frontiers | Research Topics

Analytical methods for nonlinear oscillators and solitary waves

Edited by
Chun-Hui He, Hamid M. Sedighi, Ji-Huan He, Yusry El-Dib and Dragan Marinkovic

Published in
Frontiers in Physics

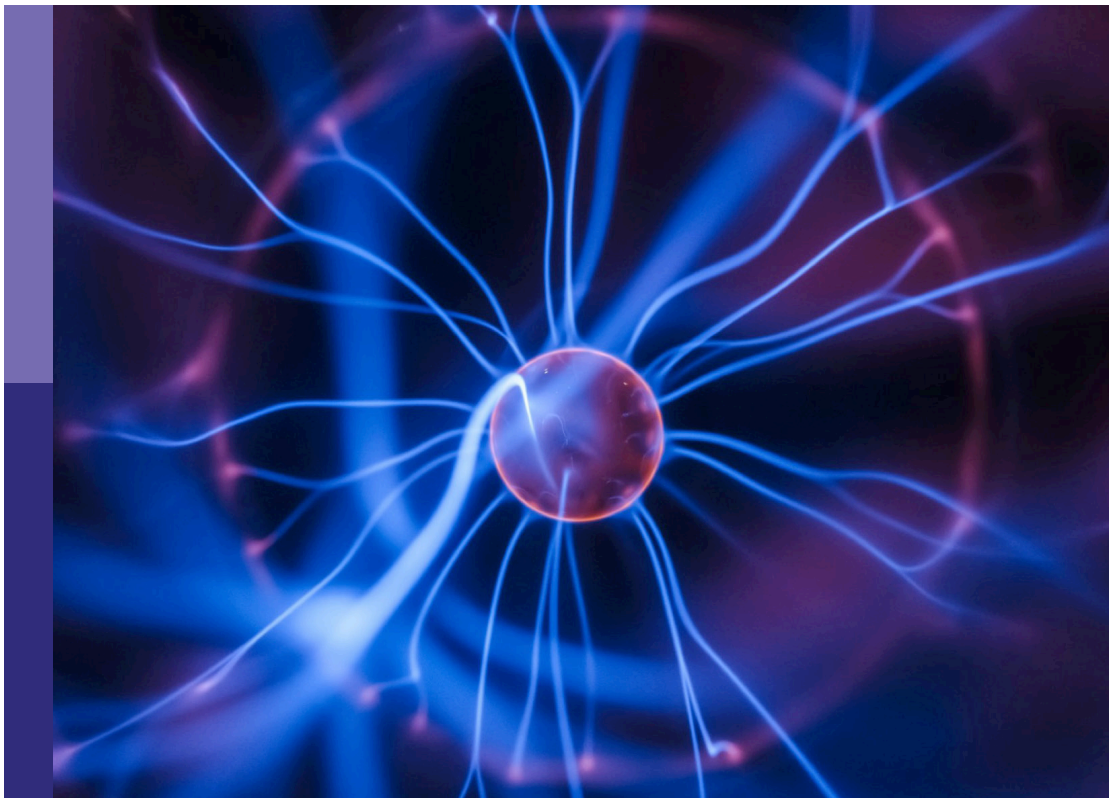

ISSN 1664-8714
ISBN 978-2-8325-3963-7
DOI 10.3389/978-2-8325-3963-7

About Frontiers

Frontiers is more than just an open access publisher of scholarly articles: it is a pioneering approach to the world of academia, radically improving the way scholarly research is managed. The grand vision of Frontiers is a world where all people have an equal opportunity to seek, share and generate knowledge. Frontiers provides immediate and permanent online open access to all its publications, but this alone is not enough to realize our grand goals.

Frontiers journal series

The Frontiers journal series is a multi-tier and interdisciplinary set of open-access, online journals, promising a paradigm shift from the current review, selection and dissemination processes in academic publishing. All Frontiers journals are driven by researchers for researchers; therefore, they constitute a service to the scholarly community. At the same time, the *Frontiers journal series* operates on a revolutionary invention, the tiered publishing system, initially addressing specific communities of scholars, and gradually climbing up to broader public understanding, thus serving the interests of the lay society, too.

Dedication to quality

Each Frontiers article is a landmark of the highest quality, thanks to genuinely collaborative interactions between authors and review editors, who include some of the world's best academicians. Research must be certified by peers before entering a stream of knowledge that may eventually reach the public - and shape society; therefore, Frontiers only applies the most rigorous and unbiased reviews. Frontiers revolutionizes research publishing by freely delivering the most outstanding research, evaluated with no bias from both the academic and social point of view. By applying the most advanced information technologies, Frontiers is catapulting scholarly publishing into a new generation.

What are Frontiers Research Topics?

Frontiers Research Topics are very popular trademarks of the *Frontiers journals series*: they are collections of at least ten articles, all centered on a particular subject. With their unique mix of varied contributions from Original Research to Review Articles, Frontiers Research Topics unify the most influential researchers, the latest key findings and historical advances in a hot research area.

Find out more on how to host your own Frontiers Research Topic or contribute to one as an author by contacting the Frontiers editorial office: frontiersin.org/about/contact

Analytical methods for nonlinear oscillators and solitary waves

Topic editors

Chun-Hui He — Xi'an University of Architecture and Technology, China
Hamid M. Sedighi — Shahid Chamran University of Ahvaz, Iran
Ji-Huan He — Soochow University, China
Yusry El-Dib — Ain Shams University, Egypt
Dragan Marinkovic — Technical University of Berlin, Germany

Citation

He, C.-H., Sedighi, H. M., He, J.-H., El-Dib, Y., Marinkovic, D., eds. (2023). *Analytical methods for nonlinear oscillators and solitary waves*. Lausanne: Frontiers Media SA. doi: 10.3389/978-2-8325-3963-7

Table of contents

frontiers | Frontiers in Physics

TYPE Editorial
PUBLISHED 03 November 2023
DOI 10.3389/fphy.2023.1309182

OPEN ACCESS

EDITED AND REVIEWED BY
Alex Hansen,
Norwegian University of Science and Technology, Norway

*CORRESPONDENCE
Chun-Hui He,
mathew_he@yahoo.com

RECEIVED 07 October 2023
ACCEPTED 23 October 2023
PUBLISHED 03 November 2023

CITATION
He C-H, He J-H, Sedighi HM, El-Dib YO, Marinkovic D and Alsolami AA (2023), Editorial: Analytical methods for nonlinear oscillators and solitary waves. *Front. Phys.* 11:1309182.
doi: 10.3389/fphy.2023.1309182

Editorial: Analytical methods for nonlinear oscillators and solitary waves

Chun-Hui He[1,2]*, Ji-Huan He[3], Hamid M. Sedighi[4], Yusry O. El-Dib[5], Dragan Marinkovic[6] and Abdulrahman Ali Alsolami[7]

[1]School of Civil Engineering, Xi'an University of Architecture and Technology, Xi'an, China, [2]School of Mathematics, China University of Mining and Technology, Xuzhou, China, [3]College of Textile and Clothing Engineering, Soochow University, Suzhou, China, [4]Mechanical Engineering Department, Faculty of Engineering, Shahid Chamran University of Ahvaz, Ahvaz, Iran, [5]Mechanical Engineering Department, Faculty of Engineering, Ain Shams University, Cairo, Egypt, [6]Department of Structural Analysis, Technical University of Berlin, Berlin, Germany, [7]Department of Mathematics, Faculty of Science, King Abdulaziz University, Jeddah, Saudi Arabia

KEYWORDS

soliton, nonlinear osciilation, fractal theory, fractional calculus, homotope perturbations method

Editorial on the Research Topic
Analytical methods for nonlinear oscillators and solitary waves

1 Introduction

Physics is mathematical, new physical phenomena require new mathematical tools. This Research Topic is an attractive introduction of some new mathematical concepts, e.g., the two-scale fractal geometry, the fractal-fractional models, the homotopy perturbation method and the frequency formulation appliable to physics. The new findings of physical phenomena using the new mathematical tools have excited physicists with their potential to reveal secrets in physics and have triggered new research frontiers in physics. Here is an overview of the Research Topic.

2 Fractional soliton vs. fractal soliton

Fractional soliton is a new concept in mathematics, in this paper, Zeng et al. studied the fractional Kdv–Burgers equation to reveal that the soliton profile is not function of t and x, but t^{η} and x^{η}, where η is the fractional order.

Fractal soliton, on the other hand, is a solitary wave moving along an unsmooth boundary or through a porous medium [1]. When an attosecond electron beam is trapped in and propagate with the laser pulse, the travelling solitary wave can be modelled in a fractal space [2], and the attosecond physics won 2023 Nobel Prize in Physics [3]. Discontinuous time appears on an attosecond (10^{-18} s) scale, so fractal time has to be adopted [4, 5], and pinpointing the fractal dimensions is tricky, especially when the studied system has not

seeming self-similarity, now He-Liu's fractal dimensions formulation [6] makes the fractal theory accessible to porous media and discontinuous time.

3 Fractional vibration vs. fractal vibration

The fractional calculus can also be applied to model the memory property of a damped vibration system. In this paper, Zhang et al. studied a fractional stochastic vibration system by taking full advantage of the memory property of the Caputo fractional derivative.

A fractal vibration system, on the other hand, works in a fractal space. The fractal vibration theory allows scientists to insight into the vibration properties on a molecule scale. The traditional vibration theory cannot model the effects of molecules or nanoparticles' size and distribution in air on the vibrating properties. Tian et al. [7] considered the effect of the air pollution on the operation of the MEMS system, and concluded that the fractal dimensions can be used for controlling the pull-in instability. In this paper, Lin and Li applied the fractal vibration theory to elucidate the ions release mechanism instead of the traditional diffusion process, opening up a flood of promising opportunities to design new hollow fibers.

4 Homotopy perturbation method

The homotopy perturbation method (HPM) was proposed by Ji-Huan He [8], a heuristic review on the method is available in Ref. [9]. In an interview with ScienceWatch.com on February 2008, Ganji http://archive.sciencewatch.com/dr/fbp/2008/08febfbp/08febGanji/ emphasized the homotopy perturbation method (HPM), "wherever a nonlinear equation is found, Dr. He's HPM will be the primary tool of discovery," and he further concluded, "He's homotopy perturbation method itself is mathematically beautiful and extremely accessible to non-mathematicians." In the last two decades, Dr. Ganji's prediction is coming true. There are many modifications of the homotopy perturbation method, among which He-Laplace method is extremely suitable for fractional calculus [10–12], and Li-He's modified homotopy perturbation method [13–15] for forced oscillators.

In this paper, Qayyum et al. found that the homotopy perturbation method is extremely suitable for the search for fractional soliton solutions, Tao et al. coupled the Aboodh transformation with the homotopy perturbation method, a new hope for fractional calculus, Buhe et al. applied the method to study forest resource and there is the possibility to extend it to other natural resources, especially the grassland resources.

5 Frequency formulation

The simpler is the better for most physical problems. So far the simplest approach to a nonlinear oscillator is He's frequency formulation [16–18]. There are many modifications, the most famous one is the Hamiltonian-based frequency-amplitude formulation [19, 20]. El-Dib extended it to time-delayed vibration systems [21]. In this paper, Niu et al. extended the frequency formulation to fractal–fractional non-linear oscillators.

6 Concluding remarks

This Research Topic of *Frontiers in Physics* consists mainly of a Research Topic of mathematics methods appliable to physics, it is to bring to the fore the many new and exciting applications of some new mathematical theories of the two-scale fractal theory and the fractal-fractional calculus, it can attract much attention from different fields, such as mathematics, physics, artificial intelligence, neural network, computer science, textile engineering, material science and others. We hope that this Research Topic will prove to be a timely and valuable reference for researchers in this Research Topic.

Author contributions

C-HH: Writing–original draft, Writing–review and editing. J-HH: Writing–review and editing. HS: Writing–review and editing. YE-D: Writing–review and editing. DM: Writing–review and editing. AA: Writing–review and editing.

Funding

The author(s) declare that no financial support was received for the research, authorship, and/or publication of this article.

Conflict of interest

The authors declare that the research was conducted in the absence of any commercial or financial relationships that could be construed as a potential conflict of interest.

The author(s) declared that they were an editorial board member of Frontiers, at the time of submission. This had no impact on the peer review process and the final decision.

Publisher's note

References

1. He JH, Qie N, He CH. Solitary waves travelling along an unsmooth boundary. *Results Phys* (2021) 24:104104. doi:10.1016/j.rinp.2021.104104

2. Duchateau G. Theoretical derivation of laser-dressed atomic states by using a fractal space. *Eur Phys J Plus* (2018) 133(5):186. doi:10.1140/epjp/i2018-12017-y

3. Castelvecchi D, Sanderson K. Physicists who built ultrafast 'attosecond' lasers win Nobel Prize. *Nature* (2023) 622:225–7. doi:10.1038/d41586-023-03047-w

4. Nottale L. On time in microphysics. *C R Acad Sci Ser* (1988) 306:341–6.

5. He JH. Fractal calculus and its geometrical explanation. *Results Phys* (2018) 10: 272–6. doi:10.1016/j.rinp.2018.06.011

6. He CH, Liu C. Fractal dimensions of a porous concrete and its effect on the concrete's strength. *Facta Universitatis Ser Mech Eng* (2023) 21:137–50. doi:10.22190/fume221215005h

7. Tian D, Ain QT, Anjum N, He CH, Cheng B. Fractal N/MEMS: from pull-in instability to pull-in stability. *Fractals* (2021) 29:2150030. doi:10.1142/s0218348x21500304

8. He JH. A coupling method of a homotopy technique and a perturbation technique for non-linear problems. *Int J Non-Linear Mech* (2000) 35:37–43. doi:10.1016/s0020-7462(98)00085-7

9. He CH, El-Dib YO. A heuristic review on the homotopy perturbation method for non-conservative oscillators. *J Low Frequency Noise, Vibration Active Control* (2022) 41(2):572–603. doi:10.1177/14613484211059264

10. Qayyum M, Afzal S, Ahmad E, Riaz MB. Fractional modeling and analysis of unsteady squeezing flow of Casson nanofluid via extended He-Laplace algorithm in Liouville-Caputo sense. *Alexandria Eng J* (2023) 73:579–91. doi:10.1016/j.aej.2023.05.010

11. Mishra HK, Nagar AK. He-laplace method for linear and nonlinear partial differential equations. *J Appl Math* (2012) 2012:180315. doi:10.1155/2012/180315

12. Chen B, Chen L, Xia ZZ. He-Laplace method for time fractional Burgers-type equations. *Therm Sci* (2023) 27(3):1947–55. doi:10.2298/tsci2303947c

13. Anjum N, He JH, Ain QT, Tian D. Li-He's modified homotopy perturbation method for doubly-clamped electrically actuated microbeams-based microelectromechanical system. *Facta Univ.-Ser Mech* (2021) 19(4):601–12. doi:10.22190/FUME210112025A

14. He JH, El-Dib YO. The enhanced homotopy perturbation method for axial vibration of strings. *Facta Univ.-Ser Mech* (2021) 19(4):735–50. doi:10.22190/fume210125033h

15. Ji QP, Wang J, Lu LX, Ge CF. Li-He's modified homotopy perturbation method coupled with the energy method for the dropping shock response of a tangent nonlinear packaging system. *J Low Frequency Noise, Vibration Active Control* (2021) 40(2): 675–82. doi:10.1177/1461348420914457

16. He JH. The simplest approach to nonlinear oscillators. *Results Phys* (2019) 15: 102546. doi:10.1016/j.rinp.2019.102546

17. Qie N, Hou WF, He JH. The fastest insight into the large amplitude vibration of a string. *Rep Mechan Eng* (2020) 2:1–5. doi:10.31181/rme200102001q

18. He JH. The simpler, the better: analytical methods for nonlinear oscillators and fractional oscillators. *J Low Frequency Noise, Vibration Active Control* (2019) 38: 1252–60. doi:10.1177/1461348419844145

19. Ma HJ. Simplified Hamiltonian-based Frequency-amplitude formulation for nonlinear vibration systems. *Facta Universitatis Ser Mech Eng* (2022) 20(2):445–55. doi:10.22190/fume220420023m

20. He JH, Hou WF, Qie N, Gepreel KA, Shirazi AH, Sedighi HM. Hamiltonian-based Frequency-amplitude formulation for nonlinear oscillators. *Facta Universitatis Ser Mech Eng* (2021) 19(2):199–208. doi:10.22190/fume201205002h

21. El-Dib YO, Elgazery NS, Gad NS. A novel technique to obtain a time-delayed vibration control analytical solution with simulation of He's formula. *Vibration & Active Control* (2023) 42:1379–89. doi:10.1177/14613484221149518

frontiers | Frontiers in Physics

TYPE Original Research
PUBLISHED 16 March 2023
DOI 10.3389/fphy.2023.1158121

OPEN ACCESS

EDITED BY
Ji-Huan He,
Soochow University, China

REVIEWED BY
Naveed Anjum,
Government College University, Faisalabad, Pakistan
Ain Qura Tul,
Guizhou University, China
Alex Elias-Zuniga,
Monterrey Institute of Technology and Higher Education (ITESM), Mexico
Dan Tian,
Xi'an University of Architecture and Technology, China

*CORRESPONDENCE
Guang-Qing Feng,
43789369@qq.com

†These authors have contributed equally to this work and share first authorship

SPECIALTY SECTION
This article was submitted to Interdisciplinary Physics, a section of the journal Frontiers in Physics

RECEIVED 03 February 2023
ACCEPTED 27 February 2023
PUBLISHED 16 March 2023

CITATION
Niu J-Y, Feng G-Q and Gepreel KA (2023), A simple frequency formulation for fractal–fractional non-linear oscillators: A promising tool and its future challenge.
Front. Phys. 11:1158121.
doi: 10.3389/fphy.2023.1158121

A simple frequency formulation for fractal–fractional non-linear oscillators: A promising tool and its future challenge

Jing-Yan Niu[1†], Guang-Qing Feng[2*†] and Khaled A. Gepreel[3,4]

[1]College of Technology, Jiaozuo Normal College, Jiaozuo, China, [2]School of Mathematics and Information Science, Henan Polytechnic University, Jiaozuo, China, [3]Taif University, Taif, Saudi Arabia, [4]Mathematics Department, Faculty of Science, Zagazig University, Zagazig, Egypt

This paper proposes a simple frequency formula developed from He's frequency formulation for fractal systems. In this approach, the initial guess can be judiciously chosen. Even the simplest initial guess leads to a highly accurate approximate solution. A detailed theoretical development is elucidated, and the solving process is given step by step. The simple calculation and reliable results have been merged into an effective tool for deeply studying fractal vibration systems, and the present approach offers a completely new angle for the fast insight into the physical properties of a non-linear vibration system in a fractal space.

KEYWORDS

frequency formula, trial solution, fractal oscillator, successive approximate solution, frequency–amplitude relationship, numerical simulation

1 Introduction

Fractal oscillations not only demonstrate the beauty of mathematics but also reveal the nature of the world and change the way people study nature. Fractal non-linear systems truly describe the dynamic problems of engineering science, and the research on them greatly expands the field of human cognition. The emergence of fractal theory makes us realize that the world is non-linear and fractals are everywhere. Fractal non-linear vibration can be close to practical problems in both depth and breadth, and it explains many phenomena through the fractal theory. Since the birth of the fractal theory, it has been used in engineering and science, for example, the fractal diffusion [1, 2], the fractal rheological model [3], the fractal control [4], the fractal solitary waves [5, 6], and the fractal oscillators [7]. The two-scale fractal calculus is used to describe transport problems in a porous medium, such as the problem of oil extraction and heat transfer of heat pipes. The porous medium is viewed as a fractal space, so non-linear vibrations in the porous medium can be modeled by fractal vibration theory [8, 9].

There are many analytical and numerical methods to find an approximate solution of a differential equation containing fractional derivatives. The homotopy perturbation method contains perturbation parameters, which have been extended to a wide range of physical applications and engineering fields by many researchers [10, 11]. He's frequency formula is a simple and powerful method for a conservation non-linear oscillator, which has been widely applied to solve non-linear oscillator problems, especially the pull-in instability found in MEMS [12, 13]. It can be extended to the fractal oscillators and non-conservative oscillators [14–21]. The applications of these non-linear oscillations do not have non-linear even functions. El-Dib proposed a modification of He's method for the case of even non-linearity [22]. The Hamiltonian-based frequency formula is a modification of He's frequency formula

[23]. The most important property of a non-linear system is the relationship between frequency and amplitude, so how to quickly estimate the frequency–amplitude relationship is an urgent problem to study. Many researchers devoted their efforts to studying fractional calculus which provides a powerful tool to characterize the periodic behavior of a non-linear oscillator [24]. He gave a tutorial review on fractal space and fractional calculus [25], Tian et al. established a fractal model for N/MEMS [26], and Li et al. studied the non-linear vibration of nanoparticles in the electrospinning process [27].

There are many analytical solutions for fractal oscillators, but the continuous solution has not been discussed so far. Existing frequency formulas cannot be formulated to correspond to the frequency of the continuous process [28]. Recently, El-Dib proposed an efficient frequency formula, which can be used to obtain successive approximate solutions for the non-linear oscillation [22]. In this paper, we illustrate the frequency formula and extend it in the differential equation with the fractional derivative. The new method will be applied to rapidly predict the frequency characteristics and determine successive approximate solutions of a fractal vibration system.

2 Two-scale fractal theory

As the fractal theory is helpful in establishing a governing equation in a fractal space, it has become a significant topic in both mathematics and mechanical engineering. The two-scale fractal derivative [29] is defined as follows:

$$\frac{dz}{dt^{\varphi}}(t_0) = \Gamma(1+\varphi) \lim_{\substack{t-t_0\to\Delta t \\ \Delta t\neq 0}} \frac{z(t)-z(t_0)}{(t-t_0)^{\varphi}} \tag{1}$$

where $\varphi \in R$.

When we observe a motion at a large scale, it may be a continuous change, while at a small scale, it may become discontinuous. Therefore, the two-scale fractal theory is a powerful mathematical tool to study the world with greater precision [30].

When $\varphi = 1$ and $\Delta t \to 0$, we can easily have $\frac{dz}{dt^1} = \Gamma(2) \lim_{\substack{t-t_0\to\Delta t \\ \Delta t\neq 0}} \frac{z(t)-z(t_0)}{t-t_0} = z'$. Similarly, when $\varphi = 2$, $\frac{dz}{dt^2} = \Gamma(3) \lim_{\substack{t-t_0\to\Delta t \\ \Delta t\neq 0}} \frac{z(t)-z(t_0)}{(t-t_0)^2} = z''$.

It is worth mentioning that the two-scale fractal derivative agrees with the traditional differential derivative when the fractal dimension φ is a positive integer.

To better understand the fractional derivative, let us take the function $z = t^{\mu}$ as an example. Using Eq. 1, we can obtain [31]

$$\frac{d}{dt^{\varphi}} t^{\mu} = \frac{\Gamma(1+\mu)\Gamma(1+\varphi-N)}{\Gamma(1+\mu-N)} t^{\mu-\varphi} \tag{2}$$

where N is a natural number, $N \le \varphi$.

Knowing the fractional derivative of the power function, the derivatives of all elementary functions will also be calculated, with the help of Taylor's series. For example, we have the following equation:

$$sint = \sum_{k=0}^{\infty} \frac{(-1)^k}{(2k+1)!} t^{2k+1}. \tag{3}$$

By using Eqs 2, 3, we can obtain

$$\frac{d}{dt^{\varphi}} sint = \sum_{k=0}^{\infty} \frac{(-1)^k}{(2k+1)!} \frac{\Gamma(2+2k)\Gamma(1+\varphi-N)}{\Gamma(2+2k-N)} t^{2k+1-\varphi} \tag{4}$$

After simple calculations, it yields the following result:

$$\frac{d}{dt^{1}} sint = \sum_{k=0}^{\infty} \frac{(-1)^k}{(2k+1)!} \frac{\Gamma(2+2k)\Gamma(1+1-1)}{\Gamma(2+2k-1)} t^{2k+1-1} = cost \tag{5}$$

and

$$\frac{d}{dt^{1.5}} sint = \sum_{k=0}^{\infty} \frac{(-1)^k}{(2k+1)!} \frac{\Gamma(2+2k)\Gamma(1+1.5-1)}{\Gamma(2+2k-1)} t^{2k+1-1.5} = \frac{\sqrt{\pi}}{2} t^{-0.5} cost \tag{6}$$

Also, we can obtain another form of the fractional derivative. It is obvious that the fractal derivative is useful and convenient to study.

3 Successive approximate solutions for fractal non-linear oscillation

We consider a general fractal non-linear oscillator in a fractal space as follows:

$$\frac{d}{dt^{\varphi}}\left(\frac{dz}{dt^{\varphi}}\right) + h(z) = 0,\ z(0) = A, \frac{dz(0)}{dt^{\varphi}} = 0 \tag{7}$$

where $h(z)$ is an odd potential function or an odd polynomial as $h(z) = a_1 z + a_3 z^3 + \ldots + a_{2n+1} z^{2n+1}$.

Let $\tau = t^{\varphi}$, Eq. 7 can be converted into its differential partner as

$$z'' + h(z) = 0,\ z(0) = A, z'(0) = 0, \tag{8}$$

where the derivative of the function z with respect to τ is defined. Here, φ is the scale dimension, and t and τ describe the small and large scales, respectively.

He rewrote Eq. 8 in the following form [12]:

$$z'' + \frac{h(z)}{z} z = 0 \tag{9}$$

where the ratio h(z)/z is the equivalent stiffness.

When Eq. 8 is approximated by a linear oscillator:

$$z'' + \omega^2 z = 0 \tag{10}$$

He has established a simple formula [12].

$$\omega_{He}{}^2 = \left.\frac{dh(z)}{dz}\right|_{z=\frac{A}{2}} \tag{11}$$

Following the analysis principle of He's frequency formula, He and Liu proposed a modified frequency formulation for a fractal vibration in the porous medium [32].

$$\omega_{HL}{}^2 = \frac{\int_0^A z^4 h(z) dz}{\int_0^A z^5 dz} \tag{12}$$

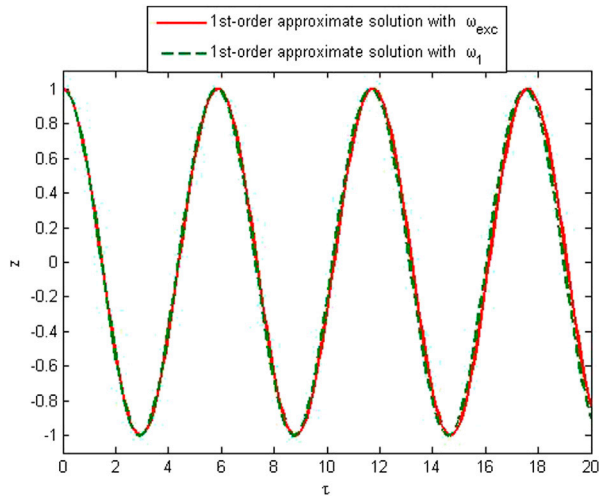

FIGURE 1
Illustration of the first-order approximate solution with $A = 1$.

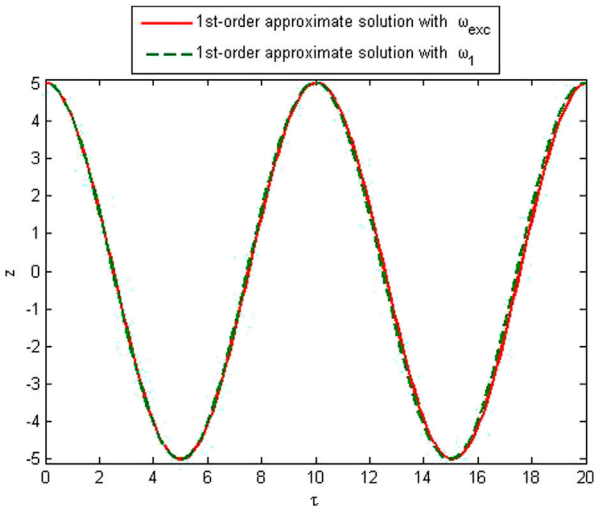

FIGURE 2
Illustration of the first-order approximate solution with $A = 5$.

El-Dib established an extended frequency–amplitude formula, which is the best and most efficient formula and can be used to obtain successive approximate solutions for the non-linear oscillations [26]. We extend this method to the fractal system and obtain high-precision approximate frequency.

In the same way as in Eqs 8, 9 can be rewritten as follows:

$$z'' + \frac{h(z)z}{z^2}z = 0 \tag{13}$$

Integrating the numerator and the denominator of the stiffness term, the frequency ω^2 with the trial solution $z = z(\tau)$ that corresponds to the initial conditions is obtained in the following form:

$$\omega^2\big|_{z=z(\tau)} = \frac{\int_0^T h(z)z d\tau}{\int_0^T z^2 d\tau} \tag{14}$$

where T is the period, $T = \frac{2\pi}{\omega}$.

Let us explain this frequency formula from another angle.

By the comparison of Eqs 8, 10, the error function needs to take the minimum value.

$$E(\omega^2) = \left|h(z) - \omega^2 z\right| \tag{15}$$

The mean square error is defined as

$$\begin{aligned} MSE(\omega^2) &= \int_0^T (h(z) - \omega^2 z)^2 d\tau, \\ &= \omega^4 \int_0^T z^2 d\tau - \omega^2 2 \int_0^T h(z)z d\tau + \int_0^T h^2(z) d\tau \end{aligned} \tag{16}$$

The aforementioned problem is equivalent to the value of ω^2, and the function $MSE(\omega^2)$ takes the minimum value. After a simple calculation, the minimum point is

$$\frac{dMSE(\omega^2)}{d\omega^2} = \omega^2 2 \int_0^T z^2 d\tau - 2 \int_0^T h(z)z d\tau = 0 \tag{17}$$

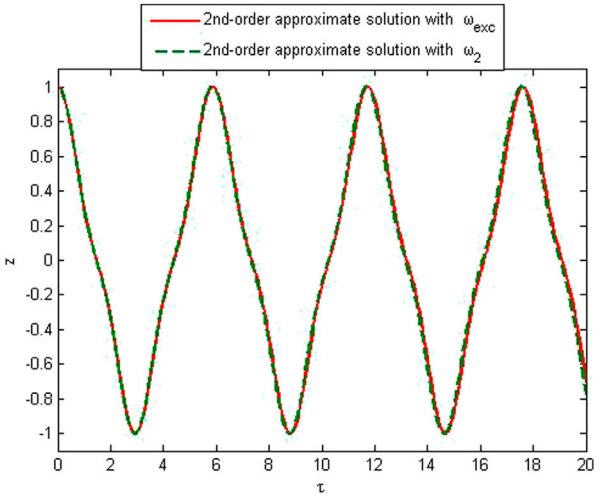

FIGURE 3
Illustration of the second-order approximate solution with $A = 1$.

The solution of Eq. 17 is Eq. 14. The aforementioned analysis process verifies the accuracy of the frequency formula. With a suitable chosen trial solution, performing the aforementioned integrals gives the corresponding frequency.

For the non-linear oscillator, $h(z) = a_1 z + a_3 z^3$, we obtain

$$\omega_{He}{}^2 = \omega_{HL}{}^2 = \omega^2\big|_{z=A\cos\omega\tau} = a_1 + \frac{3}{4}A^2 a_3 \tag{18}$$

The precision of Eq. 18 can be found by comparing it with the exact frequency [22].

$$\omega_{exc} = \frac{\pi}{2\int_0^{\pi/2} \frac{d\theta}{\sqrt{a_1 + \frac{1}{2}A^2 a_3 \left(1 + \sin^2\theta\right)}}} \tag{19}$$

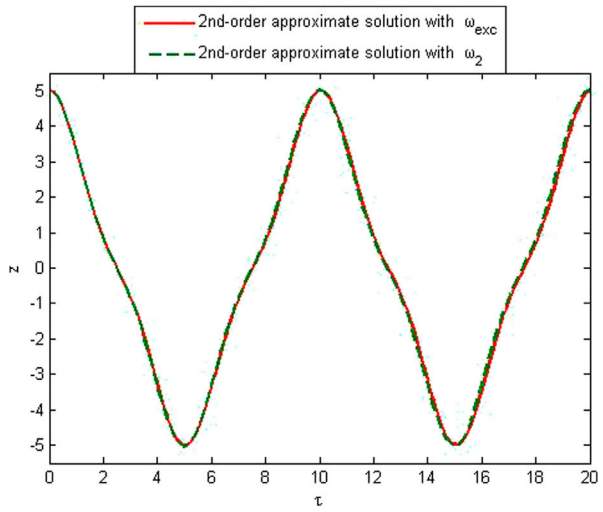

FIGURE 4
Illustration of the second-order approximate solution with $A = 5$.

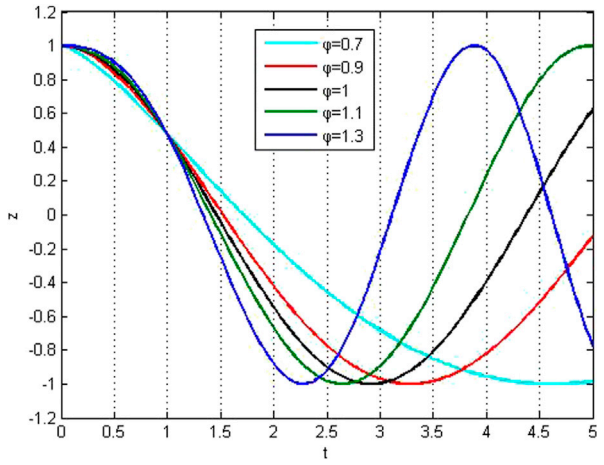

FIGURE 6
Graphing solution (28) for sequences of the parameter φ with $A = 1$.

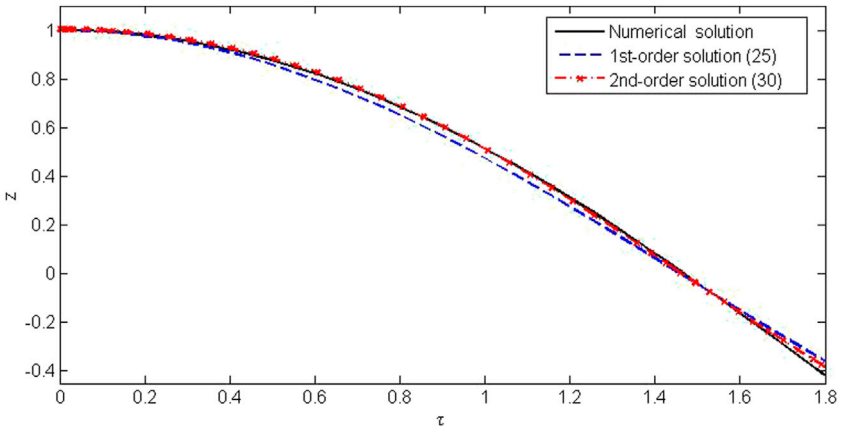

FIGURE 5
Comparison of the numerical solution with first- and second-order solutions for $A = 1$

4 Application and numerical illustration

In order to illustrate the solution process of the aforementioned method, we consider the following oscillator:

$$\frac{d}{dt^{\varphi}}\left(\frac{dz}{dt^{\varphi}}\right) + z^{\frac{1}{3}} = 0,\ z(0) = A,\ \frac{dz(0)}{dt^{\varphi}} = 0 \tag{20}$$

We consider that the general mth-order trial solution which satisfies the initial conditions can be expressed by

$$z_m(\tau) = \sum_{n=1}^{m} c_n \cos\left((2n-1)\omega_m \tau\right), \tag{21}$$

where $\tau = t^{\varphi}$ and $\sum_{n=1}^{m} c_n = A$.

Using the first-order trial solution, $z_1 = A\cos\omega_1\tau$, and employing Eq. 14, the corresponding frequency is

$$\omega_1 = \sqrt{\frac{\int_0^T (z_1)^{\frac{4}{3}} d\tau}{\int_0^T (z_1)^2 d\tau}} = \frac{1.076845}{A^{\frac{1}{3}}},\ T = \frac{2\pi}{\omega_1} \tag{22}$$

For a comparison between He–Liu's modification and the present modification, we obtain

$$\omega_{HL} = \sqrt{\frac{\int_0^A z^4 h(z) dz}{\int_0^A z^5 dz}} = \frac{1.06066}{A^{\frac{1}{3}}} \tag{23}$$

The exact frequency of Eq. 20 is ω_{exc}.

$$\omega_{\text{exc}} = \frac{2\pi}{2\sqrt{2}\int_0^A \frac{dz}{\sqrt{\int_z^A s^{\frac{1}{3}} ds}}} = \frac{1.070451}{A^{\frac{1}{3}}} \tag{24}$$

So, the relative error in the first-order approximate frequency is given by

$$\left|\frac{\omega_{exc}-\omega_1}{\omega_{exc}}\right|\times 100\% = 0.5973\% \tag{25}$$

Also, the error in He–Liu's modification is

$$\left|\frac{\omega_{exc}-\omega_{HL}}{\omega_{exc}}\right|\times 100\% = 0.9147\% \tag{26}$$

It is noticed that the present method has better precision.

The first-order approximate solution of Eq. 20 is

$$z_1 = A\cos\left(\frac{1.076845}{A^{\frac{1}{3}}}\tau\right), \tag{27}$$

that is,

$$z_1 = A\cos\left(\frac{1.076845}{A^{\frac{1}{3}}}t^{\varphi}\right) \tag{28}$$

We consider that the second-order trial solution meeting the initial conditions can be expressed as

$$z_2 = c_1\cos(\omega_2\tau) + (A-c_1)\cos(3\omega_2\tau) \tag{29}$$

Using a trigonometric formula $\cos(3\omega_2\tau) = 4cos^3(\omega_2\tau) - 3\cos(\omega_2\tau)$, we have the following equation:

$$z_2 = (4c_1-3A)\cos(\omega_2\tau) + (4A-4c_1)\cos^3(\omega_2\tau) \tag{30}$$

The least-square of the displacement is estimated as follows:

$$\int_0^T\left[(4c_1-3A)\cos(\omega_2\tau)\right]^2 d\tau = \int_0^T\left[(4A-4c_1)\cos^3(\omega_2\tau)\right]^2 d\tau,\quad T=\frac{2\pi}{\omega_2} \tag{31}$$

The solution of Eq. 31 is $c_1 = 086038A$, and substituting the value into Eq. 29, we obtain

$$z_2 = 086038A\cos(\omega_2\tau) + 0.13962A\cos(3\omega_2\tau) \tag{32}$$

Using Eq. 32 and the second-order trial solution, Eq. 14 becomes

$$\omega_2 = \sqrt{\frac{\int_0^T (z_2)^{\frac{4}{3}} d\tau}{\int_0^T (z_2)^2 d\tau}},\quad T=\frac{2\pi}{\omega_2} \tag{33}$$

After integral calculation, the second-order approximate frequency is given by

$$\omega_2 = \frac{1.074586}{A^{\frac{1}{3}}} \tag{34}$$

The percentage relative error in second-order approximate frequency is 0.3863%. Also, the second-order approximate solution of Eq. 20 is

$$z_2 = 086038A\cos\left(\frac{1.074586}{A^{\frac{1}{3}}}\tau\right) + 0.13962A\cos\left(\frac{3.223758}{A^{\frac{1}{3}}}\tau\right) \tag{35}$$

This leads to

$$z_2 = 086038A\cos\left(\frac{1.074586}{A^{\frac{1}{3}}}t^{\varphi}\right) + 0.13962A\cos\left(\frac{3.223758}{A^{\frac{1}{3}}}t^{\varphi}\right) \tag{36}$$

In order to obtain the sequential extended approximate solution and improve the accuracy of the solution, we can use a higher-order trial solution, but the solving process becomes more complex.

To verify the accuracy of the method, the approximate solution is compared with the exact solution of Eq. 20 in Figures 1–5. The comparison of the approximate frequency with the exact one is made, and relative errors have been found. It is noted that the relative error does not depend upon the amplitude; that is, the error is the same for any value of the amplitude, while it decreases with the increase in the order of approximation. Figures 1, 2 show first-order approximate solutions with different values of the amplitudes. Figures 3, 4 show second-order approximate solutions. A good agreement for various amplitudes of first- and second-order approximate frequencies can be seen from these figures. Figure 5 shows the comparison of the numerical solution obtained by the Matlab solver "ode45" with approximate solutions over a small interval.

Different values of the fractal exponent φ are considered for Eq. 28 and shown together in Figure 6. It is observed that the vibration attenuation occurs more, and the oscillation frequency becomes faster for increasing the values of the fractal exponent φ.

5 Conclusion

In this paper, a high-precision frequency is obtained by a trial solution for the first time ever, and a frequency formula determined by the trial solution is proposed for solving a fractal nonlinear vibration system. The new method is described theoretically, and an example is given to explain in detail the process of finding the higher-order approximate solution and the approximate frequency. The analysis results show that this new method can be used to obtain the frequency with high accuracy and to quickly calculate the high-order continuous solution of the fractal non-linear oscillator. The influence of the fractal derivative order on the periodic motion is visually displayed graphically. It is revealed that the fractal exponent affects the frequency characteristics greatly as that discussed in Refs. [33, 34]. Although we only discuss the oscillator with the non-zero initial condition, it is still valid for the oscillator with zero initial condition as that in micro-electromechanical systems [35], which will be discussed in the next paper.

Data availability statement

The original contributions presented in the study are included in the article/Supplementary Material; further inquiries can be directed to the corresponding author.

Author contributions

All authors listed have made a substantial, direct, and intellectual contribution to the work and approved it for publication.

Conflict of interest

The authors declare that the research was conducted in the absence of any commercial or financial relationships that could be construed as a potential conflict of interest.

Publisher's note

References

1. Xiao BQ, Huang QW, Yu BM, Long GB, Chen HX. A fractal model for predicting oxygen effective diffusivity of porous media with rough surfaces under dry and wet conditions. *Fractals* (2021) 29(3):2150076. doi:10.1142/s0218348x21500766

2. He JH, Qian MY. A fractal approach to the diffusion process of red ink in a saline water. *Therm Sci* (2022) 26(3B):2447–51. doi:10.2298/tsci2203447h

3. Zuo YT. Effect of sic particles on viscosity of 3-D print paste a fractal rheological model and experimental verification. *Therm Sci* (2021) 25(3):2405–9. doi:10.2298/tsci200710131z

4. Ma HJ. Fractal variational principle for an optimal control problem. *J Low Frequency Noise, Vibration Active Control* (2022) 41:1523–31. doi:10.1177/14613484221104647

5. Wang KL. Exact solitary wave solution for fractal shallow water wave model by He's variational method. *Mod Phys Lett B* (2022) 36(7):2150602. doi:10.1142/s0217984921506028

6. Wang KL. New variational theory for coupled nonlinear fractal Schrodinger system. *Int J Numer Methods Heat Fluid Flow* (2022) 32(2):589–97. doi:10.1108/hff-02-2021-0136

7. Shen Y, El-Dib YO. A periodic solution of the fractional sine-Gordon equation arising in architectural engineering. *J Low Frequency Noise, Vibration Active Control* (2021) 40(2):683–91. doi:10.1177/1461348420917565

8. He JH, Kou SJ, He CH, Zhang ZW, Gepreel KA. Fractal oscillation and its frequency-amplitude property. *Fractals* (2021) 29(4):2150105. doi:10.1142/s0218348x2150105x

9. Elías-Zúñiga A, Martínez-Romero O, Trejo DO, Palacios-Pineda LM. Exact steady-state solution of fractals damped and forced systems. *Results Phys* (2021) 28:104580. doi:10.1016/j.rinp.2021.104580

10. He CH, El-Dib YO. A heuristic review on the homotopy perturbation method for non-conservative oscillators. *J Low Frequency Noise, Vibration Active Control* (2022) 41(2):572–603. doi:10.1177/14613484211059264

11. He JH, Jiao ML, He CH. Homotopy perturbation method for fractal Duffing oscillator with arbitrary conditions. *Fractals* (2022) 30(9). doi:10.1142/S0218348X22501651

12. He JH. The simplest approach to nonlinear oscillators. *Results Phys* (2019) 15:102546. doi:10.1016/j.rinp.2019.102546

13. He JH, Na Q, He CH, Khaled G. Fast identification of the pull-in voltage of a nano/micro-electromechanical system. *J Low Frequency Noise, Vibration Active Control* (2022) 41:566–71. doi:10.1177/14613484211068252

14. Feng GQ. He's frequency formula to fractal undamped Duffing equation. *J Low Frequency Noise Vibration Active Control* (2021) 40:1671–6. doi:10.1177/1461348421992608

15. Elias-Zuniga A, Palacios-Pineda LM, Jimenez-Cedeno IH, Martinez-Romero O, Olvera-Trejo D. Analytical solution of the fractal cubic–quintic duffing equation. *Fractals* (2021) 29(4):2150080. doi:10.1142/s0218348x21500808

16. Elias-Zuniga A, Palacios-Pineda LM, Jiménez-Cedeño IH, Martinez-Romero O, Olvera-Trejo D. A fractal model for current generation in porous electrodes. *J Electroanalytical Chem* (2021) 880:114883. doi:10.1016/j.jelechem.2020.114883

17. Qie N, Hou WF, He JH. The fastest insight into the large amplitude vibration of a string. *Rep Mechan Eng* (2020) 2:1–5. doi:10.31181/rme200102001q

18. El-Dib YO. The frequency estimation for non-conservative nonlinear oscillation. *Zamm-z Angew Math Mech* (2021) 101:101. doi:10.1002/zamm.202100187

19. El-Dib YO. The damping Helmholtz–Rayleigh–Duffing oscillator with the non-perturbative approach. *Mathematics Comput Simulation* (2022) 194:552–62. doi:10.1016/j.matcom.2021.12.014

20. El-Dib YO. The simplest approach to solving the cubic nonlinear jerk oscillator with the non-perturbative method. *Math Meth Appl Sci* (2022) 45:5165–83. doi:10.1002/mma.8099

21. Elías-Zúñiga A, Palacios-Pineda LM, Jiménez-Cedeño IH, Martínez-Romero O, Trejo DO. He's frequency–amplitude formulation for nonlinear oscillators using Jacobi elliptic functions. *J Low Frequency Noise, Vibration Active Control* (2020) 39(4):1216–23. doi:10.1177/1461348420972820

22. El-Dib YO. Insightful and comprehensive formularization of frequency-amplitude formula for strong or singular nonlinear oscillators. *J Low Frequency Noise, Vibration Active Control* (2022) 42:89–109. doi:10.1177/14613484221118177

23. He JH. Hamiltonian approach to nonlinear oscillators. *Phys Lett A* (2010) 374:2312–4. doi:10.1016/j.physleta.2010.03.064

24. Ain QT, He JH. On two-scale dimension and its applications. *Therm Sci* (2019) 23:1707–12. doi:10.2298/tsci190408138a

25. He JH. Fractal calculus and its geometrical explanation. *Results Phys* (2018) 10:272–6. doi:10.1016/j.rinp.2018.06.011

26. Tian D, Ain QT, Anjum N, He CH, Cheng B. Fractal N/MEMS: From pull-in instability to pull-in stability. *Fractals* (2021) 29(2):2150030. doi:10.1142/s0218348x21500304

27. He JH. The simpler, the better: Analytical methods for nonlinear oscillators and fractional oscillators. *J Low Frequency Noise Vibration Active Control* (2019) 38:1252–60. doi:10.1177/1461348419844145

28. Elías-Zúñiga A, Martínez-Romero O, Palacios-Pineda LM, Olvera-Trejo D. New analytical solution of the fractal anharmonic oscillator using an ancient Chinese algorithm: Investigating how plasma frequency changes with fractal parameter values. *J Low Frequency Noise, Vibration Active Control* (2022) 41(3):833–41. doi:10.1177/14613484211070883

29. Elias-Zuniga A. On the two-scale dimension and its application for deriving a new analytical solution for the fractal Duffing's equation. *Fractals* (2022) 30(3):2250061. doi:10.1142/S0218348X2250061X

30. Elias-Zuniga A, Palacios-Pineda LM, Olvera-Trejo D, Martinez-Romero O. Recent strategy to study fractal-order viscoelastic polymer materials using an ancient Chinese algorithm and He's formulation. *J Low Frequency Noise Vibration Active Control* (2022) 41(3):842–51. doi:10.1177/14613484221085413

31. He JH, El-Dib YO. A tutorial introduction to the two-scale fractal calculus and its application to the fractal Zhiber-Shabat oscillator. *Fractals* (2021) 29(8):2150268. doi:10.1142/s0218348x21502686

32. He CH, Liu C. A modified frequency-amplitude formulation for fractal vibration systems. *Fractals* (2022) 30(3):2250046. doi:10.1142/S0218348X22500463

33. He JH, Moatimid GM, Zekry MH. Forced nonlinear oscillator in a fractal space. *Facta Univ Series: Mech Eng* (2022) 20(1):1–20.

34. Liu FJ, Zhang T, He CH, Tian D. Thermal oscillation arising in a heat shock of a porous hierarchy and its application. *Facta Univ Series: Mech Eng* (2022) 20(3):633–645.

35. Anjum N, He JH, Ain QT, Tian D. Li-He's modified homotopy perturbation method for doubly-clamped electrically actuated microbeams-based microelectromechanical system. *Facta Univ Series: Mech Eng* (2021) 19(4):601–612.

frontiers | Frontiers in Physics

TYPE Original Research
PUBLISHED 11 April 2023
DOI 10.3389/fphy.2023.1177335

OPEN ACCESS

EDITED BY
Ji-Huan He,
Soochow University, China

REVIEWED BY
Guangqing Feng,
Henan Polytechnic University, China
Muhammad Nadeem,
Qujing Normal University, China
Ain Qura Tul,
Guizhou University, China
Naveed Anjum,
Government College University, Faisalabad, Pakistan

*CORRESPONDENCE
Yuxia Wang,
wangyx094@163.com

SPECIALTY SECTION
This article was submitted to Interdisciplinary Physics, a section of the journal Frontiers in Physics

RECEIVED 01 March 2023
ACCEPTED 22 March 2023
PUBLISHED 11 April 2023

CITATION
Zeng H, Wang Y, Xiao M and Wang Y (2023), Fractional solitons: New phenomena and exact solutions. *Front. Phys.* 11:1177335. doi: 10.3389/fphy.2023.1177335

Fractional solitons: New phenomena and exact solutions

Huajun Zeng[1], Yuxia Wang[1]*, Min Xiao[1] and Ying Wang[2]

[1]Zhejiang Gongshang University, Hangzhou, Zhejiang, China, [2]School of Science, Xi'an University of Architecture and Technology, Xi'an, Shaanxi, China

The fractional solitons have demonstrated many new phenomena, which cannot be explained by the traditional solitary wave theory. This paper studies some famous fractional wave equations including the fractional KdV–Burgers equation and the fractional approximate long water wave equation by a modified tanh-function method. The solving process is given in details, and new solitons can be rigorously explained by the obtained exact solutions. This paper offers a new window for studying fractional solitons.

KEYWORDS

time-fractional KdVB model, fractional approximate long water wave model, exact solutions, fractional solitons, fractional complex transform

1 Introduction

A fractional solitary wave [1] has some special properties which cannot be explained by the traditional soliton theory. The traditional soliton is a single wave with the same shape in propagation, while the fractional soliton has some amazing memory and non-local properties, which means the present wave morphology depends upon its history. This is caused by the intrinsic property of the fractional derivative [2]. The fractal solitary waves, on the other hand, are waves traveling along an unsmooth boundary [3, 4]. And the fractal solitary wave has the local property, the unsmooth boundary affects its wave shape. Here, the two-scale fractal theory [5, 6] is adopted to figure out the basic property of the unsmooth boundary.

This paper focuses on fractional solitons, which can describe physical phenomena more accurately and reflect their intrinsic properties deeply. Therefore, fractional solitons have attracted increasing attention from both physics and oceanography. For example, shallow water waves [7, 8] can describe the effects of waves in the ocean better than other mathematical models. Shallow water waves are fluctuations in the ocean with wavelengths much greater than the depth of the water (usually more than 25 times), and the dispersion of water waves is one of the key properties in many shallow water wave models, which has obvious memory property. Fractional shallow water equations can describe the propagation of waves in dispersed media and model the hydrodynamics of lakes, estuaries, tidal stalls, and coastal waves, as well as deep-ocean tides. These fractional differential equations have a significant impact on the study of fluid motion in ocean waves and the soliton theory as well; however, a serious bottleneck was hit, that is, the fractional model is extremely difficult to be solved analytically. Therefore, many scholars focused on using different methods to find fractional solitons. For instance, the first integral method [9], the fractional sub-equation method [10], the homotopy perturbation method [11-13] and its modifications, Mohand transform–homotopy perturbation method [14, 15], two-scale transform–-homotopy perturbation method [16], Laplace transform–homotopy perturbation method [17], Li–He's modified homotopy perturbation method [18-20], the tanh-function method [21, 22] and its modification—tanh function expansion method [23]—and modified extended tanh-function method [24,25]. It is worth mentioning that fractional complex transform was first proposed by [26]; it can convert fractional differential equations directly into ordinary differential equations. This method makes a significant contribution to finding exact solutions of fractional differential

equations, and it was applied to gain insights into physical properties of the time-fractional Schrodinger equation [27] and the time-fractional Camassa–Holm equation [28].

In the current article, our concern is to find some exact solutions of the following two non-linear FPDEs *via* the modified extended tanh-function method with the fractional complex transform.

1) The time-fractional KdV–Burgers (KdVB) equation of the form [29

$$\frac{\partial^{\eta} u}{\partial t^{\eta}} + wu\frac{\partial u}{\partial x} + \rho\frac{\partial^2 u}{\partial x^2} + s\frac{\partial^3 u}{\partial x^3} = 0, \tag{1}$$

where w, ρ, and s are real constants and $0 < \eta < 1$. The KdVB equation ($\eta = 1$) is a well-known mathematical model for describing waves on shallow water surfaces; it plays an essential role in both applied mathematics and physics. This equation can be used to describe and analyze a few foremost physical contents related to liquids, dispersion, viscosity, and wave dynamics. For example, it is used to study the spread of waves in elastic tubes filled with viscous fluids [30] and to analyze the propagation of wave-like pores in shallow water [31].

However, with the increasing irregularities and non-linearities in wave motion observed by other scholars, the broader outlook establishment for this model is necessary. Therefore, an increasing number of scholars began to study the extended classical model into a new model with time-fractional derivatives to deal with what the traditional KdVB equation ($\eta = 1$) cannot do.

There have been some common methods to solve fractional KdVB equations. For instance, [32] extended the homotopy perturbation method to solve time-space fractional equations. [29] applied the residual power series method (RPSM) for finding approximate solutions of the time-fractional KdVB equation. [33] solved the time-fractional KdVB equation numerically by the Petrov–Galerkin method.

2) The fractional approximate long water wave equation is given as [34]

$$\begin{aligned} &D_t^{\eta} u - uD_x^{\eta} u - D_x^{\eta} v + aD_x^{2\eta} u = 0, \\ &D_t^{\eta} v - D_x^{\eta}(uv) - aD_x^{2\eta} v = 0, \end{aligned} \tag{2}$$

where $0 < \eta < 1$ and a is a real parameter. As a famous equation to describe the propagation of shallow water waves, it is also important for its amazing fractional solitons, so its exact solutions are much needed to gain insights deeply into the properties of the fractional solitary waves. Up to now, some explicit solutions appeared in the literature, for instance, [34] found three traveling wave solutions by the fractional sub-equation method, [35] obtained an exact solution by using the (G'/G)-method, and [36] also constructed an exact solution by the generalized Kudryashov method. Although much achievement was obtained, its full breathtaking panorama has not been offered yet.

The article is divided into the following sections: First, an introduction is given to the basic knowledge in Section 2; second, in Section 3, the general steps for the solution are given in detail; and finally, the applications and the conclusions are organized in Section 4 and Section 5, respectively.

2 Preliminaries

Regarding the definition of fractional derivatives, many mathematicians started from different perspectives and gave different definitions. Here are some definitions.

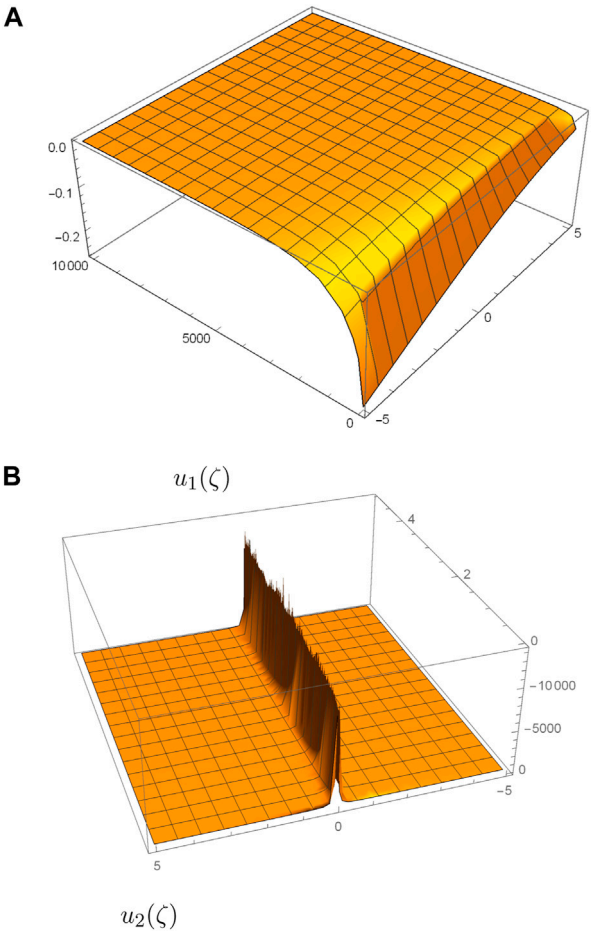

FIGURE 1
Three-dimensional plots of u1(ζ) and u2(ζ) in case 1 for η=0.5, w=1, ρ=1, s=1, l=1, L=1.

1) Caputo fractional derivative [37, 38]:

$$D_x^{\eta}[f(x)] = \frac{1}{\Gamma(n-\eta)}\int_0^x (x-t)^{n-\eta-1}\frac{\mathrm{d}^n f(t)}{\mathrm{d}t^n}\mathrm{d}t. \tag{3}$$

2) Jumarie's modified Riemann–Liouville (R–L) fractional derivative [39]:

$$D_t^{\eta} g(t) = \begin{cases} \frac{1}{\Gamma(1-\eta)}\int_0^t (t-\xi)^{-\eta-1}(g(\xi)-g(0))\mathrm{d}\xi, & \eta < 0, \\ \frac{1}{\Gamma(1-\eta)}\frac{\mathrm{d}}{\mathrm{d}t}\int_0^t (t-\xi)^{-\eta}(g(\xi)-g(0))\mathrm{d}\xi, & 0 < \eta < 1, \\ (g^{(n)}(t))^{(\eta-n)}, & n \le \eta < n+1, n \ge 1, \end{cases} \tag{4}$$

where

$$\Gamma(\eta) = \int_0^{+\infty} x^{\eta-1}e^{-x}dx, \ \eta > 0. \tag{5}$$

(3) He's fractional derivative [20, 40]:

$$D_t^{\eta} f = \frac{1}{\Gamma(n-\eta)}\frac{d^n}{dt^n}\int_{t_o}^t (s-t)^{n-\eta-1}[f_0(s) - f(s)]ds, \tag{6}$$

where $f_0(x)$ is a known function.

4) Two-scale fractal derivative [41, 42]:

$$\frac{\partial w}{\partial t^{\eta}}(t^{\eta}) = \Gamma(1+\eta)\lim_{t-t_0=4t,\triangle\neq 0}\frac{w(t^{\eta})-w(t_0^{\eta})}{(t-t_0)^{\eta}}, \tag{7}$$

where $\triangle t$ is the period required for the motion through a gap of a porous space.

In addition, there are other famous derivatives in the literature such as the Atangana–Baleanu derivative with non-local and non-singular kernel [43, 44]. In this paper, we adopt the Jumarie's modified R–L derivative definition. Some of its important properties are as follows:

$$D_t^{\eta}t^m = \frac{\Gamma(1+m)}{\Gamma(1+m-\eta)}t^{m-\eta}, \tag{8}$$

$$D_t^{\eta}(cg(x)) = cD_t^{\eta}g(x),\ c\ is\ a\ constant, \tag{9}$$

$$D_t^{\eta}\{g(\omega)+f(\omega)\} = D_t^{\eta}g(\omega)+D_t^{\eta}f(w). \tag{10}$$

3 Basic idea of the modified tanh-function expansion method

Considering the following equation

$$P(u, D_t^{\eta}u, D_x^{\gamma}u, D_t^{\eta}D_t^{\eta}u, D_t^{\eta}D_x^{\gamma}u, D_x^{\gamma}D_x^{\gamma}u, \cdots) = 0,\ \ (0<\eta,\gamma<1), \tag{11}$$

where $D_t^{\eta}u, D_x^{\gamma}u, D_t^{\eta}D_t^{\eta}u, D_t^{\eta}D_x^{\gamma}u\cdots$ are the modified R–L fractional derivatives. P presents the polynomial function. To solve this equation, by using the modified tanh-function expansion method, we divide the solution processes into three steps.

Step 1: Using the fractional complex transformation [26, 45]

$$\begin{aligned} &u(x,t) = u(\zeta),\\ &\zeta = \frac{lx^{\gamma}}{\Gamma(\gamma+1)}+\frac{kt^{\eta}}{\Gamma(\eta+1)}, \end{aligned} \tag{12}$$

where l and k are constants and $l,\ k\neq 0$. By the chain rule [45],

$$\begin{aligned} D_t^{\eta}u &= \sigma_t\frac{\partial u(\zeta)}{\mathrm{d}\zeta}D_t^{\eta}\zeta, & D_x^{\eta}u &= \sigma_x\frac{\partial u(\zeta)}{\mathrm{d}\zeta}D_x^{\eta}\zeta,\\ D_t^{2\eta}u &= (\sigma_t)^2\frac{\partial^2 u(\zeta)}{\mathrm{d}\zeta^2}D_t^{2\eta}\zeta, & D_x^{2\eta}u &= (\sigma_x)^2\frac{\partial^2 u(\zeta)}{\mathrm{d}\zeta^2}D_x^{2\eta}\zeta, \end{aligned} \tag{13}$$

where σ_t and σ_x are sigma indices. We take $\sigma_t=\sigma_x=$ L, where L is a constant. Then, substituting Eqs 12 and 13 into Eq. 11, we obtain a non-linear ODE that contains only variable ζ:

$$D(u, u', u''\cdots) = 0, \tag{14}$$

where $u' = \frac{\mathrm{d}u}{\mathrm{d}\zeta}, u'' = \frac{\mathrm{d}^2u}{\mathrm{d}\zeta^2}\cdots$ and D presents the polynomial function.

Step 2: Supposing Eq. 14 has the solution as Eq. 15

$$u(\zeta) = \sum_{i=0}^{n}a_i\Phi^i(\zeta), \tag{15}$$

where Φ is a function about ζ, and it satisfies the Riccati equation

$$\Phi' = \tau+\Phi^2, \tag{16}$$

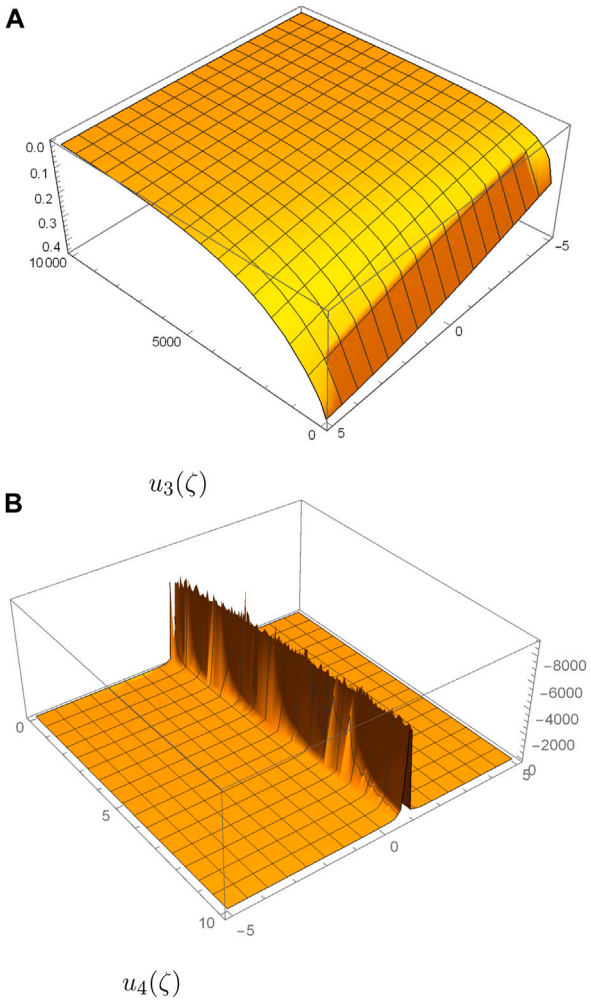

FIGURE 2
Three-dimensional plots of u3(ζ) and u4(ζ) in case 2 with η=0.5, w=1, ρ=1, s=1, l=1, L=1.

τ is a constant, and $a_i(i=0,1,2,\ldots,n)$ are undetermined constant. n is a balancing parameter which is determined by the homogeneous balance method. Φ has the following three types of solutions according to the different values of constant τ

$$\begin{cases} \Phi = -\sqrt{-\tau}\tanh\sqrt{-\tau}\,\zeta, & \tau<0,\\ \Phi = -\sqrt{-\tau}\coth\sqrt{-\tau}\,\zeta, & \tau<0,\\ \Phi = \sqrt{\tau}\tan\sqrt{\tau}\,\zeta, & \tau>0,\\ \Phi = \sqrt{\tau}\cot\sqrt{\tau}\,\zeta, & \tau>0,\\ \Phi = -\frac{1}{\zeta}, & \tau=0. \end{cases} \tag{17}$$

Step 3: Substituting Eq. 15 and 16 into Eq. 14, we obtain an iteration formulation to obtain the polynomial of Φ. Then, we get the algebraic equations about $a_i(i=0,1,2,\ldots,n)$ and l, k, L, and τ by letting the coefficients of each power and constant terms of Φ to be 0. By solving them, we calculate the values of $a_i(i=0,1,2,\ldots,n)$ and l,

k, L, and τ. Thus, the exact solution of Eq. 11 is obtained from Eqs. 15–17.

4 Applications

We choose two different and classical equations named the time-fractional KdVB equation and the fractional approximate long water wave equation for applications. By the calculations of software, we obtain the exact solutions of these two equations and the 3D plots of the obtained solutions perform well.

4.1 Solving process for the fractional Kdv–Burgers model

Taking the fractional complex transform [26, 45]

$$u(x,t) = u(\zeta),\quad \zeta = lx + \frac{kt^{\eta}}{\Gamma(\eta+1)}. \tag{18}$$

Then, the original equation Eq. (1) is converted into a non-linear ODE:

$$kLu' + lwuu' + l^2\rho u'' + l^3 s u''' = 0. \tag{19}$$

Integrating once and the integral constant is equal to zero, Eq. 19 turns into

$$2kLu + lwu^2 + 2l^2\rho u' + 2l^3 s u'' = 0, \tag{20}$$

where n is a balancing parameter. It is used to keep the balance between the term "u''" and the non-linear term "u^2"; we find $n = 2$. Therefore, Eq. 15 changed to

$$u(\zeta) = a_0 + a_1\Phi(\zeta) + a_2\Phi^2(\zeta). \tag{21}$$

Substituting Eqs 16 and 21 into Eq. 20, merging the terms of the same degree of Φ, and vanishing each coefficient of the resulted polynomials to zero, we obtain the equations for the unknowns a_0, a_1, a_2, l, k, L, and τ:

$$\begin{aligned}
&2a_0kL + 2\tau l^2\left(a_1\rho + 2a_2\tau ls\right) + a_0^2lw = 0,\\
&2a_2\tau l^2\rho + a_1\left(kL + 2\tau l^3 s + a_0lw\right) = 0,\\
&a_1l\left(2l\rho + a_1w\right) + 2a_2\left(kL + 8\tau l^3 s + a_0lw\right) = 0,\\
&2a_2l\rho + 2a_1l^2 s + a_1a_2w = 0,\\
&12l^2 s + a_2w = 0.
\end{aligned} \tag{22}$$

Solving the aforementioned set of algebraic equations in the software application, the solutions of the original equation called four generalized hyperbolic function solutions are obtained.

Case 1.

$$a_0 = -\frac{3\rho^2}{25sw},\ a_1 = -\frac{12l\rho}{5w},\ a_2 = -\frac{12l^2 s}{w},\ k = \frac{6l\rho^2}{25Ls},\ \sigma = -\frac{\rho^2}{100l^2 s^2},$$

which produces

$$u_1(\zeta) = -\frac{3\rho^2}{25sw} + \frac{6\rho^2}{25sw}\tanh\frac{\rho}{10ls}\zeta - \frac{3\rho^2}{25ws}\tanh^2\frac{\rho}{10ls}\zeta,\ \tau<0, \tag{23}$$

$$u_2(\zeta) = -\frac{3\rho^2}{25sw} + \frac{6\rho^2}{25sw}\coth\frac{\rho}{10ls}\zeta - \frac{3\rho^2}{25ws}\coth^2\frac{\rho}{10ls}\zeta,\ \tau<0, \tag{24}$$

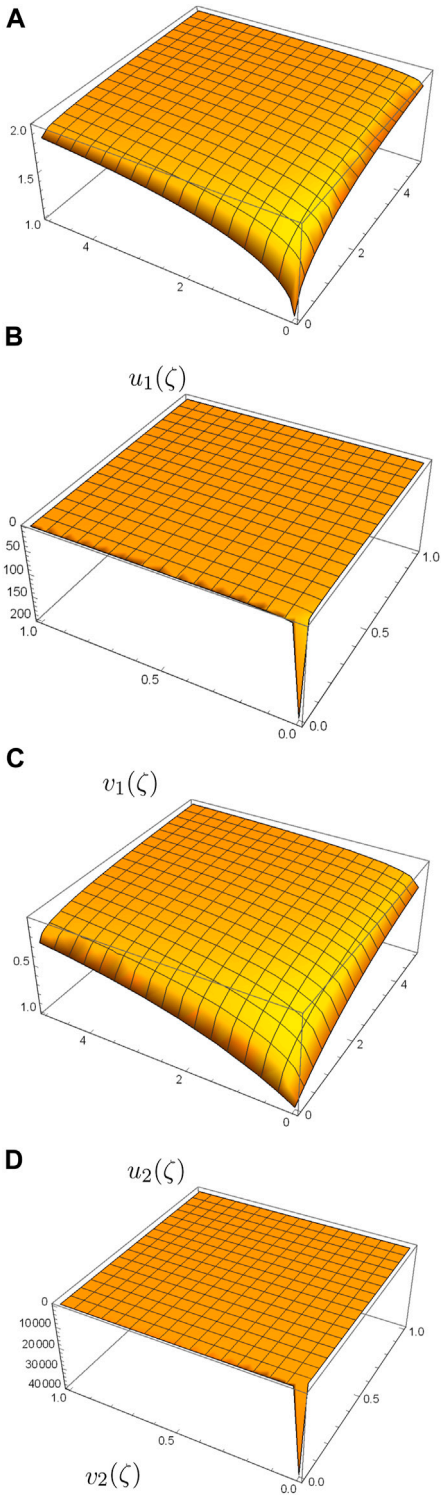

FIGURE 3
Three-dimensional plots of u1(ζ), v1(ζ)and u2(ζ), v2(ζ) of Eq. 2 for η=0.5, a=1, l=1, k=1, L=1.

where $\zeta = lx + \frac{kt^{\eta}}{\Gamma(\eta+1)}$, l is an arbitrary constant, and $l \neq 0$.

Figure 1 is the 3D plots of the obtained solutions of the KdVB equation in case 1 for $\eta = 0.5$, $w = 1$, $\rho = 1$, $s = 1$, $l = 1$, and $L = 1$.

Case 2.

$$a_0 = \frac{9\rho^2}{25sw},\ a_1 = -\frac{12l\rho}{5w},\ a_2 = -\frac{12l^2 s}{w},\ k = -\frac{6l\rho^2}{25Ls},\ \sigma = -\frac{\rho^2}{100l^2 s^2},$$

which produces

$$u_3(\zeta) = \frac{9\rho^2}{25sw} + \frac{6\rho^2}{25sw}\tanh\frac{\rho}{10ls}\zeta - \frac{3\rho^2}{25ws}\tanh^2\frac{\rho}{10ls}\zeta,\ \tau < 0, \quad (25)$$

$$u_4(\zeta) = \frac{9\rho^2}{25sw} + \frac{6\rho^2}{25sw}\coth\frac{\rho}{10ls}\zeta - \frac{3\rho^2}{25ws}\coth^2\frac{\rho}{10ls}\zeta,\ \tau < 0, \quad (26)$$

where $\zeta = lx + \frac{kt^\eta}{\Gamma(\alpha+1)}$, l is an arbitrary constant, and $l \neq 0$.

Figure 2 shows the 3D plots of the obtained solutions of the KdVB equation in case 2 for $\eta = 0.5$, $w = 1$, $\rho = 1$, $s = 1$, $l = 1$, and $L = 1$.

4.2 Solving process for the fractional approximate long water wave equation

Equation 2 is transformed into the following ODEs by applying the fractional complex transformation Li and He [26] and He et al. [45]:

$$\begin{aligned} &u(x,t) = u(\zeta),\ v(x,t) = v(\zeta),\\ &\zeta = \frac{lx^\eta}{\Gamma(\eta+1)} + \frac{kt^\eta}{\Gamma(\eta+1)}. \end{aligned} \quad (27)$$

Then, the following expressions are obtained:

$$\begin{aligned} &kLu' - luLu' - lLv' + al^2L^2u'' = 0,\\ &kLv' - lL(uv)' - al^2L^2v'' = 0. \end{aligned} \quad (28)$$

We perform the same process as mentioned previously and we obtain

$$\begin{aligned} &2ku - lu^2 - 2lv + 2al^2Lu' = 0,\\ &kv - l(uv) - al^2Lv' = 0. \end{aligned} \quad (29)$$

Balancing "v" with "$u^{2\prime\prime}$" in the first equality in Eq. 29 and "v'" with "UV" in the second equality in Eq. 29, we find $n = 1$ and $m = 2$. Therefore, Eq. 15 can be written as

$$\begin{aligned} &u(\zeta) = a_0 + a_1\Phi(\zeta),\\ &v(\zeta) = b_0 + b_1\Phi(\zeta) + b_2\Phi^2(\zeta). \end{aligned} \quad (30)$$

Substituting Eq. 16 and 30 into Eq. 29, merging the terms of the same degree of Φ, and making the coefficient of each item in the result equal to zero, we obtain the equations for the unknowns a_0, a_1, b_0, b_1, b_2, a, k, l, L, and τ

$$\begin{aligned} &2a_0k - a_0{}^2l + 2l(-b_0 + aa_1lL\tau) = 0,\\ &a_0a_1l + b_1l - a_1k = 0,\\ &a_1{}^2 + 2b_2 - 2aa_1lL = 0,\\ &-a_0b_0l + b_0k - ab_1l^2L\tau = 0,\\ &b_1k - a_0b_1l - a_1b_0l - 2ab_2l^2\ L\tau = 0,\\ &b_2k - a_0b_2l - a_1b_1l - ab_1l^2L = 0,\\ &a_1 + 2alL = 0. \end{aligned} \quad (31)$$

Solving the equations, we have

$$a_0 = \frac{k}{l},\ a_1 = -2alL,\ b_0 = \frac{k^2}{l^2},\ b_1 = 0,\ b_2 = -4a^2l^2L^2,\ \tau = -\frac{k^2}{4a^2l^4L^2}. \quad (32)$$

Finally, from Eqs 17, 27, 30 and 32, we obtain the following generalized hyperbolic function solutions of Eq. 2:

$$u_1(\zeta) = \frac{k}{l} + \frac{k}{l}\tanh\frac{k}{2al^2L}\zeta,\ \tau < 0, \quad (33)$$

$$v_1(\zeta) = \frac{k^2}{l^2} - \frac{k^2}{l^2}\tanh^2\frac{k}{2al^2\ L}\zeta,\ \tau < 0, \quad (34)$$

and

$$u_2(\zeta) = \frac{k}{l} + \frac{k}{l}\coth\frac{k}{2al^2L}\zeta,\ \tau < 0, \quad (35)$$

$$v_2(\zeta) = \frac{k^2}{l^2} - \frac{k^2}{l^2}\coth^2\frac{k}{2al^2\ L}\zeta,\ \tau < 0, \quad (36)$$

where $\zeta = \frac{lx^\eta}{\Gamma(\eta+1)} + \frac{kt^\eta}{\Gamma(\eta+1)}$, l and k are arbitrary constants, and $l, k \neq 0$.

Figure 3 shows the 3D plots of the obtained solutions of Eq. 2 for $\eta = 0.5$, $a = 1$, $l = 1$, $k = 1$, and $L = 1$.

5 Conclusion

In this paper, some attractive properties of the fractional solitons are elucidated through two examples, and this paper proposes a total new concept on the fractional soliton theory and gives a rigorous mathematical tool to gain deep insights into the physical properties of the fractional solitary solutions, which are practically applicable in many fields. Additionally, this paper also reveals the simplicity, comprehensibility, and effectiveness of the modified extended tanh-function method.

We anticipate that this paper offers a flood of opportunities for finding new physical phenomena of the fractional solitons, and this paper can be used as a good paradigm for future research.

Data availability statement

The original contributions presented in the study are included in the article/supplementary material; further inquiries can be directed to the corresponding author.

Author contributions

All authors listed have made a substantial, direct, and intellectual contribution to the work and approved it for publication.

Funding

This work is supported by the Shaanxi Provincial Education Department (No. 21JK0735) and the National Natural Science Foundation of China (No. 12201485).

Conflict of interest

The authors declare that the research was conducted in the absence of any commercial or financial relationships that could be construed as a potential conflict of interest.

Publisher's note

References

1. Tian Y, Liu J. Direct algebraic method for solving fractional fokas equation. *Therm Sci* (2021) 25:2235–44. doi:10.2298/TSCI200306111T

2. Sun HG, Chen W, Wei H, Chen YQ. A comparative study of constant-order and variable-order fractional models in characterizing memory property of systems. *Eur Phys J Spec Top* (2011) 193:185–92. doi:10.1140/epjst/e2011-01390-6

3. He JH, Hou WF, He CH, Saeed T, Hayat T. Variational approach to fractal solitary waves. *Fractals* (2021) 29:1–5. doi:10.1142/S0218348X21501991

4. He JH, Na Q, He CH. Solitary waves travelling along an unsmooth boundary. *Results Phys* (2021) 24:104104. doi:10.1016/j.rinp.2021.104104

5. Qian MY, He JH. Two-scale thermal science for modern life–making the impossible possible. *Therm Sci* (2022) 26:2409–12. doi:10.2298/TSCI2203409Q

6. Anjum N, Ain QT, Li XX. Two-scale mathematical model for tsunami wave. *GEM - Int J Geomathematics* (2021) 12:10. doi:10.1007/s13137-021-00177-z

7. Çerdik YH. New analytic solutions of the space-time fractional broer–kaup and approximate long water wave equations. *J Ocean Eng Sci* (2018) 3:295–302. doi:10.1016/j.joes.2018.10.004

8. Ling WW, Wu PX. A fractal variational theory of the broer-kaup system in shallow water waves. *Therm Sci* (2021) 25:2051–6. doi:10.2298/TSCI180510087L

9. Lu B. The first integral method for some time fractional differential equations. *J Math Anal Appl* (2012) 395:684–93. doi:10.1016/j.jmaa.2012.05.066

10. Alzaidy JF. The fractional sub-equation method and exact analytical solutions for some nonlinear fractional pdes. *Am J Math Anal* (2013) 1:14–9. doi:10.12691/ajma-1-1-3

11. He JH. Homotopy perturbation technique. *Comp Methods Appl Mech Eng* (1999) 178:257–62. doi:10.1016/S0045-7825(99)00018-3

12. He JH. A coupling method of a homotopy technique and a perturbation technique for non-linear problems. *Int J Non-Linear Mech* (2000) 35:37–43. doi:10.1016/S0020-7462(98)00085-7

13. He JH, El-Dib YO. Homotopy perturbation method with three expansions. *J Math Chem* (2021) 59:1139–50. doi:10.1007/s10910-021-01237-3

14. Nadeem M, He JH, Islam A. The homotopy perturbation method for fractional differential equations: Part 1 mohand transform. *Int J Numer Methods Heat Fluid Flow* (2021) 31:3490–504. doi:10.1108/HFF-11-2020-0703

15. Fang JH, Nadeem M, Habib M, Karim S, Wahash H. A new iterative method for the approximate solution of klein-gordon and sine-gordon equations. *J Funct Spaces* (2022) 1:1–9. doi:10.1155/2022/5365810

16. Nadeem M, He JH. The homotopy perturbation method for fractional differential equations: Part 2, two-scale transform. *Int J Numer Methods Heat Fluid Flow* (2022) 32:559–67. doi:10.1108/HFF-01-2021-0030

17. Filobello-Nino U, Vazquez-Leal H, Khan Y, Perez-Sesma A, Diaz-Sanchez A, Jimenez-Fernandez VM, et al. Laplace transform-homotopy perturbation method as a powerful tool to solve nonlinear problems with boundary conditions defined on finite intervals. *Comput Appl Math* (2015) 34:1–16. doi:10.1007/s40314-013-0073-z

18. Li XX, He CH. Homotopy perturbation method coupled with the enhanced perturbation method. *J Low Frequency Noise, Vibration Active Control* (2019) 38:1399–403. doi:10.1177/1461348418800554

19. Anjum N, He JH, Ain QT, Tian D. Li-he's modified homotopy perturbation method for doubly-clamped electrically actuated microbeams-based microelectromechanical system. *Facta Universitatis, Ser Mech Eng* (2021) 19:601–12. doi:10.22190/FUME210112025A

20. He JH, El-Dib YO. The enhanced homotopy perturbation method for axial vibration of strings. *Facta Universitatis, Ser Mech Eng* (2021) 19:735–50. doi:10.22190/FUME210125033H

21. Duffy BR, Parkes EJ. Travelling solitary wave solutions to a seventh-order generalized kdv equation. *Phys Lett A* (1996) 214:271–2. doi:10.1016/0375-9601(96)00184-3

22. Parkes EJ, Duffy BR. Travelling solitary wave solutions to a compound kdv-burgers equation. *Phys Lett A* (1997) 229:217–20. doi:10.1016/S0375-9601(97)00193-X

23. Fan EG. Extended tanh-function method and its applications to nonlinear equations. *Phys Lett A* (2000) 277:212–8. doi:10.1016/S0375-9601(00)00725-8

24. Elwakil S, El-Labany S, Zahran M, Sabry R. Modified extended tanh-function method for solving nonlinear partial differential equations. *Phys Lett A* (2002) 299:179–88. doi:10.1016/S0375-9601(02)00669-2

25. Elwakil S, El-Labany S, Zahran M, Sabry R. Modified extended tanh-function method and its applications to nonlinear equations. *Appl Math Comput* (2005) 161:403–12. doi:10.1016/j.amc.2003.12.035

26. Li ZB, He JH. Fractional complex transform for fractional differential equations. *Math Comput Appl* (2010) 15:970–3. doi:10.3390/mca15050970

27. Ain QT, He JH, Anjum N, Ali M. The fractional complex transform: A novel approach to the time-fractional schrodinger equation. *Fractals* (2020) 28:2050141. doi:10.1142/S0218348X20501418

28. Anjum N, Ain QT. Application of he's fractional derivative and fractional complex transform for time fractional camassa-holm equation. *Therm Sci* (2020) 24:3023–30. doi:10.2298/TSCI190930450A

29. Senol M, Tasbozan O, Kurt A. Numerical solutions of fractional burgers' type equations with conformable derivative. *Chin J Phys* (2019) 58:75–84. doi:10.1016/j.cjph.2019.01.001

30. Johnson RS. A non-linear equation incorporating damping and dispersion. *J Fluid Mech* (1970) 42:49–60. doi:10.1017/S0022112070001064

31. Benney DJ. Long waves on liquid films. *J Math Phys* (1966) 45:150–5. doi:10.1002/sapm1966451150

32. Wang Q. Homotopy perturbation method for fractional kdv-burgers equation. *Chaos, Solitons & Fractals* (2008) 35:843–50. doi:10.1016/j.chaos.2006.05.074

33. Gupta AK, Ray SS. On the solution of time-fractional KdV–Burgers equation using Petrov–Galerkin method for propagation of long wave in shallow water. *Chaos, Solitons & Fractals* (2018) 116:376–80. doi:10.1016/j.chaos.2018.09.046

34. Yan LM. New travelling wave solutions for coupled fractional variant Boussinesq equation and approximate long water wave equation. *Int J Numer Methods Heat Fluid Flow* (2015) 25:33–40. doi:10.1108/hff-04-2013-0126

35. Guner O, Atik H, Kayyrzhanovich AA. New exact solution for space-time fractional differential equations via g′/g-expansion method. *Optik - Int J Light Electron Opt* (2017) 130:696–701. doi:10.1016/j.ijleo.2016.10.116

36. Kaplan M, Akbulut A. Application of two different algorithms to the approximate long water wave equation with conformable fractional derivative. *Arab J Basic Appl Sci* (2018) 25:77–84. doi:10.1080/25765299.2018.1449348

37. Yang XJ. *Advanced local fractional calculus and its applications*. New York: World Science Publisher (2012).

38. Habib S, Batool A, Islam A, Nadeem M, He JH. Study of nonlinear hirota-satsuma coupled kdv and coupled mkdv system with time fractional derivative. *Fractals* (2021) 29:2150108. doi:10.1142/S0218348X21501085

39. Jumarie G. Modified riemann-liouville derivative and fractional Taylor series of nondifferentiable functions further results. *Comput Math Appl* (2006) 51:1367–76. doi:10.1016/j.camwa.2006.02.001

40. He JH. A tutorial review on fractal spacetime and fractional calculus. *Int J Theor Phys* (2014) 53:3698–718. doi:10.1007/s10773-014-2123-8

41. He JH. Fractal calculus and its geometrical explanation. *Results Phys* (2018) 10:272–6. doi:10.1016/j.rinp.2018.06.011

42. Ain QT, He JH. On two-scale dimension and its applications. *Therm Sci* (2019) 23:1707–12. doi:10.2298/TSCI190408138A

43. Atangana A, Baleanu D. New fractional derivatives with nonlocal and non-singular kernel: Theory and application to heat transfer model. *Therm Sci* (2016) 20:763–9. doi:10.2298/TSCI160111018A

44. Ain QT, Sathiyaraj T, Nadeem M, Mwanakatwe PK, Kandege Mwanakatwe P. Abc fractional derivative for the alcohol drinking model using two-scale fractal dimension. *Complexity* (2022) 8531858:1–11. doi:10.1155/2022/8531858

45. He JH, Elagan S, Li Z. Geometrical explanation of the fractional complex transform and derivative chain rule for fractional calculus. *Phys Lett A* (2012) 376:257–9. doi:10.1016/j.physleta.2011.11.030

frontiers | Frontiers in Physics

TYPE Original Research
PUBLISHED 17 April 2023
DOI 10.3389/fphy.2023.1167797

OPEN ACCESS

EDITED BY
Ji-Huan He,
Soochow University, China

REVIEWED BY
Muhammad Nadeem,
Qujing Normal University, China
Naveed Anjum,
Government College University
Faisalabad, Pakistan
Guangqing Feng,
Henan Polytechnic University, China

*CORRESPONDENCE
Rania Saadeh,
rsaadeh@zu.edu.jo,
raniaraed2011@gmail.com

SPECIALTY SECTION
This article was submitted to Interdisciplinary Physics, a section of the journal Frontiers in Physics

RECEIVED 16 February 2023
ACCEPTED 23 March 2023
PUBLISHED 17 April 2023

CITATION
El-Ajou A, Al-ghananeem H, Saadeh R, Qazza A and Oqielat MN (2023), A modern analytic method to solve singular and non-singular linear and non-linear differential equations.
Front. Phys. 11:1167797.
doi: 10.3389/fphy.2023.1167797

A modern analytic method to solve singular and non-singular linear and non-linear differential equations

Ahmad El-Ajou[1], Haneen Al-ghananeem[1], Rania Saadeh[2]*, Ahmad Qazza[2] and Moa'ath N. Oqielat[1]

[1]Department of Mathematics, Faculty of Science, Al Balqa Applied University, Salt, Jordan, [2]Department of Mathematics, Faculty of Science, Zarqa University, Zarqa, Jordan

This article circumvents the Laplace transform to provide an analytical solution in a power series form for singular, non-singular, linear, and non-linear ordinary differential equations. It introduces a new analytical approach, the Laplace residual power series, which provides a powerful tool for obtaining accurate analytical and numerical solutions to these equations. It demonstrates the new approach's effectiveness, accuracy, and applicability in several ordinary differential equations problem. The proposed technique shows the possibility of finding exact solutions when a pattern to the series solution obtained exists; otherwise, only rough estimates can be given. To ensure the accuracy of the generated results, we use three types of errors: actual, relative, and residual error. We compare our results with exact solutions to the problems discussed. We conclude that the current method is simple, easy, and effective in solving non-linear differential equations, considering that the obtained approximate series solutions are in closed form for the actual results. Finally, we would like to point out that both symbolic and numerical quantities are calculated using Mathematica software.

KEYWORDS

ordinary differential equations, Laplace transforms, power series, approximate solutions, laurent series

1 Introduction

A differential equation or a system of differential equations, along with proper boundary and initial conditions (ICs), is one of the most common outputs when mathematical modeling describes physical, biological, or chemical phenomena. Finding ordinary or partial differential equations and analyzing their solutions are at the heart of applied mathematics [1].

Since ancient times, differential equations have attracted the interest of researchers and scientists from two sides. The first is how to use them to express phenomena and issues that interest them in their specializations and research. On the other hand, there is the question of how to solve these equations. There are a limited number of differential equations, especially linear ones, whose solutions can be determined using the well-known traditional methods based on finite and simple algebraic operations. In contrast, there are many kinds of differential equations that still require the search for simple and accurate solutions. For this reason, the interest of mathematicians in previous decades was and is still in the investigation

for analytical and sometimes numerical methods to solve these forms of differential equations.

Many analytical, numerical, and numero-analytical techniques have been proposed previously and recently to provide solutions for differential equations with initial or boundary conditions, such as the Laplace and Fourier transforms method [2], the Adomian decomposition method [3–5], the variational iteration method [6–8], the homotopy perturbation method [9–11], the homotopy analysis method [12, 13], the differential transformation method [14–16], the finite difference method [17], the predictor–corrector method [18, 19], the first integral method [20, 21], the Adams–Bashforth Molten method [22], the new iterative method [23, 24], the Crank–Nicolson method [25, 26], the reproducing kernel method [27, 28], the Laplace Adomian decomposition method [11, 29, 30], the He–Laplace method [31–33], and others [34–36].

Recently, Eriqat et al. [37] presented a new hybrid method in which they combined the Laplace transform (LT) method with the residual power series (PS) method to establish series solutions of the pantograph equation. This method is called the LRPS method, and it simulates the residual PS method but with a different construction and view. It uses the limit concept instead of the concept of the derivative as in the residual PS method. The LRPS method uses the LT to transfer the given differential equation to a new algebraic equation in a new space. The obtained algebraic equation is solved by assuming that it is a solution that has a Laurent series (LS) form. The values of the coefficients of the LS are determined by utilizing the limit at infinity. Then, the inverse LT is used to transfer the LS, which is the solution of the algebraic equation in the Laplace space, to the initial space. Thus, we have obtained the solution to the original problem in the form of PS.

Indeed, the LRPS method is similar to the He–Laplace method's [31–33] idea of searching for the solution of differential equations in Laplace space. The He–Laplace technique uses the variational iteration method or homotopy perturbation method to solve the just-transformed Laplace space. In contrast, the LRPS method uses the PS method to solve that equation using the Laurent series instead of the Taylor series. In addition, the LRPS method is just an easy and fast technique for finding the PS solution coefficients of the differential equations.

The LRPS method has won the admiration and interest of many researchers due to its ease, speed, and efficiency in arriving at exact or accurate approximate solutions to many equations. In addition, the LT was employed in dealing with non-linear problems because it is known that the LT deals only with some categories of linear equations. In 2021, El-Ajou [38] adapted the LRPS method to establish solitary solutions of non-linear time-fractional dispersive partial differential equations and to introduce a vector series solution of some types of hyperbolic system of Caputo time-fractional partial differential equations with variable coefficients [39]. Recently, the LRPS method was used for solving time-fractional Navier–Stokes equations [40], fuzzy quadratic Riccati DEs [41], Lane–Emden equations of fractional order [42], a system of fractional initial value problems (IVPs) [43], autonomous n-dimensional fractional non-linear systems [44], and others [45–49].

Despite the extensive publication of research dealing with the new method, all works dealt with specific problems devoid of complexity and generality. Therefore, we aim in this manuscript, first, to employ the LRPS method to provide exact or accurate approximate analytic series solutions to linear ordinary differential equations (ODEs) in their general form, whether their coefficients are constants or analytical functions, which have the following formula:

$$\frac{d^n y}{dt^n} = L_t\left[y(t)\right] + g(t), t \geq 0. \tag{1.1}$$

Subject to the ICs,

$$y(0) = y_0, y'(0) = y_1, \ldots, y^{(n-1)}(0) = y_{n-1}, \tag{1.2}$$

where L_t is a linear differential operator of order $(n-1)$ with coefficients being analytic functions. This general equation is difficult to solve by the direct PS method. Herein lays the importance and novelty of the aim of this research.

Since in our world, most events are essentially non-linear and modeled by non-linear equations, the study of non-linear issues is critical in mathematics and physics, engineering, economics, and other disciplines. Solving non-linear problems is difficult, and getting an analytical approximation of a given problem is often more complicated than getting a numerical one. Therefore, the second aim of this paper is to establish analytic approximate solutions to the general form of non-linear ODEs, which have the following form using the proposed method (LRPS method):

$$\frac{d^n y}{dt^n} = f\left(t, y(t), \frac{dy}{dt}, \frac{d^2 y}{dt^2}, \ldots, \frac{d^{n-1} y}{dt^{n-1}}\right), t \geq 0. \tag{1.3}$$

Subject to the ICs,

$$y(0) = y_0, \; y'(0) = y_1, \ldots, y^{(n-1)}(0) = y_{n-1}, \tag{1.4}$$

where f is an analytic function on $[0, \infty)$.

The third objective of this article is to provide a series solution to the singular ODEs, whether linear or non-linear. This type of equation is of great interest to researchers in providing analytical solutions to it, as it appears in the models of many natural phenomena, as well as the difficulty of providing solutions to it.

To determine the efficiency and applicability of the method, we test for three types of errors: exact error, relative error, and residual error. We present the numerical results of the resulting solutions through prepared and organized tables. In addition, we sketch the obtained approximate solution by the proposed method along with the exact solution if we can obtain it to make the comparison on the one hand and to determine the period of convergence to solve the series on the other hand.

2 Basic facts of the LT and PS

In this section, we overview essential facts about the LT and the PS, along with some properties that are needed in this article.

Definition 2.1: [50]). We assume that $y(t)$ is a continuous function defined for $t \geq 0$ and let $s \in I \subseteq \mathbb{R}$. Then, the LT of $y(t)$ is the function Y(s), denoted and defined as follows:

$$Y(s) = \mathcal{L}\left[y(t)\right](s) = \int_0^\infty e^{-st} y(t) dt, \tag{2.1}$$

where the improper integral is the convergence on an interval of s, which represents the domain of $Y(s)$.

Also, the inverse LT of a function $Y(s), s \in I$ is the function $y(t), t \geq 0$ that is denoted and defined as

$$y(t) = \mathcal{L}^{-1}[Y(s)](t) = \int_{c-i\infty}^{c+i\infty} e^{st} Y(s) ds, c = \mathrm{Re}(s) > c_0, \tag{2.2}$$

where c_0 lies in the right-half plane of the absolute convergence of the Laplace integral.

Lemma 2.1: [50]). Suppose that $y(t)$ and $x(t)$ are both continuous functions defined on $[0, \infty)$, $Y(s) = \mathcal{L}[y(t)]$, $X(s) = \mathcal{L}[x(t)]$, and η, λ are constants. Then, we have the following properties:

1) $\mathcal{L}[e^{\lambda t} y(t)] = Y(s - \lambda)$
2) $\mathcal{L}[t^n y(t)] = (-1)^n \frac{d^n}{ds^n} Y(s)$
3) $\mathcal{L}[y(\lambda t)] = \frac{1}{\lambda} Y(\frac{s}{\lambda}), \lambda > 0$
4) $\mathcal{L}^{-1}[\eta Y(s) + \lambda X(s)]$
$= \eta \mathcal{L}^{-1}[Y(s)] + \lambda \mathcal{L}^{-1}[X(s)] = \eta\, y(t) + \lambda x(t)$

5) $\lim_{s \to \infty} sY(s) = y(0)$
6) $\mathcal{L}[y^{(n)}(t)] = s^n \mathcal{L}[y] - \sum_{k=0}^{n-1} s^{n-k-1} y^{(k)}(0)$

Definition 2.2: [51]). A series that has the representation

$$\sum_{n=-\infty}^{\infty} c_n (s - s_0)^n = \sum_{n=1}^{\infty} \frac{c_{-n}}{(s - s_0)^n} + \sum_{n=0}^{\infty} c_n (s - s_0)^n \tag{2.3}$$

is called the LS about $s = s_0$, where s is the variable and c_n's are the coefficients of the series. The series $\sum_{n=0}^{\infty} c_n (s - s_0)^n$ is known as the analytic or regular part of the LS, while $\sum_{n=1}^{\infty} \frac{c_{-n}}{(s-s_0)^n}$ is known as the singular or the principal part of the LS.

Theorem 2.1: [50]). Let $y(t)$ be an analytic function defined on the domain D: $\xi_1 < |t - t_0| < \xi_2$. Then, $y(t)$ can be expanded as a PS as follows:

$$y(t) = \sum_{n=0}^{\infty} c_n (t - t_0)^n, \tag{2.4}$$

which is valid for $\xi_1 < |t - t_0| < \xi_2$.

Theorem 2.2: If $Y(s) = \mathcal{L}[y(t)]$ has an LS representation about $s = 0$,

$$Y(s) = \frac{c_0}{s} + \sum_{n=1}^{\infty} \frac{c_n}{s^{n+1}}, s > 0, \tag{2.5}$$

then $c_n = y^{(n)}(0), n = 0, 1, 2, \ldots$.

Proof. Suppose that $Y(s)$ can be represented by the LS expansion as in Eq. 2.5. So,

$$sY(s) = c_0 + \sum_{n=1}^{\infty} \frac{c_n}{s^n}, s > 0. \tag{2.6}$$

According to part (5) of Lemma 2.1, we have $c_0 = y(0)$.

Multiplying Eq. 2.6 by s gives the following expansion:

$$s^2 Y(s) - y(0)s = c_1 + \sum_{n=2}^{\infty} \frac{c_n}{s^n}, s > 0. \tag{2.7}$$

Using part (5) of Lemma 2.1, it is obvious that

$$\begin{aligned} c_1 &= \lim_{s \to \infty} \left(c_1 + \sum_{n=2}^{\infty} \frac{c_n}{s^n} \right) = \lim_{s \to \infty} \left(s^2 Y(s) - sy(0) \right) \\ &= \lim_{s \to \infty} s\left(sY(s) - y(0) \right) = \lim_{s \to \infty} s\left(\mathcal{L}[y'(t)] \right) = y'(0). \end{aligned}$$

Similarly, multiplying Eq. 2.7 by s gives the following expansion:

$$s\left(s^2 Y(s) - y(0)s - y'(0) \right) = c_2 + \sum_{n=3}^{\infty} \frac{c_n}{s^n}, s > 0. \tag{2.8}$$

Again, by parts (5) and (6) of Lemma 2.1, we have

$$\begin{aligned} c_2 &= \lim_{s \to \infty} \left(c_2 + \sum_{n=3}^{\infty} \frac{c_n}{s^n} \right) = \lim_{s \to \infty} s\left(s^2 Y(s) - sy(0) - y'(0) \right) \\ &= \lim_{s \to \infty} s\left(\mathcal{L}[y''(t)] \right) = y''(0). \end{aligned}$$

Now, we can find out the general formula for the coefficient c_n. However, we can get it by multiplying Eq. 2.6 by s^{n+1} and taking the limit of the resulting equation as $s \to \infty$; then, we find that $c_n = y^{(n)}(0), n = 0, 1, 2, \ldots$. Thus, the proof is now complete.

Theorem 2.3: assume that $\mathcal{L}[y(t)] = Y(s)$ can be represented as in Eq. 2.6. If $|s\,\mathcal{L}[y^{(n)}(t)]| \leq K$, on $0 < s \leq d$, then the reminder $R_n(s)$ of the expansion of the LS appearing in Theorem 2.2 will satisfy the relation

$$|R_n(s)| \leq \frac{K}{s^{n+2}}, 0 < s \leq d\,. \tag{2.9}$$

Proof.

First, we assume that for $r = 0, 1, 2, \ldots, n+1$, $\mathcal{L}[y^{(r)}(t)](s)$ is defined on $0 < s \leq d$. Also, we assume the following:

$$\left| s\,\mathcal{L}\left[\left(y^{(n+1)} \right)(t) \right] \right| \leq K, 0 < s \leq d\,. \tag{2.10}$$

From the definition of the reminder $R_n(s) = Y(s) - \sum_{i=0}^{n} \frac{y^{(i)}(0)}{s^{i+1}}$, one can acquire

$$\begin{aligned} s^{n+2} R_n(s) &= s^{n+2} Y(s) - \sum_{m=0}^{n} s^{(n+1-m)} y^{(m)}(0) \\ &= s\left(s^{n+1} Y(s) - \sum_{i=0}^{n} s^{(n-m)} y^{(m)}(0) \right) = s\,\mathcal{L}\left[y^{(n+1)}(t) \right]. \end{aligned} \tag{2.11}$$

Eq. 2.10 and Eq. 2.11 lead to the conclusion that $|s^{(n+1)\alpha+1} R_n(s)| \leq K$. Thus,

$$-K \leq s^{n+2} R_n(s) \leq K, \; 0 < s \leq d\,. \tag{2.12}$$

The inequality $|R_n(s)| \leq \frac{K}{s^{n+2}}$ can be discovered by reformulating Eq. 2.12, and so, we got the result.

3 Constructing series solutions to ODEs

In this section, we first use the LRPS method to solve linear ODEs in preparation for solving non-linear ODEs. What is worth noting is the possibility of solving non-linear ODEs, which cannot be carried out using the traditional LT method. We will use the construction that we will get to solve non-linear ODEs when solving singular ODEs, whether linear or non-linear, and this is what we will see in Section 3.3.

3.1 LRPS method for solving linear ODEs

In this section, we demonstrate the steps of the LRPS method for solving linear ODEs. The basic idea of the proposed method is to apply the LT to the linear ODEs and then use the LRPS approach to construct a series solution, in LS form, to the transformed equation. Then, we transform the obtained solution into the required solution in the original space.

To illustrate the idea of the LRPS method in constructing series solutions to the linear ODEs, we consider problems (1.1) and (1.2), considering that L_t is a linear differential operator given by

$$L_t = a_{n-1}(t)\frac{\mathrm{d}^{n-1}}{\mathrm{d}t^{n-1}} + \ldots + a_1(t)\frac{\mathrm{d}}{\mathrm{d}t} + a_0(t), \tag{3.1}$$

where $a_0(t), a_1(t), ..., a_{n-1}(t)$ and $g(t)$ are arbitrary analytic functions that depend only on t, $y(t)$ is the unknown function of the independent variables t, and I is an open interval.

To generate the LRPS solution of the IVP (1.1) and (1.2), first, we apply the LT to both sides of Eq. 1.1 to obtain

$$\mathcal{L}\left[y^{(n)}(t)\right] = \mathcal{L}\left[L_t[y(t)]\right] + \mathcal{L}[g(t)], t \in I. \tag{3.2}$$

Using ICs (1.2) and some properties of the LT, Eq. 3.2 becomes

$$Y(s) = \sum_{i=0}^{n-1}\frac{y_i}{s^{i+1}} + \frac{1}{s^n}\mathcal{L}\left[L_t\left[\mathcal{L}^{-1}[Y(s)]\right]\right] + \frac{G(s)}{s^n}, s > 0. \tag{3.3}$$

We assume that $Y(s)$ in Eq. 3.3 has an expansion in the LS form as

$$Y(s) = \sum_{i=0}^{\infty}\frac{c_i}{s^{1+i}}, s > 0. \tag{3.4}$$

Depending on Theorem 2.3 and the given conditions in Eq. 1.2, the first n-coefficients of the expansion (3.4) can be determined, so it can be rewritten as follows:

$$Y(s) = \sum_{i=0}^{n-1}\frac{y_i}{s^{i+1}} + \sum_{i=n}^{\infty}\frac{c_i}{s^{1+i}}, s > 0. \tag{3.5}$$

The kth-truncated series of $Y(s)$ is given by

$$Y_k(s) = \sum_{i=0}^{n-1}\frac{y_i}{s^{i+1}} + \sum_{i=n}^{k}\frac{c_i}{s^{1+i}}, s > 0. \tag{3.6}$$

Thus, one can conclude

$$Y_n(s) = \sum_{i=0}^{n-1}\frac{y_i}{s^{i+1}} + \frac{c_n}{s^{1+n}}, s > 0. \tag{3.7}$$

To find the values of the unknown coefficients in series (3.7), we define the Laplace residual function (LRF) of Eq. 3.3 as

$$LRes(s) = Y(s) - \sum_{i=0}^{n-1}\frac{y_i}{s^{i+1}} - \frac{1}{s^n}\mathcal{L}\left[L_t\left[\mathcal{L}^{-1}[Y(s)]\right]\right] - \frac{G(s)}{s^n}, s > 0 \tag{3.8}$$

and the kth LRF as

$$LRes_k(s) = Y_k(s) - \sum_{i=0}^{n-1}\frac{y_i}{s^{i+1}} - \frac{1}{s^n}\mathcal{L}\left[L_t\left[\mathcal{L}^{-1}[Y_k(s)]\right]\right] - \frac{G(s)}{s^n}, s > 0. \tag{3.9}$$

It is clear that $Lim_{k\to\infty}LRes_k(s) = LRes(s)$, $LRes(s) = 0$, and thus, $s^k LRes(s) = 0$ for $s > 0$ and $k = 0, 1, 2, 3, \ldots$. Therefore, $Lim_{s\to\infty}(s^k LRes(s)) = 0$. Moreover,

$$Lim_{s\to\infty}\left(s^{k+1}LRes(s)\right) = Lim_{s\to\infty}\left(s^{k+1}LRes_k(s)\right) = 0, k = 1, 2, 3, \ldots \tag{3.10}$$

Substituting the first nth-truncated series in Eq. 3.7 into the nth LRF to obtain

$$LRes_n(s) = \frac{c_n}{s^{1+n}} - \frac{1}{s^n}\mathcal{L}\left[L_t\left[\mathcal{L}^{-1}\left[\sum_{i=0}^{n-1}\frac{y_i}{s^{i+1}} + \frac{c_n}{s^{1+n}}\right]\right]\right] - \frac{G(s)}{s^n}, s > 0. \tag{3.11}$$

Running the inverse LT in Eq. 3.11, we get

$$LRes_n(s) = \frac{c_n}{s^{1+n}} - \frac{1}{s^n}\mathcal{L}\left[L_t\left[\sum_{i=0}^{n-1}\frac{y_i}{i!}t^i + \frac{c_n}{n!}t^n\right]\right] - \frac{G(s)}{s^n}, s > 0. \tag{3.12}$$

Since the coefficients of the linear operator in Eq. 3.1 are analytic functions, they can be expressed as

$$a_r(t) = \sum_{j=0}^{\infty}\lambda_{rj}t^j, r = 0, 1, \ldots, n-1, \tag{3.13}$$

where

$$\lambda_{rj} = \frac{a_r^{(j)}(0)}{j!}, r = 0, 1, \ldots, n-1, j = 0, 1, 2, \ldots. \tag{3.14}$$

So, the linear operator L_t in Eq. 3.1 can be expressed as

$$L_t = \sum_{r=0}^{n-1}\left(\sum_{j=0}^{\infty}\lambda_{rj}t^j\right)\frac{d^r}{dt^r}. \tag{3.15}$$

Running the operator L_t on Eq. 3.12 according to its new form in Eq. 3.15, we get

$$LRes_n(s) = \frac{c_n}{s^{1+n}} - \frac{1}{s^n}\mathcal{L}\left[\sum_{r=0}^{n-1}\sum_{j=0}^{\infty}\left(\frac{c_n\lambda_{rj}}{(n-r)!}t^{n+j-r} + \sum_{i=r}^{n-1}\frac{\lambda_{rj}y_i}{(i-r)!}t^{i+j-r}\right)\right] - \frac{G(s)}{s^n}. \tag{3.16}$$

Finally, we run the LT in Eq. 3.16 to obtain the required form of the nth LRF:

$$LRes_n(s) = \frac{c_n}{s^{1+n}} - \frac{G(s)}{s^n} - \frac{1}{s^n}\sum_{r=0}^{n-1}\sum_{j=0}^{\infty}\left(\frac{c_n\lambda_{rj}}{(n-r)!}\frac{(n+j-r)!}{s^{1+n+j-r}} + \sum_{i=r}^{n-1}\frac{\lambda_{rj}y_i}{(i-r)!}\frac{(i+j-r)!}{s^{1+j+i-r}}\right). \tag{3.17}$$

Now, multiplying Eq. 3.17 by s^{n+1}, we get the following function:

$$s^{n+1}LRes_n(s) = c_n - sG(s) - \sum_{r=0}^{n-1}\sum_{j=0}^{\infty}\frac{c_n\lambda_{rj}}{(n-r)!}\frac{(n+j-r)!}{s^{n+j-r}} - \sum_{r=0}^{n-1}\sum_{j=0}^{\infty}\sum_{i=r}^{n-1}\frac{\lambda_{rj}y_i}{(i-r)!}\frac{(i+j-r)!}{s^{j+i-r}}. \tag{3.18}$$

Taking the limit at infinity to Eq. 3.18, according to Eq. 3.10, we get

$$c_n = g(0) + \sum_{r=0}^{n-1}\lambda_{r0}y_r. \tag{3.19}$$

Thus, the first approximation of the solution of Eq. 3.3 is

$$Y_n(s) = \frac{y_0}{s} + \frac{y_1}{s^2} + \frac{y_2}{s^3} + \ldots + \frac{y_{n-1}}{s^n} + \frac{1}{s^{n+1}}\left(g(0) + \sum_{r=0}^{n-1}\lambda_{r0}y_r\right). \tag{3.20}$$

Following that, one can find the value of the coefficient c_{n+1}; to do that, we substitute the $(n+1)$th-truncated series, $Y_{n+1}(s) = \frac{y_0}{s} + \frac{y_1}{s^2} + \frac{y_2}{s^3} + \ldots + \frac{y_{n-1}}{s^n} + \frac{c_n}{s^{n+1}} + \frac{c_{n+1}}{s^{n+2}}$, into the $(n+1)$th LRF to get the following:

$$LRes_{n+1}(s) = \frac{c_n}{s^{n+1}} + \frac{c_{n+1}}{s^{n+2}} - \frac{1}{s^n}\mathcal{L}\left[L_t\left[\mathcal{L}^{-1}\left[\sum_{i=0}^{n-1}\frac{y_i}{s^{i+1}} + \frac{c_n}{s^{1+n}} + \frac{c_{n+1}}{s^{n+2}}\right]\right]\right] - \frac{G(s)}{s^n}. \tag{3.21}$$

Performing the previous steps, we obtain the final form of the $(n+1)$th LRF:

$$LRes_{n+1}(s) = \frac{c_n}{s^{n+1}} + \frac{c_{n+1}}{s^{n+2}} - \frac{G(s)}{s^n} - \frac{1}{s^n}\sum_{r=0}^{n-1}\sum_{j=0}^{\infty}\left(\frac{c_{n+1}\lambda_{rj}}{(n+1-r)!}\frac{(n+1+j-r)!}{s^{2+n+j-r}} + \frac{c_n\lambda_{rj}}{(n-r)!}\frac{(n+j-r)!}{s^{1+n+j-r}} + \sum_{i=r}^{n-1}\frac{\lambda_{rj}y_i}{(i-r)!}\frac{(i+j-r)!}{s^{1+j+i-r}}\right). \tag{3.22}$$

Again, we multiply Eq. 3.22 by s^{n+2} to obtain

$$s^{n+2}\mathrm{LRes}_{n+1}(s) = c_{n+1} - s^2G(s) + sg(0) + s\sum_{r=0}^{n-1}\lambda_{r0}y_r - \sum_{r=0}^{n-1}\sum_{j=0}^{\infty}\left(\frac{c_{n+1}\lambda_{rj}}{(n+1-r)!}\frac{(n+1+j-r)!}{s^{n+j-r}} + \frac{c_n\lambda_{rj}}{(n-r)!}\frac{(n+j-r)!}{s^{n+j-r-1}} + \sum_{i=r}^{n-1}\frac{\lambda_{rj}y_i}{(i-r)!}\frac{(i+j-r)!}{s^{i+j-r-1}}\right). \tag{3.23}$$

Computing the limit at infinity to both sides of the last equation and using Eq. 3.10, we get

$$c_{n+1} = g'(0) + c_n\lambda_{(n-1)0} + 1!\sum_{r=0}^{n-1}\lambda_{r1}y_r + \sum_{r=0}^{n-2}\lambda_{r0}y_{r+1}. \tag{3.24}$$

So, the second approximation of the solution of Eq. 3.3 is

$$Y_{n+1}(s) = \frac{y_0}{s} + \frac{y_1}{s^2} + \frac{y_2}{s^3} + \ldots + \frac{y_{n-1}}{s^n} + \frac{1}{s^{n+1}}\left(g(0) + \sum_{r=0}^{n-1}\lambda_{r0}y_r\right) + \frac{1}{s^{n+2}}\left(g'(0) + \left(g(0) + \sum_{r=0}^{n-1}\lambda_{r0}y_r\right)\lambda_{(n-1)0} + \sum_{r=0}^{n-1}\lambda_{r1}y_r + \sum_{r=0}^{n-2}\lambda_{r0}y_{r+1}\right). \tag{3.25}$$

Like the previous steps, we have

$$c_{n+2} = g''(0) + c_{n+1}\lambda_{(n-1)0} + c_n\lambda_{(n-2)0} + \frac{2!}{1!}c_n\lambda_{(n-1)1} + 2!\left(\sum_{r=0}^{n-1}\lambda_{r2}y_r + \sum_{r=0}^{n-2}\lambda_{r1}y_{r+1} + \sum_{r=0}^{n-3}\lambda_{r0}y_{r+2}\right). \tag{3.26}$$

Repeating the steps, one can obtain

$$c_{n+3} = g'''(0) + 3!\sum_{i=0}^{2}\sum_{r=0}^{i}\frac{c_{(n+2-i)}\lambda_{(n-1-i+r)r}}{(3-r)!} + 3!\left(\sum_{i=0}^{3}\sum_{r=0}^{n-1-i}\frac{\lambda_{r(3-i)}y_{(r+i)}}{i!}\right). \tag{3.27}$$

Considering a pattern of the obtained coefficients, we easily deduce the coefficient c_{n+k} as follows:

$$c_{n+k} = g^{(k)}(0) + k!\sum_{i=0}^{k-1}\sum_{r=0}^{i}\frac{c_{(n+k-1-i)}\lambda_{(n-1-i+r)r}}{(k-r)!} + k!\left(\sum_{i=0}^{k}\sum_{r=0}^{n-1-i}\frac{\lambda_{r(k-i)}y_{(r+i)}}{i!}\right), \quad k = 0, 1, \ldots. \tag{3.28}$$

According to Eq. 3.14, the recurrence relation (3.28) becomes as follows:

$$c_{n+k} = g^{(k)}(0) + \sum_{i=0}^{k-1}\sum_{r=0}^{i}\binom{k}{r}c_{(n+k-1-i)}\,a^{(r)}_{(n-1-i+r)}(0) + \left(\sum_{i=0}^{k}\sum_{r=0}^{n-1-i}\binom{k}{i}y_{(r+i)}a_r^{(k-i)}(0)\right). \tag{3.29}$$

Thus, we can express the $(k+1)$th-approximate solution of Eq. 3.3 by the following formula:

$$Y_{n+k}(s) = \sum_{i=0}^{n-1}\frac{y_i}{s^{i+1}} + \sum_{i=0}^{k}\frac{c_{n+i}}{s^{1+i+n}}, s > 0, \quad k = 0, 1, \ldots.. \tag{3.30}$$

Therefore, the exact solution of Eq. 3.3 can be expressed as

$$Y(s) = \sum_{i=0}^{n-1}\frac{y_i}{s^{i+1}} + \sum_{i=0}^{\infty}\frac{c_{n+i}}{s^{1+i+n}}. \tag{3.31}$$

Substituting the result in Eq. 3.29 into Eq. 3.31 and running the inverse LT gives the solutions of IVP (1.1) and (1.2) as follows:

TABLE 1 The exact and the 10^{th} approximate solutions of the IVP (4.1) and (4.2) and the actual and relative errors at $a = 3$ and $b = -2$.

t	$y(t)$	$y_{10}(t)$	$Act.err.(t)$	$Rel.err.(t)$
0.0	0	0	0	–
0.1	0.044244	0.044244	1.45827×10^{-15}	3.29600×10^{-14}
0.2	0.196077	0.196077	4.34332×10^{-12}	2.21511×10^{-11}
0.3	0.489605	0.489605	3.82242×10^{-10}	7.80716×10^{-10}
0.4	0.967566	0.967566	9.21045×10^{-9}	9.51919×10^{-9}
0.5	1.683357	1.683357	1.09149×10^{-7}	6.48398×10^{-8}
0.6	2.703517	2.703516	8.25760×10^{-7}	3.05439×10^{-7}
0.7	4.110778	4.110774	4.58384×10^{-6}	1.11508×10^{-6}
0.8	6.007802	6.007782	2.02872×10^{-5}	3.37681×10^{-6}
0.9	8.521765	8.521689	7.55276×10^{-5}	8.86290×10^{-6}
1.0	11.809970	11.809724	2.45341×10^{-4}	2.07741×10^{-5}

$$y(t) = \sum_{i=0}^{n-1} \frac{y_i}{i!} t^i + \sum_{i=0}^{\infty} \frac{t^{i+n}}{(i+n)!} \left(g^{(i)}(0) + \sum_{j=0}^{i-1} \sum_{r=0}^{j} \binom{i}{r} c_{(n+i-1-j)}\, a_{(n-1-j+r)}^{(r)}(0) + \sum_{j=0}^{i} \sum_{r=0}^{n-1-j} \binom{i}{j} y_{(r+j)}\, a_r^{(i-j)}(0) \right). \tag{3.32}$$

3.2 The LRPS method for solving non-linear ODEs

This section introduces the steps of the LRPS approach in solving non-linear ODEs. To explain the methodology of the proposed method in constructing series solutions to this class, we consider IVP (1.3) and (1.4).

To generate the LRPS solution of the IVP (1.3) and (1.4), we consider the first step; that is, operating the LT to Eq. 1.3 and utilizing conditions (1.4), we obtain

$$Y(s) = \sum_{i=0}^{n-1} \frac{y_i}{s^{i+1}} + \frac{1}{s^n} \Psi\left(s, Y(s), \frac{dY}{ds}, \frac{d^2Y}{ds^2}, \ldots, \frac{d^mY}{ds^m} \right), s > 0, \tag{3.33}$$

where Ψ is a multivariable function of $s, Y(s), \frac{dY}{ds}, \frac{d^2Y}{ds^2}$, and $\frac{d^mY}{ds^m}$, $m \in \mathbb{N}$.

We assume that $Y(s)$ given in Eq. 3.33 can be expanded as in Eq. 3.4. According to the conditions given in Eq. 1.4 and Theorem 2.3, series (3.4) also has the form in Eq. 3.5, and the kth-truncated series of $Y(s)$ will be like Eq. 3.6.

To set the values of the unknown coefficients in Eq. 3.6, according to Eq. 3.33, we define the LRF of Eq. 3.33 as

$$LRes(s) = Y(s) - \sum_{i=0}^{n-1} \frac{y_i}{s^{i+1}} - \frac{1}{s^n} \Psi\left(s, Y(s), \frac{dY}{ds}, \frac{d^2Y}{ds^2}, \ldots, \frac{d^mY}{ds^m} \right), s > 0 \tag{3.34}$$

and the kth LRF as

$$LRes_k(s) = Y_k(s) - \sum_{i=0}^{n-1} \frac{y_i}{s^{i+1}} - \frac{1}{s^n} \Psi\left(s, Y_k(s), \frac{dY_k}{ds}, \frac{d^2Y_k}{ds^2}, \ldots, \frac{d^mY_k}{ds^m} \right), s > 0. \tag{3.35}$$

According to the form of $Y_k(s)$ as in Eq. 3.6, it is clear that $\Psi(s, Y_k(s), \frac{dY_k}{ds}, \frac{d^2Y_k}{ds^2}, \ldots, \frac{d^mY_k}{ds^m})$ has a finite LS as follows:

$$\Psi\left(s, Y_k(s), \frac{dY_k}{ds}, \frac{d^2Y_k}{ds^2}, \ldots, \frac{d^mY_k}{ds^m} \right) = \sum_{i=0}^{k} \frac{\phi(c_n, c_{n+1}, \ldots, c_{n+i})}{s^{1+i}}, s > 0, \tag{3.36}$$

where ϕ is a multivariable function of $c_n, c_{n+1}, \ldots, c_{n+i}$, for $i = 0, 1, \ldots, k$.

Substituting the expansions (3.6) and (3.36) in (3.35) gives the following expansion form of the kth LRF:

$$LRes_k(s) = \sum_{i=n}^{k} \frac{c_i}{s^{1+i}} - \sum_{i=0}^{k} \frac{\phi(c_n, c_{n+1}, \ldots, c_{n+i})}{s^{1+n+i}}, s > 0. \tag{3.37}$$

Thus, the nth LRF is

$$LRes_n(s) = \frac{c_n}{s^{1+n}} - \sum_{i=0}^{k} \frac{\phi(c_n, c_{n+1}, \ldots, c_{n+i})}{s^{1+n+i}}, s > 0. \tag{3.38}$$

Now, we multiply Eq. 3.38 by s^{n+1} to get

$$s^{n+1} LRes_n(s) = c_n - \sum_{i=0}^{k} \frac{\phi(c_n, c_{n+1}, \ldots, c_{n+i})}{s^i}, s > 0. \tag{3.39}$$

Now, applying the limit as $s \to \infty$ to both sides of Eq. 3.39 and using the fact in Eq. 3.10, we can easily determine the value of c_n by solving the following equation for c_n:

$$c_n = \phi(c_n). \tag{3.40}$$

In the same manner, we find the value of the coefficient c_{n+1} by substituting the $(n+1)$th-truncated series, $Y_n(s) = \sum_{i=0}^{n-1} \frac{y_i}{s^{1+i}} + \frac{c_n}{s^{1+n}}$, into the $(n+1)$th LRF to get the following:

$$LRes_{n+1}(s) = \frac{c_{n+1}}{s^{2+n}} - \sum_{i=0}^{k} \frac{\phi(c_n, c_{n+1}, \ldots, c_{n+i})}{s^{2+n+i}}, s > 0. \tag{3.41}$$

Multiplying s^{n+2} by both sides of Eq. 3.41, we get the following function:

$$s^{n+2} LRes_{n+1}(s) = c_{n+1} - \sum_{i=1}^{k} \frac{\phi(c_n, c_{n+1}, \ldots, c_{n+i})}{s^{i-1}}, s > 0. \tag{3.42}$$

Applying the limit at infinity to Eq. 3.42, we obtain the algebraic equation:

$$c_{n+1} = \phi(c_{n+1}). \tag{3.43}$$

Solving Eq. 3.43 implicitly for c_{n+1} determines the second unknown coefficient in Eq. 3.6.

Similarly, we compute the third coefficient c_{n+2} by substituting the $(n+2)$th-truncated series, $Y_{n+2}(s) = \frac{y_0}{s} + \frac{y_1}{s^2} + \frac{y_2}{s^3} + \ldots + \frac{y_{n-1}}{s^n} + \frac{c_n}{s^{n+1}} + \frac{c_{n+1}}{s^{n+2}} + \frac{c_{n+2}}{s^{n+3}}$, into the $(n+2)$th LRF to get the following function:

TABLE 2 The exact and the 10^{th} approximate solutions of the IVP (4.7) and (4.8) and the actual and relative errors.

t	$y_{10}(t)$	$y(t)$	$Act.err.(t)$	$Rel.err.(t)$
0.0	1	1	0	0
0.1	0.889966	0.889966	9.16853×10^{-14}	1.03021×10^{-13}
0.2	0.759453	0.759453	3.85420×10^{-10}	5.07496×10^{-10}
0.3	0.607144	0.607144	5.23038×10^{-8}	8.61472×10^{-8}
0.4	0.430542	0.430540	1.76504×10^{-6}	4.09960×10^{-6}
0.5	0.225375	0.225347	2.81962×10^{-5}	1.25123×10^{-4}
0.6	−0.015603	−0.015888	2.85811×10^{-4}	1.79887×10^{-2}
0.7	−0.304937	−0.307110	2.17319×10^{-3}	7.07626×10^{-3}
0.8	−0.664860	−0.678886	1.40298×10^{-2}	2.06658×10^{-2}
0.9	−1.135230	−1.224997	8.97720×10^{-2}	7.32834×10^{-2}

$$LRes_{n+2}(s) = \frac{c_{n+2}}{s^{n+3}} - \sum_{i=0}^{k} \frac{\phi(c_n, c_{n+1}, \ldots, c_{n+i})}{s^{1+n+i}}, s > 0. \tag{3.44}$$

Multiplying Eq. 3.44 by s^{n+3} gives

$$s^{n+3}\mathrm{LRes}_{n+2}(s) = c_{n+2} - \phi(c_n) - \phi(c_{n+1}) - \phi(c_{n+2}) - \sum_{i=2}^{k} \frac{\phi(c_n, c_{n+1}, \ldots, c_{n+i})}{s^{i-2}}, s > 0. \tag{3.45}$$

According to fact (3.10), we obtain

$$c_{n+2} = \phi(c_n) + \phi(c_{n+1}) + \phi(c_{n+2}). \tag{3.46}$$

Solving Eq. 3.46 for c_{n+2} sets another coefficient in Eq. 3.6.

The value of the third unknown coefficient c_{n+3} can be obtained by similar arguments and by solving the following equation:

$$c_{n+3} = \phi(c_n) + \phi(c_{n+1}) + \phi(c_{n+2}) + \phi(c_{n+3}). \tag{3.47}$$

Considering the pattern of the obtained coefficients, we easily conclude the coefficient c_{n+k} from the following implicit formula of c_{n+k}:

$$c_{n+k} = \phi(c_n) + \phi(c_{n+1}) + \phi(c_{n+2}) + \phi(c_{n+3}) + \ldots + \phi(c_{n+k}). \tag{3.48}$$

Thus, we can express the $(k+1)$th-approximate solution of Eq. 3.33 in the following shape:

$$Y_{n+k}(s) = \sum_{i=0}^{n-1} \frac{y_i}{s^{i+1}} + \sum_{i=0}^{k} \frac{\phi(c_n, c_{n+1}, \ldots, c_{n+i})}{s^{1+n+i}}, s > 0, \ k = 0, 1, \ldots. \tag{3.49}$$

Therefore, the exact analytic solution of Eq. 3.33 is written in a series form:

$$Y(s) = \sum_{i=0}^{n-1} \frac{y_i}{s^{i+1}} + \sum_{i=0}^{\infty} \frac{\phi(c_n, c_{n+1}, \ldots, c_{n+i})}{s^{1+n+i}}. \tag{3.50}$$

Running the inverse LT to Eq. 3.50 gives the solution of Eq. 1.3 and Eq. 1.4 in a series expansion as

$$y(t) = \sum_{i=0}^{n-1} \frac{y_i}{i!} t^i + \sum_{i=0}^{\infty} \frac{\phi(c_n, c_{n+1}, \ldots, c_{n+i})}{(i+n)!} t^{i+n}. \tag{3.51}$$

3.3 The LRPS method for solving singular-value problems

This section presents the LRPS method's procedure for handling singular-value problems. To do this, let us consider the following singular-value problem:

$$\frac{1}{t^k} \frac{d^n y}{dt^n} = f\left(t, y(t), \frac{dy}{dt}, \frac{d^2 y}{dt^2}, \ldots, \frac{d^{n-1} y}{dt^{n-1}}\right), t \in I, m, k \in \mathbb{N}. \tag{3.52}$$

Subject to the ICs

$$y(0) = y_0, y'(0) = y_1, \ldots, y^{(n-1)}(0) = y_{n-1}. \tag{3.53}$$

To solve the initial-singular value problems (3.52) and (3.53), we first multiply Eq. 3.52 by t^k to get

$$\frac{d^n y}{dt^n} = t^k f\left(t, y(t), \frac{dy}{dt}, \frac{d^2 y}{dt^2}, \ldots, \frac{d^{n-1} y}{dt^{n-1}}\right). \tag{3.54}$$

Now applying LT to Eq. 3.54 and using ICs (3.53), we get

$$Y(s) = \sum_{i=0}^{n-1} \frac{y_i}{s^{i+1}} + \frac{1}{s^n} \mathcal{L}\left[\mathcal{L}^{-1}\left[\frac{k!}{s^{k+1}}\right] \mathcal{L}^{-1}\left[\Psi\left(s, Y(s), \frac{dY}{ds}, \frac{d^2 Y}{ds^2}, \ldots, \frac{d^m Y}{ds^m}\right)\right]\right], s > 0. \tag{3.55}$$

Now, suppose that the function Y(s) can be expressed in the form of the expansion of (3.4), and so on. We can complete the steps described in the previous Section 3.2 to obtain the required solution.

4 Applications to linear and non-linear problems

This section presents seven interesting problems with wide applications in physics and other sciences that are discussed and solved by the LRPS method.

Problem 4.1: consider the following composite oscillation equation:

$$\frac{d^2 y}{dt^2} - a\frac{dy}{dt} - by(t) = 8, t \geq 0, \tag{4.1}$$

with respect to the initial condition

$$y(0) = 0, y'(0) = 0. \tag{4.2}$$

Comparing Eq. 4.1 with Eq. 1.1 concludes that $a_1(t) = a, a_0(t) = b$, and $g(x) = 8$. Using the results obtained in Section 3.1, we can deduce $\lambda_{10} = a, \lambda_{11} = \lambda_{12} = \lambda_{13} = \ldots = 0$ and $\lambda_{00} = b, \lambda_{01} = \lambda_{02} = \lambda_{03} = \ldots = 0$. According to the recurrence relation in Eq. 3.29, we can see that $c_2 = 8$, $c_3 = 8a$, $c_4 = 8(b + a^2), c_5 = 8(a^3 + 2ab)$, $c_6 = 8(a^4 + 3a^2 b + b^2)$, $c_7 = 8(a^5 + 4a^3 b + 3ab^2)$, $c_8 = 8(a^6 + 5a^4 b + 6a^2 b^2 + b^3)$, $c_9 = 8(a^7 + 6a^5 b + 10a^3 b^2 + 4ab^3)$, and $c_{10} = 8(a^8 + 7a^6 b +$

TABLE 3 The 10^{th} approximate LRPS solution of the IVP (4.24) and (4.25) and the residual and relative errors.

t	$y_{10}(t)$	$Res.err.(t)$	$Rel.err.(t)$
0.0	1	0	0
0.1	0.990008	1.49429×10^{-20}	4.90918×10^{-9}
0.2	0.960133	6.11918×10^{-17}	3.23767×10^{-7}
0.3	0.910671	7.93635×10^{-15}	3.88428×10^{-6}
0.4	0.842113	2.50409×10^{-13}	2.35678×10^{-5}
0.5	0.755133	3.64141×10^{-12}	1.00077×10^{-4}
0.6	0.650575	3.24397×10^{-11}	3.46087×10^{-4}
0.7	0.529442	2.06065×10^{-10}	1.06956×10^{-3}
0.8	0.392875	1.02189×10^{-9}	3.20192×10^{-3}
0.9	0.242133	4.19437×10^{-9}	1.04964×10^{-2}
1.0	0.078569	1.48293×10^{-8}	6.06363×10^{-2}

$15a^4b^2 + 10a^2b^3 + b^4$). Therefore, the 10th approximation of the solution of the IVP (4.1) and (4.2) will be as follows:

$$\begin{aligned} y_{10}(t) = {} & \frac{8}{2!}t^2 + \frac{8a}{3!}t^3 + \frac{8(b+a^2)}{4!}t^4 + \frac{8(a^3+2ab)}{5!}t^5 \\ & + \frac{8(a^4+3a^2b+b^2)}{6!}t^6 + \frac{8(a^5+4a^3b+3ab^2)}{7!}t^7 \\ & + \frac{8(a^6+5a^4b+6a^2b^2+b^3)}{8!}t^8 + \frac{8(a^7+6a^5b+10a^3b^2+4ab^3)t^9}{9!} \\ & + \frac{8(a^8+7a^6b+15a^4b^2+10a^2b^3+b^4)t^{10}}{10!}. \end{aligned} \tag{4.3}$$

It is easy to check if the exact solution of Eq. 4.1 and Eq. 4.2 is as follows:

$$y(t) = \frac{4}{bc}\left((c+a)e^{\frac{1}{2}(a-c)t} + (c-a)e^{\frac{1}{2}(a+c)t}\right) - \frac{8}{b}, c = \sqrt{a^2+4b}. \tag{4.4}$$

To analyze the accuracy of the approximate solution in Eq. 4.3 and determine the interval of convergence, we introduce and compute two types of error, actual and relative errors that are defined, respectively, as follows:

$$Act.Err.(t) = \left|y(t) - y_{10}(t)\right| \tag{4.5}$$

and

$$Rel.Err.(t) = \left|\frac{y(t) - y_{10}(t)}{y(t)}\right|. \tag{4.6}$$

For analysis and comparison of the exact and approximate solutions of IVP (4.1) and (4.2), Table 1 shows the numerical results of this problem. It displays the exact and approximate results in addition to the actual and relative errors at different values of t within the interval $[0, 1]$. The results indicate that the errors increase when the value of t increases. It is known that by increasing the number of terms in the series solution, the error decreases and the convergence period of the truncated series increases. It should be noted that we can extend the convergence period using the multi-stage technique.

Problem 4.2: consider the following Bessel's equation:

$$(1-t^2)y''(t) - 2ty'(t) + 2y(t) = 0. \tag{4.7}$$

Subject to the ICs,

$$y(0) = 1,\ y'(0) = -1. \tag{4.8}$$

According to the existence and uniqueness theorem, it is clear that the IVPs (4.7) and (4.8) have a unique solution in the interval $(-1, 1)$, so we seek to get this solution *via* the LRPS method. To reach our goal and be able to rely on the construction obtained in Section 3.1, it is necessary to rewrite Eq. 4.7 as follows:

$$y''(t) = \frac{2t}{(1-t^2)}y'(t) - \frac{2}{(1-t^2)}y(t), 0 \le t < 1. \tag{4.9}$$

Comparing Eq. 4.7 with Eq. 1.1, we find that

$$L_t = \frac{2t}{(1-t^2)}\frac{d}{dt} - \frac{2}{(1-t^2)}, a_1(t) = \frac{2t}{(1-t^2)}, a_0(t) = \frac{-2}{(1-t^2)}, \tag{4.10}$$

where $a_0(t)$ and $a_1(t)$ are analytic functions on $[0, 1)$.

Since the coefficients of the linear operator in Eq. 4.10 are analytic functions, they can be expressed as McLaurin expansions as follows:

$$a_0(t) = \sum_{j=0}^{\infty} -2t^{2j}, a_1(t) = \sum_{j=0}^{\infty} 2t^{2j+1}. \tag{4.11}$$

So, according to Eq. 4.11 and Eq. 3.14, we have

$$\begin{aligned} & \lambda_{0(2j)} = \frac{a_0^{(2j)}(0)}{(2j)!} = -2, \lambda_{0(2j+1)} = \frac{a_0^{(2j+1)}(0)}{(2j+1)!} = 0, j = 0, 1, 2, \ldots \\ & \lambda_{1(2j)} = \frac{a_1^{(2j)}(0)}{(2j)!} = 0, \lambda_{1(2j+1)} = \frac{a_1^{(2j+1)}(0)}{(2j+1)!} = 2, j = 0, 1, 2, \ldots \end{aligned} \tag{4.12}$$

Comparing with the general formula (3.29), we can find the values of the coefficients as follows:

$$\begin{aligned} c_2 &= \lambda_{00}y_0 + \lambda_{10}y_1 = -2, \\ c_3 &= c_2\lambda_{10} + \lambda_{01}y_0 + \lambda_{11}y_1 + \lambda_{00}y_1 = 0, \\ c_4 &= c_3\lambda_{10} + c_2\lambda_{00} + 2!c_2\lambda_{11} + 2(\lambda_{02}y_0 + \lambda_{12}y_1 + \lambda_{01}y_1) = -8, \\ c_5 &= c_4\lambda_{10} + c_3\lambda_{00} + 3c_3\lambda_{11} + 3c_2\lambda_{01} + 6c_2\lambda_{12} + 6(\lambda_{03}y_0 + \lambda_{13}y_1 + \lambda_{02}y_1) = 0 \\ c_6 &= c_5\lambda_{10} + c_4\lambda_{00} + 4c_4\lambda_{11} + 4c_3\lambda_{01} + 12c_3\lambda_{12} + 12c_2\lambda_{02} + 24c_2\lambda_{13} \\ &\quad +24(\lambda_{04}y_0 + \lambda_{14}y_1 + \lambda_{03}y_1) = -144 \\ c_7 &= c_6\lambda_{10} + c_5\lambda_{00} + 5c_5\lambda_{11} + 5c_4\lambda_{01} + 20c_4\lambda_{12} + 20c_3\lambda_{02} + 60c_3\lambda_{13} + 60c_2\lambda_{03} \\ &\quad + 120c_2\lambda_{14} + 120(\lambda_{04}y_1 + \lambda_{05}y_0 + \lambda_{15}y_1) = 0 \\ c_8 &= c_7\lambda_{10} + c_6\lambda_{00} + 6c_6\lambda_{11} + 6c_5\lambda_{01} + 30c_5\lambda_{12} + 30c_4\lambda_{02} + 120c_4\lambda_{13} + 120c_3\lambda_{03} \\ &\quad +360c_3\lambda_{14} + 360c_2\lambda_{04} + 720c_2\lambda_{15} + 720(\lambda_{05}y_1 + \lambda_{06}y_0 + \lambda_{16}y_1) = -5760 \\ c_9 &= c_7\lambda_{00} + 7c_6\lambda_{01} + 42c_5\lambda_{02} + 210c_4\lambda_{03} + 840c_3\lambda_{04} + 2520c_2\lambda_{05} + c_8\lambda_{10} \\ &\quad +7c_7\lambda_{11} + 42c_6\lambda_{12} + 210c_5\lambda_{13} + 840c_4\lambda_{14} + 2520c_3\lambda_{15} + 5040c_2\lambda_{16} \\ &\quad +5040(\lambda_{07}y_0 + \lambda_{17}y_1 + \lambda_{06}y_1) = 0 \\ c_{10} &= c_8\lambda_{00} + 8c_7\lambda_{01} + 56c_6\lambda_{02} + 336c_5\lambda_{03} + 1680c_4\lambda_{04} + 6720c_3\lambda_{05} \\ &\quad + 20160c_2\lambda_{06} + c_9\lambda_{10} + 8c_8\lambda_{11} + 56c_7\lambda_{12} + 336c_6\lambda_{13} + 1680c_5\lambda_{14} \\ &\quad + 6720c_4\lambda_{15} + 20160c_3\lambda_{16} + 40320c_2\lambda_{17} + 40320(\lambda_{08}y_0 + \lambda_{18}y_1 + \lambda_{07}y_1) \\ &= -403200. \end{aligned}$$

Therefore, the LRPS solution to Problem 4.2 can be expressed in the following series form:

$$y(t) = 1 - t - t\left(t + \frac{t^3}{3} + \frac{t^5}{5} + \frac{t^7}{7} + \frac{t^9}{9} + \ldots\right). \tag{4.13}$$

TABLE 4 The 8^{th} approximate LRPS solution of the IVP (4.40) and (4.41) and the residual and relative errors.

t	$y_{10}(t)$	$Res.err.(t)$	$Rel.err.(t)$
0.0	3.141592	0	0
0.1	3.143436	6.17550×10^{-12}	3.88412×10^{-9}
0.2	3.149766	3.46550×10^{-9}	2.54577×10^{-7}
0.3	3.162007	1.47389×10^{-7}	2.96588×10^{-6}
0.4	3.181938	2.19032×10^{-6}	1.70131×10^{-5}
0.5	3.211770	1.83429×10^{-5}	6.60961×10^{-5}
0.6	3.254229	1.07003×10^{-4}	2.00356×10^{-4}
0.7	3.312664	4.86480×10^{-4}	5.10802×10^{-4}
0.8	3.391178	1.84223×10^{-3}	1.14494×10^{-3}
0.9	3.494777	6.06308×10^{-3}	2.32075×10^{-3}
1.0	3.629549	1.78494×10^{-2}	4.33494×10^{-3}

The expansion in (4.13) is the same expansion as that of the function $\tan^{-1}(t)$. Therefore, the exact solution of the IVP (4.7) and (4.8) has the following closed form:

$$y(t) = 1 - t - t\tan^{-1}(t), 0 \le t < 1. \tag{4.14}$$

Table 2 shows the numerical results of Problem 4.2. It shows the exact and approximate results in addition to the actual and relative errors at different values of $t \in [0, 09]$. The displayed data are acceptable and can be improved by increasing the order of the approximation.

Problem 4.3: consider the following non-linear nonhomogeneous ODE:

$$y^{(3)}(t) + y^2(t) + \cos t\, y'(t) = 1 - \cos t. \tag{4.15}$$

Subject to the ICs,

$$y(0) = 0, y'(0) = 1, y''(0) = 0. \tag{4.16}$$

Similar to the previous problems, we operate the LT on both sides of Eq. 4.15 and employ the ICs (4.16). Then, we obtain the following equation in the Laplace space:

$$Y(s) = \frac{1}{s^2} - \frac{1}{s^3}\mathcal{L}\left[\left(\mathcal{L}^{-1}[Y(s)]\right)^2\right] - \frac{1}{s^3}\mathcal{L}\left[\mathcal{L}^{-1}\left[\frac{s}{1+s^2}\right]\mathcal{L}^{-1}[sY(s)]\right] + \frac{1}{s^4} - \frac{1}{s^2(1+s^2)}, s > 0. \tag{4.17}$$

We assume that the solution of Eq. 4.17 has the same LS expansion as in Eq. 3.4. According to ICs (4.16), the kth-truncated series of $Y(s)$ becomes

$$Y_k(s) = \frac{1}{s^2} + \sum_{i=3}^{k} \frac{c_i}{s^{1+i}}, s > 0. \tag{4.18}$$

To set the value of the unknown coefficients in series (4.18), we utilize the kth LRF of Eq. 3.17, which is defined as

$$\mathrm{LRes}_k(s) = Y_k(s) - \frac{1}{s^2} + \frac{1}{s^3}\mathcal{L}\left[\left(\mathcal{L}^{-1}[Y_k(s)]\right)^2\right] + \frac{1}{s^3}\mathcal{L}\left[\mathcal{L}^{-1}\left[\frac{s}{1+s^2}\right]\mathcal{L}^{-1}[sY_k(s)]\right] - \frac{1}{s^4} + \frac{1}{s^2(1+s^2)}, s > 0. \tag{4.19}$$

To determine the coefficient c_3, we substitute $Y_3(s) = \frac{1}{s^2} + \frac{c_3}{s^4}$ into $\mathrm{LRes}_3(s)$ and run the operators in Eq. 4.19 to get the following rational function:

$$\mathrm{LRes}_3(s) = \frac{c_3}{s^4} - \frac{1}{s^4} + \frac{2}{s^2(1+s^2)} + \frac{2}{s^6} + \frac{8c_3}{s^8} + \frac{c_3}{(1+s^2)^3} - \frac{3c_3}{s^2(1+s^2)^3} + \frac{20c_3^2}{s^{10}}. \tag{4.20}$$

Employing fact (3.10), the solution of the equation $\lim_{s\to\infty} s^4 \mathrm{LRes}_3(s) = 0$ for c_3 introduces $c_3 = -1$.

Similarly, to find out the value of the second unknown coefficient c_4, we substitute $Y_4(s) = \frac{1}{s^2} + \frac{1}{s^4} + \frac{c_4}{s^5}$ into the 4^{th}-LRF to get the following:

$$LRes_4(s) = \frac{c_3}{s^5} + \frac{2}{s^6} - \frac{8}{s^8} + \frac{20}{s^{10}} - \frac{1}{(1+s^2)^3} + \frac{3}{s^2(1+s^2)^3} - \frac{2}{s^4+s^6} - \frac{70c_3}{s^{11}} + \frac{10c_3}{s^9} + \frac{c_3}{s^3(1+s^2)^4} - \frac{6c_3}{s(1+s^2)^4} + \frac{sc_3}{(1+s^2)^4} + \frac{70c_3^2}{s^{12}}, s > 0. \tag{4.21}$$

Utilizing fact (3.10) *via* Eq. 4.21 gives $c_4 = 0$. Using the same procedure as mentioned above, we can find more coefficients for series (4.18). Some of them are $c_5 = 1, c_6 = 0, c_7 = -1, c_8 = 0, c_9 = 1, c_{10} = 0, c_{11} = -1$. So, the series solution to Eq. 4.31 has the following LS:

$$Y(s) = \frac{1}{s^2} - \frac{1}{s^4} + \frac{1}{s^6} - \frac{1}{s^8} + \frac{1}{s^{10}} - \frac{1}{s^{12}} + \ldots. \tag{4.22}$$

Therefore, the LRPS solution to Eq. 4.15 and Eq. 4.16 can be expressed in the following series form:

$$y(t) = t - \frac{t^3}{3!} + \frac{t^5}{5!} - \frac{t^7}{7!} + \frac{t^9}{9!} - \frac{t^{11}}{11!} + \ldots, \tag{4.23}$$

which is the expansion of the exact solution $y(t) = \sin(t)$.

Problem 4.4: consider the following non-linear pantograph equation:

$$\frac{d^2y}{dt^2} = -2y^2\left(\frac{t}{2}\right), t \ge 0. \tag{4.24}$$

Subject to the ICs,

$$y(0) = 1, y'(0) = 0. \tag{4.25}$$

Following the same procedure as in the previous problems, we can express the LRPS solution to IVP (4.24) and (4.25) in the form

$$y(t) = 1 - t^2 + \frac{t^4}{12} - \frac{7t^6}{1440} + \frac{127t^8}{1290240} - \frac{10879t^{10}}{7431782400} + \ldots. \tag{4.26}$$

Since we cannot predict the pattern in the coefficients of the series solution in Eq. 4.26, we cannot reach the exact solution.

TABLE 5 The 10^{th} approximate LRPS solution of the IVP (4.46) and (4.47) and the residual and relative errors.

t	$y_{10}(t)$	$Res.err.(t)$	$Rel.err.(t)$
0.0	0	0	0
0.1	1.66589×10^{-4}	2.79119×10^{-12}	1.21224×10^{-8}
0.2	1.33102×10^{-3}	1.07260×10^{-9}	2.99609×10^{-7}
0.3	4.48384×10^{-3}	2.75171×10^{-8}	1.60237×10^{-6}
0.4	1.06044×10^{-2}	1.83659×10^{-7}	3.90207×10^{-6}
0.5	2.06612×10^{-2}	4.28369×10^{-9}	3.15208×10^{-6}
0.6	3.56173×10^{-2}	7.03832×10^{-6}	1.40973×10^{-5}
0.7	5.64404×10^{-2}	5.66213×10^{-5}	7.81978×10^{-5}
0.8	8.41213×10^{-2}	2.83838×10^{-4}	2.45959×10^{-4}
0.9	1.19699×10^{-1}	1.09913×10^{-3}	6.12036×10^{-4}
1.0	1.64304×10^{-1}	3.57492×10^{-3}	1.32164×10^{-3}

Therefore, we test the results using the residual and relative errors, which are defined as follows, respectively:

$$Res.Err.(t) = \left|\mathcal{L}^{-1}\left[LRes_k(s)\right]\right| = \left|\frac{d^2y_k}{dt^2} + 2y_k^2\left(\frac{t}{2}\right)\right|, \tag{4.27}$$

$$Rel.Err.(t) = \left|\frac{y_k(t) - y_{k/2}(t)}{y_k(t)}\right|. \tag{4.28}$$

Table 3 shows the numerical results of Problem 4.4. It displays the 10th approximate solution in addition to the residual and relative errors at different values of t within the interval $[0, 1]$. The results indicate that the LRPS solution is acceptable mathematically in the period $[0, 1]$.

Problem 4.5: consider the following homogenous linear singular ODE:

$$(\sin t)y'' - 2(\cos t)y' - (\sin t)y = 0, 0 < t < \pi, \tag{4.29}$$

with respect to the ICs:

$$y(0) = 2, y'(0) = 0. \tag{4.30}$$

We apply the LT on both sides of Eq. 4.29 and use the ICs in Eq. 4.30 to obtain the following symbolic algebraic equation in the Laplace space:

$$\mathcal{L}\left[\mathcal{L}^{-1}\left[\frac{1}{1+s^2}\right]\mathcal{L}^{-1}\left[s^2Y(s) - 2s\right]\right] - 2\mathcal{L}\left[\mathcal{L}^{-1}\left[\frac{1}{1+s^2}\right]\mathcal{L}^{-1}\left[sY(s) - 2\right]\right] - \mathcal{L}\left[\mathcal{L}^{-1}\left[\frac{1}{1+s^2}\right]\mathcal{L}^{-1}\left[Y(s)\right]\right] = 0, s > 0. \tag{4.31}$$

Suppose that the solution of Eq. 4.31 has a LS expansion as in Eq. 3.4. According to ICs (4.30), the kth-truncated series (3.6) can be expressed as

$$Y_k(s) = \frac{2}{s} + \sum_{i=2}^{k} \frac{c_i}{s^{1+i}}, s > 0. \tag{4.32}$$

To set the unknown coefficient in series (4.32), we define the kth LRF of Eq. 4.31 as follows:

$$\begin{aligned} \mathrm{LRes}_k(s) = {} & \mathcal{L}\left[\mathcal{L}^{-1}\left[\frac{1}{1+s^2}\right]\mathcal{L}^{-1}\left[s^2Y_k(s) - 2s\right]\right] \\ & -2\mathcal{L}\left[\mathcal{L}^{-1}\left[\frac{1}{1+s^2}\right]\mathcal{L}^{-1}\left[sY_k(s) - 2\right]\right] \\ & -\mathcal{L}\left[\mathcal{L}^{-1}\left[\frac{1}{1+s^2}\right]\mathcal{L}^{-1}\left[Y_k(s)\right]\right], s > 0. \end{aligned} \tag{4.34}$$

We substitute $Y_2(s) = \frac{2}{s} + \frac{c_2}{s^3}$ into $\mathrm{LRes}_2(s)$ and run the operators in Eq. 4.34 to get the following function:

$$\begin{aligned} \mathrm{LRes}_2(s) = {} & -\frac{2}{(1+s^2)^3} + \frac{4c_2}{(1+s^2)^3} - \frac{4s^2}{(1+s^2)^3} - \frac{c_2s^2}{(1+s^2)^3} \\ & - \frac{2s^4}{(1+s^2)^3} - \frac{c_2s^4}{(1+s^2)^3}. \end{aligned} \tag{4.35}$$

Solving the equation $\lim_{s\to\infty} s^2\mathrm{LRes}_2(s) = 0$ gives $c_2 = -2$. Thus, the first approximation of the solution of Eq. 4.31 is $Y_2(s) = \frac{2}{s} - \frac{2}{s^3}$.

Again, we substitute 3rd-truncated series, $Y_3(s) = \frac{2}{s} - \frac{2}{s^3} + \frac{c_3}{s^4}$, into the 3rd LRF to get the following:

$$\mathrm{LRes}_3(s) = \frac{-10}{(1+s^2)^4} + \frac{12c_3s}{(1+s^2)^4} - \frac{12s^2}{(1+s^2)^4} + \frac{4c_3s^3}{(1+s^2)^4} - \frac{2s^4}{(1+s^2)^4}. \tag{4.36}$$

Consequently, the equation $\lim_{s\to\infty} s^3\mathrm{LRes}_3(s) = 0$ gives $c_3 = 0$.

Likewise, we substitute the 4th-truncated series, $Y_4(s) = \frac{2}{s} - \frac{2}{s^3} + \frac{c_4}{s^5}$, into the 4th LRF to get the following:

$$\begin{aligned} \mathrm{LRes}_4(s) = {} & \frac{-10}{(1+s^2)^5} - \frac{4c_4}{(1+s^2)^5} - \frac{22s^2}{(1+s^2)^5} + \frac{21c_4s^2}{(1+s^2)^5} - \frac{14s^4}{(1+s^2)^5} \\ & + \frac{10c_4s^4}{(1+s^2)^5} - \frac{2s^6}{(1+s^2)^5} + \frac{c_4s^6}{(1+s^2)^5}. \end{aligned} \tag{4.37}$$

Solving the equation $\lim_{s\to\infty} s^4\mathrm{LRes}_4(s) = 0$ gives $c_4 = 2$. Applying the same procedure for $k = 5, 6, 7, 8$ leads to $c_5 = 0$, $c_6 = -2$, $c_7 = 0$, and $c_8 = 2$. Thus, we conclude that the solution of Eq. 4.31 has the following expansion:

$$Y(s) = \frac{2}{s} - \frac{2}{s^3} + \frac{2}{s^5} - \frac{2}{s^7} + \frac{2}{s^9} - \ldots. \tag{4.38}$$

Applying the inverse LT to Eq. 4.38 gives the LRPS solution to the IVP (4.29) and (4.30) in the following PS form:

$$y(t) = 2\left(1 - \frac{t^2}{2!} + \frac{t^4}{4!} - \frac{t^6}{6!} + \frac{t^8}{8!} - \ldots\right). \tag{4.39}$$

It is clear that the closed form of the exact solution of IVP (4.50) and (4.51) is $y(t) = 2\cos(t)$.

Problem 4.6: consider the following non-homogeneous nonlinear Lane–Emden singular ODE:

$$y''(t) + \frac{2}{t}y'(t) - t\sin y(t) = e^{2t}, t \in (0, 2), \tag{4.40}$$

considering the ICs:

$$y(0) = \pi, y'(0) = 0. \tag{4.41}$$

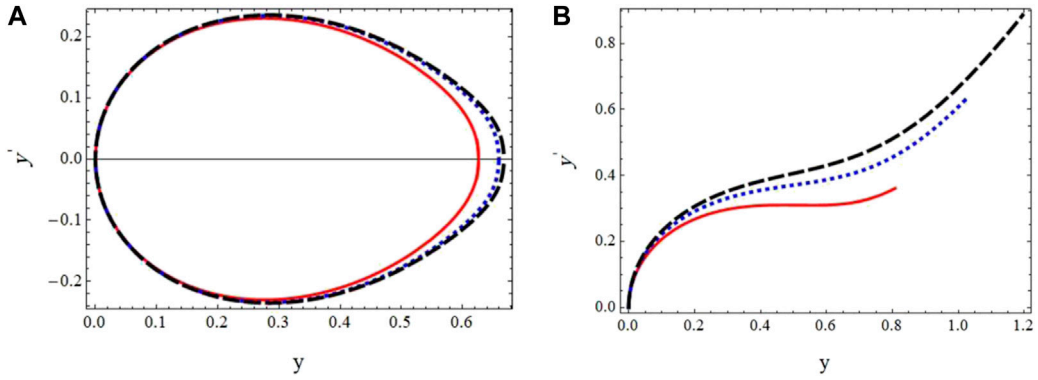

FIGURE 1
Phase trajectories at different values of θ. **(A)** Solid line: $\theta = 0.2$; dotted line: $\theta = 0.203$; and dashed line: $\theta = 0.203632188$. **(B)** Solid line: $\theta = 0.2037$; dotted line: $\theta = 0.25$; and dashed line: $\theta = 0.3$.

Using similar arguments to the previous problem, one can obtain the series solution of the LT of the IVP (4.40) and (4.41) as follows:

$$Y(s) = \frac{\pi}{s} + \frac{\frac{1}{3}}{s^3} + \frac{1}{s^4} + \frac{\frac{12}{5}}{s^5} + \frac{\frac{14}{3}}{s^6} + \frac{\frac{60}{7}}{s^7} + \frac{15}{s^8} + \frac{28}{s^9} + \frac{\frac{2588}{45}}{s^{10}} + \ldots. \quad (4.42)$$

Applying the inverse LT on Eq. 4.42 gives the LRPS solution of the IVP (4.40) (4.41) in the following series form:

$$y(t) = \pi + \frac{t^2}{6} + \frac{t^3}{6} + \frac{t^4}{10} + \frac{7t^5}{180} + \frac{t^6}{84} + \frac{t^7}{336} + \frac{t^8}{1440} + \frac{647t^9}{4082400} + \ldots. \quad (4.43)$$

There is no pattern between the series terms in Eq. 4.43. So, it is difficult to predict the exact solution formula. Thus, we suffice with the approximate solution we got for Problem 4.6. It is worth noting that the more terms we calculate for the LRPS solution, the longer the series convergence interval and the higher the accuracy of the solution. Therefore, we test the 8th approximate LRPS solution for Problem 4.6 using the residual and relative errors, which are defined as follows, respectively:

$$\begin{aligned} Res.Err.(t) &= \left|\mathcal{L}^{-1}\left[LRes_8(s)\right]\right| \\ &= \left|t - e^{2t}t + 2t^2 + 2t^3 + \frac{4t^4}{3} + \frac{2t^5}{3} \right. \\ &\quad \left. + \frac{4t^6}{15} + \frac{4t^7}{45} + \frac{8t^8}{315} + \frac{t^9}{1512} - \frac{13t^{10}}{4320} - \frac{1003t^{11}}{255150} - \frac{113221t^{12}}{32659200}\right|, \end{aligned} \quad (4.44)$$

$$\begin{aligned} Rel.Err.(t) &= \left|\frac{y_8(t) - y_4(t)}{y_8(t)}\right| \\ &= \left|\frac{\frac{t^6}{84} + \frac{t^7}{336} + \frac{t^8}{1440} + \frac{647t^9}{4082400}}{\pi + \frac{t^2}{6} + \frac{t^3}{6} + \frac{t^4}{10} + \frac{7t^5}{180} + \frac{t^6}{84} + \frac{t^7}{336} + \frac{t^8}{1440} + \frac{647t^9}{4082400}}\right|. \end{aligned} \quad (4.45)$$

Table 4 shows the numerical results of Problem 4.6. It illustrates the 8th approximate solution in addition to the residual and relative errors at different values of t within the interval $[0, 1]$. Similar to the results in the previous tables, the data are good for the period $[0, 1]$.

Problem 4.7: We consider the following micro-electromechanical system (MEMS) [52]:

$$y'' + y + \frac{\theta}{y-1} = 0, \theta > 0, \quad (4.46)$$

with the ICs:

$$y(0) = y'(0) = 0. \quad (4.47)$$

This dynamic differential equation is used to describe the wire's movement as a point mass, where y is the dimensionless distance and θ is a voltage-related parameter.

Simulating the previous examples, the LT of the IVP (4.46) and (4.47) is given by the following algebraic equation:

$$\mathcal{L}\left[\mathcal{L}^{-1}\left[s^2Y(s)\right]\mathcal{L}^{-1}\left[Y(s)\right]\right] - s^2Y(s) + \mathcal{L}\left[\left(\mathcal{L}^{-1}\left[Y(s)\right]\right)^2\right] - Y(s) + \frac{1}{s^2} = 0, s > 0. \quad (4.48)$$

Applying the arguments and processes of the LRPS method, one can obtain the LRPS solution to the algebraic Eq. 4.48 as follows:

$$Y(s) = \frac{\theta}{s^3} + \frac{\theta(\theta-1)}{s^5} + \frac{\theta(1-2\theta+7\theta^2)}{s^7} - \frac{\theta(1-3\theta+39\theta^2-127\theta^3)}{s^9} + \frac{\theta(1-4\theta+168\theta^2-1678\theta^3+4369\theta^4)}{s^{11}} + \ldots. \quad (4.49)$$

Applying the inverse LT to Eq. 4.49 gives the LRPS solution of the IVP (4.46) (4.47) as follows:

$$y(t) = \frac{\theta t^2}{2} + \frac{\theta(\theta-1)t^4}{4!} + \frac{\theta(1-2\theta+7\theta^2)t^6}{6!} - \frac{\theta(1-3\theta+39\theta^2-127\theta^3)t^8}{8!} + \frac{\theta(1-4\theta+168\theta^2-1678\theta^3+4369\theta^4)t^{10}}{10!} + \ldots. \quad (4.50)$$

To test the accuracy of the obtained solution given in (4.50), we compute the residual and relative errors to the 10th approximation of the solution. Table 5 shows the 10th approximate solution in addition to the residual and relative errors at different values of t within the interval $[0, 1]$. The results indicate that the obtained solution is acceptable mathematically.

On the other hand, what specialists in MEMS system implementations are most interested in is the pull-in phenomenon analysis. The MEMS system in Eq. 4.46 and Eq. 4.47 conducts either periodically or unsteadily. This behavior depends on the value of the voltage-related parameter, θ. At small values of θ, the solution of the system is stable and periodic, whereas at large values of θ, it becomes

unstable, called pull-in instability. Figure 1 shows that the system is stable and periodic at θ values less than or equal to the critical value ($\theta = 0.203632188$) [52], and it becomes unstable at θ values greater than the critical one.

5 Conclusion

This study aims to test the efficiency of the LRPS method in finding series solutions for ODEs, which are difficult to solve in the analytical methods. We have succeeded in providing a solution to the general form of linear ODEs whose coefficients are analytical functions as an exact solution in a PS form. We also dealt with non-linear ODEs in the proposed technique and found approximate solutions with high accuracy. The biggest surprise is the success of the LRPS method in providing series solutions for the equations about the singular points that coincide with the exact results in some examples. Using the LRPS method, there is no longer an obstacle to obtaining a PS solution for a broad class of ODEs. In addition, the idea of the method circumvented the use of the LT to solve non-linear equations to which the LT is difficult to apply. In addition to the method's efficiency in arriving at exact solutions, LRPS is easy and fast in finding the coefficients of a series solution. There is no doubt that we can use the new method to solve other sets of equations that we did not have to deal with in previous studies, such as using it to solve partial differential equations, integral equations, integrodifferential equations, and linear or non-linear, as well as algebraic equations. We should not forget that the method has not been applied to solve differential equations with boundary conditions. All these and other topics will be under research by our research team in the next stage.

Data availability statement

The original contributions presented in the study are included in the article/Supplementary Material; further inquiries can be directed to the corresponding author.

Author contributions

All authors listed have made a substantial, direct, and intellectual contribution to the work and approved it for publication.

Conflict of interest

The authors declare that the research was conducted in the absence of any commercial or financial relationships that could be construed as a potential conflict of interest.

Publisher's note

All claims expressed in this article are solely those of the authors and do not necessarily represent those of their affiliated organizations, or those of the publisher, the editors, and the reviewers. Any product that may be evaluated in this article, or claim that may be made by its manufacturer, is not guaranteed or endorsed by the publisher.

References

1. King A, Billingham J, Otto S. *Differential equations: Linear, nonlinear, ordinary and partial*. Cambridge: Cambridge University Press (2003).

2. Huntley E, Pickering WM, Zinober ASI. The numerical solution of linear time-dependent partial differential equations by the Laplace and fast Fourier transforms. *J Comput Phys* (1978) 27(2):256–71. doi:10.1016/0021-9991(78)90008-6

3. Adomian G. A review of the decomposition method and some recent results for nonlinear equations. *Comput Maths Appl* (1991) 21(5):101–27. doi:10.1016/0898-1221(91)90220-x

4. Evans DJ, Raslan KR. The Adomian decomposition method for solving delay differential equation. *Int J Comput Maths* (2005) 82(1):49–54. doi:10.1080/00207160412331286815

5. Ibijola EA, Adegboyegun BJ, Halid OY. On Adomian Decomposition Method (ADM) for numerical solution of ordinary differential equations. *Adv Nat Appl Sci* (2008) 2(3):165–70.

6. He JH. Approximate solution of nonlinear differential equations with convolution product nonlinearities. *Comput Methods Appl Mech Eng* (1998) 167(1-2):69–73. doi:10.1016/s0045-7825(98)00109-1

7. He JH. Variational iteration method–a kind of non-linear analytical technique: Some examples. *Int J non-linear Mech* (1999) 34(4):699–708. doi:10.1016/s0020-7462(98)00048-1

8. Abbasbandy S. Numerical solution of non-linear Klein–Gordon equations by variational iteration method. *Int J Numer Methods Eng* (2007) 70(7):876–81. doi:10.1002/nme.1924

9. Anjum N, He JH, Ain QT, Tian D. Li-He's modified homotopy perturbation method for doubly-clamped electrically actuated microbeams-based microelectromechanical system. *Facta Universitatis, Ser Mech Eng* (2021) 19(4):601–12. þ. doi:10.22190/fume210112025a

10. Anjum N, He JH. Homotopy perturbation method for N/MEMS oscillators. In: *Mathematical methods in the applied sciences* (2020). þ.

11. Saadeh R. Numerical algorithm to solve a coupled system of fractional order using a novel reproducing kernel method. *Alexandria Eng J* (2021) 60(5):4583–91. doi:10.1016/j.aej.2021.03.033

12. Liao W, Zhu J, Khaliq AQ. An efficient high-order algorithm for solving systems of reaction-diffusion equations. *Numer Methods Partial Differential Equations* (2002) 18(3):340–54. doi:10.1002/num.10012

13. Abbasbandy S. Soliton solutions for the Fitzhugh–Nagumo equation with the homotopy analysis method. *Appl Math Model* (2008) 32(12):2706–14. doi:10.1016/j.apm.2007.09.019

14. Pukhov G. *Taylor transforms and their application in electrical engineering and electronics (Russian book)*. Kiev: Izdatel'stvo Naukova Dumka (1978). p. 259. p, In Russian.

15. Pukhov GE. *Differential transformations of functions and equations*. Kiev: Naukova Dumka (1980). p. 54–7. (in Russian).

16. Abbasov TEYMURAZ, Bahadir AR. The investigation of the transient regimes in the nonlinear systems by the generalized classical method. *Math Probl Eng* (2005) 2005(5):503–19. doi:10.1155/mpe.2005.503

17. Chawla M. A fourth-order tridiagonal finite difference method for general non-linear two-point boundary value problems with mixed boundary conditions. *IMA J Appl Maths* (1978) 21(1):83–93. doi:10.1093/imamat/21.1.83

18. Ascher UM, Ruuth SJ, Wetton BT. Implicit-explicit methods for time-dependent partial differential equations. *SIAM J Numer Anal* (1995) 32(3):797–823. doi:10.1137/0732037

19. Burrage K, Tian T. Predictor-corrector methods of runge--kutta type for stochastic differential equations. *SIAM J Numer Anal* (2002) 40(4):1516–37. doi:10.1137/s0036142900372677

20. Feng Z, Knobel R. Traveling waves to a Burgers–Korteweg–de Vries-type equation with higher-order nonlinearities. *J Math Anal Appl* (2007) 328(2):1435–50. doi:10.1016/j.jmaa.2006.05.085

21. Eslami M, Fathi Vajargah B, Mirzazadeh M, Biswas A. Application of first integral method to fractional partial differential equations. *Indian J Phys* (2014) 88(2):177–84. doi:10.1007/s12648-013-0401-6

22. Ascher UM, Petzold LR. *Computer methods for ordinary differential equations and differential-algebraic equations*. Philadelphia, PA: Society for Industrial and Applied Mathematics (1998). p. 61.

23. Ostrowski AM. *Solution of equations and systems of equations: Pure and applied mathematics: A series of monographs and textbooks, vol. 9*. Amsterdam: Elsevier (2016).

24. Hueso JL, Martínez E, Teruel C. Multipoint efficient iterative methods and the dynamics of Ostrowski's method. *Int J Comput Maths* (2019) 96(9):1687–701. doi:10.1080/00207160.2015.1080354

25. Li D, Zhang C. Nonlinear stability of discontinuous Galerkin methods for delay differential equations. *Appl Maths Lett* (2010) 23(4):457–61. doi:10.1016/j.aml.2009.12.003

26. Zaibin Z, Zhizhong S. A Crank-Nicolson scheme for a class of delay nonlinear parabolic differential equations. *J Numerica Methods Comput Appl* (2010) 31(2):131.

27. Zhou Y, Cui M, Lin Y. Numerical algorithm for parabolic problems with non-classical conditions. *J Comput Appl Maths* (2009) 230(2):770–80. doi:10.1016/j.cam.2009.01.012

28. Geng F, Cui M. A reproducing kernel method for solving nonlocal fractional boundary value problems. *Appl Maths Lett* (2012) 25(5):818–23. doi:10.1016/j.aml.2011.10.025

29. Khuri SA. A Laplace decomposition algorithm applied to a class of nonlinear differential equations. *J Appl Math* (2001) 1(4):141–55. doi:10.1155/s1110757x01000183

30. Kiymaz O. An algorithm for solving initial value problems using Laplace Adomian decomposition method. *Appl Math Sci* (2009) 3:1453–9.

31. Nadeem M, He JH. He–Laplace variational iteration method for solving the nonlinear equations arising in chemical kinetics and population dynamics. *J Math Chem* (2021) 59:1234–45. doi:10.1007/s10910-021-01236-4

32. Rehman S, Hussain A, Rahman JU, Anjum N, Munir T. Modified Laplace based variational iteration method for the mechanical vibrations and its applications. *acta mechanica et automatica* (2022) 16(2):98–102. þ. doi:10.2478/ama-2022-0012

33. Anjum N, He JH. Laplace transform: Making the variational iteration method easier. *Appl Maths Lett* (2019) 92:134–8. þ. doi:10.1016/j.aml.2019.01.016

34. He K, Nadeem M, Habib S, Sedighi HM, Huang D. Analytical approach for the temperature distribution in the casting-mould heterogeneous system. *Int J Numer Methods Heat Fluid flow* (2022) 32(3):1168–82. þ. doi:10.1108/hff-03-2021-0180

35. Fang J, Nadeem M, Habib M, Karim S, Wahash HA. A new iterative method for the approximate solution of klein-gordon and sine-gordon equations. *J Funct Spaces* (2022) 2022:1–9. doi:10.1155/2022/5365810þ

36. Anjum N, Suleman M, Lu D, He JH, Ramzan M. Numerical iteration for nonlinear oscillators by Elzaki transform. *J Low Frequency Noise, Vibration Active Control* (2020) 39(4):879–84. þ. doi:10.1177/1461348419873470

37. Eriqat T, El-Ajou A, Oqielat MN, Al-Zhour Z, Momani S. A new attractive analytic approach for solutions of linear and nonlinear neutral fractional pantograph equations. *Chaos, Solitons and Fractals* (2020) 138:109957. doi:10.1016/j.chaos.2020.109957

38. El-Ajou A. Adapting the Laplace transform to create solitary solutions for the nonlinear time-fractional dispersive PDEs via a new approach. *The Eur Phys J Plus* (2021) 136(2):229–2. doi:10.1140/epjp/s13360-020-01061-9

39. El-Ajou A, Al-Zhour Z. A vector series solution for a class of hyperbolic system of Caputo time-fractional partial differential equations with variable coefficients. *Front Phys* (2021) 9:525250. doi:10.3389/fphy.2021.525250

40. Burqan A, El-Ajou A, Saadeh R, Al-Smadi M. A new efficient technique using Laplace transforms and smooth expansions to construct a series solution to the time-fractional Navier-Stokes equations. *Alexandria Eng J* (2022) 61(2):1069–77. doi:10.1016/j.aej.2021.07.020

41. Oqielat MN, El-Ajou A, Al-Zhour Z, Eriqat T, Al-Smadi M. A new approach to solving fuzzy quadratic Riccati differential equations. *Int J Fuzzy Logic Intell Syst* (2022) 22(1):23–47. þ. doi:10.5391/ijfis.2022.22.1.23

42. Saadeh R, Burqan A, El-Ajou A. Reliable solutions to fractional Lane-Emden equations via Laplace transform and residual error function. *Alexandria Eng J* (2022) 61(12):10551–62. doi:10.1016/j.aej.2022.04.004

43. Salah E, Qazza A, Saadeh R, El-Ajou A. A hybrid analytical technique for solving multi-dimensional time-fractional Navier-Stokes system. *AIMS Maths* (2023) 8(1):1713–36. doi:10.3934/math.2023088

44. Alquran M, Ali M, Alshboul O. Explicit solutions to the time-fractional generalized dissipative Kawahara equation. *J Ocean Eng Sci* (2022) 1–5. doi:10.1016/j.joes.2022.02.013

45. Eriqat T, Oqielat MN, Al-Zhour Z, Khammash G, El-Ajou A, Alrabaiah H. Exact and numerical solutions of higher-order fractional partial differential equations: A new analytical method and some applicationsþ. *Pramana* (2022) 96(4):207þ. doi:10.1007/s12043-022-02446-4

46. Saadeh R, Ala'yed O, Qazza A. Analytical solution of coupled hirota–satsuma and KdV equations. *Fractal and Fractional* (2022) 6(12), 694. þdoi:10.3390/fractalfract6120694

47. Saadeh R, Qazza A, Amawi K. A new approach using integral transform to solve cancer models. *Fractal and Fractional* (2022) 6(9), 490.þdoi:10.3390/fractalfract6090490

48. El-Ajou A, Oqielat MN, Al-Zhour Z, Momani S. A class of linear non-homogenous higher order matrix fractional differential equations: Analytical solutions and new techniqueþ. *Fractional Calculus Appl Anal* (2020) 23(2), 356–77. doi:10.1515/fca-2020-0017

49. Eriqat T, Oqielat MN, Al-Zhour Z, El-Ajou A, Bataineh A. Revisited Fisher's equation and logistic system model: A new fractional approach and some modificationsþ. *Int J Dyn Control* (2022) 11, 555–63. doi:10.1007/s40435-022-01020-5

50. Nagle RK, Saff EB, Snider AD. *Fundamentals of differential equations*. United States: Pearson (2018).

51. Zill DG, Shanahan PD. *A first course in complex analysis with applications*. London: Jones & Bartlett Learning (2013).

52. Feng GQ, Niu JY. The analysis for the dynamic pull-in of a micro-electromechanical systemþ. *J Low Frequency Noise, Vibration Active Control* (2022) 146134842211455. doi:10.1177/14613484221145588

frontiers | Frontiers in Physics

TYPE Original Research
PUBLISHED 27 April 2023
DOI 10.3389/fphy.2023.1168795

OPEN ACCESS

EDITED BY
Hamid M. Sedighi,
Shahid Chamran University of Ahvaz, Iran

REVIEWED BY
Szabolcs Fischer,
Széchenyi István University, Hungary
Santanu Saha Ray,
National Institute of Technology Rourkela, India
Magaji Adamu Yunbunga,
Abubakar Tafawa Balewa University, Nigeria

*CORRESPONDENCE
Naveed Anjum,
xsnaveed@yahoo.com

RECEIVED 18 February 2023
ACCEPTED 03 April 2023
PUBLISHED 27 April 2023

CITATION
Tao H, Anjum N and Yang Y-J (2023), The Aboodh transformation-based homotopy perturbation method: new hope for fractional calculus. *Front. Phys.* 11:1168795. doi: 10.3389/fphy.2023.1168795

The Aboodh transformation-based homotopy perturbation method: new hope for fractional calculus

Huiqiang Tao[1], Naveed Anjum[2]* and Yong-Ju Yang[3]

[1]School of Mathematics and Statistics, Huanghuai University, Zhumadian, China, [2]Department of Mathematics, Government College University, Faisalabad, Pakistan, [3]School of Mathematics and Statistics, Nanyang Normal University, Nanyang, China

Fractional differential equations can model various complex problems in physics and engineering, but there is no universal method to solve fractional models precisely. This paper offers a new hope for this purpose by coupling the homotopy perturbation method with Aboodh transform. The new hybrid technique leads to a simple approach to finding an approximate solution, which converges fast to the exact one with less computing effort. An example of the fractional casting-mold system is given to elucidate the hope for fractional calculus, and this paper serves as a model for other fractional differential equations.

KEYWORDS

homotopy perturbation method, Aboodh transform, He's polynomials, fractional differential equation, two-scale fractal theory

1 Introduction

Fractional calculus has triggered much interest in both physics and mathematics [1, 2]. Traditional differential equations cannot accurately represent many physical problems, and the fractional partner can provide deeper insight into these complex physical phenomena with ease. In general, this newly developed field is for studying real-world applications in the fractal space, so most literature labeled it as the fractal–fractional calculus [3–5] or the local fractional calculus on the Cantor set [6]. A continuum medium, e.g., water or air, becomes a fractal space (porous medium) when we observe it on a molecule's scale. Any phenomena arising in molecules' perturbation have to be modeled by the fractal–fractional model [7]. As an example, we consider a nanoparticle's motion in the air, which is stochastic and difficult to be modeled by the traditional differential equation; however, if the air is considered as a fractal space on a molecule's scale, its motion is determinate and can be modeled by the fractal–fractional model. So, we need two scales for a porous medium; one is large enough so that the continuum assumption works, and the other is small enough so that the porosity can be measured, as pointed out by Ji-Huan He that "seeing with a single scale is always unbelieving" [8]. Another example is the motion of the Moon, which is naturally periodic; however, if we measure its motion at an extremely far distance, its motion becomes stochastic, and the Heisenberg-like uncertainty principle works for the Moon [9]. He and Qian showed that the fractal diffusion process in water depends on the fractal dimensions [10], and other scientists also discussed the fractional advection–reaction–diffusion process [11] and the fractal diffusion–reaction process [12]. A cocoon's air/moisture permeability and its thermal property can best be revealed by the

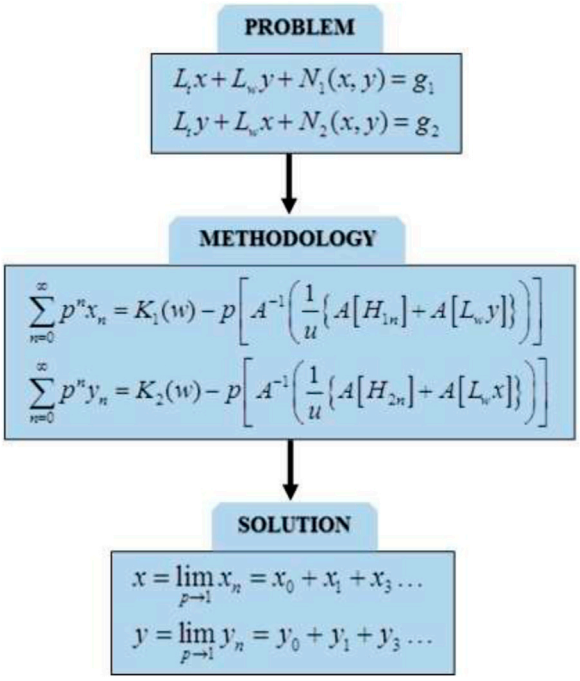

GRAPHICAL ABSTRACT

fractal–fractional model [13, 14], and the fractal micro-electromechanical systems show even more amazing properties [15–18].

Fractional calculus is a good and reliable tool for scientists and engineers but a mixed blessing for practical applications because an intractable problem arises; that is, fractional models are extremely difficult to be solved. Researchers have been racing to test various analytical methods which were originally proposed to solve traditional differential equations. Though there are many famous analytical methods in the literature, for example, the homotopy perturbation method [19–23] and its various modifications [24–26], the decomposition method [27], the variational iteration method [28–30], the exp-function method [31], and the differential transform method [32], so far, there is not a universal approach to solving exactly fractional differential equations, and this paper offers a new hope for this purpose by coupling the homotopy perturbation method [33, 34] and the Aboodh transform [35].

The homotopy perturbation method (HPM) was first proposed by Chinese mathematician Prof. Ji-Huan He in the later 1990s [33]; it is mathematically simple and physically insightful. The method is equally suitable for linear or non-linear, homogeneous or inhomogeneous, and initial and/or boundary value problems. The solution is expressed in an infinite series and typically converges to the exact solution. The HPM is now considered a matured tool for almost all kinds of problems, and many researchers have used this method for an accurate insight into the solution properties of a complex problem [36–38].

The Aboodh transform (AT) was proposed by Aboodh [35] and derived from the classical Fourier integral. This transform is now considered a simple technique for solving linear differential equations but is unable to solve non-linear ones. By coupling AT with the HPM, one has the capability to solve linear and non-linear problems, and a lot of literature works have been witnessed to utilize this coupling for solving various types of problems. Using AT–HPM, Manimegalai et al. [39] solved strongly non-linear oscillators with great success. Jani and Singh [40] found it had obvious advantages over the decomposition method, Yasmin [41] revealed the dynamic behavior of the fractional convection–reaction–diffusion process, and Jani and Singh [42] extended it to the soliton theory.

Though much work was achieved, in this study, we will show that AT–HPM is a universal tool for fractional calculus. As an example, we consider the time-fractional casting-mold system which is used in manufacturing various medical equipment, ranging from injections to the COVID-19 tool-kit [43]. The significant findings reveal that AT–HPM is an accurate and effective approach that reduces the computational work with fast convergence ratio.

2 Aboodh transform-based homotopy perturbation technique

This section is divided into two sections. In the first section, the methodology will be proposed, and the convergence of the suggested technique will be discussed in the second section.

TABLE 1 Aboodh transform of some elementary functions.

$f(t)$	1	t	t^n	e^{bt}	$\sin bt$	$\cos bt$	$\sinh bt$	$\cosh bt$
$F(u)$	$\frac{1}{u^2}$	$\frac{1}{u^3}$	$\frac{n!}{u^{n+2}}$	$\frac{1}{u^2-bu}$	$\frac{b}{u(u^2+b^2)}$	$\frac{1}{u^2+b^2}$	$\frac{b}{u(u^2-b^2)}$	$\frac{1}{u^2-b^2}$

2.1 Methodology

In this section, we give a brief introduction to the Aboodh transform [35] and homotopy perturbation method [33, 34].

If f is a continuous piecewise function of time t, then the Aboodh transform of $f(t)$ is $F(u)$ that can be expressed as follows [35]:

$$A[f(t)] = F(u) = \frac{1}{u}\int_0^\infty f(t)e^{-ut}dt,\ t \geq 0,\ k_1 \leq u \leq k_2, \tag{1}$$

where k_1 and k_2 are positive and can be finite or infinite. $f(t)$ is considered a function of the exponential order, which assures the convergence of the integrand. e^{-ut} is the kernel of the transform, and u is the transform variable. Table 1 includes the Aboodh transformation of some elementary functions helpful for this manuscript. This table can also be used for inverse Aboodh transform.

The Aboodh transform of the partial derivative of time can be obtained using the following formula:

$$A\left[\frac{\partial^n f(w,t)}{\partial t^n}\right] = u^n F(w,u) - \sum_{k=0}^{n-1}\frac{1}{u^{2-n+k}}\frac{\partial^k f(w,0)}{\partial t^k}, \tag{2}$$

where w is the independent variable. Now, suppose the general system of PDEs is expressed as

$$\begin{aligned} L_t x + L_w y + N_1(x,y) &= g_1, \\ L_t y + L_w x + N_2(x,y) &= g_2, \end{aligned} \tag{3}$$

where L is the linear operator, N_1, N_2 are the non-linear operators, x, y are the dependent variables, and g_1, g_2 are the inhomogeneous functions. We assume the initial conditions as

$$\begin{aligned} x(w,0) &= h_1(w), \\ y(w,0) &= h_2(w), \end{aligned} \tag{4}$$

where h_1 and h_2 are known functions of the independent variable w. The methodology composed of initially applying the Aboodh transform to both sides of the system of equations written in Eq. 3 and then employing the given initial conditions expressed in Eq. 4, thus yielding

$$\begin{aligned} A[L_t x] + A[L_w y] + A[N_1(x,y)] &= A[g_1], \\ A[L_t y] + A[L_w x] + A[N_2(x,y)] &= A[g_2]. \end{aligned} \tag{5}$$

By employing the differential characteristic of Aboodh transform, we can express Eq. 3 as

$$\begin{aligned} uA[x(w,t)] - \frac{x(w,0)}{u} + A[L_w y] + A[N_1(x,y)] &= A[g_1], \\ uA[y(w,t)] - \frac{y(w,0)}{u} + A[L_w x] + A[N_2(x,y)] &= A[g_2], \end{aligned} \tag{6}$$

and after using the initial conditions, we have

$$\begin{aligned} A[x(w,t)] &= \frac{h_1(w)}{u^2} - \frac{1}{u}A[L_w y] - \frac{1}{u}A[N_1(x,y)] + \frac{1}{u}A[g_1], \\ A[y(w,t)] &= \frac{h_2(w)}{u^2} - \frac{1}{u}A[L_w x] - \frac{1}{u}A[N_2(x,y)] + \frac{1}{u}A[g_2] \end{aligned}$$

or

$$\begin{aligned} x(w,t) &= K_1(w) - A^{-1}\left(\frac{1}{u}\{A[N_1(x,y)] + A[L_w y]\}\right), \\ y(w,t) &= K_2(w) - A^{-1}\left(\frac{1}{u}\{A[N_2(x,y)] + A[L_w x]\}\right), \end{aligned} \tag{7}$$

where $K_1(w)$ and $K_2(w)$ denote the terms arising from the initial condition. According to the standard homotopy perturbation method [33, 34], the solution x and y can be expanded into an infinite series as

$$x = \sum_{n=0}^{\infty} p^n x_n, \quad y = \sum_{n=0}^{\infty} p^n y_n, \tag{8}$$

where $p \in [0,1]$ is the embedding parameter. Also, the non-linear terms N_1 and N_2 can be written as

$$N_1(x,y) = \sum_{n=0}^{\infty} p^n H_{1n}(x,y), \quad N_2(x,y) = \sum_{n=0}^{\infty} p^n H_{2n}(x,y), \tag{9}$$

where H_{1n} and H_{2n} are He's polynomials [44] and can be generated by the recursive formula

$$H_n(x_0, x_1, \cdots, x_n) = \frac{1}{n!}\frac{\partial^n}{\partial p^n}\left[N\left(\sum_{i=0}^{\infty} p^i x_i\right)\right]\Bigg|_{p=0}, \quad n = 0, 1, 2, \cdots. \tag{10}$$

By substituting Eqs 7, 8 in Eq. 6, we get

$$\begin{aligned} \sum_{n=0}^{\infty} p^n x_n &= K_1(w) - p\left[A^{-1}\left(\frac{1}{u}\{A[H_{1n}] + A[L_w y]\}\right)\right], \\ \sum_{n=0}^{\infty} p^n y_n &= K_2(w) - p\left[A^{-1}\left(\frac{1}{u}\{A[H_{2n}] + A[L_w x]\}\right)\right]. \end{aligned} \tag{11}$$

Comparing the coefficients of like powers of p, we have

$$\begin{aligned} &p^0\colon\ x_0 = K_1(w), \\ &p^1\colon\ x_1 = -A^{-1}\left(\frac{1}{u}\{A[H_{10}] + A[L_w y_0]\}\right), \\ &p^2\colon\ x_2 = -A^{-1}\left(\frac{1}{u}\{A[H_{11}] + A[L_w y_1]\}\right), \\ &\vdots \end{aligned} \tag{12}$$

$$\begin{aligned} &p^0\colon\ y_0 = K_2(w), \\ &p^1\colon\ y_1 = -A^{-1}\left(\frac{1}{u}\{A[H_{20}] + A[L_w x_0]\}\right), \\ &p^2\colon\ y_2 = -A^{-1}\left(\frac{1}{u}\{A[H_{21}] + A[L_w x_1]\}\right). \\ &\vdots \end{aligned} \tag{13}$$

We can obtain the best approximation for the solution as

$$\begin{aligned} x &= \lim_{p\to 1} x_n = x_0 + x_1 + x_3 + \cdots, \\ y &= \lim_{p\to 1} y_n = y_0 + y_1 + y_3 + \cdots. \end{aligned} \tag{14}$$

2.2 Convergence analysis

To show that the series solution of the system in Eq. 14 converges to the solution of Eq. 3, we are to prove the sufficient condition of the convergence, and the following theorem will help us.

Theorem: We assume that X and Y are Banach spaces and $M\colon X \to Y$ is a non-linear contractive mapping such that

$$\forall s, s^* \in X\colon \|M(s) - M(s^*)\| \leq \lambda\|s - s^*\|, 0 < \lambda < 1.$$

Then, according to Banach's fixed point theorem, M has a unique fixed point μ, that is, $M(\mu) = \mu$. Supposing that the sequence in Eq. 14 can be written as

$$S_n = M(S_{n-1}),\ S_{n-1} = \sum_{i=0}^{n-1} S_i, n = 1, 2, 3, \cdots$$

and considering that $S_0 = s_0 \in B_r(s), where\ B_r(s) = \{s^* \in X \mid \|s^* - s\| < r\}$, we have

(i) $S_n \in B_r(s)$
(ii) $\lim_{n\to\infty} S_n = s$

Proof: (i) By the principle of mathematical induction, for $n = 1$, we have

$$\|S_1 - s\| = \|M(S_0) - M(s)\| \le \lambda\|s_0 - s\|.$$

Assuming $\|S_{n-1} - s\| \le \lambda^{n+1}\|s_0 - s\|$ as an induction hypothesis, we get

$$\|S_n - s\| = \|M(S_{n-1}) - M(s)\| \le \lambda\|S_{n-1} - s\| \le \lambda^n\|s_0 - s\|.$$

By employing the definition of $B_r(s)$, we have

$$\|S_n - s\| \le \lambda^n\|s_0 - s\| \le \lambda^n r < r \text{ which implies } S_n \in B_r(s).$$

(ii) As $\|S_n - s\| \le \lambda^n\|s_0 - s\|$ and $\lim_{n\to\infty} \lambda^n = 0$,

$$\lim_{n\to\infty} \|S_n - s\| = 0, that\ is, \lim_{n\to\infty} S_n = s.$$

Hence, the given statement is proved.

3 Numerical examples

In this section, three examples are presented to illustrate the idea explained in Section 2. First, we will study the method for a homogeneous linear system of PDEs. Second, the analytical solution will be obtained for an inhomogeneous linear system of PDEs. Finally, the inhomogeneous non-linear system of PDEs will be examined.

3.1 The system of homogeneous linear PDEs

We consider the following linear system:

$$\begin{aligned} x_t + y_w - (x + y) &= 0, \\ y_t + x_w - (x + y) &= 0, \end{aligned} \tag{15}$$

with initial conditions

$$\begin{aligned} x(w, 0) &= \sinh w, \\ y(w, 0) &= \cosh w. \end{aligned} \tag{16}$$

By employing the Aboodh transform method, we have

$$\begin{aligned} uA[x(w,t)] - \frac{x(w,0)}{u} &= -A[y_w] + A[x + y], \\ uA[y(w,t)] - \frac{y(w,0)}{u} &= -A[x_w] + A[x + y]. \end{aligned} \tag{17}$$

Using the initial conditions given in Eq. 16, we reach

$$\begin{aligned} A[x(w,t)] &= \frac{\sinh w}{u^2} - \frac{1}{u}(A[y_w] - A[x + y]), \\ A[y(w,t)] &= \frac{\cosh w}{u^2} - \frac{1}{u}(A[x_w] - A[x + y]) \end{aligned} \tag{18}$$

or

$$\begin{aligned} x(w,t) &= \sinh w - A^{-1}\left(\frac{1}{u}(A[y_w] - A[x + y])\right), \\ y(w,t) &= \cosh w - A^{-1}\left(\frac{1}{u}(A[x_w] - A[x + y])\right). \end{aligned} \tag{19}$$

The Aboodh transform-based homotopy perturbation method considers a series solution given by

$$x(w,t) = \sum_{n=0}^{\infty} p^n x_n(w,t),\ \ y(w,t) = \sum_{n=0}^{\infty} p^n y_n(w,t). \tag{20}$$

By using the aforestated equation, the system of equations in Eq. 19 gets the form

$$\begin{aligned} \sum_{n=0}^{\infty} p^n x_n(w,t) &= \sinh w - pH_1(x_n, y_n) = \sinh w \\ &\quad - pA^{-1}\left(\frac{1}{u}A\left[\left(\sum_{n=0}^{\infty} p^n y_n(w,t)\right)_w - \left(\sum_{n=0}^{\infty} p^n x_n(w,t) + \sum_{n=0}^{\infty} p^n y_n(w,t)\right)\right]\right), \\ \sum_{n=0}^{\infty} p^n y_n(w,t) &= \cosh w - pH_2(x_n, y_n) = \cosh w \\ &\quad - pA^{-1}\left(\frac{1}{u}A\left[\left(\sum_{n=0}^{\infty} p^n x_n(w,t)\right)_w - \left(\sum_{n=0}^{\infty} p^n x_n(w,t) + \sum_{n=0}^{\infty} p^n y_n(w,t)\right)\right]\right). \end{aligned} \tag{21}$$

By comparing like powers of p from the aforestated equation, we obtain

$$p^0: \begin{cases} x_0(w,t) = \sinh w \\ y_0(w,t) = \cosh w, \end{cases} \tag{22}$$

$$p^1: \begin{cases} x_0(w,t) = t\cosh w \\ y_0(w,t) = t\sinh w, \end{cases} \tag{23}$$

$$p^2: \begin{cases} x_0(w,t) = \dfrac{t^2}{2}\sinh w \\ y_0(w,t) = \dfrac{t^2}{2}\cosh w, \end{cases} \tag{24}$$

$$\vdots$$

$$\vdots$$

Hence, the series solution by using Eq. 14 can be expressed as

$$\begin{aligned} x(w,t) &= \left(1 + \frac{t^2}{2!} + \frac{t^4}{4!} + \cdots\right)\sinh w + \left(t + \frac{t^3}{3!} + \frac{t^5}{5!} + \cdots\right)\cosh w, \\ y(w,t) &= \left(1 + \frac{t^2}{2!} + \frac{t^4}{4!} + \cdots\right)\cosh w + \left(t + \frac{t^3}{3!} + \frac{t^5}{5!} + \cdots\right)\sinh w \end{aligned} \tag{22a}$$

or in a closed form as

$$\begin{aligned} x(w,t) &= \sinh(w + t), \\ y(w,t) &= \cosh(w + t), \end{aligned} \tag{23a}$$

which is the exact solution of Eq. 15.

3.2 The system of inhomogeneous linear PDEs

Suppose the following inhomogeneous linear system of PDEs:

$$\begin{aligned} x_t - y_w - (x-y) &= -2, \\ y_t + x_w - (x-y) &= -2, \end{aligned} \tag{24a}$$

with initial conditions

$$\begin{aligned} x(w,0) &= 1 + e^w, \\ y(w,0) &= -1 + e^w. \end{aligned} \tag{25}$$

Applying the Aboodh transform on each side of the equations in Eq. 24 and then putting on the given initial conditions, we obtain

$$\begin{aligned} A[x(w,t)] &= \frac{1+e^w}{u^2} - \frac{2}{u^3} + \frac{1}{u}\left(A[y_w] + A[(x-y)]\right), \\ A[y(w,t)] &= \frac{-1+e^w}{u^2} - \frac{2}{u^3} + \frac{1}{u}\left(A[(x-y)] - A[x_w]\right) \end{aligned} \tag{26}$$

or

$$\begin{aligned} x(w,t) &= 1 + e^w - 2t + A^{-1}\left(\frac{1}{u}\left(A[y_w] + A[(x-y)]\right)\right), \\ y(w,t) &= -1 + e^w - 2t + A^{-1}\left(\frac{1}{u}\left(A[(x-y)] - A[x_w]\right)\right). \end{aligned} \tag{27}$$

By using the Aboodh transform-based homotopy perturbation method, the series solution is expressed by

$$x(w,t) = \sum_{n=0}^{\infty} p^n x_n(w,t), \quad y(w,t) = \sum_{n=0}^{\infty} p^n y_n(w,t). \tag{28}$$

The system of equations in Eq. 27 gets the following form after employing the aforestated equation:

$$\begin{aligned} \sum_{n=0}^{\infty} p^n x_n(w,t) &= 1 + e^w - 2t + p\left\{A^{-1}\left(\frac{1}{u}A\left[\left(\sum_{n=0}^{\infty} p^n y_n(w,t)\right)_w\right.\right.\right. \\ &\quad \left.\left.\left. + \left(\sum_{n=0}^{\infty} p^n x_n(w,t) - \sum_{n=0}^{\infty} p^n y_n(w,t)\right)\right]\right)\right\}, \\ \sum_{n=0}^{\infty} p^n y_n(w,t) &= -1 + e^w - 2t \\ &\quad + p\left\{A^{-1}\left(\frac{1}{u}A\left[\left(\sum_{n=0}^{\infty} p^n x_n(w,t) - \sum_{n=0}^{\infty} p^n y_n(w,t)\right)\right.\right.\right. \\ &\quad \left.\left.\left. - \left(\sum_{n=0}^{\infty} p^n y_n(w,t)\right)_w\right]\right)\right\}. \end{aligned} \tag{29}$$

By comparing the coefficient of like powers of p, we have

$$p^0: \begin{cases} x_0(w,t) = 1 + e^w - 2t \\ y_0(w,t) = -1 + e^w - 2t, \end{cases} \tag{30}$$

$$p^1: \begin{cases} x_1(w,t) = te^w + 2t \\ y_1(w,t) = -te^w + 2t, \end{cases} \tag{31}$$

$$p^2: \begin{cases} x_2(w,t) = \dfrac{t^2}{2!}e^w \\ y_2(w,t) = \dfrac{t^2}{2!}e^w, \end{cases} \tag{32}$$

$$p^3: \begin{cases} x_3(w,t) = \dfrac{t^3}{3!}e^w \\ y_3(w,t) = -\dfrac{t^3}{3!}e^w, \end{cases} \tag{33}$$

$$\vdots$$

Therefore, the solution in the form of an infinite series by using Eq. 14 can be expressed as

$$\begin{aligned} x(w,t) &= 1 + e^w\left(1 + t + \frac{t^2}{2!} + \frac{t^3}{3!} + \cdots\right), \\ y(w,t) &= -1 + e^w\left(1 - t + \frac{t^2}{2!} - \frac{t^3}{3!} + \cdots\right) \end{aligned} \tag{34}$$

or in its convergent form as

$$\begin{aligned} x(w,t) &= 1 + e^{w+t}, \\ y(w,t) &= -1 + e^{w-t}, \end{aligned} \tag{35}$$

which is the exact solution of Eq. 24.

3.3 The system of inhomogeneous non-linear PDEs

Suppose the following inhomogeneous non-linear system of PDEs:

$$\begin{aligned} x_t + x_w y + x &= 1, \\ y_t - x y_w + y &= 1, \end{aligned} \tag{36}$$

with initial conditions

$$\begin{aligned} x(w,0) &= e^w, \\ y(w,0) &= e^{-w}. \end{aligned} \tag{37}$$

Employing the Aboodh transform on each side of the equations in Eq. 36 and then applying the given initial conditions give

$$\begin{aligned} x(w,u) &= \frac{e^w}{u^2} + \frac{1}{u^3} - \frac{1}{u}\left(A[xy_w] + A[x]\right), \\ y(w,u) &= \frac{e^{-w}}{u^2} + \frac{1}{u^3} + \frac{1}{u}\left(A[xy_w] + A[y]\right). \end{aligned} \tag{38}$$

Taking the inverse Aboodh transform on each side, we obtain

$$\begin{aligned} x(w,t) &= e^w + t - A^{-1}\left(\frac{1}{u}\left(A[xy_w] + A[x]\right)\right), \\ y(w,t) &= e^{-w} + t + A^{-1}\left(\frac{1}{u}\left(A[xy_w] + A[y]\right)\right). \end{aligned} \tag{39}$$

According to the Aboodh transform-based homotopy perturbation method, the solution functions $x(w,t)$ and $y(w,t)$ are series solutions, and inserting these series into both sides of each equation of the system yields

$$\begin{aligned} \sum_{n=0}^{\infty} p^n x_n(w,t) &= e^w + t - p\left\{A^{-1}\left(\frac{1}{u}\left(A\left[\sum_{n=0}^{\infty} p^n H_{1n}(x,y)\right]\right) + \sum_{n=0}^{\infty} p^n x_n(w,t)\right)\right\}, \\ \sum_{n=0}^{\infty} p^n y_n(w,t) &= e^{-w} + t + p\left\{A^{-1}\left(\frac{1}{u}\left(A\left[\sum_{n=0}^{\infty} p^n H_{2n}(x,y)\right]\right) + \sum_{n=0}^{\infty} p^n y_n(w,t)\right)\right\}, \end{aligned} \tag{40}$$

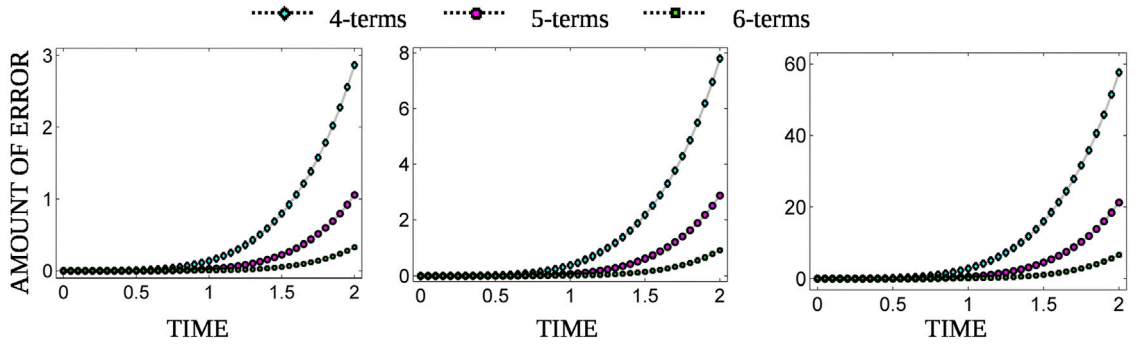

FIGURE 1
Error estimations for the casting process at $\beta = 1$ and $x = 0.5, 1, 2$.

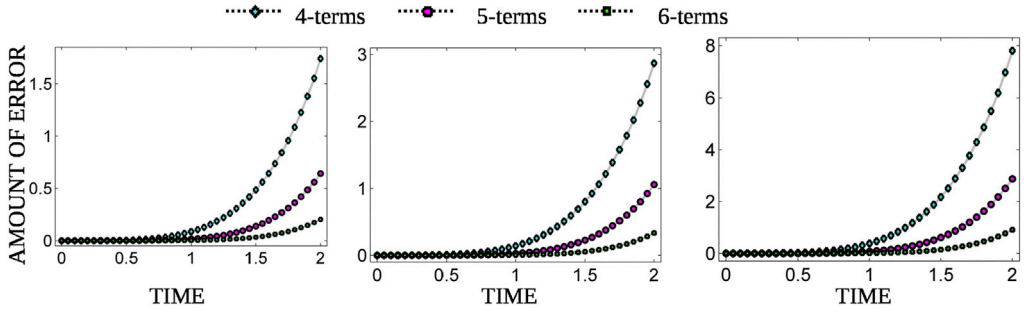

FIGURE 2
Error estimations for the molding process at $\beta = 1$ and $x = 0.5, 1, 2$.

where the non-linear terms $x_w y$ and $x y_w$ are denoted by He's polynomials $H_{1n}(x, y)$ and $H_{2n}(x, y)$, respectively. A few He's polynomials are

$$\begin{aligned} H_{10}(x,y) &= y_0 x_{0w}, \\ H_{11}(x,y) &= y_1 x_{0w} + y_0 x_{1w}, \\ H_{12}(x,y) &= y_2 x_{0w} + y_1 x_{1w} + y_0 x_{2w}, \\ &\vdots \\ &\vdots \end{aligned} \tag{41}$$

$$\begin{aligned} H_{20}(x,y) &= x_0 y_{0w}, \\ H_{21}(x,y) &= x_1 y_{0w} + x_0 y_{1w}, \\ H_{22}(x,y) &= x_2 y_{0w} + x_1 y_{1w} + x_0 y_{2w}, \\ &\vdots \\ &\vdots \end{aligned} \tag{42}$$

By comparing the coefficient of like powers of p, we have

$$p^0: \begin{cases} x_0(w,t) = e^w + t \\ y_0(w,t) = e^{-w} + t, \end{cases} \tag{43}$$

$$p^1: \begin{cases} x_1(w,t) = -\left(t + \dfrac{t^2}{2!} + te^w + \dfrac{t^2}{2!}e^w\right) \\ y_1(w,t) = -\left(t + \dfrac{t^2}{2!} + te^{-w} + \dfrac{t^2}{2!}e^{-w}\right) \end{cases}, \tag{44}$$

$$p^2: \begin{cases} x_2(w,t) = \dfrac{t^2}{2!} + t^2 e^w \\ y_2(w,t) = \dfrac{t^2}{2!} + t^2 e^{-w}, \end{cases} \tag{45}$$

$$\vdots$$
$$\vdots$$

Therefore, the solution in the form of an infinite series by using Eq. 14 can be expressed as

$$\begin{aligned} x(w,t) &= e^w\left(1 - t + \frac{t^2}{2!} - \frac{t^3}{3!} + \cdots\right), \\ y(w,t) &= e^{-w}\left(1 + t + \frac{t^2}{2!} + \frac{t^3}{3!} + \cdots\right) \end{aligned} \tag{46}$$

or in its convergent form as

$$\begin{aligned} x(w,t) &= e^{w-t}, \\ y(w,t) &= e^{-w+t}, \end{aligned} \tag{47}$$

which is the exact solution of Eq. 36.

4 Time-fractional casting-mold system

Now, we turn back to a time-fractional casting-mold system which models the temperature distribution in the casting and molding processes. For this, two heat conduction equations are used with initial and Dirichlet boundary conditions [45]. The mathematical model is depicted as follows:

$$\begin{aligned} \frac{\partial^{\beta} Z(t,x)}{\partial t^{\beta}} &= a\frac{\partial^2 Z(t,x)}{\partial x^2}, \\ \frac{\partial^{\beta} N(t,x)}{\partial t^{\beta}} &= b\frac{\partial^2 N(t,x)}{\partial x^2}, \end{aligned} \tag{48}$$

where a, b are parameters, Z, N are functions of time t and space x that represent the temperature on casting and molding plates, respectively, and β is the fractal dimension. For more details on the modeling aspect of the aforementioned model, readers can see [45].

It is necessary to point out that Eq. 48 was originally studied in [45], where the series solution was presented and no closed-form solution was formulated. Our aim here is to overcome the main shortcomings in [45] and to offer a totally new hope for numerical approximation. To this end, applying the Aboodh transform in the aforementioned system, we have

$$\begin{aligned} A[Z(t,x)] &= \frac{1}{u^{\beta}}\left(\sum_{k=0}^{m-1}\frac{Z^{(k)}(0,x)}{u^{2-\beta+k}} + A\left[a\frac{\partial^2 Z(t,x)}{\partial x^2}\right]\right), \\ A[N(t,x)] &= \frac{1}{u^{\beta}}\left(\sum_{k=0}^{m-1}\frac{N^{(k)}(0,x)}{u^{2-\beta+k}} + A\left[b\frac{\partial^2 N(t,x)}{\partial x^2}\right]\right). \end{aligned} \tag{49}$$

Now, by inverse Aboodh transformation, we obtain

$$\begin{aligned} Z(t,x) &= A^{-1}\left[\frac{1}{u^{\beta}}\left(\sum_{k=0}^{m-1}\frac{Z^{(k)}(0,x)}{u^{2-\beta+k}} + A\left[a\frac{\partial^2 Z(t,x)}{\partial x^2}\right]\right)\right], \\ N(t,x) &= A^{-1}\left[\frac{1}{u^{\beta}}\left(\sum_{k=0}^{m-1}\frac{N^{(k)}(0,x)}{u^{2-\beta+k}} + A\left[b\frac{\partial^2 N(t,x)}{\partial x^2}\right]\right)\right], \end{aligned} \tag{50}$$

which can further be written as

$$\begin{aligned} Z(t,x) &= Z(0,x) + A^{-1}\left[\frac{1}{u^{\beta}}\left(A\left[a\frac{\partial^2 Z(t,x)}{\partial x^2}\right]\right)\right], \\ N(t,x) &= N(0,x) + A^{-1}\left[\frac{1}{u^{\beta}}\left(A\left[b\frac{\partial^2 N(t,x)}{\partial x^2}\right]\right)\right]. \end{aligned} \tag{51}$$

According to the standard HPM [33, 34], the solution Z and N can be expanded into a finite series as

$$Z = \sum_{m=0}^{\infty} p^m Z_m, \quad N = \sum_{m=0}^{\infty} p^m N_m. \tag{52}$$

By substituting Eq. 52 in Eq. 51, the solution can be written as

$$\begin{aligned} \sum_{m=0}^{\infty} p^m Z_m &= Z(0,x) + p\left(A^{-1}\left[\frac{1}{u^{\beta}}\left(A\left[a\frac{\partial^2 Z(t,x)}{\partial x^2}\right]\right)\right]\right), \\ \sum_{m=0}^{\infty} p^m N_m &= N(0,x) + p\left(A^{-1}\left[\frac{1}{u^{\beta}}\left(A\left[a\frac{\partial^2 Z(t,x)}{\partial x^2}\right]\right)\right]\right). \end{aligned} \tag{53}$$

Equating coefficients of powers of p, we yield the following:

$$p^0: \begin{cases} Z_0(t,x) = Z(0,x) \\ N_0(t,x) = N(0,x), \end{cases} \tag{54}$$

$$p^1: \begin{cases} Z_1(t,x) = A^{-1}\left[\frac{1}{u^{\beta}}A(aZ_0)\right] \\ N_1(t,x) = A^{-1}\left[\frac{1}{u^{\beta}}A(bN_0)\right], \end{cases} \tag{55}$$

$$p^2: \begin{cases} Z_2(t,x) = A^{-1}\left[\frac{1}{u^{\beta}}A(aZ_1)\right] \\ N_2(t,x) = A^{-1}\left[\frac{1}{u^{\beta}}A(bN_1)\right], \end{cases} \tag{56}$$

$$\vdots \qquad \vdots$$

The approximate solution can be obtained as

$$\begin{aligned} Z &= Z_0 + Z_1 + Z_2 + \cdots, \\ N &= N_0 + N_1 + N_2 + \cdots. \end{aligned} \tag{57}$$

4.1 Example

We consider the system expressed in Eq. 48 for the case $a = 1, b = 1, Z(0,x) = e^{2x}, N(0,x) = e^{x}$. By utilizing Eqs 54–56, we have

$$\begin{aligned} Z_0 &= e^{2x}, \quad N_0 = e^{x}, \\ Z_1 &= \frac{e^{2x}t^{\beta}}{\Gamma(1+\beta)}, \quad N_1 = \frac{e^{x}t^{\beta}}{\Gamma(1+\beta)}, \\ Z_2 &= \frac{e^{2x}t^{2\beta}}{\Gamma(1+2\beta)}, \quad N_2 = \frac{e^{x}t^{2\beta}}{\Gamma(1+2\beta)}, \\ Z_3 &= \frac{e^{2x}t^{3\beta}}{\Gamma(1+3\beta)}, \quad N_3 = \frac{e^{x}t^{3\beta}}{\Gamma(1+3\beta)}, \\ &\vdots \qquad\qquad \vdots \end{aligned}$$

By employing Eq. 57, the solution can be written as

$$\begin{aligned} Z(t,x) &= e^{2x} + \frac{e^{2x}t^{\beta}}{\Gamma(1+\beta)} + \frac{e^{2x}t^{2\beta}}{\Gamma(1+2\beta)} + \frac{e^{2x}t^{3\beta}}{\Gamma(1+3\beta)} + \cdots, \\ N(t,x) &= e^{x} + \frac{e^{x}t^{\beta}}{\Gamma(1+\beta)} + \frac{e^{x}t^{2\beta}}{\Gamma(1+2\beta)} + \frac{e^{x}t^{3\beta}}{\Gamma(1+3\beta)} + \cdots. \end{aligned} \tag{58}$$

The expressions are similar to those obtained by the fractional complex transform [46–49]. In the closed form, we obtain

$$Z(t,x) = \sum_{k=0}^{n} \frac{e^{2x}t^{k\beta}}{\Gamma(1+k\beta)} = e^{2x}E_{\beta}\left(t^{\beta}\right),$$
$$N(t,x) = \sum_{k=0}^{n} \frac{e^{x}t^{k\beta}}{\Gamma(1+k\beta)} = e^{x}E_{\beta}\left(t^{\beta}\right), \tag{59}$$

where $E_{\beta}(t^{\beta})$ is the Mittag-Leffler function [50]. One can check that Eq. 59 is an exact solution of Eq. 48 for the said parameters.

4.2 Results and discussion

This section is devoted to test the applicability and validity of the suggested technique for the time-fractional casting-mold system over the series-based solution of the same model.

Figures 1, 2 present the errors of the series solutions obtained by the HPM [45] for the fractal dimension $\beta = 1$. It is observed that for all the parameters and for both casting and molding processes, the errors grow exponentially for the case of a series solution [45] and can be reduced by adding more terms in the solution. On the other hand, the suggested solution has the exact solution, and there is no chance of error even for a larger range of t. Therefore, based on these findings, we can say that the proposed technique is more effective than the previous method [45].

5 Conclusion

The Aboodh transform-based homotopy perturbation method is successfully employed to solve traditional differential equations and fractional differential equations successfully. This approach has been shown to have the potential to solve both linear and non-linear problems. For a linear system, the exact solution is predicted, while for a non-linear system, with the help of He's polynomials, a series solution is obtained, which converges fast to the exact one. So, the method pushes the progress of non-linear science and will make a "big change" to increase the number of practical applications, and this paper serves as a model for other applications.

Data availability statement

The original contributions presented in the study are included in the article/Supplementary Materials; further inquiries can be directed to the corresponding author.

Author contributions

Conceptualization: HT and NA; methodology: NA and YY; validation: NA and YY; writing—original draft preparation: HT and YY; writing—review and editing: HT, NA, and YY; supervision: HT and YY; and funding acquisition: YY. All authors read and agreed to the published version of the manuscript.

Funding

The study was supported by the Natural Science Foundation of Henan Province (No. 222300420507); National Natural Science Foundation of China (No. 12171193), Key Scientific Research Project of High Education Institutions of Henan Province (No. 23A110019), Science and Technology Research Projects of Henan Province (No. 182102110292), Basic and Frontier Technology Research Project of Henan Province (Nos. 12300410398 and 132300410084), and Zhumadian Key Laboratory of Statistical Computing and Data Modeling [No. (2022)12].

Conflict of interest

The authors declare that the research was conducted in the absence of any commercial or financial relationships that could be construed as a potential conflict of interest.

Publisher's note

All claims expressed in this article are solely those of the authors and do not necessarily represent those of their affiliated organizations, or those of the publisher, the editors, and the reviewers. Any product that may be evaluated in this article, or claim that may be made by its manufacturer, is not guaranteed or endorsed by the publisher.

References

1. Hong BJ. Exact solutions for the conformable fractional coupled nonlinear Schrodinger equations with variable coefficients. *J Low Frequency Noise, Vibration Active Control* (2023) 146134842211354. doi:10.1177/14613484221135478

2. He JH, He CH, Saeed T. A fractal modification of Chen-Lee-Liu equation and its fractal variational principle. *Int J Mode Phys B* (2021) 35(21):2150214. doi:10.1142/s0217979221502143

3. Wang KL, Wei CF. Fractal soliton solutions for the fractal-fractional shallow water wave equation arising in ocean engineering. *Alexandria Eng J* (2023) 65(2023):859–65. doi:10.1016/j.aej.2022.10.024

4. Feng GQ, Niu JY. An analytical solution of the fractal toda oscillator. *Results Phys* (2023) 44:106208. doi:10.1016/j.rinp.2023.106208

5. He JH, Qie N, He CH. Solitary waves travelling along an unsmooth boundary. *Results Phys* (2021) 24:104104. doi:10.1016/j.rinp.2021.104104

6. Yang XJ, Srivastava HM, He JH, Baleanu D. Cantor-type cylindrical-coordinate method for differential equations with local fractional derivatives. *Phys Lett A* (2013) 377(28-30):1696–700. doi:10.1016/j.physleta.2013.04.012

7. He JH. Fractal calculus and its geometrical explanation. *Results Phys* (2018) 10: 272–6. doi:10.1016/j.rinp.2018.06.011

8. He JH. Seeing with a single scale is always unbelieving: From magic to two-scale fractal. *Therm Sci* (2021) 25(2):1217–9. doi:10.2298/tsci2102217h

9. He JH. Frontier of modern textile engineering and short remarks on some topics in physics. *Int J Nonlinear Sci Numer Simulation* (2010) 11(7):555–63. doi:10.1515/ijnsns.2010.11.7.555

10. He JH, Qian MY. A fractal approach to the diffusion process of red ink in a saline water. *Therm Sci* (2022) 26(3B):2447–51. doi:10.2298/tsci2203447h

11. Dai DD, Ban TT, Wang YL, Zhang W. The piecewise reproducing kernel method for the time variable fractional order advection-reaction-diffusion equations. *Therm Sci* (2021) 25(2B):1261–8. doi:10.2298/tsci200302021d

12. Lin L, Qiao Y. Fractal diffusion-reaction model for a porous electrode. *Therm Sci* (2021) 25(2):1305–11. doi:10.2298/tsci191212026l

13. Liu FJ, Zhang T, He CH, Tian D. Thermal oscillation arising in a heat shock of a porous hierarchy and its application. *Facta Universitatis Ser Mech Eng* (2022) 20(3): 633–45. doi:10.22190/fume210317054l

14. Xue RJ, Liu FJ. A Fractional model and its application to heat prevention coating with cocoon-like hierarchy. *Therm Sci* (2022) 26(3):2493–8. doi:10.2298/tsci2203493x

15. Tian D, Ain QT, Anjum N, He CH, Cheng B. Fractal N/MEMS: From pull-in instability to pull-in stability. *Fractals* (2021) 29:2150030. doi:10.1142/s0218348x21500304

16. Tian D, He CH. A fractal micro-electromechanical system and its pull-in stability. *J Low Frequency Noise Vibration Active Control* (2021) 40(3):1380–6. doi:10.1177/1461348420984041

17. He JH, Yang Q, He CH, Li HB, Buhe E. Pull-in stability of a fractal MEMS system and its pull-in plateau. *Fractals* (2023) 30. doi:10.1142/S0218348X22501857

18. He CH. A variational principle for a fractal nano/microelectromechanical (N/MEMS) system. *Int J Numer Methods Heat Fluid Flow* (2023) 33(1):351–9. doi:10.1108/hff-03-2022-0191

19. Anjum N, He JH. Higher-order homotopy perturbation method for conservative nonlinear oscillators generally and microelectromechanical systems' oscillators particularly. *Int J Mod Phys B* (2020) 34:2050313. doi:10.1142/S0217979220503130

20. He CH, El-Dib YO. A heuristic review on the homotopy perturbation method for non-conservative oscillators. *J Low Frequency Noise, Vibration Active Control* (2022) 41(2):572–603. doi:10.1177/14613484211059264

21. Anjum N, He JH. Homotopy perturbation method for N/MEMS oscillators. *Math Methods Appl Sci* (2020). doi:10.1002/mma.6583

22. He JH, Jiao ML, He CH. Homotopy perturbation method for fractal Duffing oscillator with arbitrary conditions. *Fractals* (2023) 30. doi:10.1142/S0218348X22501651

23. He JH, Moatimid GM, Zekry MH. Forced nonlinear oscillator in a fractal space. *Facta Universitatis Ser Mech Eng* (2022) 20(1):001–20. doi:10.22190/fume220118004h

24. Li XX, He CH (2019). Homotopy perturbation method coupled with the enhanced perturbation method, *J Low Frequency Noise Vibration Active Control* 38, þ1399–403. doi:10.1177/1461348418800554

25. Anjum N, He JH, Ain QT, Tian D. Li-He's modified homotopy perturbation method for doubly-clamped electrically actuated microbeams-based microelectromechanical system. *Facta Universitatis Ser Mech Eng* (2021) 19(4):601–12. doi:10.22190/fume210112025a

26. He JH, El-Dib YO. The enhanced homotopy perturbation method for axial vibration of strings. *Facta Universitatis Ser Mech Eng* (2021) 19(4):735–50. doi:10.22190/fume210125033h

27. Wazwaz AM. The decomposition method applied to systems of partial differential equations and to the reaction–diffusion Brusselator model. *Appl Math Comput* (2000) 110:251–64. doi:10.1016/s0096-3003(99)00131-9

28. Wang SQ, He JH. Variational iteration method for solving integro-differential equations. *Phys Lett A* (2007) 367(3):188–91. doi:10.1016/j.physleta.2007.02.049

29. Wang SQ. A variational approach to nonlinear two-point boundary value problems. *Comput Math Appl* (2009) 58(11):2452–5. doi:10.1016/j.camwa.2009.03.050

30. Shen YY, Huang XX, Kwak K, Yang B, Wang S. Subcarrier-pairing-based resource optimization for OFDM wireless powered relay transmissions with time switching scheme. *IEEE Trans Signal Process* (2016) 65(5):1130–45. doi:10.1109/tsp.2016.2628351

31. Chen QL, Sun ZQ. The exact solution of the non-linear Schrodinger equation by the exp-function method. *Therm Sci* (2021) 25(3B):2057–62. doi:10.2298/tsci200301088c

32. Güzel N, Kurulay M. Solution of shiff systems by using differential transform method. *Journal of Science and Technology of Dumlupinar University* (2008) 16:49–60.

33. He JH. Homotopy perturbation technique. *Comp Methods Appl Mech Eng* (1999) 178:257–62. doi:10.1016/s0045-7825(99)00018-3

34. He JH, He CH, Alsolami AA. A good initial guess for approximating nonlinear oscillators by the homotopy perturbation method. *Facta Universitatis, Ser Mech Eng* (2023). doi:10.22190/FUME230108006H

35. Aboodh KS. Application of new transform "Aboodh transform" to partial differential equations. *Glob J Pure Appl Math* (2014) 10(2):249–54.

36. Peker HA, Cuha FA. Application of Kashuri Fundo transform and homotopy perturbation methods to fractional heat transfer and porous media equations. *Therm Sci* (2022) 26(4):2877–84. doi:10.2298/tsci2204877p

37. Anjum N, He JH. Two modifications of the homotopy perturbation method for nonlinear oscillators. *J Appl Comput Mech* (2020) 2020:2482. doi:10.22055/JACM.2020.34850.2482

38. Nadeem M, Li FQ. He-Laplace method for nonlinear vibration systems and nonlinear wave equations. *J Low Frequency Noise, Vibration Active Control* (2019) 38(3-4):1060–74. doi:10.1177/1461348418818973

39. Manimegalai K, Zephania C F S, Bera PK, Bera P, Das SK, Sil T. Study of strongly nonlinear oscillators using the Aboodh transform and the homotopy perturbation method. *Eur Phys J Plus* (2019) 134:462–71. doi:10.1140/epjp/i2019-12824-6

40. Jani HP, Singh TR. Aboodh transform homotopy perturbation method for solving fractional-order Newell-Whitehead-Segel equation. *Math Methods Appl Sci* (2022). doi:10.1002/mma.8886

41. Yasmin H. Application of Aboodh homotopy perturbation transform method for fractional-order convection–reaction–diffusion equation within caputo and atangana–baleanu operators. *Symmetry* (2023) 15(2):453. doi:10.3390/sym15020453

42. Jani HP, Singh TR. A robust analytical method for regularized long wave equations. *Iranian J Sci Technol Trans A: Sci* (2022) 46(6):1667–79. doi:10.1007/s40995-022-01380-9

43. Xu RH, Yang LB, Qin Z. Design, manufacture, and testing of customized sterilizable respirator. *J Mech Behav Biomed Mater* (2022) 131:105248. doi:10.1016/j.jmbbm.2022.105248

44. Ghorbani A. Beyond adomian polynomials: He polynomials. *Chaos Solitons Fractals* (2009) 39:1486–92. doi:10.1016/j.chaos.2007.06.034

45. Luo XK, Nadeem M, Asjad MI, Abdo MS. A computational approach for the calculation of temperature distribution in casting-mould heterogeneous system with fractional order. *Comput Math Methods Med* (2022) 2022:1–10. doi:10.1155/2022/3648277

46. Li ZB, He JH. Fractional complex transform for fractional differential equations. *Math Comput Appl* (2010) 15(5):970–3. doi:10.3390/mca15050970

47. He JH, Elagan SK, Li ZB. Geometrical explanation of the fractional complex transform and derivative chain rule for fractional calculus. *Phys Lett A* (2012) 376(4): 257–9. doi:10.1016/j.physleta.2011.11.030

48. Ain QT, He JH, Anjum N, Ali M. The fractional complex transform: A novel approach to the time-fractional schrödinger equation. *Fractals* (2021) 28(7):2050141. doi:10.1142/s0218348x20501418

49. He JH, El-Dib YO. A tutorial introduction to the two-scale fractal calculus and its application to the fractal Zhiber-Shabat Oscillator. *Fractals* (2021) 29:2150268. doi:10.1142/s0218348x21502686

50. Haubold HJ, Mathai AM, Saxena RK. Mittag-leffler functions and their applications. *J Appl Math* (2011) 2011:1–51. doi:10.1155/2011/298628

10.3389/fphy.2023.1168795

Nomenclature

f	continuous piecewise function
A	Aboodh transform operator
w	independent variable
L	Linear operator
x, y	dependent variable
p	purturbation parameter
A^{-1}	inverse Aboodh transform operator
M	mapping from X to Y
λ	parameter
Z	temperature at casting plate
$E_\beta(.)$	Mittag-Leffler function
β	fractal dimension
t	time
u	transformed variable
g_1, g_2	functions of independent variables
N_1, N_2	Nonlinear operators
K_1, K_2	functions of variable w
H	He's polynomials
X, Y	Banach spaces
μ	fixed point
s, s^*	elements of Banach space
N	temperature at molding plate
$\Gamma(.)$	Gamma function
a, b	parameters of casting and molding

frontiers | Frontiers in Physics

TYPE Original Research
PUBLISHED 17 May 2023
DOI 10.3389/fphy.2023.1185846

OPEN ACCESS

EDITED BY
Ji-Huan He,
Soochow University, China

REVIEWED BY
Ying Wang,
Xi'an University of Architecture and Technology, China
Kangle Wang,
Henan Polytechnic University, China
Baojian Hong,
Nanjing Institute of Technology (NJIT), China

*CORRESPONDENCE
Wenbo Wang,
wenbowangmath@ynu.edu.cn

RECEIVED 14 March 2023
ACCEPTED 02 May 2023
PUBLISHED 17 May 2023

CITATION
Li G, Qiu C, Cheng B and Wang W (2023), On the asymptotically cubic generalized quasilinear Schrödinger equations with a Kirchhoff-type perturbation. *Front. Phys.* 11:1185846. doi: 10.3389/fphy.2023.1185846

On the asymptotically cubic generalized quasilinear Schrödinger equations with a Kirchhoff-type perturbation

Guofa Li[1], Chong Qiu[2], Bitao Cheng[1] and Wenbo Wang[3]*

[1]Key Laboratory of Analytical Mathematics and Intelligent Computing for Yunnan Provincial, Department of Education and College of Mathematics and Statistics, Qujing Normal University, Qujing, China, [2]Faculty of Mathematics and Physics, Huaiyin Institute of Technology, Huaian, China, [3]Department of Mathematics and Statistics, Yunnan University, Kunming, China

In this paper, we consider the non-existence and existence of solutions for a generalized quasilinear Schrödinger equation with a Kirchhoff-type perturbation. When the non-linearity $h(u)$ shows critical or supercritical growth at infinity, the non-existence result for a quasilinear Schrödinger equation is proved via the Pohožaev identity. If $h(u)$ shows asymptotically cubic growth at infinity, the existence of positive radial solutions for the quasilinear Schrödinger equation is obtained when b is large or equal to 0 and b is equal to 0 by the variational methods. Moreover, some properties are established as the parameter b tends to be 0.

KEYWORDS

quasilinear Schrödinger equations, Kirchhoff-type perturbation, asymptotically cubic growth, non-existence, positive solutions

1 Introduction

The Schrödinger equation [1] is of paramount importance in physics, and there are many modifications in literature, for example, the Chen–Lee–Liu equation [2] and stochastic Schrödinger equation [3]. However, the generalized quasilinear Schrödinger equation with a Kirchhoff-type perturbation was rarely studied in literature, which can be written as

$$\left(1+b\int_{\mathbb{R}^3} g^2(u)|\nabla u|^2dx\right)\left[-\operatorname{div}\left(g^2(u)\nabla u\right)+g(u)g'(u)|\nabla u|^2\right]+V(x)u=h(u), \quad (1.1)$$

where $x\in\mathbb{R}^3, b\geq 0, V\colon \mathbb{R}^3\to\mathbb{R}$ and $h\colon \mathbb{R}\to\mathbb{R}$ are continuous functions, $g\in C^1(\mathbb{R},\mathbb{R}^+)$ satisfies (g_1), g is even, $g'(t)\leq 0$, $g(0)=1$, $\lim_{t\to+\infty} g(t)=l, l\in(0,1)$, and $\forall\ t\geq 0$.

When $b=0$, Eq. 1.1 is reduced to the following quasilinear Schrödinger equation:

$$-\operatorname{div}\left(g^2(u)\nabla u\right)+g(u)g'(u)|\nabla u|^2+V(x)u=h(u), \quad x\in\mathbb{R}^3. \quad (1.2)$$

According to [4], let $g(u)=\sqrt{1+2\left(\varphi'\left(|u|^2\right)\right)^2u^2}$, then, Eq. 1.2 is transformed into

$$-\triangle u-\left[\triangle\left(\varphi\left(|u|^2\right)\right)\right]\varphi'\left(|u|^2\right)u+V(x)u=h(u), \quad x\in\mathbb{R}^3. \quad (1.3)$$

It is well-known that the classical case is $\varphi(s)=s$ or $\varphi(s)=\sqrt{1+s}$ [5–12].

For Eq. 1.1, another interesting question is $b>0$. When $g(t)=1$ for all $t\in\mathbb{R}$, it is reduced to the following classical Kirchhoff equation:

$$-\left(1+b\int_{\mathbb{R}^3}|\nabla u|^2dx\right)\Delta u+V(x)u=h(u),\quad x\in\mathbb{R}^3. \tag{1.4}$$

It is well-known that Eq. 1.4 is related to the stationary analog of the following Kirchhoff-type equation:

$$u_{tt}+\left(1+b\int_{\mathbb{R}^3}|\nabla u|^2dx\right)\Delta u+V(x)u=h(u),\quad x\in\mathbb{R}^3, \tag{1.5}$$

which was proposed by Kirchhoff as an extension of the classical D'Alembert's wave equation for free vibrations of elastic strings [13,14]. More physical background can be found in [15] and the references therein. Based on the aforementioned analysis, it is necessary to study Eq. 1.1.

1.1 Related works and main results

At first, let us briefly review the predecessors' pioneering works about the problem [16–20]. However, to the best of our knowledge, there are no works involving Eq. 1.1 when the non-linearity $h(u)$ is asymptotically cubic at infinity. More information about the asymptotically cubic problems is given in [21,22] and the references therein. The main goal of the present paper is to investigate this problem. Precisely, we suppose that

(V_1) $V(x)=V(|x|), 0<V_0\le V(x)\le V_\infty:=\lim_{|x|\to+\infty}V(x)<\infty$;
(V_2) $V\in C^1(\mathbb{R}^3,\mathbb{R})$ and $\langle\nabla V(x),x\rangle\le 0,\forall\ x\in\mathbb{R}^3$;
(h_1) $h\in C(\mathbb{R},\mathbb{R})$, $h(t)=0,\forall\ t\le 0$, and $\lim_{t\to 0}\frac{h(t)}{t}=0$;
(h_2) $\lim_{|t|\to+\infty}\frac{|h(t)|}{|t|^3}=\gamma,\gamma>bl^4\lambda_1$, where

$$\lambda_1:=\inf\left\{\left(\int_{\mathbb{R}^3}|\nabla w|^2dx\right)^2:w\in\mathcal{H},\quad\int_{\mathbb{R}^3}|w|^4dx=1\right\}$$

and $\mathcal{H}$ is defined in Section 2;

(h_3) $\frac{1}{4}h(t)t\ge H(t)$ for all $t>0$, where $H(t)=\int_0^t h(s)ds$.

Remark 1.1: For example, $h(t)=\frac{\gamma t^5}{1+t^2}$. By direct calculations, we have

$$H(t)=\frac{\gamma t^4}{4}-\frac{\gamma t^2}{2}+\frac{\gamma}{2}\ln(1+t^2).$$

It is easy to observe that h satisfies the assumption (h_1) – (h_3).

The first result involves non-existence for the Kirchhoff-type perturbation problem.

Theorem 1.1: Assume that (g_1) holds with $\frac{1}{3}\le l\le 1$ and $\langle\nabla V(x),x\rangle\ge 0$. For any $b>0$, Eq. 1.1 has no non-trivial solutions with $h(u)=|u|^{p-2}u$, $p\ge 6$.

The next result describes the existence for generalized quasilinear Schrödinger equations with the Kirchhoff term.

Theorem 1.2: Assume that (V_1), (V_2), (g_1), (h_1), and (h_2) are satisfied. Then, Eq. 1.1 has a positive radial solution.

The third result shows the existence for generalized quasilinear Schrödinger equations without the Kirchhoff term.

Theorem 1.3: Assume that (V_1), (V_2), (g_1), and (h_1) – (h_3) are satisfied. Then, Eq. 1.2 has a positive radial solution.

Compared with Theorem 1.2, without the Kirchhoff term $\int_{\mathbb{R}^3}g^2(u)|\nabla u|^2dx$, we find that we need to add the condition (h_3). Until now, we have not been able to remove it. A natural question is that what happens if Kirchhoff-type perturbation occurs, that is, when $b\to 0$, can we build a relationship between Theorem 1.2 and 1.3? In this regard, we state the following.

Theorem 1.4: Assume that (V_1), (V_2), (g_1), and (h_1) – (h_3) hold and $\{u_{b_n}\}\subset\mathcal{H}$ are the positive radial solutions obtained in Theorem 1.2 for each $n\in\mathbb{N}$. Then, $u_{b_n}\to u_0$ in $\mathcal{H}$ as $b_n\to 0$, $n\to\infty$, where u_0 is a positive radial solution for Eq. 1.2.

1.2 Our contributions and methods

We should mention that our results are new since we focus on the asymptotically cubic case. Compared with [16,19,20], we know that in Theorem 1.1, our non-linear term in the autonomy problem Eq. 1.1 is supercritical, so we invoke the Pohožaev-type identity. As for Theorem 1.2, the problem is asymptotically 3-linear at infinity (*i.e.*, $h(t)\sim t^3$), so it is different from [16]. We take full advantage of the condition h_2, and this is our paper's highlight. We borrow the idea from [16], but we require more elaborate estimates (see Lemma 3.2–3.4) to prove Theorem 1.3. It is worth pointing out that in Theorem 1.3, it seems that the condition (h_3) is fussy, but our pursuit is not to relax the condition. Our condition (h_3) is different from ([16], h_5), and we adopt the idea from [23], Lemma 2.2 to obtain mountain pass geometry (see Lemma 3.5). Finally, we study the behavior of the positive radial solutions as $b\to 0$. Since we do not know whether u_0 is unique, we cannot draw the conclusion that u_0 is obtained in Theorem 1.2.

1.3 Organization

This paper is organized as follows. Section 2 provides some preliminaries, and Section 3 is divided into three parts, which will prove Theorems 1.1–1.3, respectively. The proof of Theorem 1.4 is given in Section 3. Throughout this paper, the following notations are used:

- $\|u\|_p$ $(1<p\le\infty)$ is the norm in $L^p(\mathbb{R}^3)$;
- $\to$ and $\rightharpoonup$ denote strong and weak convergence, respectively;
- $\langle\cdot,\cdot\rangle$ denotes the duality pairing between a Banach space and its dual space;
- $o_n(1)$ denotes $o_n(1)\to 0$ as $n\to\infty$.

2 Preliminary results

Since the condition (V_1), we use the work space

$$\mathcal{H}:=\{u\in H^1(\mathbb{R}^3):u(x)=u(|x|)\},$$

equipped with the norm

$$\|u\|_{\mathcal{H}}^2=\int_{\mathbb{R}^3}\left(|\nabla u|^2+V(x)u^2\right)dx. \tag{2.1}$$

According to [16], the energy functional associated with Eq. 1.1 is

$$I_b(u)=\frac{1}{2}\int_{\mathbb{R}^3}g^2(u)|\nabla u|^2dx+\frac{1}{2}\int_{\mathbb{R}^3}V(x)|u|^2dx+\frac{b}{4}\left(\int_{\mathbb{R}^3}g^2(u)|\nabla u|^2dx\right)^2-\int_{\mathbb{R}^3}H(u)dx,$$

where $H(t)=\int_0^t h(s)ds$. We require the change of variable [24–27]

$$v = G(u) = \int_0^u g(t)dt, \tag{2.2}$$

and $I(u)$ can be reduced to

$$J_b(v) = \frac{1}{2}\int_{\mathbb{R}^3} |\nabla v|^2 dx + \frac{1}{2}\int_{\mathbb{R}^3} V(x)|G^{-1}(v)|^2 dx + \frac{b}{4}\left(\int_{\mathbb{R}^3} |\nabla v|^2 dx\right)^2 - \int_{\mathbb{R}^3} H(G^{-1}(v))dx, \tag{2.3}$$

where $G^{-1}(v)$ is the inverse of $G(u)$.

Clearly, we have the following lemma (see [16]).

Lemma 2.1: *Assume that* (V_1) *holds. If* $v \in \mathcal{H}$ is a critical point of J_b, then $u = G^{-1}(v)$ is a weak solution of Eq. 1.1.

3 Proof of the main results

3.1 Proof of Theorem 1.1

By a standard argument in [28], we can obtain the following Pohožaev type.

Lemma 3.1: If $v \in \mathcal{H}$ is a weak solution of Eq. 1.1 with $h(t) = |t|^{p-2}t$, $p \geq 6$, then v satisfies

$$\frac{1}{2}\int_{\mathbb{R}^3} |\nabla v|^2 dx + \frac{3}{2}\int_{\mathbb{R}^3} V(x)|G^{-1}(v)|^2 dx + \frac{1}{2}\int_{\mathbb{R}^3} \langle \nabla V(x), x\rangle |G^{-1}(v)|^2 dx + \frac{b}{2}\left(\int_{\mathbb{R}^3} |\nabla v|^2 dx\right)^2 = \frac{3}{p}\int_{\mathbb{R}^3} |G^{-1}(v)|^p dx.$$

Based on the identity, we can provide the proof of Theorem 1.1. Indeed, v satisfies

$$\int_{\mathbb{R}^3} |\nabla v|^2 dx + \int_{\mathbb{R}^3} V(x)\frac{G^{-1}(v)}{g(G^{-1}(v))}vdx + b\left(\int_{\mathbb{R}^3} |\nabla v|^2 dx\right)^2 = \int_{\mathbb{R}^3} \frac{|G^{-1}(v)|^{p-2}G^{-1}(v)}{g(G^{-1}(v))}vdx.$$

Since $\frac{1}{3} \leq l \leq 1$, using (5) of Lemma 2.1 in [29], jointly with $\langle \nabla V(x), x\rangle \geq 0$, we can obtain $0 = u = G^{-1}(v)$.

3.2 Proof of Theorem 1.2

This section provides the proof of Theorem 1.2. Clearly, as mentioned previously, we are devoted to studying the functional J_b [Eq. 2.3]. Since our case is asymptotically cubic, it is hard to prove the boundedness of the PS-sequences of J_b. Hence, we use [30], Theorem 1.1 to find a special bounded PS-sequence of $J_{b,\mu}$, where

$$J_{b,\mu}(v) := \frac{1}{2}\int_{\mathbb{R}^3} |\nabla v|^2 dx + \frac{1}{2}\int_{\mathbb{R}^3} V(x)|G^{-1}(v)|^2 dx + \frac{b}{4}\left(\int_{\mathbb{R}^3} |\nabla v|^2 dx\right)^2 - \mu\int_{\mathbb{R}^3} H(G^{-1}(v))dx,$$

$\mu \in [1, 2]$. We have the following lemma.

Lemma 3.2: Assume that (h_1)–(h_2) are satisfied, then

(i) for $\mu \in [1, 2]$, there exists $v \in \mathcal{H}\backslash\{0\}$ such that $J_{b,\mu}(v) < 0$.
(ii) there exists $\rho, \alpha > 0$ such that $J_{b,\mu}(v) \geq \alpha$ and $\|v\|_{\mathcal{H}} = \rho$.

Proof. (i) It is well-known that $\lambda_1 > 0$ is attained [([31]; Section 1.7)]. In other words, $\phi \in \mathcal{H}$ satisfied $\int_{\mathbb{R}^3} |\phi|^4 dx = 1$ and $\phi > 0$ such that

$$\lambda_1 = \left(\int_{\mathbb{R}^3} |\nabla\phi|^2 dx\right)^2.$$

In view of (h_2), $1 < \frac{1}{l^2}$, and $1 \leq \mu \leq 2$, jointly with (3) and (4) of Lemma 2.1 in [29], we have

$$\begin{aligned}
&\lim_{t\to+\infty} \frac{J_{b,\mu}(t\phi)}{t^4} \\
&< \lim_{t\to+\infty}\left[\frac{1}{l^2 t^2}\|\phi\|_{\mathcal{H}}^2 + \frac{b}{4}\left(\int_{\mathbb{R}^3} |\nabla\phi|^2 dx\right)^2 - \mu\int_{\mathbb{R}^3} \frac{H(G^{-1}(t\phi))}{|G^{-1}(t\phi)|^4}\frac{|G^{-1}(t\phi)|^4}{|t\phi|^4}|\phi|^4 dx\right] \\
&\leq \frac{b}{4}\left(\int_{\mathbb{R}^3} |\nabla\phi|^2 dx\right)^2 - \frac{b\lambda_1}{4}\int_{\mathbb{R}^3} |\phi|^4 dx \\
&= 0.
\end{aligned}$$

Hence, when t is large, let $v := t\phi$, and we obtain the results.

(ii) Let $\varepsilon \in (0, \frac{l^2 V_0}{2\mu})$, then we obtain

$$J_{b,\mu}(v) \geq \frac{1}{2}\int_{\mathbb{R}^3} |\nabla v|^2 dx + \frac{1}{2}\int_{\mathbb{R}^3} \left(V_0 - \frac{\mu\varepsilon}{l^2}\right)|v|^2 dx - \frac{C_\varepsilon \mu}{q l^q}\int_{\mathbb{R}^3} |v|^q dx. \tag{3.1}$$

Hence, we can choose $\|v\|_{\mathcal{H}} = \rho > 0$ small enough such that $J_{b,\mu}(v) > 0$.

Define

$$A(v) := \frac{1}{2}\int_{\mathbb{R}^3} [|\nabla v|^2 + V(x)|G^{-1}(v)|^2]dx + \frac{b}{4}\left(\int_{\mathbb{R}^3} |\nabla v|^2 dx\right)^2,$$
$$B(v) := \int_{\mathbb{R}^3} H(G^{-1}(v))dx.$$

It is deduced from (V_1) and (3) of Lemma 2.1 in [29] that

$$A(v) > \frac{1}{2}\|v\|_{\mathcal{H}}^2 \to +\infty, \quad \text{as} \quad \|v\|_{\mathcal{H}} \to \infty, \quad \forall\ v \in \mathcal{H}.$$

Moreover, from (h_1), it can be observed that $B(v) = \int_{\mathbb{R}^3} H(G^{-1}(v))dx \geq 0, \forall\ v \in \mathcal{H}$.

Using [30], Theorem 1.1 or [16], Theorem 4.1, it shows that for a.e. $\mu \in [1, 2]$, there is a bounded $(PS)_{c_\mu}$ sequence $\{v_n\} \subset \mathcal{H}$, where c_μ is the mountain pass level.

Lemma 3.3: Up to a subsequence, $v_n \to v_\mu$ in $\mathcal{H}$.

Proof: Since $\{v_n\} \subset \mathcal{H}$ is bounded, up to a subsequence, there exists $v_\mu \in \mathcal{H}$ such that $v_n \rightharpoonup v_\mu$, in $\mathcal{H}$, $v_n \to v_\mu$, in $L^p(\mathbb{R}^3)$ for $2 < p < 6$, and $v_n(x) \to v_\mu(x)$ a.e. $x \in \mathbb{R}^3$. Obviously, $J'_{b,\mu}(v_\mu) = 0$. Then,

$$\begin{aligned}
o_n(1) &= \langle J'_{b,\mu}(v_n) - J'_{b,\mu}(v_\mu), v_n - v_\mu\rangle \\
&= \int_{\mathbb{R}^3} |\nabla(v_n - v_\mu)|^2 dx + \int_{\mathbb{R}^3} V(x)\left[\frac{G^{-1}(v_n)}{g(G^{-1}(v_n))} - \frac{G^{-1}(v_\mu)}{g(G^{-1}(v_\mu))}\right](v_n - v_\mu)dx + b\left[\int_{\mathbb{R}^3} |\nabla v_n|^2 dx\int_{\mathbb{R}^3} \nabla v_n \nabla(v_n - v_\mu)dx\right. \\
&\quad \left. - \int_{\mathbb{R}^3} |\nabla v_\mu|^2 dx\int_{\mathbb{R}^3} \nabla v_\mu \nabla(v_n - v_\mu)dx\right] \\
&\quad - \mu\int_{\mathbb{R}^3} \left[\frac{h(G^{-1}(v_n))}{g(G^{-1}(v_n))} - \frac{h(G^{-1}(v_\mu))}{g(G^{-1}(v_\mu))}\right](v_n - v_\mu)dx.
\end{aligned} \tag{3.2}$$

We define φ: $\mathbb{R} \to \mathbb{R}$ by $\varphi(t) = G^{-1}(t)/g(G^{-1}(t))$. Noting that $l < g(t) \leq 1$ for $t \in \mathbb{R}$, jointly with [29], (2) of Lemma 2.1, we have

$$\varphi'(t) = \frac{1}{g^2(G^{-1}(t))}\left[1 - \frac{G^{-1}(t)g'(G^{-1}(t))}{g(G^{-1}(t))}\right] \geq \frac{1}{g^2(G^{-1}(t))} \geq 1.$$

According to the mean value theorem, for any $x \in \mathbb{R}^3$, there exists a function $\xi(x)$ between $v_\mu(x)$ and $v_n(x)$ such that

$$\int_{\mathbb{R}^3} V(x)\left[\frac{G^{-1}(v_n)}{g(G^{-1}(v_n))} - \frac{G^{-1}(v_\mu)}{g(G^{-1}(v_\mu))}\right](v_n - v_\mu)dx = \int_{\mathbb{R}^3} V(x)\varphi'(\xi)|v_n - v_\mu|^2 dx \geq \int_{\mathbb{R}^3} V(x)|v_n - v_\mu|^2 dx. \tag{3.3}$$

It is easy to check that

$$\begin{aligned}&\int_{\mathbb{R}^3}|\nabla v_n|^2 dx \int_{\mathbb{R}^3} \nabla v_n \nabla(v_n - v_\mu)dx - \\ &\int_{\mathbb{R}^3}|\nabla v_\mu|^2 dx \int_{\mathbb{R}^3} \nabla v_\mu \nabla(v_n - v_\mu)dx \\ &= \int_{\mathbb{R}^3}\left[|\nabla v_n|^2 - |\nabla v_\mu|^2\right]dx \int_{\mathbb{R}^3} \nabla v_n \nabla(v_n - v_\mu)dx \\ &+ \int_{\mathbb{R}^3}|\nabla v_\mu|^2 dx \int_{\mathbb{R}^3}|\nabla(v_n - v_\mu)|^2 dx \\ &\to 0, \quad n \to \infty .\end{aligned} \tag{3.4}$$

Noting that [29], (3) of Lemma 2.1, we obtain

$$\begin{aligned}&\left|\int_{\mathbb{R}^3}\left[\frac{h(G^{-1}(v_n))}{g(G^{-1}(v_n))} - \frac{h(G^{-1}(v_\mu))}{g(G^{-1}(v_\mu))}\right](v_n - v_\mu)dx\right| \\ &\leq C\int_{\mathbb{R}^3}\left(|v_n| + |v_n|^{q-1} + |v_\mu| + |v_\mu|^{q-1}\right)|v_n - v_\mu|dx.\end{aligned} \tag{3.5}$$

Therefore, $v_n \to v_\mu$ in $\mathcal{H}$.

It is easy to check the following lemma.

Lemma 3.4: If $v \in \mathcal{H}$ is a critical point of $J_{b,\mu}(v)$, then v satisfies

$$\frac{1}{2}\int_{\mathbb{R}^3}|\nabla v|^2 dx + \frac{3}{2}\int_{\mathbb{R}^3} V(x)|G^{-1}(v)|^2 dx + \frac{1}{2}\int_{\mathbb{R}^3}\langle \nabla V(x), x\rangle |G^{-1}(v)|^2 dx + \frac{b}{2}\left(\int_{\mathbb{R}^3}|\nabla v|^2 dx\right)^2 = 3\mu\int_{\mathbb{R}^3} H(G^{-1}(v))dx.$$

Up to this point, we can prove Theorem 1.3. In fact, it is deduced from Lemma 3.2 and 3.3 that there exists $\{\mu_n\} \subset [1, 2]$ such that $\lim_{n\to\infty}\mu_n = 1, v_{\mu_n} \in \mathcal{H}$ satisfies $J_{b,\mu_n}(v_{\mu_n}) = c_{\mu_n} > 0, J'_{b,\mu_n}(v_{\mu_n}) = 0$. Next, we prove $\{v_{\mu_n}\}$ is bounded in $\mathcal{H}$. Since the map $\mu \to c_\mu$ is non-increasing, combining with Lemma 3.4 and condition (V_2), we obtain

$$\begin{aligned}M &\geq J_{b,\mu_n}(v_{\mu_n}) \\ &= \frac{1}{3}\int_{\mathbb{R}^3}|\nabla v_{\mu_n}|^2 dx - \frac{1}{6}\int_{\mathbb{R}^3}\langle \nabla V(x), x\rangle |G^{-1}(v_{\mu_n})|^2 dx + \frac{b}{12}\left(\int_{\mathbb{R}^3}|\nabla v_{\mu_n}|^2 dx\right)^2 \\ &\geq \frac{1}{3}\int_{\mathbb{R}^3}|\nabla v_{\mu_n}|^2 dx.\end{aligned} \tag{3.6}$$

It is easy to check that

$$\begin{aligned}&\int_{\mathbb{R}^3}|\nabla v_{\mu_n}|^2 dx + \int_{\mathbb{R}^3} V(x)\frac{G^{-1}(v_{\mu_n})}{g(G^{-1}(v_{\mu_n}))}v_{\mu_n}dx + b\left(\int_{\mathbb{R}^3}|\nabla v_{\mu_n}|^2 dx\right)^2 \\ &= \mu_n\int_{\mathbb{R}^3}\frac{h(G^{-1}(v_{\mu_n}))}{g(G^{-1}(v_{\mu_n}))}v_{\mu_n}dx \\ &\leq \frac{\varepsilon\mu_n}{l^2}\int_{\mathbb{R}^3}|v_{\mu_n}|^2 dx + \frac{C_\varepsilon\mu_n}{l^6}\int_{\mathbb{R}^3}|v_{\mu_n}|^6 dx \\ &\leq \frac{\varepsilon\mu_n}{l^2}\int_{\mathbb{R}^3}|v_{\mu_n}|^2 dx + \frac{C_\varepsilon\mu_n S}{l^6}\left(\int_{\mathbb{R}^3}|\nabla v_{\mu_n}|^2 dx\right)^3 \\ &\leq \frac{\varepsilon\mu_n}{l^2}\int_{\mathbb{R}^3}|v_{\mu_n}|^2 dx + \frac{C_\varepsilon\mu_n S}{l^6}(3M)^3.\end{aligned}$$

Moreover, using (3) and (5) of Lemma 2.1 in [29], it is deduced from condition (V_1) that

$$\int_{\mathbb{R}^3} V_0|v_{\mu_n}|^2 dx \leq \int_{\mathbb{R}^3}|\nabla v_{\mu_n}|^2 dx + \int_{\mathbb{R}^3} V(x)\frac{G^{-1}(v_{\mu_n})}{g(G^{-1}(v_{\mu_n}))}v_{\mu_n}dx + b\left(\int_{\mathbb{R}^3}|\nabla v_{\mu_n}|^2 dx\right)^2 \leq \frac{\varepsilon\mu_n}{l^2}\int_{\mathbb{R}^3}|v_{\mu_n}|^2 dx + \frac{C_\varepsilon\mu_n S}{l^6}(3M)^3.$$

Let $\varepsilon = \frac{l^2 V_0}{2\mu_n}$, then we obtain

$$\int_{\mathbb{R}^3}|v_{\mu_n}|^2 dx \leq \frac{2SC_\varepsilon\mu_n}{l^6 V_0}(3M)^3. \tag{3.7}$$

From Eqs 3.6, 3.7, we know that $\{v_{\mu_n}\}$ is bounded in $\mathcal{H}$.

A subsequence of $\{v_{\mu_n}\}$ is selected and also denoted by $\{v_n\}$, such that $v_n \rightharpoonup v$ in $\mathcal{H}$. Similar to the proof of Lemma 3.3, we obtain $v_n \to v$ in $\mathcal{H}$. It is well-known that $\mu \mapsto c_\mu$ is continuous from the left [([16], Theorem 4.1)]. So,

$$\begin{aligned}\lim_{n\to\infty} J_b(v_{\mu_n}) &= \lim_{n\to\infty}\left[J_{b,\mu_n}(v_{\mu_n}) + (\mu_n - 1)\int_{\mathbb{R}^3} H(G^{-1}(v_{\mu_n}))dx\right] \\ &= \lim_{n\to\infty} c_{\mu_n} = \tilde{c}.\end{aligned}$$

In addition,

$$\begin{aligned}\lim_{n\to\infty}\langle J'_b(v_{\mu_n}), \psi\rangle &= \lim_{n\to\infty}\left[\langle J'_{b,\mu_n}(v_{\mu_n}), \quad \psi\rangle + (\mu_n - 1)\int_{\mathbb{R}^3}\frac{h(G^{-1}(v_{\mu_n}))}{g(G^{-1}(v_{\mu_n}))}\psi dx\right] \\ &= 0,\end{aligned}$$

for any $\psi \in C_0^\infty(\mathbb{R}^3)$, which means that $J'_b(v) = 0$ satisfies $J_b(v) = \tilde{c} > 0$. Let $v^- = \min\{v, 0\}$. Using (3) and (5) of Lemma 2.1 in [29], we have

$$\begin{aligned}0 &= \langle J'_b(v), v^-\rangle \\ &= \int_{\mathbb{R}^3}\left(|\nabla v^-|^2 + V(x)\frac{G^{-1}(v^-)}{g(G^{-1}(v^-))}v^-\right)dx \\ &\geq \int_{\mathbb{R}^3}\left(|\nabla v^-|^2 + V(x)|v^-|^2\right)dx.\end{aligned} \tag{3.8}$$

It shows that $v^- \equiv 0$. Applying the strong maximum principle, we obtain $v(x) > 0$.

3.3 Proof of Theorem 1.3

This section studies the case $\frac{1}{4}h(t)t \geq H(t)$ for all $t > 0$ and without the Kirchhoff term $\int_{\mathbb{R}^3} g^2(u)|\nabla u|^2 dx$. At first, let us check the mountain pass geometry of the functional J_0.

Lemma 3.5: Assume that (h_1)–(h_2) are satisfied, then

(i) there exists $v \in \mathcal{H}\backslash\{0\}$ such that $J_0(v) < 0$.
(ii) there exist $\rho, \alpha > 0$ such that $J_0(v) \geq \alpha$, $\|v\|_{\mathcal{H}} = \rho$.

Proof (i) Motivated by Lemma 2.2 of [23], we need to study the following equation:

$$-\Delta v + V_\infty\frac{G^{-1}(v)}{g(G^{-1}(v))} = \frac{h(G^{-1}(v))}{g(G^{-1}(v))}, \quad x \in \mathbb{R}^3. \tag{3.9}$$

The corresponding functional is $J_{0,\infty}(v)$. We also define the mountain pass min–max level

$$c_\infty = \inf_{\xi\in\Gamma_\infty}\max_{t\in[0,1]} J_{0,\infty}(\xi(t)),$$

where

$$\Gamma_\infty = \{\xi \in C([0,1], \mathcal{H}: \xi(0) = 0 \neq \xi(1), \quad J_{0,\infty}(\xi(1)) < 0\}.$$

By the standard arguments, it shows that $w \in H^1(\mathbb{R}^N)$ is a solution of Eq. 3.9, which satisfies $J_{0,\infty}(w) = c_\infty$. A continuous path α: $[0, +\infty) \to \mathcal{H}$ is defined by $\alpha(t)(x) = w(x/t)$, if $t > 0$ and $\alpha(0) = 0$. Taking the derivative, we know that

$$\frac{d}{dt}J_{0,\infty}(\alpha(t)) = \frac{1}{2}\int_{\mathbb{R}^3}|\nabla w|^2dx + \frac{3}{2}t^2\int_{\mathbb{R}^3}V_\infty|G^{-1}(w)|^2dx - 3t^2\int_{\mathbb{R}^3}H(G^{-1}(w))dx.$$

Since w is a solution of Eq. 3.9, it satisfies the Pohožaev identity,

$$\frac{1}{2}\int_{\mathbb{R}^3}|\nabla w|^2dx + \frac{3}{2}\int_{\mathbb{R}^3}V_\infty|G^{-1}(w)|^2dx = 3\int_{\mathbb{R}^3}H(G^{-1}(w))dx.$$

Therefore,

$$\frac{d}{dt}J_{0,\infty}(\alpha(t)) = \frac{1}{2}(1-t^2)\int_{\mathbb{R}^3}|\nabla w|^2dx.$$

The map $t \mapsto J_{0,\infty}(\alpha(t))$ achieves the maximum value at $t = 1$. By choosing $L > 0$ sufficiently large, we have $J_{0,\infty}(\alpha(L)) < 0$. Taking $\zeta(t) = \alpha(tL)$, we have $\zeta \in \Gamma_\infty$. If $\zeta_y(t) := w(\frac{\cdot - y}{tL})$, noting that (V_1), we obtain

$$J_0(\zeta_y(1)) = J_{0,\infty}(\zeta_y(1)) + \frac{1}{2}\int_{\mathbb{R}^3}(V(x+y) - V_\infty)|G^{-1}(\zeta_y(1))|^2dx < 0, \quad \text{for } |y| \text{ is large.}$$

Choosing $e = \zeta_y(1)$, we can obtain the result.

(ii) Similar to (*ii*) of Lemma 3.2, we obtain

$$J_0(v) \geq \frac{1}{2}\int_{\mathbb{R}^3}(|\nabla v|^2 + V(x)|v|^2)dx - \int_{\mathbb{R}^3}\left(\frac{\varepsilon}{2}|G^{-1}(v)|^2 + \frac{C_\varepsilon}{q}|G^{-1}(v)|^q\right)dx \geq \frac{C}{4}\|v\|^2_{\mathcal{H}} - \frac{C_1C_\varepsilon}{ql^q}\|v\|^q_{\mathcal{H}}.$$

Hence, choosing $\|v\|_{\mathcal{H}} = \rho > 0$ small enough, we can obtain the desired conclusion.

Therefore, there is a (PS) c_0 sequence $\{v_n\} \subset \mathcal{H}$ where c_0 is the mountain pass level of the J_0.

Lemma 3.6: $\{v_n\}$ is bounded.

Proof: Since $G^{-1}(v_n)g(G^{-1}(v_n)) \in \mathcal{H}$, jointly with (h_3) and [29], (2) of Lemma 2.1], we obtain

$$c + o_n(1) = J_0(v_n) - \frac{1}{4}\langle J_0'(v_n), G^{-1}(v_n)g(G^{-1}(v_n))\rangle \geq \frac{1}{4}\|v_n\|^2_{\mathcal{H}}.$$

Hence, $\{v_n\}$ is bounded in $\mathcal{H}$.

Similar to Lemma 3.3, we obtain the following result.

Lemma 3.7: Up to a subsequence, $v_n \to v$ in $\mathcal{H}$.

Proof of Theorem 1.3: It deduces from lemmas 3.5, 3.6, and 3.7 that Eq. 1.2 has a non-trivial solution v. Similar to Eq. 3.8, we know that $v(x) > 0, x \in \mathbb{R}^3$.

4 Asymptotic properties of the positive radial solution

Proof of Theorem 1.4: If v_{b_n} is a critical point of J_{b_n}, which is obtained in Theorem 1.2 for each $n \in \mathbb{N}$. Similar to the proof of Lemma 3.2, for $b_n \to 0$, $n \to \infty$, $\{v_{b_n}\}$ is a $(PS)_c$ sequence, which is bounded in $\mathcal{H}$. There exists a subsequence of $\{b_n\}$, still denoted by $\{b_n\}$, such that $v_{b_n} \rightharpoonup v_0$ in $\mathcal{H}$. It is easy to obtain

$$\begin{aligned}\|v_{b_n} - v_0\|^2_{\mathcal{H}} \leq{}& \langle J_{b_n}'(v_{b_n}) - J_0'(v_0), v_{b_n} - v_0\rangle \\ &- b_n\int_{\mathbb{R}^3}|\nabla v_{b_n}|^2dx\int_{\mathbb{R}^3}\nabla v_{b_n}\nabla(v_{b_n} - v_0)dx \\ &+ \int_{\mathbb{R}^3}\left[\frac{h(G^{-1}(v_{b_n}))}{g(G^{-1}(v_{b_n}))} - \frac{h(G^{-1}(v_0))}{g(G^{-1}(v_0))}\right](v_{b_n} - v_0)dx \\ ={}& o_n(1).\end{aligned}$$

On one hand, in view of (3) of Lemma 2.1 in [29], we can use the Lebesgue dominated convergence theorem to obtain

$$\lim_{n\to\infty}\int_{\mathbb{R}^3}V(x)\frac{G^{-1}(v_{b_n})\phi}{g(G^{-1}(v_{b_n}))}dx = \int_{\mathbb{R}^3}V(x)\frac{G^{-1}(v_0)\phi}{g(G^{-1}(v_0))}dx,$$

$$\lim_{n\to\infty}\int_{\mathbb{R}^3}\frac{h(G^{-1}(v_{b_n}))\phi}{g(G^{-1}(v_{b_n}))}dx = \int_{\mathbb{R}^3}\frac{h(G^{-1}(v_0))\phi}{g(G^{-1}(v_0))}dx.$$

On the other hand, we have $\langle J_{b_n}'(v_{b_n}), \phi\rangle = o_n(1)$ and $\langle J_0'(v_0), \phi\rangle = o_n(1)$. Moreover,

$$\lim_{n\to\infty}\int_{\mathbb{R}^3}\nabla v_{b_n}\nabla\phi dx = \int_{\mathbb{R}^3}\nabla v_0\nabla\phi dx,$$

$$\lim_{n\to\infty}b_n\int_{\mathbb{R}^3}|\nabla v_{b_n}|^2dx\int_{\mathbb{R}^3}\nabla v_{b_n}\nabla\phi dx = 0.$$

Thus,

$$\int_{\mathbb{R}^3}\nabla v_0\nabla\phi dx + \int_{\mathbb{R}^3}V(x)\frac{G^{-1}(v_0)}{g(G^{-1}(v_0))}\phi dx = \int_{\mathbb{R}^3}\frac{h(G^{-1}(v_0))}{g(G^{-1}(v_0))}\phi dx.$$

It shows that v_0 is a positive solution of Eq. 1.2.

Data availability statement

The original contributions presented in the study are included in the article/Supplementary Material, further inquiries can be directed to the corresponding author.

Author contributions

All authors listed have made a substantial, direct, and intellectual contribution to the work and approved it for publication.

Funding

This work was supported by the National Natural Science Foundation of China (Grant Nos 12261075 and 12261076), Yunnan Local Colleges Applied Basic Research Projects (Grant Nos 202001BA070001-032 and 202101BA070001-280), the Technology Innovation Team of University in Yunnan Province (Grant No. 2020CXTD25), and Yunnan Fundamental Research Projects (Grant Nos 202201AT070018 and 202105AC160087). WW was supported in part by the Yunnan Province Basic Research Project for Youths (202301AU070001) and the Xingdian Talents Support Program of Yunnan Province.

Conflict of interest

The authors declare that the research was conducted in the absence of any commercial or financial relationships that could be construed as a potential conflict of interest.

Publisher's note

References

1. Feit M, Fleck J, Steiger A. Solution of the Schrödinger equation by a spectral method. *J Comput Phys* (1982) 47:412–33. doi:10.1016/0021-9991(82)90091-2

2. He J, He C, Saeed T. A fractal modification of chen-lee-liu equation and its fractal variational principle. *Internat J Mod Phys. B* (2021) 35:2150214. doi:10.1142/S0217979221502143

3. Almutairi A. Stochastic solutions to the non-linear Schrödinger equation in optical fiber. *Therm Sci* (2022) 26:185–90. doi:10.2298/tsci22s1185a

4. Deng Y, Peng S, Yan S. Positive soliton solutions for generalized quasilinear Schrödinger equations with critical growth. *J Differential Equations* (2015) 258:115–47. doi:10.1016/j.jde.2014.09.006

5. Alves C, Wang Y, Shen Y. Soliton solutions for a class of quasilinear Schrödinger equations with a parameter. *J Differential Equations* (2015) 259:318–43. doi:10.1016/j.jde.2015.02.030

6. Bouard A, Hayashi N, Saut J. Global existence of small solutions to a relativistic non-linear Schrödinger equation. *Comm Math Phys* (1997) 189:73–105. doi:10.1007/s002200050191

7. Brizhik L, Eremko A, Piette B, Zakrzewski W. Static solutions of a*D*-dimensional modified non-linear Schr dinger equation. *Non-linearity* (2003) 16:1481–97. doi:10.1088/0951-7715/16/4/317

8. Li G, Huang Y, Liu Z. Positive solutions for quasilinear Schrödinger equations with superlinear term. *Complex Var. Elliptic Equ* (2020) 65:936–55. doi:10.1080/17476933.2019.1636791

9. Li Q, Wu X. Existence, multiplicity, and concentration of solutions for generalized quasilinear Schrödinger equations with critical growth. *J Math Phys* (2017) 58:041501. doi:10.1063/1.4982035

10. Shen Y, Wang Y. Soliton solutions for generalized quasilinear Schrödinger equations. *Nonlinear Anal* (2013) 80:194–201. doi:10.1016/j.na.2012.10.005

11. Shi H, Chen H. Positive solutions for generalized quasilinear Schrödinger equations with potential vanishing at infinity. *Appl Math Lett* (2016) 61:137–42. doi:10.1016/j.aml.2016.06.004

12. Shen Y, Wang Y. Standing waves for a class of quasilinear Schrödinger equations. *Complex Var. Elliptic Equ* (2016) 61:817–42. doi:10.1080/17476933.2015.1119818

13. Kirchhoff G. Mechanik *(leipzig: Teubner)* (1883).

14. He J, El-dib Y. The enhanced homotopy perturbation method for axial vibration of strings. *Facta Universitatis Ser Mech Eng* (2021) 19:735–50. doi:10.22190/FUME210125033H

15. Wang K. Construction of fractal soliton solutions for the fractional evolution equations with conformable derivative. *Fractals* (2023) 31:2350014. doi:10.1142/S0218348X23500147

16. Chen J, Tang X, Cheng B. Existence and nonexistence of positive solutions for a class of generalized quasilinear Schrödinger equations involving a Kirchhoff-type perturbation with critical sobolev exponent. *J Math Phys* (2018) 59:021505. doi:10.1063/1.5024898

17. Cheng B, Tang X. Ground state sign-changing solutions for asymptotically 3-linear Kirchhoff-type problems. *Complex Var. Elliptic Equ* (2017) 62:1093–116. doi:10.1080/17476933.2016.1270272

18. Feng R, Tang C. Ground state sign-changing solutions for a Kirchhoff equation with asymptotically 3-linear nonlinearity. *Qual Theor Dyn. Syst.* (2021) 20:91–19. doi:10.1007/s12346-021-00529-y

19. Li F, Zhu X, Liang Z. Multiple solutions to a class of generalized quasilinear Schrödinger equations with a Kirchhoff-type perturbation. *J Math Anal Appl* (2016) 443:11–38. doi:10.1016/j.jmaa.2016.05.005

20. Shen L. Existence and nonexistence results for generalized quasilinear Schrödinger equations of Kirchhoff type in. *Appl Anal* (2020) 99:2465–88. doi:10.1080/00036811.2019.1569225$\mathbb{R}^{3}$

21. Li G, Cheng B, Huang Y. Positive solutions for asymptotically 3-linear quasilinear Schrödinger equations. *Electron J Differential Equations* (2020) 2020:1–17. Available at: http://ejde.math.txstate.edu.

22. Wang W, Yu Y, Li Y. On the asymptotically cubic fractional Schrödinger-Poisson system. *Appl Anal* (2021) 100:695–713. doi:10.1080/00036811.2019.1616695

23. Lehrer R, Maia L, Squassina M. Asymptotically linear fractional Schrödinger equations. *Complex Var. Elliptic Equ* (2015) 60:529–58. doi:10.1080/17476933.2014.948434

24. Chu C, Liu H. Existence of positive solutions for a quasilinear Schrödinger equation. *Nonlinear Anal RWA* (2018) 44:118–27. doi:10.1016/j.nonrwa.2018.04.007

25. Colin M, Jeanjean L. Solutions for a quasilinear schrödinger equation: A dual approach. *Nonlinear Anal* (2004) 56:213–26. doi:10.1016/j.na.2003.09.008

26. Liang Z, Gao J, Li A. Infinitely many solutions to a quasilinear Schrödinger equation with a local sublinear term. *Appl Math Lett* (2019) 89:22–7. doi:10.1016/j.aml.2018.09.015

27. Shen Y, Wang Y. Standing waves for a relativistic quasilinear asymptotically Schrödinger equation. *Appl Anal* (2016) 95:2553–64. doi:10.1080/00036811.2015.1100296

28. Severo U, Gloss E, Silva E. On a class of quasilinear Schrödinger equations with superlinear or asymptotically linear terms. *J Differential Equations* (2017) 263:3550–80. doi:10.1016/j.jde.2017.04.040

29. Li G, Huang Y. Positive solutions for generalized quasilinear Schrödinger equations with asymptotically linear nonlinearities. *Appl Anal* (2021) 100:1051–66. doi:10.1080/00036811.2019.1634256

30. Jeanjean L. On the existence of bounded Palais–Smale sequences and application to a Landesman–Lazer-type problem set on $\mathbb{R}^N$. *Proc Roy Soc Edin* (1999) 129A:787–809. doi:10.1017/S0308210500013147$\mathbb{R}^{n}$

31. Willem M. *Minimax theorems, progress in nonlinear differential equations and their applications.* Boston, MA: Birkhäuser Boston, Inc. (1996). p. 24.

frontiers | Frontiers in Physics

TYPE Mini Review
PUBLISHED 31 May 2023
DOI 10.3389/fphy.2023.1210400

OPEN ACCESS

EDITED BY
Chun-Hui He,
Xi'an University of Architecture and Technology, China

REVIEWED BY
Junfeng Lu,
Zhejiang Gongshang University, China
Fujuan Liu,
Soochow University, China

*CORRESPONDENCE
Ya Li,
liya@zstu.edu.cn

RECEIVED 22 April 2023
ACCEPTED 16 May 2023
PUBLISHED 31 May 2023

CITATION
Lin L and Li Y (2023), A mini-review on release oscillation in a hollow fiber. *Front. Phys.* 11:1210400. doi: 10.3389/fphy.2023.1210400

A mini-review on release oscillation in a hollow fiber

Ling Lin[1] and Ya Li[2,3]*

[1]Ningbo Advanced Textile Technology & Fashion CAD Key Laboratory, Zhejiang Fashion Institute of Technology, Ningbo, China, [2]Zhejiang Sci-Tech University, College of Textile Science and Engineering (International Silk College), Hangzhou, China, [3]Laimei Technology Co., Ltd., Changxing, Huzhou, Zhejiang, China

This mini-review aims at strengthening the links among textile science, physics, and mathematics. The state-of-the-art technology for silver ions' release from hollow fibers is reviewed, its bottleneck problems are identified, and some open problems are elucidated. The release oscillation opens a new era for modern applications of hollow fibers containing silver ions.

KEYWORDS

hollow fiber, ions release, capillary rise, antibacterial property, nanofluid, fractal, fractional calculus (FC)

1 Introduction

Hollow fibers have obvious advantages in that they are low density and have good flexibility. Natural hollow fibers have even more amazing properties, for example, polar bear hairs have remarkable thermal properties [1, 2]. Wang et al. elucidated the biomechanism of the hollow hair of the polar bear using the fractal calculus with great success [3], Cui et al. designed a biomimetic textile with good thermal insulation [4], and Liu et al. found a new phenomenon of thermal oscillation in the thermal insulation [5]. Hollow-fiber liquid-phase microextractionare is highly efficient for extraction of heavy metals and pharmaceuticals [6–8]. The corresponding solvent, which should be of low polarity and immiscible with water, is immobilized in the pores in the wall of hollow fibers and serves as a supported liquid membrane. A larger number of reports have been published on the development of hollow fibers as a green sample preparation technique requiring only a few microliters of organic solvent per sample. Due to the protection of the acceptor phase by the supported liquid membrane, hollow fibers are amenable to highly complex samples such as plasma, whole blood, urine, saliva, breast milk, tap water, surface water, pond water, seawater, and soil slurries [9].

The physical process of hollow fiber spinning always involves four steps: solution formulation, extrusion, coagulation, and coagulated fiber treatment [10]. Thus far, the electrospinning technique has been considered as a versatile and efficient method for the fabrication of membranes with highly interconnected pore structures [11]. The flexibility of device construction for electrospinning and the diversity of the post-treatment process to electrospun membrane leaves vast scope for researchers to tailor the membrane structures and properties; thus, polymeric nano-scale hollow fibers via electrospinning technology have become popular, for example, bubble electrospinning might be a good candidate for hollow fiber fabrication [12, 13].

This paper focuses on artificial hollow fibers containing silver particles [14, 15], with an emphasis on the release oscillation [16–18].

2 Antibacterial mechanism

Hollow fibers containing silver ions are widely used for antibacterial and antifouling applications [19, 20]; when the fibers are submerged in water, silver ions are gradually released from the inner wall into the water.

Viruses and bacteria are generally quite small [21–23]. In particular, some deadly viruses (e.g., the COVID-19 virus) have a complex unsmooth surface, and a small surface has high surface energy (geometric potential) [24–26], which can easily absorb silver nanoparticles around the surface. The absorbed nanoparticles make viruses and bacteria inactive [24].

On the other hand, silver ions react with water when ions are adhered to the surface of bacteria or viruses:

$$Ag^{+}+H_2O \rightarrow AgOH + H^{+} \tag{1}$$

Bacteria and viruses will be killed due to their exsiccosis and hydrogen ions can react with macromolecules, which is the mechanism of the antibacterial property of the hollow fibers containing silver ions. Of course, however, a high concentration of silver ions will be also harmful to human cells.

3 Capillary effect and diffusion process

The inner diameter of hollow fibers greatly affects the ions release. A smaller diameter implies a higher capillary rise [27, 28]; as a result, more ions can dissolve in water and the diffusion process makes the ions release into the outside of the hollow fiber. Han and He unlocked the secret of hollow fibers' antifouling properties using the capillary effect [29]. Environmental temperature and saline water will affect the ions' diffusion process [30–33].

Though hollow fibers with thinner diameters have better capillary effect, the corresponding fabrication needs more costs, meanwhile, the inner wall surface area is less, so there are less loaded ions. The effects of the temperature on the diffusion process and viruses and bacteria's metabolism should also be considered, as well as additionally the nanofluid mechanics [34–37] being of paramount importance in studying the optimal design of the hollow fiber's geometrical structure and its effect on its antibacterial properties.

4 Release oscillation and frequency property

Due to environmental perturbation, the water in hollow fibers is vibrated periodically, the mechanism of which was first found in [17]. The vibrating water accelerates the release process; however, the non-linear vibrations make it difficult to predict its frequency properties. The governing equation can be expressed as [17].

$$\frac{d^2u}{dt^2} + \frac{a+bu}{(L_0-u)(u+u_0)} = 0 \tag{2}$$

with initial conditions

$$u(0) = 0, u'(0) = A \tag{3}$$

where u is the capillary rise, a, b, and L_0 are constants. The physical understanding represented by each physical parameter is referred to reference [17], and A is the initial velocity.

Solving Eq. 2 effectively is still an open problem. The possible methods to solve Eq. 2 with the initial conditions of Eq. 3 include mainly the homotopy perturbation method [38, 39], the Li-He method [40–42], frequency-amplitude formulation [43], and the variational principle [44].

For u, Eq. 2 can be approximately expressed as

$$\frac{d^2u}{dt^2} + \frac{a+bu}{u_0L_0}\left(1+\frac{u}{L_0}\right)\left(1-\frac{u}{u_0}\right) = 0 \tag{4}$$

or

$$\frac{d^2u}{dt^2} + \frac{a}{u_0L_0} + \frac{1}{u_0L_0}\left(\frac{a}{L_0} - \frac{a}{u_0} + b\right)u + \frac{1}{u_0L_0}\left(-\frac{a}{u_0L_0} + \frac{b}{L_0} - \frac{b}{u_0}\right)u^2 - \frac{b}{(u_0L_0)^2}u^3 = 0 \tag{5}$$

This equation was studied in [45]; the quadratic non-linearity will gradually consume the vibrating energy, and finally the vibrating motion will stop (see the discussion in [46]).

5 Fractal-fractional model for ions release

The unsmooth surface of the inner wall of the hollow fiber is another important factor affecting the release process. Because any physical laws are scale-dependent, the same phenomenon may lead to debating theories if observed using different scales [47]. Capillary effect plays an important role in the heat transmission of porous media and capillary vibration significantly affects the capillary rise or capillary pressure; therefore, the mass transfer or heat transfer will be greatly affected [48]. Most capillary vibrations in the literatures have assumed that the capillary tube is small and uniform; however, capillary tubes are non-uniform in most porous media [24, 48]. The capillary fluid moves extremely slowly, and its vibrations near its equilibrium have an extremely low frequency [48]. Owing to two types of capillary pressures (positive capillary pressure and negative capillary pressure), the capillary pressure from porous media should be taken into consideration [11]. Furthermore, capillary pressure is affected by pore size, capillary pressure with different pore sizes has been analyzed for the hydrophobic-hydrophilic interface in detail, such as electrospun hollow nanofibers used in oil/water separation [11].

The capillary effect has wide applications for microelectromechanical systems and microfluidics devices, in which the capillary vibration significantly affects its mass transmission [48]. Nanofluid mechanics can be directly used for describing the releasing process for the smooth boundary, so the unsmooth boundary makes the release more difficult, but it is amazing Wolfgang Pauli (1900–1958) once said that "God made the bulk, the surface was invented by the devil". The unsmooth surface determines the release process and it can be modeled by the two-scale fractal dimension [49] with ease. In the fractal space, Liu et al. established a fractional model for the silver ions' release

oscillation [50]. The fractal-fractional model offers a new window for studying the effect of the unsmooth boundary on the release process. Fan et al. concluded that the fractal calculus plays an important role in unlocking the mechanisms of natural fibers [51]. Lu et al. provided two numerical approaches for finding the approximated solutions of the time fractional Boussinesq-Burgers equations without any linearization or complicated computation, including the homotopy perturbation transform method and the method based on the fractional complex transform and homotopy perturbation method [52]. Afterwards, a numerical approach was proposed for finding the approximated solutions of a fractal modification of the Yao-Cheng oscillator based on the two-scale fractal transformation and the global residue harmonic balance method with He's fractal derivative as well [53]. They also proposed a combined technique for solving the fractional modification of the non-linear oscillator with coordinate-dependent mass [54]. Meanwhile, the numerical sensitive analysis of the approximations were further considered with respect to different amplitudes and parameters, confirming their high efficiency and stability [53, 54]. Considering that two-scale thermodynamics observes the same phenomenon using two different scales, fractal calculus is adopted to establish governing equations, and fractal variational principles are discussed for 1-D fluid mechanics [47], modeling the ions' release process from an unsmooth boundary of the inner wall of the hollow fibers might be possible.

6 Conclusion

Hollow fibers are now a research Frontier in textile engineering, nanofluid mechanics, material science, non-linear science, physics, and mathematics. This mini-review article provides a panoramic view of the recent studies in this meaningful direction. It is still an open problem to model the ions' release process from an unsmooth boundary of the inner wall of the hollow fibers; a mathematical model for the fractal release oscillation might be more attractive and promising. There is much opportunity and challenge, so this article should be the beginning of future research, not only a review.

Author contributions

All authors listed have made a substantial, direct, and intellectual contribution to the work and approved it for publication.

Funding

The authors thank the Zhejiang Provincial Natural Science Foundation of China under Grant No. LQ21E030016 and the China Postdoctoral Science Foundation under Grant No. 2021M692866.

Conflict of interest

Author YL works at Zhejiang Sci-Tech University, and also is a joint postdoctoral fellow of Laimei Technology Co., Ltd., Changxing

The remaining author declares that the research was conducted in the absence of any commercial or financial relationships that could be construed as a potential conflict of interest.

Publisher's note

References

1. He JH, Wang QL, Sun J. Can polar bear hairs absorb environmental energy? *Therm Sci* (2011) 15:911–3. doi:10.2298/TSCI1103911H

2. Wang QL, He JH, Liu Z. Intelligent nanomaterials for solar energy harvesting: From polar bear hairs to unsmooth nanofiber fabrication. *Front Bioeng Biotech* (2022) 10: 926253. doi:10.3389/fbioe.2022.926253

3. Wang QL, Shi XY, He JH, Li ZB. Fractal calculus and its application to explanation of biomechanism of polar bear hairs. *Fractals* (2018) 26(6):1850086. doi:10.1142/S0218348X1850086X

4. Cui Y, Gong HX, Wang YJ, Li DW, Bai H. A thermally insulating textile inspired by polar bear hair. *Adv Mater* (2018) 30(14):1706807. doi:10.1002/adma.201706807

5. Liu FJ, Zhang T, He CH, Tian D. Thermal oscillation arising in a heat shock of a porous hierarchy and its application. *Facta Univ.-Ser Mech* (2022) 20(3):633–45. doi:10.22190/FUME210317054L

6. Abulhassani J, Manzoori JL, Amjadi M. Hollow fiber based-liquid phase microextraction using ionic liquid solvent for preconcentration of lead and nickel from environmental and biological samples prior to determination by electrothermal atomic absorption spectrometry. *J Hazard Mater* (2010) 176(1-3):481–6. doi:10.1016/j.jhazmat.2009.11.054

7. Esrafili A, Baharfar M, Tajik M, Yamini Y, Ghambarian M. Two-phase hollow fiber liquid-phase microextraction. *Trac-trend Anal Chem* (2018) 108:314–22. doi:10.1016/j.trac.2018.09.015

8. Shariati S, Yamini Y, Esrafili A. Carrier mediated hollow fiber liquid phase microextraction combined with HPLC-UV for preconcentration and determination of some tetracycline antibiotics. *J Chromatogr B* (2009) 877(4):393–400. doi:10.1016/j.jchromb.2008.12.042

9. Khan WA, Arain MB, Yamini Y, Shah N, Kazi TG, Pedersen-Bjergaard S, et al. Hollow fiber-based liquid phase microextraction followed by analytical instrumental techniques for quantitative analysis of heavy metal ions and pharmaceuticals. *J Pharm Anal* (2020) 10(2):109–22. doi:10.1016/j.jpha.2019.12.003

10. Feng CY, Khulbe KC, Matsuura T, Ismail AF. Recent progresses in polymeric hollow fiber membrane preparation, characterization and applications. *Sep Purif Technol* (2013) 111:43–71. doi:10.1016/j.seppur.2013.03.017

11. Wang HX, Zhou H, Niu HT, Zhang J, Du Y, Lin T. Dual-layer superamphiphobic/superhydrophobic-oleophilic nanofibrous membranes with unidirectional oil-transport ability and strengthened oil-water separation performance. *Adv Mater Inter* (2015) 2(4): 1400506. doi:10.1002/admi.201400506

12. Huang Y, Xiao C, Huang Q, Liu H, Zhao J. Progress on polymeric hollow fiber membrane preparation technique from the perspective of green and sustainable development. *Chem Eng J* (2021) 403:126295. doi:10.1016/j.cej.2020.126295

13. Li Y, Chen RX, Liu FJ. Comparison between electrospun and Bubbfil-spun Polyether sulfone fibers. *Matéria-Brazil* (2014) 19:363–9. doi:10.1590/S1517-70762014000400006

14. Lin L, Gong WZ, Wang X, Li XG, Wang SY. Preparation and characterizations of antibacterial PET-based hollow fibers containing silver particles. *Mater Lett* (2011) 65(9):1375–7. doi:10.1016/j.matlet.2011.02.006

15. Lin L, Gong WZ, Wang SY. Hollow PET fibers containing silver particles as antibacterial materials. *J Text Inst* (2011) 102(5):419–23. doi:10.1080/00405000.2010.486185

16. Lin L, Yao SW, Li HG. Silver ion release from Ag/PET hollow fibers: Mathematical model and its application to food packing. *J Eng Fiber Fabr* (2020) 15: 1558925020935448. doi:10.1177/1558925020935448

17. Lin L, Yao SW. Release oscillation in a hollow fiber - Part 1: Mathematical model and fast estimation of its frequency. *J Low Freq N A* (2019) 38(3-4):1703–7. doi:10.1177/1461348419836347

18. Lin L, Li HG, Liu YP. Release oscillation in a hollow fiber - Part 2: The effect of its frequency on ions release and experimental verification. *J Low Freq N A* (2021) 40(2):1067–71. doi:10.1177/1461348419874973

19. Yu DG, Teng MY, Chou WL, Yang MC. Characterization and inhibitory effect of antibacterial PAN-based hollow fiber loaded with silver nitrate. *J Membr Sci.* (2003) 225(1-2):115–23. doi:10.1016/j.memsci.2003.08.010

20. Behboudi A, Jafarzadeh Y, Yegani R. Enhancement of antifouling and antibacterial properties of PVC hollow fiber ultrafiltration membranes using pristine and modified silver nanoparticles. *J Environ Chem Eng* (2018) 6(2):1764–73. doi:10.1016/j.jece.2018.02.031

21. He JH. Fatalness of virus depends upon its cell fractal geometry. *Chaos Soliton Fract* (2008) 38(5):1390–3. doi:10.1016/j.chaos.2008.04.018

22. Liu YP, Yan RY, Zhang XH. A possible way for preventing the novel coronavirus. *Therm Sci* (2022) 26(3):2677–81. doi:10.2298/TSCI200308331L

23. Li LJ. Thermal therapy for eye diseases. *Therm Sci* (2020) 24(4):2319–24. doi:10.2298/TSCI2004319L

24. Li XX, He JH. Nanoscale adhesion and attachment oscillation under the geometric potential. Part 1: The formation mechanism of nanofiber membrane in the electrospinning. *Result Phys* (2019) 12:1405–10. doi:10.1016/j.rinp.2019.01.043

25. Fan J, Zhang YR, Liu Y. Explanation of the cell orientation in a nanofiber membrane by the geometric potential theory. *Result Phys* (2019) 15:102537. doi:10.1016/j.rinp.2019.102537

26. Tian D, Li XX, He JH. Geometrical potential and nanofiber membrane's highly selective adsorption property. *Adsorpt Sci Technol* (2019) 37(5-6):367–88. doi:10.1177/0263617418813826

27. Jin X, Liu MN, Pan F. Low frequency of a deforming capillary vibration, part 1: Mathematical model. *J Low Freq N A* (2019) 38:1676–80. doi:10.1177/1461348419856227

28. Bin C, Lu JF, Xia ZZ. Numerical investigation of the fractal capillary oscillator. *J Low Freq N A* (2023) 2023. doi:10.1177/14613484221131245

29. Han CY, He JH. Effect of fabric surface's cleanliness on its moisture/air permeability. *Therm Sci* (2021) 25(2):1517–21. doi:10.2298/TSCI2102517H

30. Zhou CJ, Tian D, He JH. Highly selective penetration of red ink in a saline water. *Therm Sci* (2019) 23(4):2265–70. doi:10.2298/TSCI1904265Z

31. He JH, Qian MY. A fractal approach to the diffusion process of red ink in a saline water. *Therm Sci* (2022) 26(3B):2447–51. doi:10.2298/TSCI2203447H

32. Qian MY, He JH. Two-scale thermal science for modern life-Making the Impossible Possible. *Therm Sci* (2022) 26(3B):2409–12.

33. Liu YP, Wang CC, Li SJ. A fractal Langmuir kinetic equation and its solution structure. *Therm Sci* (2021) 25(2):1351–4. doi:10.2298/TSCI200320033L

34. Kumar K, Chauhan PR, Kumar R, Bharj RS. Irreversibility analysis in Al_2O_3-water nanofluid flow with variable property. *Facta Univ.-Ser Mech* (2022) 20(3):503–18. doi:10.22190/FUME210308050K

35. He J, Elgazery NS, Elagamy K. Efficacy of a modulated viscosity-dependent temperature/nanoparticles concentration parameter on a nonlinear radiative electromagneto-nanofluid flow along an elongated stretching sheet. *J Appl Computat Mech* (2023) 9(3):848–60. doi:10.22055/jacm.2023.42294.3905

36. He JH, Abd-Elazem NY. The carbon nanotube-embedded boundary layer theory for energy harvesting. *Facta Univ.-Ser Mech* (2022) 20(2):211–35. doi:10.22190/FUME220221011H

37. Zhang H, Nikolov A, Wasan D. Dewetting film dynamics inside a capillary using a micellar nanofluid. *Langmuir* (2014) 30(31):9430–5. doi:10.1021/la502387j

38. He CH, Amer TS, Tian D. Controlling the kinematics of a spring-pendulum system using an energy harvesting device. *J Low Freq N A* (2022) 41(3):1234–57. doi:10.1177/14613484221077474

39. He CH, El-Dib YO. A heuristic review on the homotopy perturbation method for non-conservative oscillators. *J Low Freq N A* (2022) 41(2):572–603. doi:10.1177/14613484211059264

40. Anjum N, He JH, Ain QT, Tian D. Li-He's modified homotopy perturbation method for doubly-clamped electrically actuated microbeams-based microelectromechanical system. *Facta Univ.-Ser Mech* (2021) 19(4):601–12. doi:10.22190/FUME210112025A

41. He JH, El-Dib YO. The enhanced homotopy perturbation method for axial vibration of strings. *Facta Univ.-Ser Mech* (2021) 19(4):735–50. doi:10.22190/FUME210125033H

42. Ji QP, Wang J, Lu LX, Ge CF. Li-He's modified homotopy perturbation method coupled with the energy method for the dropping shock response of a tangent nonlinear packaging system. *J Low Freq N A* (2021) 40(2):675–82. doi:10.1177/1461348420914457

43. He CH, Liu C. A modified frequency-amplitude formulation for fractal vibration systems. *Fractals* (2022) 30(3):2250046. doi:10.1142/S0218348X22500463

44. He CH. A variational principle for a fractal nano/microelectromechanical (N/MEMS) system. *Int J Numer Method H* (2023) 33(1):351–9. doi:10.1108/HFF-03-2022-0191

45. He CH, Tian D, Moatimid GM. Hybrid Rayleigh-van der pol-duffing oscillator: Stability analysis and controller. *J Low Freq N A* (2022) 41(1):244–68. doi:10.1177/14613484211026407

46. He JH, Yang Q, He CH. *Pull-down instability of the quadratic nonlinear oscillators*. Serbia: Facta Univ.-Ser. Mech. (2023). doi:10.22190/FUME230114007H

47. He JH, Ain QT. New promises and future challenges of fractal calculus: From two-scale thermodynamics to fractal variational principle. *Therm Sci* (2020) 24(2A):659–81. doi:10.2298/TSCI200127065H

48. Xiao J, Liu MN, Pan F, Li YP, Fan J. Low frequency of a deforming capillary vibration, part 1: Mathematical model. *J Low Freq Noise V A* (2019) 38(3-4):1676–80. doi:10.1177/14613484198562

49. He CH, Liu C. Fractal dimensions of a porous concrete and its effect on the concrete's strength. *Facta Univ.-Ser Mech* (2023) 2023. doi:10.22190/FUME221215005H

50. Liu HY, Li ZM, Yao YJ. A fractional nonlinear system for release oscillation of silver ions from hollow fibers. *J Low Freq N A* (2019) 38(1):88–92. doi:10.1177/1461348418814122

51. Fan J, Yang X, Liu Y. Fractal calculus for analysis of wool fiber: Mathematical insight of its biomechanism. *J Eng Fiber Fabr* (2019) 2019:14. doi:10.1177/1558925019872200

52. Lu J, Sun Y. Numerical approaches to time fractional boussinesq-burgers equations. *Fractals* (2021) 29(08):2150244. doi:10.1142/S0218348X21502443

53. Lu J, Chen L. Numerical analysis of a fractal modification of Yao-Cheng oscillator. *Result Phys* (2022) 38:105602. doi:10.1016/j.rinp.2022.105602

54. Lu J, Ma L. Numerical analysis of a fractional nonlinear oscillator with coordinate-dependent mass. *Result Phys* (2022) 43:106108. doi:10.1016/j.rinp.2022.106108

frontiers | Frontiers in Physics

TYPE Original Research
PUBLISHED 02 June 2023
DOI 10.3389/fphy.2023.1178154

OPEN ACCESS

EDITED BY
Ji-Huan He,
Soochow University, China

REVIEWED BY
Guangqing Feng,
Henan Polytechnic University, China
Naveed Anjum,
Government College University,
Faisalabad, Pakistan

*CORRESPONDENCE
Hijaz Ahmad,
ahmad.hijaz@uninettuno.it

RECEIVED 02 March 2023
ACCEPTED 20 April 2023
PUBLISHED 02 June 2023

CITATION
Qayyum M, Ahmad E, Tauseef Saeed S, Ahmad H and Askar S (2023), Homotopy perturbation method-based soliton solutions of the time-fractional (2+1)-dimensional Wu–Zhang system describing long dispersive gravity water waves in the ocean.
Front. Phys. 11:1178154.
doi: 10.3389/fphy.2023.1178154

Homotopy perturbation method-based soliton solutions of the time-fractional (2+1)-dimensional Wu–Zhang system describing long dispersive gravity water waves in the ocean

Mubashir Qayyum[1], Efaza Ahmad[1], Syed Tauseef Saeed[1], Hijaz Ahmad[2,3,4]* and Sameh Askar[5]

[1]Department of Sciences and Humanities, National University of Computer and Emerging Sciences, Lahore, Pakistan, [2]Section of Mathematics, International Telematic University Uninettuno, Roma, Italy, [3]Operational Research Center in Healthcare, Near East University, Mersin, Turkey, [4]Department of Computer Science and Mathematics, Lebanese American University, Beirut, Lebanon, [5]Department of Statistics and Operations Research, College of Science, King Saud University, Riyadh, Saudi Arabia

Physical phenomena and natural disasters, such as tsunamis and floods, are caused due to dispersive water waves and shallow waves caused by earthquakes. In order to analyze and minimize damaging effects of such situations, mathematical models are presented by different researchers. The Wu–Zhang (WZ) system is one such model that describes long dispersive waves. In this regard, the current study focuses on a non-linear (2 + 1)-dimensional time-fractional Wu–Zhang (WZ) system due to its importance in capturing long dispersive gravity water waves in the ocean. A Caputo fractional derivative in the WZ system is considered in this study. For solution purposes, modification of the homotopy perturbation method (HPM) along with the Laplace transform is used to provide improved results in terms of accuracy. For validity and convergence, obtained results are compared with the fractional differential transform method (FDTM), modified variational iteration method (mVIM), and modified Adomian decomposition method (mADM). Analysis of results indicates the effectiveness of the proposed methodology. Furthermore, the effect of fractional parameters on the given model is analyzed numerically and graphically at both integral and fractional orders. Moreover, Caputo, Caputo–Fabrizio, and Atangana–Baleanu approaches of fractional derivatives are applied and compared graphically in the current study. Analysis affirms that the proposed algorithm is a reliable tool and can be used in higher dimensional fractional systems in science and engineering.

KEYWORDS

Wu–Zhang system, fractional-order system, homotopy perturbation, Laplace transform, Caputo, Atangana–Baleanu, Caputo–Fabrizio

Abbreviations: WZ, Wu–Zhang; DEs, differential equations; PDEs, partial differential equations; FDEs, fractional differential equations; HPM, homotopy perturbation method; HLM, He–Laplace method; mVIM, modified variation iteration method; mADM, modified Adomian decomposition method; FRDTM, fractional reduced differential transform method.

1 Introduction

The study of differential equations (DEs) is a pivotal topic as they capture most of the real-world phenomena, i.e., earthquakes [1, 2], natural gas consumption [3, 4], current flow [5], and cooking [6]. These equations can additionally be characterized into linear and non-linear differential equations. Many important and interesting phenomena like electrical circuits [7, 8], DNA sequencing [9, 10], disease modeling and analysis [11, 12], and food chain models [13, 14] are captured through differential equations. Since the order of a DE describes the nature and scope of the captured phenomena, it is therefore important for researchers to cater fractional-order derivatives for a more general study of the physical aspects of the considered phenomena. Fractional models allow better understanding of model dynamics and facilitate researchers to accurately predict changes in the physical systems. The chaos theory [15], nanotechnology [16], fluid flow [17], cosmology [18], and robotics [19] use differential equations for problem formulation. These equations also frequently appear in many branches of mathematics [20, 21], finance [22], economy [23], and biology [24].

The phrase "fractal" was first created in 1975 by mathematician Benoit Mandelbrot [25]. It is a geometric shape that exhibits the same level of non-regularity on all scales. Fractals are infinite patterns, which we frequently see in nature. Snowflakes, trees, mountains, clouds, and coastlines represent fractals as they are highly uneven at both large and small scales. Many important models including the diffusion model of red ink [26] and thin films [27], the vibration model for a concrete beam [28] and electronic devices [29], and the COVID-19 mathematical model [30] contain fractal geometry. The distinction between fractional and fractal is that the former is a statement of a fractional number, while the latter is a geometric figure that is similar at all scales.

The Wu–Zhang system [31] contains non-linear partial differential equations (PDEs) and deals with the motion of water waves in oceans. In 1996, three sets of model equations were first derived by Wu and Zhang and named the Wu–Zhang system of PDEs [31]. This system is used to customize several harbor and coastal designs. This non-linear (2 + 1)-dimensional fractional system describes shallow water dispersive long gravity waves in two horizontal directions, which are given as

$$\begin{aligned}
&\frac{\partial^{\zeta}\mathcal{U}}{\partial \mathrm{t}^{\zeta}}+\mathcal{U}\frac{\partial \mathcal{U}}{\partial x}+\mathcal{V}\frac{\partial \mathcal{U}}{\partial y}+\frac{\partial \mathcal{W}}{\partial x}=0,\\
&\frac{\partial^{\zeta}\mathcal{V}}{\partial \mathrm{t}^{\zeta}}+\mathcal{U}\frac{\partial \mathcal{V}}{\partial x}+\mathcal{V}\frac{\partial \mathcal{V}}{\partial y}+\frac{\partial \mathcal{W}}{\partial y}=0,\\
&\frac{\partial^{\zeta}\mathcal{W}}{\partial \mathrm{t}^{\zeta}}+\frac{\partial(\mathcal{U}\mathcal{W})}{\partial x}+\frac{\partial(\mathcal{V}\mathcal{W})}{\partial y}+\frac{1}{3}\left(\frac{\partial^{3}\mathcal{U}}{\partial x^{3}}+\frac{\partial^{3}\mathcal{U}}{\partial x\partial y^{2}}+\frac{\partial^{3}\mathcal{V}}{\partial x^{2}\partial y}+\frac{\partial^{3}\mathcal{V}}{\partial y^{3}}\right)=0,
\end{aligned} \tag{1}$$

where $\mathcal{U}$ and $\mathcal{V}$ represent the velocities at the surface of water in x and y directions, while $\mathcal{W}$ depicts the elevation of water waves. The aforementioned WZ system is a time fraction, while Wang and He [32] concluded that when time is fractional, space must also be fractional. This is called Wang–He's spatiotemporal fractional relationship (for more details see [32]). Due to the substantial importance of WZ systems, many scholars have attempted to solve and analyze these systems through variety of methodologies like mVIM [33], ADM [34, 35], extended tanh and exp–function method [36], and dynamical analysis method [37]. Recently, for more generalized solutions and predictions, the WZ systems are also attempted fractionally by few of the scientists. Kaur and Gupta discussed dispersion analysis of the (2 + 1)-dimensional time-fractional WZ system [38]. Patel and Patel investigated the fractional-order WZ system analytically [39]. Different approaches of fractional derivatives can be utilized, such as Caputo [40], Atangana–Baleanu [41], Caputo–Fabrizio [42], and He's fractional derivative [43].

In order to solve such highly non-linear fractional systems, many analytical and numerical methodologies are utilized by different researchers. Anjum et al. [44] applied Li–He's modified homotopy perturbation approach to solve the microelectromechanical system. Baitiche et al. [45] used the monotone iterative method for fractional DEs with non-linearity at the boundary. Do et al. [46] extended Chebyshev wavelets to two-dimensional fractional DEs. Hashemi et al. [47] investigated multi-term FDEs using minimization techniques. Tian and Liu utilized the modified exp-function to fractional PDEs in [48]. Furthermore, to solve complex problems, the enhanced homotopy methods can be found in [49, 50]. In this study, a hybrid algorithm is proposed by mixing the classical homotopy perturbation method [51, 52] with the Laplace transform [53] along with different fractional derivatives (Atangana–Baleanu, Caputo–Fabrizio, and Caputo) for a highly non-linear time-fractional (2 + 1)-dimensional WZ system. In the rest of the paper, Section 2 contains preliminary definitions. Section 3 contains the proposed methodology for handling time-fractional (2 + 1)-dimensional WZ system, whereas proof of convergence and error analysis are given in Section 4. Solution and results and discussion are given in Sections 5 and 6, respectively, while a conclusion is given in Section 7.

2 Basic definitions

Definition 1: For a function $\mathcal{U}(t,x,y)$, the Caputo's time-fractional derivative ${}^{C}\mathcal{D}_{t}^{\zeta}$ is [54]

$${}^{C}\mathcal{D}_{t}^{\zeta}\mathcal{U}(t,x,y)=\frac{1}{\Gamma(q-\zeta)}\int_{0}^{t}(t-G)^{q-\zeta-1}\mathcal{U}^{(q)}(G,x,y)dG,\quad q-1<\zeta\le q. \tag{2}$$

Definition 2: According to [55], one can express the Laplace transform $\mathbf{L}$ of the function $\mathcal{U}(t,x,y)$ that has been subjected to the Caputo's time-fractional derivative ${}^{C}\mathcal{D}_{t}^{\zeta}$.

$$\mathbf{L}\left\{{}^{C}\mathcal{D}_{t}^{\zeta}\mathcal{U}(t,x,y)\right\}=s^{\zeta}\mathbf{L}\{\mathcal{U}(t,x,y)\}-\sum_{p=0}^{q-1}s^{\zeta-p-1}\mathcal{U}^{(p)}(0,x,y),\quad q-1<\zeta\le q. \tag{3}$$

Definition 3: The Caputo–Fabrizio's time-fractional derivative ${}^{CF}\mathcal{D}_{t}^{\zeta}$ of a function $\mathcal{U}(t,x,y)$ is [42]

$${}^{CF}\mathcal{D}_{t}^{\zeta}\mathcal{U}(t,x,y)=\frac{1}{1-\zeta}\int_{0}^{t}e^{\frac{-\zeta(t-G)}{1-\zeta}}\frac{\partial\mathcal{U}(G,x,y)}{\partial G}dG,\qquad 0<\zeta<1. \tag{4}$$

Definition 4: The Laplace transform **L** of the Caputo–Fabrizio's time-fractional derivative ${}^{CF}\mathcal{D}_t^{\zeta}$ of a function $\mathcal{U}(t,x,y)$ is given as [56]

$$\mathbf{L}\left\{{}^{CF}\mathcal{D}_t^{\zeta+q}\mathcal{U}(t,x,y)\right\} = \frac{s^{q+1}\mathbf{L}\{\mathcal{U}(t,x,y)\} - \sum_{p=0}^{q} s^{q-p}\mathcal{U}^{(p)}(0,x,y)}{s+\zeta(1-s)}, \qquad 0<\zeta\le 1. \tag{5}$$

Definition 5: A function $\mathcal{U}(t,x,y)$ in the sense of Atangana–Baleanu's time-fractional derivative ${}^{AB}\mathcal{D}_t^{\zeta}$ is stated as [41]

$${}^{AB}\mathcal{D}_t^{\zeta}\mathcal{U}(t,x,y) = \frac{\mathbb{K}(\zeta)}{1-\zeta}\int_0^t E_{\zeta}\left[-\frac{\zeta(t-G)^{\zeta}}{1-\zeta}\right]\frac{\partial\mathcal{U}(G,x,y)}{\partial G}dG, \qquad 0<\zeta\le 1. \tag{6}$$

Here, $\mathbb{K}(\zeta)$ is a normalization function with properties $\mathbb{K}(0) = \mathbb{K}(1) = 1$.

Definition 6: The Laplace transform **L** connected with Atangana–Baleanu time-fractional derivative ${}^{AB}\mathcal{D}_t^{\zeta}$ of a function $\mathcal{U}(t,x,y)$ can be described as [57]

$$\mathbf{L}\left\{{}^{AB}\mathcal{D}_t^{\zeta}\mathcal{U}(t,x,y)\right\} = AB(\zeta).\frac{s^{\zeta}\mathbf{L}\{\mathcal{U}(t,x,y)\} - s^{\zeta-1}\mathcal{U}(0,x,y)}{s^{\zeta}(1-\zeta)+\zeta}, \qquad 0\le\zeta\le 1. \tag{7}$$

Here, $AB(\zeta)$ is a normalization function.

Definition 7: He's fractional derivative of a function $\mathcal{U}(t,x,y)$ can be defined by [43]

$$\mathcal{D}_t^{\zeta}\mathcal{U}(t,x,y) = \frac{1}{\Gamma(q-\zeta)}\frac{d^q}{dt^q}\int_{t_0}^{t}(G-t)^{q-\zeta-1}[\mathcal{U}_0(G,x,y)-\mathcal{U}(G,x,y)]dG, \quad q-1<\zeta\le q. \tag{8}$$

Definition 8: The core idea behind the **two-scale dimension** [58, 59], which commonly arises in the non-linear problem, is that while self-similarity is difficult to uncover in practical applications, fractal structures self-assemble on all scales. Creating models with the two-scale dimension allows for the successful description of various physical events.

Definition 9: **A Banach space** $\mathbb{B}$ is a normed space $\|.\|$, which is complete with respect to the metric derived from its norm.

3 Hybrid algorithm for (2 + 1)-dimensional time-fractional systems

Consider a (2 + 1)-dimensional, time-fractional system as

$$\begin{aligned}
&\mathcal{D}_t^{\zeta}\mathcal{A}1(t,x,y) + \mathcal{L}[\mathcal{A}r(t,x,y)] + \mathcal{N}[\mathcal{A}r(t,x,y)] - \mathfrak{l}(t,x,y) = 0,\\
&\mathcal{D}_t^{\zeta}\mathcal{A}2(t,x,y) + \mathcal{L}[\mathcal{A}r(t,x,y)] + \mathcal{N}[\mathcal{A}r(t,x,y)] - \mathfrak{m}(t,x,y) = 0,\\
&\mathcal{D}_t^{\zeta}\mathcal{A}3(t,x,y) + \mathcal{L}[\mathcal{A}r(t,x,y)] + \mathcal{N}[\mathcal{A}r(t,x,y)] - \mathfrak{n}(t,x,y) = 0,\\
&r = 1,2,3,\ t>0,\\
&q-1<\zeta\le q,
\end{aligned} \tag{9}$$

that has initial conditions

$$\begin{aligned}
\mathcal{A}1(0,x,y) &= \mathcal{J}1,\\
\mathcal{A}2(0,x,y) &= \mathcal{J}2,\\
\mathcal{A}3(0,x,y) &= \mathcal{J}3,
\end{aligned} \tag{10}$$

where the unknown functions $\mathcal{A}1(t,x,y)$, $\mathcal{A}2(t,x,y)$, and $\mathcal{A}3(t,x,y)$ have time-fractional derivatives, and $\mathcal{D}_t^{\zeta}$, $\mathfrak{l}(t,x,y)$, $\mathfrak{m}(t,x,y)$, and $\mathfrak{n}(t,x,y)$ are some of its known functions. The symbols $\mathcal{N}$ and $\mathcal{L}$ represent non-linear and linear operators, respectively.

The procedure will start by applying the Laplace transform on (9), which gives

$$\begin{aligned}
&\mathcal{L}\left\{\mathcal{D}_t^{\zeta}[\mathcal{A}1(t,x,y)]\right\} + \mathcal{L}\{\mathcal{L}[\mathcal{A}r(t,x,y)] + \mathcal{N}[\mathcal{A}r(t,x,y)]\\
&\quad - \mathfrak{l}(t,x,y)\} = 0, \mathcal{L}\left\{\mathcal{D}_t^{\zeta}[\mathcal{A}2(t,x,y)]\right\} + \mathcal{L}\{\mathcal{L}[\mathcal{A}r(t,x,y)]\\
&\quad + \mathcal{N}[\mathcal{A}r(t,x,y)] - \mathfrak{m}(t,x,y)\} = 0, \mathcal{L}\left\{\mathcal{D}_t^{\zeta}[\mathcal{A}3(t,x,y)]\right\}\\
&\quad + \mathcal{L}\{\mathcal{L}[\mathcal{A}r(t,x,y)] + \mathcal{N}[\mathcal{A}r(t,x,y)] - \mathfrak{n}(t,x,y)\} = 0.
\end{aligned} \tag{11}$$

Now, by utilizing the basic definitions given in Section 2, we can find the Laplace transform of the fractional derivative. Definition (2) gives

$$\begin{aligned}
&\mathcal{L}[\mathcal{A}1(t,x,y)] - \left(\frac{1}{s^{\zeta}}\right)\sum_{p=0}^{q-1} s^{\zeta-p-1}\mathcal{A}1^{(p)}(0,x,y)\\
&+ \left(\frac{1}{s^{\zeta}}\right)\mathcal{L}\{\mathcal{L}[\mathcal{A}r(t,x,y)] + \mathcal{N}[\mathcal{A}r(t,x,y)] - \mathfrak{l}(t,x,y)\} = 0,\\
&\mathcal{L}[\mathcal{A}2(t,x,y)] - \left(\frac{1}{s^{\zeta}}\right)\sum_{p=0}^{q-1} s^{\zeta-p-1}\mathcal{A}2^{(p)}(0,x,y)\\
&+ \left(\frac{1}{s^{\zeta}}\right)\mathcal{L}\{\mathcal{L}[\mathcal{A}r(t,x,y)] + \mathcal{N}[\mathcal{A}r(t,x,y)] - \mathfrak{m}(t,x,y)\} = 0,\\
&\mathcal{L}[\mathcal{A}3(t,x,y)] - \left(\frac{1}{s^{\zeta}}\right)\sum_{p=0}^{q-1} s^{\zeta-p-1}\mathcal{A}3^{(p)}(0,x,y)\\
&+ \left(\frac{1}{s^{\zeta}}\right)\mathcal{L}\{\mathcal{L}[\mathcal{A}r(t,x,y)] + \mathcal{N}[\mathcal{A}r(t,x,y)] - \mathfrak{n}(t,x,y)\} = 0.
\end{aligned} \tag{12}$$

The homotopy of the system is

$$\begin{aligned}
&\mathcal{H}_1 = (1-s)(\mathcal{L}\{\mathcal{A}1(t,x,y)\} - \mathcal{A}1_0(t,x,y)) + s\Big(\mathcal{L}\{\mathcal{A}1(t,x,y)\}\\
&-\left(\frac{1}{s^{\zeta}}\right)\sum_{p=0}^{q-1} s^{\zeta-p-1}\mathcal{A}1^{(p)}(0,x,y) + \left(\frac{1}{s^{\zeta}}\right)\mathcal{L}\{\mathcal{L}[\mathcal{A}r(t,x,y)] + \mathcal{N}[\mathcal{A}r(t,x,y)]\\
&-\mathfrak{l}(t,x,y)\}), \mathcal{H}_2 = (1-s)(\mathcal{L}\{\mathcal{A}2(t,x,y)\} - \mathcal{A}2_0(t,x,y))\\
&+s\Big(\mathcal{L}\{\mathcal{A}2(t,x,y)\} - \left(\frac{1}{s^{\zeta}}\right)\sum_{p=0}^{q-1} s^{\zeta-p-1}\mathcal{A}2^{(p)}(0,x,y) + \left(\frac{1}{s^{\zeta}}\right)\mathcal{L}\{\mathcal{L}[\mathcal{A}r(t,x,y)]\\
&+\mathcal{N}[\mathcal{A}r(t,x,y)] - \mathfrak{m}(t,x,y)\}), \mathcal{H}_3 = (1-s)(\mathcal{L}\{\mathcal{A}3(t,x,y)\}\\
&-\mathcal{A}3_0(t,x,y)) + s\Big(\mathcal{L}\{\mathcal{A}3(t,x,y)\} - \left(\frac{1}{s^{\zeta}}\right)\sum_{p=0}^{q-1} s^{\zeta-p-1}\mathcal{A}3^{(p)}(0,x,y)\\
&+\left(\frac{1}{s^{\zeta}}\right)\mathcal{L}\{\mathcal{L}[\mathcal{A}r(t,x,y)] + \mathcal{N}[\mathcal{A}r(t,x,y)] - \mathfrak{n}(t,x,y)\}),
\end{aligned} \tag{13}$$

where $\mathcal{A}1_0$, $\mathcal{A}2_0$, and $\mathcal{A}3_0$ are initial guesses. Expansion of $\mathcal{A}1(t,x,y)$, $\mathcal{A}2(t,x,y)$, and $\mathcal{A}3(t,x,y)$ in power series with respect to s leads to

$$\begin{aligned}
\mathcal{A}1(t,x,y) &= \mathcal{A}1_0(t,x,y) + s^1\mathcal{A}1_1(t,x,y) + s^2\mathcal{A}1_2(t,x,y) + \ldots\\
\mathcal{A}2(t,x,y) &= \mathcal{A}2_0(t,x,y) + s^1\mathcal{A}2_1(t,x,y) + s^2\mathcal{A}2_2(t,x,y) + \ldots\\
\mathcal{A}3(t,x,y) &= \mathcal{A}3_0(t,x,y) + s^1\mathcal{A}3_1(t,x,y) + s^2\mathcal{A}3_2(t,x,y) + \ldots
\end{aligned} \tag{14}$$

After substituting Eq. 14 in (13) and then comparing similar coefficients of s, we obtainAt s^1

$$\begin{aligned}
&\mathcal{L}\{\mathcal{A}1_1(t,x,y)\}+\mathcal{A}1_0(t,x,y)-\left(\frac{1}{s^\zeta}\right)\sum_{p=0}^{q-1}s^{\zeta-p-1}\mathcal{A}1^{(p)}(0,x,y)\\
&+\left(\frac{1}{s^\zeta}\right)\mathcal{L}\{\mathcal{L}[\mathcal{A}r_0(t,x,y)]\ +\mathcal{N}[\mathcal{A}r_0(t,x,y)]-\mathfrak{l}(t,x,y)\}=0,\\
&\mathcal{L}\{\mathcal{A}2_1(t,x,y)\}+\mathcal{A}2_0(t,x,y)-\left(\frac{1}{s^\zeta}\right)\sum_{p=0}^{q-1}s^{\zeta-p-1}\mathcal{A}2^{(p)}(0,x,y)\\
&+\left(\frac{1}{s^\zeta}\right)\mathcal{L}\{\mathcal{L}[\mathcal{A}r_0(t,x,y)]\ +\mathcal{N}[\mathcal{A}r_0(t,x,y)]-\mathfrak{m}(t,x,y)\}=0,\\
&\mathcal{L}\{\mathcal{A}3_1(t,x,y)\}+\mathcal{A}3_0(t,x,y)-\left(\frac{1}{s^\zeta}\right)\sum_{p=0}^{q-1}s^{\zeta-p-1}\mathcal{A}3^{(p)}(0,x,y)\\
&+\left(\frac{1}{s^\zeta}\right)\mathcal{L}\{\mathcal{L}[\mathcal{A}r_0(t,x,y)]\ +\mathcal{N}[\mathcal{A}r_0(t,x,y)]-\mathfrak{n}(t,x,y)\}=0.
\end{aligned}\tag{15}$$

The inverse Laplace transform leads to

$$\begin{aligned}
&\mathcal{A}1_1(t,x,y)+\mathcal{L}^{-1}\left\{\mathcal{A}1_0(t,x,y)-\left(\frac{1}{s^\zeta}\right)\sum_{p=0}^{q-1}s^{\zeta-p-1}\mathcal{A}1^{(p)}(0,x,y)\right\}+\mathcal{L}^{-1}\left\{\left(\frac{1}{s^\zeta}\right)\right.\\
&\left.\mathcal{L}\{\mathcal{L}[\mathcal{A}r_0(t,x,y)]+\mathcal{N}[\mathcal{A}r_0(t,x,y)]-\mathfrak{l}(t,x,y)\right\}=0,\\
&\mathcal{A}2_1(t,x,y)+\mathcal{L}^{-1}\left\{\mathcal{A}2_0(t,x,y)-\left(\frac{1}{s^\zeta}\right)\sum_{p=0}^{q-1}s^{\zeta-p-1}\mathcal{A}2^{(p)}(0,x,y)\right\}+\mathcal{L}^{-1}\left\{\left(\frac{1}{s^\zeta}\right)\right.\\
&\left.\mathcal{L}\{\mathcal{L}[\mathcal{A}r_0(t,x,y)]+\mathcal{N}[\mathcal{A}r_0(t,x,y)]-\mathfrak{m}(t,x,y)\right\}=0,\\
&\mathcal{A}3_1(t,x,y)+\mathcal{L}^{-1}\left\{\mathcal{A}3_0(t,x,y)-\left(\frac{1}{s^\zeta}\right)\sum_{p=0}^{q-1}s^{\zeta-p-1}\mathcal{A}3^{(p)}(0,x,y)\right\}+\mathcal{L}^{-1}\left\{\left(\frac{1}{s^\zeta}\right)\right.\\
&\left.\mathcal{L}\{\mathcal{L}[\mathcal{A}r_0(t,x,y)]+\mathcal{N}[\mathcal{A}r_0(t,x,y)]-\mathfrak{n}(t,x,y)\right\}=0.
\end{aligned}\tag{16}$$

At s^k

$$\begin{aligned}
&\mathcal{L}\{\mathcal{A}1_k(t,x,y)\}+\left(\frac{1}{s^\zeta}\right)\mathcal{L}\{\mathcal{L}[\mathcal{A}r_{k-1}(t,x,y)]+\mathcal{N}[\mathcal{A}r_{k-1}(t,x,y)]\}=0,\\
&\mathcal{L}\{\mathcal{A}2_k(t,x,y)\}+\left(\frac{1}{s^\zeta}\right)\mathcal{L}\{\mathcal{L}[\mathcal{A}r_{k-1}(t,x,y)]+\mathcal{N}[\mathcal{A}r_{k-1}(t,x,y)]\}=0,\\
&\mathcal{L}\{\mathcal{A}3_k(t,x,y)\}+\left(\frac{1}{s^\zeta}\right)\mathcal{L}\{\mathcal{L}[\mathcal{A}r_{k-1}(t,x,y)]+\mathcal{N}[\mathcal{A}r_{k-1}(t,x,y)]\}=0.
\end{aligned}\tag{17}$$

Operating the inverse Laplace transform gives the following:

$$\begin{aligned}
&\mathcal{A}1_k(t,x,y)+\mathcal{L}^{-1}\left\{\left(\frac{1}{s^\zeta}\right)\mathcal{L}\{\mathcal{L}[\mathcal{A}r_{k-1}(t,x,y)]+\mathcal{N}[\mathcal{A}r_{k-1}(t,x,y)]\}\right\}=0,\\
&\mathcal{A}2_k(t,x,y)+\mathcal{L}^{-1}\left\{\left(\frac{1}{s^\zeta}\right)\mathcal{L}\{\mathcal{L}[\mathcal{A}r_{k-1}(t,x,y)]+\mathcal{N}[\mathcal{A}r_{k-1}(t,x,y)]\}\right\}=0,\\
&\mathcal{A}3_k(t,x,y)+\mathcal{L}^{-1}\left\{\left(\frac{1}{s^\zeta}\right)\mathcal{L}\{\mathcal{L}[\mathcal{A}r_{k-1}(t,x,y)]+\mathcal{N}[\mathcal{A}r_{k-1}(t,x,y)]\}\right\}=0.
\end{aligned}\tag{18}$$

The approximate solution of the given general time-fractional, (2 + 1)-dimensional PDE system is

$$\begin{aligned}
\tilde{\mathcal{A}}1&=\mathcal{A}1_0(t,x,y)+\mathcal{A}1_1(t,x,y)+\mathcal{A}1_2(t,x,y)+\mathcal{A}1_3(t,x,y)+\cdots,\\
\tilde{\mathcal{A}}2&=\mathcal{A}2_0(t,x,y)+\mathcal{A}2_1(t,x,y)+\mathcal{A}2_2(t,x,y)+\mathcal{A}1_3(t,x,y)+\cdots,\\
\tilde{\mathcal{A}}3&=\mathcal{A}3_0(t,x,y)+\mathcal{A}3_1(t,x,y)+\mathcal{A}3_2(t,x,y)+\mathcal{A}3_3(t,x,y)+\cdots.
\end{aligned}\tag{19}$$

Residual errors of the system are

$$\begin{aligned}
\mathfrak{Res}1&=\mathcal{D}_t^\zeta[\tilde{\mathcal{A}}1]+\mathcal{L}[\tilde{\mathcal{A}}r]+\mathcal{N}[\tilde{\mathcal{A}}r]-\mathfrak{l}(t,x,y),\\
\mathfrak{Res}2&=\mathcal{D}_t^\zeta[\tilde{\mathcal{A}}2]+\mathcal{L}[\tilde{\mathcal{A}}r]+\mathcal{N}[\tilde{\mathcal{A}}r]-\mathfrak{m}(t,x,y),\\
\mathfrak{Res}3&=\mathcal{D}_t^\zeta[\tilde{\mathcal{A}}3]+\mathcal{L}[\tilde{\mathcal{A}}r]+\mathcal{N}[\tilde{\mathcal{A}}r]-\mathfrak{n}(t,x,y).
\end{aligned}\tag{20}$$

The same procedure can be extended to a system that comprises more than three equations.

4 Convergence and error analysis of the hybrid algorithm for (2 + 1)-dimensional fractional systems

4.1 Convergence

Theorem 1: If a Banach space has $\mathcal{A}r_n(t,x,y)$ and $\mathcal{A}r(t,x,y)$ defined in it for $r = 1, 2, 3$, then, the series solution of a fractional (2 + 1)-D system in Eq. 19 converges to the solution of (9) for a constant $\mu \in (0,1)$.

Proof: Let us define the sequence of partial sums of Eq. 19 as Qr_n. To demonstrate that $Qr_n(t, x, y)$ forms a Cauchy sequence in the Banach space, we can proceed by using

$$\begin{aligned}
\|Qr_{n+1}(t,x,y)-Qr_n(t,x,y)\|&=\|\mathcal{A}r_{n+1}(t,x,y)\|\\
&\le\mu\|\mathcal{A}r_n(t,x,y)\|\\
&\le\mu^2\|\mathcal{A}r_{n-1}(t,x,y)\|\\
&\le\ldots\le\mu^{n+1}\|\mathcal{A}r_0(t,x,y)\|.
\end{aligned}\tag{21}$$

If Qr_n and Qr_m are partial sums with $n \ge m$ and $n, m \in \mathbf{N}$, then utilization of triangle inequality gives

$$\begin{aligned}
\|Qr_n-Qr_m\|&=\|(Qr_n(t,x,y)-Qr_{n-1}(t,x,y))+(Qr_{n-1}(t,x,y)\\
&\quad-Qr_{n-2}(t,x,y))+\cdots+(Qr_{m+1}(t,x,y)\\
&\quad-Qr_m(t,x,y))\|\le\|Qr_n(t,x,y)-Qr_{n-1}(t,x,y)\|\\
&\quad+\|Qr_{n-1}(t,x,y)-Qr_{n-2}(t,x,y)\|\\
&\quad+\cdots+\|Qr_{m+1}(t,x,y)-Qr_m(t,x,y)\|.
\end{aligned}\tag{22}$$

From Eq. 21, we get

$$\begin{aligned}
\|Qr_n-Qr_m\|&\le\mu^n\|\mathcal{A}r_0(t,x,y)\|+\mu^{n-1}\|\mathcal{A}r_0(t,x,y)\|\\
&\quad+\cdots+\mu^{m+1}\|\mathcal{A}r_0(t,x,y)\|\le(\mu^n+\mu^{n-1}+\cdots+\mu^{m+1})\\
\|\mathcal{A}r_0(t,x,y)\|&\le\mu^{m+1}(\mu^{n-m-1}+\mu^{n-m-2}+\cdots+\mu+1)\\
\|\mathcal{A}r_0(t,x,y)\|&\le\mu^{m+1}\left(\frac{1-\mu^{n-m}}{1-\mu}\right)\|\mathcal{A}r_0(t,x,y)\|.
\end{aligned}\tag{23}$$

Given $0 < \mu < 1$, hence, $1 - \mu^{n-m} < 1$. Thus, we have

$$\|Qr_n-Qr_m\|\le\frac{\mu^{m+1}}{1-\mu}\ max\ |\mathcal{A}r_0(t,x,y)|,\qquad\forall\ t\in[0,T].\tag{24}$$

Since $\mathcal{A}r_0$ is bounded, so

$$\lim_{n,m\to\infty}\|Qr_n(t,x,y)-Qr_m(t,x,y)\|=0.\tag{25}$$

Thus, $Qr_n(t, x, y)$ is a Cauchy sequence in the Banach space, and hence, the given statement is proved.

4.2 Error estimation

Theorem 1: One can determine the maximum absolute truncation error of the solution (19) for a fractional (2 + 1)-dimensional system (9) by using the following expression:

TABLE 1 He–Laplace errors for different values of ζ, when $a = d = 0.13$, $b = 0.11$, $c = 0.12$, $x = 3$, and $y = 6$. Here, $\mathcal{R}_u$, $\mathcal{R}_v$, $\mathcal{R}_w$, and $\mathcal{R}$ represent residual errors of $\mathcal{U}$, $\mathcal{V}$, $\mathcal{W}$, and system errors, respectively.

ζ	t	$\mathcal{R}_u$	$\mathcal{R}_v$	$\mathcal{R}_w$	$\mathcal{R}$
0.1	0.1	9.81×10^{-7}	1.07×10^{-6}	1.95×10^{-6}	1.33×10^{-6}
	0.3	1.69×10^{-6}	1.84×10^{-6}	3.38×10^{-6}	2.30×10^{-6}
	0.5	2.17×10^{-6}	2.37×10^{-6}	4.36×10^{-6}	2.97×10^{-6}
	0.7	2.56×10^{-6}	2.80×10^{-6}	5.16×10^{-6}	3.51×10^{-6}
	0.9	2.90×10^{-6}	3.17×10^{-6}	5.86×10^{-6}	3.98×10^{-6}
	0.1	8.75×10^{-9}	9.54×10^{-9}	9.87×10^{-9}	9.39×10^{-9}
	0.3	1.02×10^{-7}	1.11×10^{-7}	1.17×10^{-7}	1.10×10^{-7}
0.45	0.5	3.19×10^{-7}	3.48×10^{-7}	3.71×10^{-7}	3.46×10^{-7}
	0.7	6.76×10^{-7}	7.37×10^{-7}	7.94×10^{-7}	7.36×10^{-7}
	0.9	1.18×10^{-6}	1.29×10^{-6}	1.40×10^{-6}	1.29×10^{-6}
	0.1	1.27×10^{-10}	1.39×10^{-10}	6.70×10^{-11}	1.11×10^{-10}
	0.3	6.22×10^{-9}	6.78×10^{-9}	3.34×10^{-9}	5.45×10^{-9}
0.71	0.5	3.78×10^{-8}	4.12×10^{-8}	2.06×10^{-8}	3.23×10^{-8}
	0.7	1.23×10^{-7}	1.35×10^{-7}	6.87×10^{-8}	1.09×10^{-7}
	0.9	2.99×10^{-7}	3.27×10^{-7}	1.68×10^{-7}	2.65×10^{-7}
	0.1	1.48×10^{-12}	1.62×10^{-12}	9.78×10^{-14}	1.06×10^{-12}
	0.3	2.87×10^{-10}	3.13×10^{-10}	2.03×10^{-11}	2.07×10^{-10}
0.96	0.5	3.31×10^{-9}	3.61×10^{-9}	2.49×10^{-10}	2.39×10^{-9}
	0.7	1.65×10^{-8}	1.80×10^{-8}	1.32×10^{-9}	1.19×10^{-8}
	0.9	5.48×10^{-8}	5.98×10^{-8}	4.63×10^{-9}	3.98×10^{-8}

$$\left|\mathcal{A}r(t,x,y) - \sum_{j=0}^{m} \mathcal{A}r_j(t,x,y)\right| \le \frac{\mu^{m+1}}{1-\mu}\|\mathcal{A}r_0(t,x,y)\|. \tag{26}$$

Proof: From Eq. 23, we have

$$\|\mathcal{A}r(t,x,y) - Qr_m\| \le \mu^{m+1}\left(\frac{1-\mu^{n-m}}{1-\mu}\right)\|\mathcal{A}r_0(t,x,y)\|. \tag{27}$$

Since $0 < \mu < 1$, therefore, $1 - \mu^{n-m} < 1$. Thus, we have

$$\left|\mathcal{A}r(t,x,y) - \sum_{j=0}^{m} \mathcal{A}r_j(t,x,y)\right| \le \frac{\mu^{m+1}}{1-\mu}\|\mathcal{A}r_0(t,x,y)\|. \tag{28}$$

5 Solution and analysis of the time-fractional Wu–Zhang system

Consider the following coupled time-fractional (2 + 1)-dimensional WZ system [39]:

$$\begin{aligned}
&\frac{\partial^\zeta \mathcal{U}}{\partial t^\zeta} + \mathcal{U}\frac{\partial \mathcal{U}}{\partial x} + \mathcal{V}\frac{\partial \mathcal{U}}{\partial y} + \frac{\partial \mathcal{W}}{\partial x} = 0,\\
&\frac{\partial^\zeta \mathcal{V}}{\partial t^\zeta} + \mathcal{U}\frac{\partial \mathcal{V}}{\partial x} + \mathcal{V}\frac{\partial \mathcal{V}}{\partial y} + \frac{\partial \mathcal{W}}{\partial y} = 0,\\
&\frac{\partial^\zeta \mathcal{W}}{\partial t^\zeta} + \frac{\partial(\mathcal{U}\mathcal{W})}{\partial x} + \frac{\partial(\mathcal{V}\mathcal{W})}{\partial y} + \frac{1}{3}\left(\frac{\partial^3 \mathcal{U}}{\partial x^3} + \frac{\partial^3 \mathcal{U}}{\partial x \partial y^2} + \frac{\partial^3 \mathcal{V}}{\partial x^2 \partial y} + \frac{\partial^3 \mathcal{V}}{\partial y^3}\right) = 0,\\
&0 < \zeta \le 1
\end{aligned} \tag{29}$$

that has the initial conditions

$$\begin{aligned}
\mathcal{U}(0,x,y) &= -\frac{d+ac}{b} + \frac{2\sqrt{3}}{3} b \tanh(bx+cy),\\
\mathcal{V}(0,x,y) &= a + \frac{2\sqrt{3}}{3} c \tanh(bx+cy),\\
\mathcal{W}(0,x,y) &= \frac{2}{3}(b^2+c^2)\operatorname{sech}^2(bx+cy),
\end{aligned} \tag{30}$$

where $\mathcal{U}$ and $\mathcal{V}$ represent the velocity at the surface of water in the x and y directions, respectively, and $\mathcal{W}$ depicts the elevation of the water waves. a, b, c, and d are the non-zero arbitrary constants. The exact solution of (29) at $\zeta = 1$ is

$$\begin{aligned}
\mathcal{U}(t,x,y) &= -\frac{d+ac}{b} + \frac{2\sqrt{3}}{3} b \tanh(bx+cy+dt),\\
\mathcal{V}(t,x,y) &= a + \frac{2\sqrt{3}}{3} c \tanh(bx+cy+dt),\\
\mathcal{W}(t,x,y) &= \frac{2}{3}(b^2+c^2)\operatorname{sech}^2(bx+cy+dt).
\end{aligned} \tag{31}$$

Solution: The initial step of the He–Laplace procedure is the application of the Laplace transform on both sides of Eq. 29, which gives

$$\begin{aligned}
&\mathbf{L}\left\{\frac{\partial^\zeta \mathcal{U}}{\partial t^\zeta}\right\} + \mathbf{L}\left\{\mathcal{U}\frac{\partial \mathcal{U}}{\partial x} + \mathcal{V}\frac{\partial \mathcal{U}}{\partial y} + \frac{\partial \mathcal{W}}{\partial x}\right\} = 0, \mathbf{L}\left\{\frac{\partial^\zeta \mathcal{V}}{\partial t^\zeta}\right\}\\
&+ \mathbf{L}\left\{\mathcal{U}\frac{\partial \mathcal{V}}{\partial x} + \mathcal{V}\frac{\partial \mathcal{V}}{\partial y} + \frac{\partial \mathcal{W}}{\partial y}\right\} = 0, \mathbf{L}\left\{\frac{\partial^\zeta \mathcal{W}}{\partial t^\zeta}\right\}\\
&+ \mathbf{L}\left\{\frac{\partial(\mathcal{U}\mathcal{W})}{\partial x} + \frac{\partial(\mathcal{V}\mathcal{W})}{\partial y} + \frac{1}{3}\left(\frac{\partial^3 \mathcal{U}}{\partial x^3} + \frac{\partial^3 \mathcal{U}}{\partial x \partial y^2}\right.\right.\\
&\left.\left. + \frac{\partial^3 \mathcal{V}}{\partial x^2 \partial y} + \frac{\partial^3 \mathcal{V}}{\partial y^3}\right)\right\} = 0.
\end{aligned} \tag{32}$$

Utilization of the Laplace transform on the Caputo's time-fractional derivative (2) leads to

$$\begin{aligned}
&\mathbf{L}\{\mathcal{U}(t,x,y)\} - \frac{1}{s}\left(-\frac{d+ac}{b} + \frac{2\sqrt{3}}{3} b \tanh(bx+cy)\right)\\
&+ \left(\frac{1}{s^\zeta}\right)\mathbf{L}\left\{\mathcal{U}\frac{\partial \mathcal{U}}{\partial x} + \mathcal{V}\frac{\partial \mathcal{U}}{\partial y} + \frac{\partial \mathcal{W}}{\partial x}\right\} = 0,\\
&\mathbf{L}\{\mathcal{V}(t,x,y)\} - \frac{1}{s}\left(a + \frac{2\sqrt{3}}{3} c \tanh(bx+cy)\right)\\
&+ \left(\frac{1}{s^\zeta}\right)\mathbf{L}\left\{\mathcal{U}\frac{\partial \mathcal{V}}{\partial x} + \mathcal{V}\frac{\partial \mathcal{V}}{\partial y} + \frac{\partial \mathcal{W}}{\partial y}\right\} = 0,\\
&\mathbf{L}\{\mathcal{W}(t,x,y)\} - \frac{1}{s}\left(\frac{2}{3}(b^2+c^2)\operatorname{sech}^2(bx+cy)\right) + \left(\frac{1}{s^\zeta}\right)\\
&\times \mathbf{L}\left\{\frac{\partial(\mathcal{U}\mathcal{W})}{\partial x} + \frac{\partial(\mathcal{V}\mathcal{W})}{\partial y} + \frac{1}{3}\left(\frac{\partial^3 \mathcal{U}}{\partial x^3} + \frac{\partial^3 \mathcal{U}}{\partial x \partial y^2} + \frac{\partial^3 \mathcal{V}}{\partial x^2 \partial y} + \frac{\partial^3 \mathcal{V}}{\partial y^3}\right)\right\} = 0.
\end{aligned} \tag{33}$$

We construct homotopies of the aforementioned system as

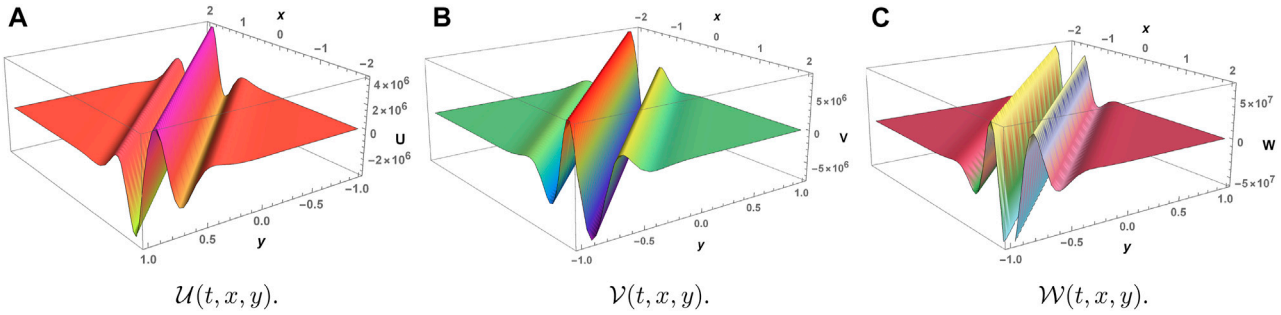

FIGURE 1
Graphical illustration of the He–Laplace solution at $\zeta = 1$, $a = c = 2$, $b = d = 1$, and $t = 2$.

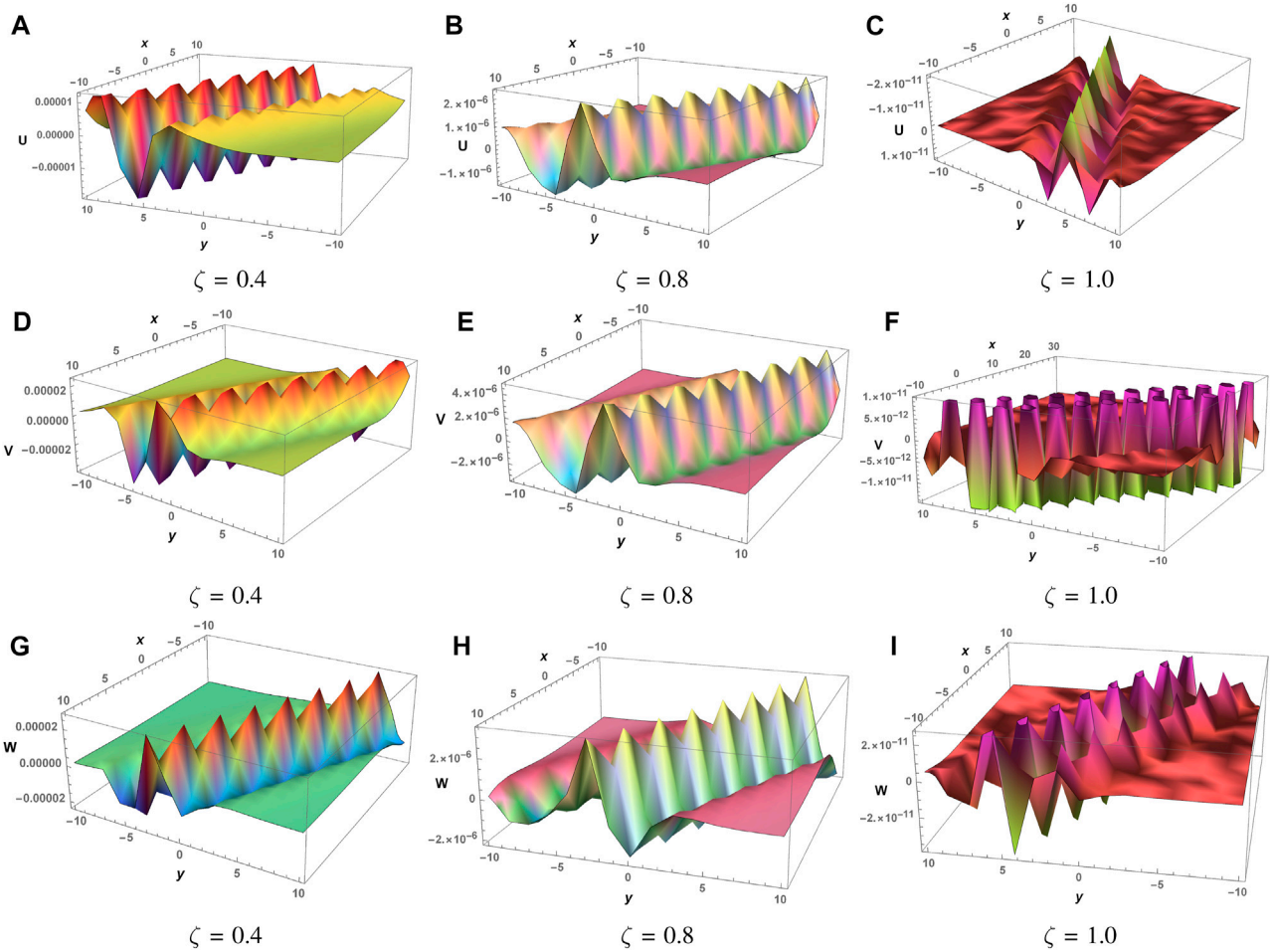

FIGURE 2
Error analysis at different values of the fractional parameter ζ, when $a = c = 0.2$, $b = d = 0.1$, and $t = 2$.

TABLE 2 Error comparison of the He–Laplace algorithm with other methods, when $\zeta = 1$, $a = b = 0.1$, $c = d = 0.01$, $t = 5$, and $y = 20$.

		Exact	HLM	HLM	FRDTM	mADM	mVIM
	x	Sol	Sol	Error	Error [39]	Error [39]	Error [39]
$\mathcal{U}$	−40	−0.22534	−0.22534	0	0	4.33×10^{-10}	1.21×10^{-5}
	−30	−0.22453	−0.22453	1.38×10^{-17}	1.00×10^{-10}	3.59×10^{-9}	8.93×10^{-5}
	−20	−0.21870	−0.21870	0	2.00×10^{-10}	2.44×10^{-8}	6.36×10^{-4}
	−10	−0.18334	−0.18334	1.38×10^{-17}	2.30×10^{-9}	1.02×10^{-7}	3.60×10^{-3}
	0	−0.08171	−0.08171	3.46×10^{-18}	3.23×10^{-9}	3.04×10^{-7}	6.44×10^{-3}
	10	−0.01204	−0.01204	1.38×10^{-17}	8.30×10^{-10}	8.92×10^{-3}	1.91×10^{-4}
	20	0.00293	0.00293	0	1.00×10^{-10}	5.19×10^{-9}	2.91×10^{-4}
	30	0.00512	0.00512	0	0	1.37×10^{-9}	4.01×10^{-5}
	40	0.00542	0.00542	0	0	2.07×10^{-10}	5.44×10^{-6}
	−40	0.08846	0.08846	0	0	6.33×10^{-11}	5.96×10^{-8}
	−30	0.08854	0.08854	1.73×10^{-18}	1.00×10^{-11}	3.39×10^{-10}	4.34×10^{-7}
	−20	0.08912	0.08912	0	2.00×10^{-11}	2.43×10^{-9}	2.91×10^{-6}
	−10	0.09266	0.09266	4.33×10^{-19}	2.30×10^{-10}	1.02×10^{-8}	1.07×10^{-5}
$\mathcal{V}$	0	0.10282	0.10282	1.73×10^{-18}	3.00×10^{-10}	3.05×10^{-8}	5.87×10^{-6}
	10	0.10979	0.10979	1.73×10^{-18}	0	8.96×10^{-9}	7.18×10^{-6}
	20	0.11129	0.11129	0	0	5.39×10^{-10}	1.30×10^{-6}
	30	0.11151	0.11151	0	0	1.07×10^{-10}	1.84×10^{-7}
	40	0.11154	0.11154	0	0	2.07×10^{-11}	2.50×10^{-8}
	−40	0.00001	0.00001	2.87×10^{-21}	1.11×10^{-12}	5.70×10^{-11}	2.73×10^{-6}
	−30	0.00010	0.00010	8.01×10^{-20}	6.50×10^{-12}	4.11×10^{-10}	1.98×10^{-5}
	−20	0.00076	0.00076	1.57×10^{-19}	1.85×10^{-11}	2.63×10^{-9}	1.30×10^{-4}
	−10	0.00401	0.00401	1.77×10^{-19}	6.20×10^{-11}	8.87×10^{-11}	4.14×10^{-4}
$\mathcal{W}$	0	0.00632	0.00632	2.11×10^{-18}	7.96×10^{-10}	3.83×10^{-8}	1.15×10^{-4}
	10	0.00188	0.00188	6.50×10^{-20}	2.07×10^{-10}	1.48×10^{-8}	2.26×10^{-5}
	20	0.00029	0.00029	2.70×10^{-20}	8.60×10^{-12}	5.89×10^{-11}	6.97×10^{-7}
	30	0.00004	0.00004	1.68×10^{-20}	3.31×10^{-12}	1.52×10^{-10}	1.99×10^{-7}
	40	5.4×10^{-6}	5.4×10^{-6}	3.53×10^{-21}	4.90×10^{-13}	2.41×10^{-11}	2.87×10^{-8}

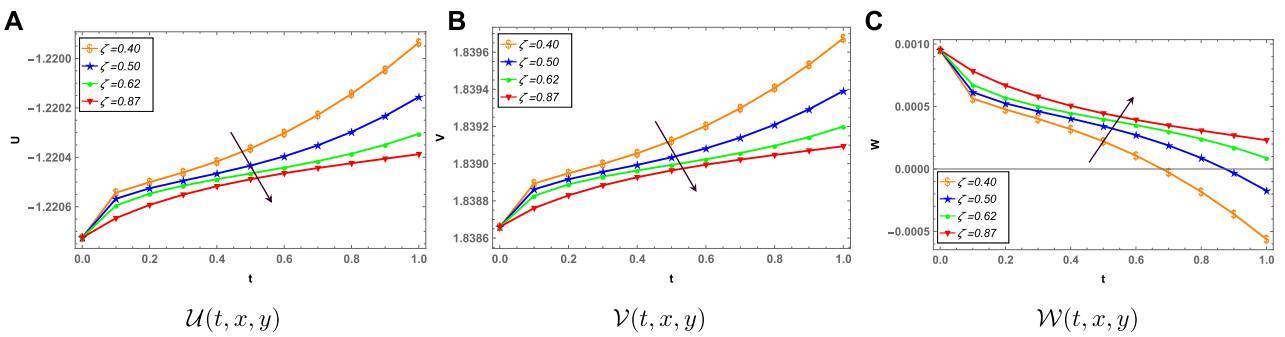

FIGURE 3
Effect of the fractional parameter ζ on the water surface level, when $a = 0.8$, $c = 0.9$, $b = d = 0.7$, $y = 3$, and $x = 2$.

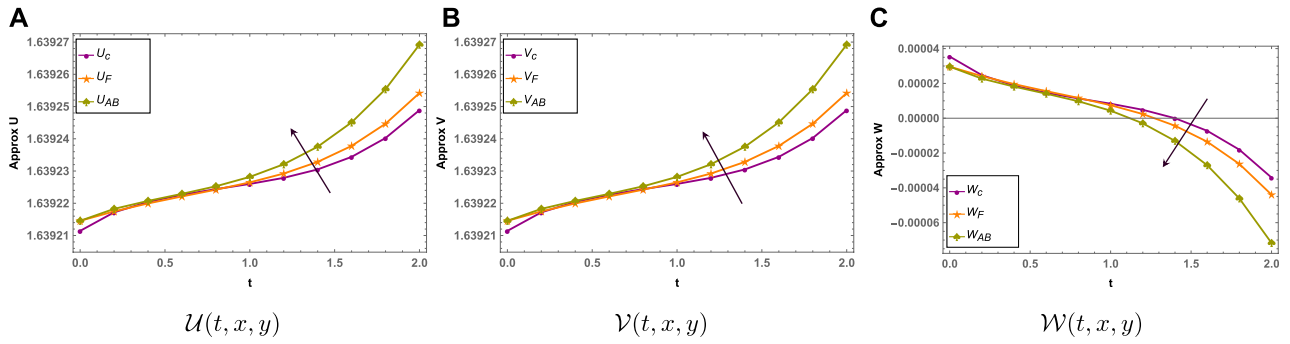

FIGURE 4
Comparison of Caputo, Caputo–Fabrizio, and Atangana–Baleanu fractional derivative approaches on the solution profile, when $a = 0.6$, $b = 0.8$, $c = 0.9$, $d = 0.7$, $y = 2$, and $x = 5$.

$$H_1 = (1-p)\left(\mathbf{L}\{\mathcal{U}(t,x,y)\} - \mathcal{U}_0(t,x,y)\right) + p\left(\mathbf{L}\{\mathcal{U}(t,x,y)\} - \frac{1}{s}\left(-\frac{d+ac}{b} + \frac{2\sqrt{3}}{3}b\tanh(bx+cy)\right)\right) + \left(\frac{1}{s^{\zeta}}\right)\mathbf{L}\left\{\mathcal{U}\frac{\partial\mathcal{U}}{\partial x} + \mathcal{V}\frac{\partial\mathcal{U}}{\partial y} + \frac{\partial\mathcal{W}}{\partial x}\right\}\Big), H_2 = (1-p)\left(\mathbf{L}\{\mathcal{V}(t,x,y)\}\right.$$
$$\left. - \mathcal{V}_0(t,x,y)\right) + p\left(\mathbf{L}\{\mathcal{V}(t,x,y)\} - \frac{1}{s}\left(a + \frac{2\sqrt{3}}{3}c\tanh(bx+cy)\right)\right) + \left(\frac{1}{s^{\zeta}}\right)\mathbf{L}\left\{\mathcal{U}\frac{\partial\mathcal{V}}{\partial x} + \mathcal{V}\frac{\partial\mathcal{V}}{\partial y} + \frac{\partial\mathcal{W}}{\partial y}\right\}\Big), H_3 = (1-p)\left(\mathbf{L}\{\mathcal{W}(t,x,y)\}\right.$$
$$\left. - \mathcal{W}_0(t,x,y)\right) + p\left(\mathbf{L}\{\mathcal{W}(t,x,y)\} - \frac{1}{s}\left(\frac{2}{3}(b^2+c^2)\mathrm{sech}^2(bx+cy)\right)\right) + \left(\frac{1}{s^{\zeta}}\right)\mathbf{L}\left\{\frac{\partial(\mathcal{U}\mathcal{W})}{\partial x} + \frac{\partial(\mathcal{V}\mathcal{W})}{\partial y} + \frac{1}{3}\left(\frac{\partial^3\mathcal{U}}{\partial x^3} + \frac{\partial^3\mathcal{U}}{\partial x\partial y^2} + \frac{\partial^3\mathcal{V}}{\partial x^2\partial y} + \frac{\partial^3\mathcal{V}}{\partial y^3}\right)\right\}\Big), \tag{34}$$

where $\mathcal{U}_0(t,x,y)$, $\mathcal{V}_0(t,x,y)$, and $\mathcal{W}_0(t,x,y)$ are the initial guesses.

$$\begin{aligned}\mathcal{U}_0(t,x,y) &= -\frac{d+ac}{b} + \frac{2\sqrt{3}}{3}b\tanh(bx+cy),\\ \mathcal{V}_0(t,x,y) &= a + \frac{2\sqrt{3}}{3}c\tanh(bx+cy),\\ \mathcal{W}_0(t,x,y) &= \frac{2}{3}(b^2+c^2)\mathrm{sech}^2(bx+cy).\end{aligned} \tag{35}$$

In the next step, we will expand $\mathcal{U}(t,x,y)$, $\mathcal{V}(t,x,y)$, and $\mathcal{W}(t,x,y)$ in Taylor's series form with respect to p as

$$\begin{aligned}\mathcal{U}(t,x,y) &= \sum_{m=1}^{\infty} p^m\mathcal{U}_m,\\ \mathcal{V}(t,x,y) &= \sum_{m=1}^{\infty} p^m\mathcal{V}_m,\\ \mathcal{W}(t,x,y) &= \sum_{m=1}^{\infty} p^m\mathcal{W}_m.\end{aligned} \tag{36}$$

Substitution of Eq. 36 into Eq. 34 and then comparison of a similar coefficient with respect to p givesthe first-order problem

$$\mathbf{L}\{\mathcal{U}_1(t,x,y)\} + \mathcal{U}_0(t,x,y) - \frac{1}{s}\left(-\frac{d+ac}{b} + \frac{2\sqrt{3}}{3}b\tanh(bx+cy)\right) + \left(\frac{1}{s^{\zeta}}\right)\mathbf{L}\left\{\mathcal{U}_0\frac{\partial\mathcal{U}_0}{\partial x} + \mathcal{V}_0\frac{\partial\mathcal{U}_0}{\partial y} + \frac{\partial\mathcal{W}_0}{\partial x}\right\} = 0, \mathbf{L}\{\mathcal{V}_1(t,x,y)\} - \mathcal{V}_0(t,x,y)$$
$$- \frac{1}{s}\left(a + \frac{2\sqrt{3}}{3}c\tanh(bx+cy)\right) + \left(\frac{1}{s^{\zeta}}\right)\mathbf{L}\left\{\mathcal{U}_0\frac{\partial\mathcal{V}_0}{\partial x} + \mathcal{V}_0\frac{\partial\mathcal{V}_0}{\partial y} + \frac{\partial\mathcal{W}_0}{\partial y}\right\} = 0, \mathbf{L}\{\mathcal{W}_1(t,x,y)\} - \mathcal{W}_0(t,x,y) - \frac{1}{s}\left(\frac{2}{3}(b^2+c^2)\mathrm{sech}^2(bx+cy)\right)$$
$$+ \left(\frac{1}{s^{\zeta}}\right)\mathbf{L}\left\{\frac{\partial\mathcal{U}_0\mathcal{W}_0}{\partial x} + \frac{\partial\mathcal{V}_0\mathcal{W}_0}{\partial y} + \frac{1}{3}\left(\frac{\partial^3\mathcal{U}_0}{\partial x^3} + \frac{\partial^3\mathcal{U}_0}{\partial x\partial y^2} + \frac{\partial^3\mathcal{V}_0}{\partial x^2\partial y} + \frac{\partial^3\mathcal{V}_0}{\partial y^3}\right)\right\} = 0, \tag{37}$$

with the condition

$$\begin{aligned}\mathcal{U}_1(0,x,y) &= 0,\\ \mathcal{V}_1(0,x,y) &= 0,\\ \mathcal{W}_1(0,x,y) &= 0.\end{aligned} \tag{38}$$

By operating the inverse Laplace transform, the solution at first order is

$$\begin{aligned}\mathcal{U}_1(t,x,y) &= -\frac{4bd^2t^{2\zeta}\tanh(bx+cy)\mathrm{sech}^2(bx+cy)}{\sqrt{3}\Gamma(2\zeta+1)},\\ \mathcal{V}_1(t,x,y) &= -\frac{4cd^2t^{2\zeta}\tanh(bx+cy)\mathrm{sech}^2(bx+cy)}{\sqrt{3}\Gamma(2\zeta+1)},\\ \mathcal{W}_1(t,x,y) &= \frac{4(b^2+c^2)d^2t^{2\zeta}(\cosh(2(bx+cy)) - 2)\mathrm{sech}^4(bx+cy)}{3\Gamma(2\zeta+1)}.\end{aligned} \tag{39}$$

The second-order problem is

$$\begin{aligned}&\mathbf{L}\{\mathcal{U}_2(t,x,y)\} + \left(\frac{1}{s^{\zeta}}\right)\mathbf{L}\left\{\mathcal{U}_1\frac{\partial\mathcal{U}_1}{\partial x} + \mathcal{V}_1\frac{\partial\mathcal{U}_1}{\partial y} + \frac{\partial\mathcal{W}_1}{\partial x}\right\} = 0,\\ &\mathbf{L}\{\mathcal{V}_2(t,x,y)\} + \left(\frac{1}{s^{\zeta}}\right)\mathbf{L}\left\{\mathcal{U}_1\frac{\partial\mathcal{V}_1}{\partial x} + \mathcal{V}_1\frac{\partial\mathcal{V}_1}{\partial y} + \frac{\partial\mathcal{W}_1}{\partial y}\right\} = 0,\\ &\mathbf{L}\{\mathcal{W}_2(t,x,y)\} + \left(\frac{1}{s^{\zeta}}\right)\mathbf{L}\left\{\frac{\partial\mathcal{U}_1\mathcal{W}_1}{\partial x} + \frac{\partial\mathcal{V}_1\mathcal{W}_1}{\partial y} + \frac{1}{3}\left(\frac{\partial^3\mathcal{U}_1}{\partial x^3} + \frac{\partial^3\mathcal{U}_1}{\partial x\partial y^2} + \frac{\partial^3\mathcal{V}_1}{\partial x^2\partial y} + \frac{\partial^3\mathcal{V}_1}{\partial y^3}\right)\right\} = 0\end{aligned} \tag{40}$$

that has the condition

$$\begin{aligned}\mathcal{U}_2(0,x,y) &= 0,\\ \mathcal{V}_2(0,x,y) &= 0,\\ \mathcal{W}_2(0,x,y) &= 0.\end{aligned} \tag{41}$$

The inverse of the Laplace transform gives

$$\begin{aligned}\mathcal{U}_2(t,x,y) &= \frac{2bdt^{\zeta}\operatorname{sech}^2(bx+cy)}{\sqrt{3}\Gamma(\zeta+1)},\\ \mathcal{V}_2(t,x,y) &= \frac{2cdt^{\zeta}\operatorname{sech}^2(bx+cy)}{\sqrt{3}\Gamma(\zeta+1)},\\ \mathcal{W}_2(t,x,y) &= -t^{\zeta}\Big(\frac{4}{3}db^2\tanh(bx+cy)\operatorname{sech}^2(bx+cy)+\frac{4}{3}c^2\\ &\quad d\tanh(bx+cy)\operatorname{sech}^2(bx+cy)\Big)\Big/\Gamma(\zeta+1).\end{aligned} \tag{42}$$

The same procedure is applied for higher-order problems. Thus, the approximate solution at the higher order of the (2 + 1)-dimensional Wu–Zhang system can be obtained by

$$\begin{aligned}\tilde{\mathcal{U}} &= \sum_{m=0}^{\infty}\mathcal{U}_m(t,x,y),\\ \tilde{\mathcal{V}} &= \sum_{m=0}^{\infty}\mathcal{V}_m(t,x,y),\\ \tilde{\mathcal{W}} &= \sum_{m=0}^{\infty}\mathcal{W}_m(t,x,y).\end{aligned} \tag{43}$$

By replacing the approximate solutions (43) in the given system (29), we obtain residual errors

$$\begin{aligned}R1 &= \frac{\partial^{\zeta}\tilde{\mathcal{U}}}{\partial t^{\zeta}}+\tilde{\mathcal{U}}\frac{\partial\tilde{\mathcal{U}}}{\partial x}+\tilde{\mathcal{V}}\frac{\partial\tilde{\mathcal{U}}}{\partial y}+\frac{\partial\tilde{\mathcal{W}}}{\partial x},\\ R2 &= \frac{\partial^{\zeta}\tilde{\mathcal{V}}}{\partial t^{\zeta}}+\tilde{\mathcal{U}}\frac{\partial\tilde{\mathcal{V}}}{\partial x}+\tilde{\mathcal{V}}\frac{\partial\tilde{\mathcal{V}}}{\partial y}+\frac{\partial\tilde{\mathcal{W}}}{\partial y},\\ R3 &= \frac{\partial^{\zeta}\tilde{\mathcal{W}}}{\partial t^{\zeta}}+\frac{\partial\tilde{\mathcal{U}}\tilde{\mathcal{W}}}{\partial x}+\frac{\partial\tilde{\mathcal{V}}\tilde{\mathcal{W}}}{\partial y}+\frac{1}{3}\Big(\frac{\partial^3\tilde{\mathcal{U}}}{\partial x^3}+\frac{\partial^3\tilde{\mathcal{U}}}{\partial x\partial y^2}+\frac{\partial^3\tilde{\mathcal{V}}}{\partial x^2\partial y}+\frac{\partial^3\tilde{\mathcal{V}}}{\partial y^3}\Big).\end{aligned} \tag{44}$$

6 Results and discussion

The objective of this study is to propose a new soliton solution of the non-linear time-fractional Wu–Zhang system. This (2 + 1)-dimensional system describes the phenomena of long dispersive waves. The current section is focused on the numerical and graphical results of the WZ system through a hybrid approach by using homotopy perturbation with the Laplace transform, which is known as the He–Laplace algorithm (method). Initially, solutions are captured through the He–Laplace algorithm, considering the fractional derivative in Caputo sense. The obtained results are then analyzed at both fractional and integral orders. Table 1 depicts the residual error at $\mathcal{U},\mathcal{V},\mathcal{W}$ along with overall system errors at various fractional parameter values. These errors clearly indicate the reliability of proposed methodology across the complete fractional domain. It is also observed that error is reduced when fractional parameter approaches one.

Table 2 shows the comparison of results obtained through He–Laplace and other methods at the integer order that is $\zeta = 1$. This numerical comparison indicates that He–Laplace surpasses other mentioned schemes in terms of accuracy. Figure 1 depicts the He–Laplace solution of the WZ system in 3D at the integer order. This graphical illustration confirms that in the WZ system, surface water velocities in x and y directions are very high, while elevation in water waves decreases with time. Error analysis at $\zeta = 0.4$, 0.8, and 1 as 3D structures can be seen from Figure 2 for $\mathcal{U}$, $\mathcal{V}$, and $\mathcal{W}$, respectively. At $\zeta = 1$, the errors are lesser than $\zeta = 0.8$, and the same can be observed in case of $\zeta = 0.4$.

The impact of the fractional parameter on the water surface is depicted in Figure 3. Research findings indicate that a rise in ζ results in a reduction of the water surface velocity, in both the x and y directions. However, water wave elevation ($\mathcal{W}$) shows inverse behavior in this case. Comparative analysis of different fractional derivative approaches (Atangana–Baleanu, Caputo–Fabrizio, and Caputo) on the solution profile can be seen in Figure 4. Analysis of this figure shows that water surface velocities are highest in the Atangana–Baleanu fractional approach as compared to Caputo and Caputo–Fabrizio fractional approaches. On the other hand, $\mathcal{W}$ depicts opposite behavior as compared to $\mathcal{U}$ and $\mathcal{V}$.

7 Conclusion

In this article , a hybrid approach is proposed to solve and analyze the highly non-linear time-fractional (2 + 1)-dimensional WZ system, which is famous for capturing long dispersive waves. A hybrid approach in which homotopy perturbation is combined with the Laplace transform along with different fractional derivatives is proposed for the solution and analysis of the fractional WZ system. Efficiency of the obtained solution is checked over the entire fractional domain to show the validity and convergence of the proposed methodology. Error analysis is also performed in comparison with other well-known numerical methods, which confirms the efficiency of the proposed approach. Graphical analysis shows that water surface velocities increase, while surface elevation decreases, when fractional parameter increases. Also, it is noted that the Atangana–Baleanu approach uplifts water velocities in x and y directions more than Caputo and Caputo–Fabrizio approaches. Analysis of the results also concludes that the proposed method is a reliable technique, which can be extended to more complex fractional systems.

Data availability statement

The original contributions presented in the study are included in the article/Supplementary Material; further inquiries can be directed to the corresponding author.

Author contributions

Conceptualization: MQ. Data curation: EA. Formal analysis: ST. Validation: EA. Writing—original draft: MQ and SS.

Writing—review editing: HA and SA. All authors contributed to the article and approved the submitted version.

Funding

This Project is funded by King Saud University, Riyadh, Saudi Arabia.

Acknowledgments

Research Supporting Project number (RSP2023R167), King Saud University, Riyadh, Saudi Arabia.

Conflict of interest

The authors declare that the research was conducted in the absence of any commercial or financial relationships that could be construed as a potential conflict of interest.

Publisher's note

All claims expressed in this article are solely those of the authors and do not necessarily represent those of their affiliated organizations, or those of the publisher, the editors, and the reviewers. Any product that may be evaluated in this article, or claim that may be made by its manufacturer, is not guaranteed or endorsed by the publisher.

References

1. Dzerjinsky RI. The earthquake attributes disjunctive form analysis at the quickest form change directions. In: *Lecture notes in networks and systems*. Springer International Publishing (2021). p. 96–101.

2. Hirano S. Source time functions of earthquakes based on a stochastic differential equation. *Scientific Rep* (2022) 12(1):3936. doi:10.1038/s41598-022-07873-2

3. Zheng C, Wu W-Z, Xie W, Li Q. A MFO-based conformable fractional nonhomogeneous grey Bernoulli model for natural gas production and consumption forecasting. *Appl Soft Comput* (2021) 99:106891. doi:10.1016/j.asoc.2020.106891

4. Liu C, Wu W-Z, Xie W, Zhang T, Zhang J. Forecasting natural gas consumption of China by using a novel fractional grey model with time power term. *Energ Rep* (2021) 7(788–797):788–97. doi:10.1016/j.egyr.2021.01.082

5. Akbar MA, Abdul Kayum M, Osman MS, Abdel-Aty A-H, Eleuch H. Analysis of voltage and current flow of electrical transmission lines through mZK equation. *Results Phys* (2021) 20:103696. doi:10.1016/j.rinp.2020.103696

6. Bidkhori P, Karizaki VM. Diffusion and kinetic modeling of water absorption process during soaking and cooking of chickpea. *Legume Sci* (2021) 4(1). doi:10.1002/leg3.116

7. Ahmadova A, Mahmudov NI. Langevin differential equations with general fractional orders and their applications to electric circuit theory. *J Comput Appl Math* (2021) 388:113299. doi:10.1016/j.cam.2020.113299

8. Khader MM, Gómez-Aguilar JF, Adel M. Numerical study for the fractional RL, RC, and RLC electrical circuits using legendre pseudo-spectral method. *Int J Circuit Theor Appl* (2021) 49(10):3266–85. doi:10.1002/cta.3103

9. Caro LAP, Mendoza R, Mendoza VMP. Application of genetic algorithm with multi-parent crossover on an inverse problem in delay differential equations. In: PROCEEDINGS OF THE INTERNATIONAL CONFERENCE ON MATHEMATICAL SCIENCES AND TECHNOLOGY 2020 (MATHTECH 2020): Sustainable Development of Mathematics and Mathematics in Sustainability Revolution. AIP Publishing (2021).

10. Chen Y, Luo Y, Liu Q, Xu H, Zhang D. Any equation is a forest: Symbolic genetic algorithm for discovering open-form partial differential equations (sga-pde) (2021).

11. Salazar-Viedma M, Gabriel Vergaño-Salazar J, Pastenes L, D'Afonseca V. Simulation model for hashimoto autoimmune thyroiditis disease. *Endocrinology* (2021) 162(12):bqab190. doi:10.1210/endocr/bqab190

12. Guzzi PH, Petrizzelli F, Mazza T. Disease spreading modeling and analysis: A survey. *Brief Bioinform* (2022) 23(4). doi:10.1093/bib/bbac230

13. Sahoo D, Samanta GP. Comparison between two tritrophic food chain models with multiple delays and anti-predation effect. *Int J Biomath* (2021) 14(03). doi:10.1142/s1793524521500108

14. Mondal B, Ghosh U, Rahman MS, Saha P, Sarkar S. Studies of different types of bifurcations analyses of an imprecise two species food chain model with fear effect and non-linear harvesting. *Math Comput Simul* (2022) 192:111–35. doi:10.1016/j.matcom.2021.08.019

15. Ahmad Z, Ali F, Khan N, Khan I. Dynamics of fractal-fractional model of a new chaotic system of integrated circuit with mittag-leffler kernel. *Chaos, Solitons and Fractals* (2021) 153:111602. doi:10.1016/j.chaos.2021.111602

16. Ayub A, Sabir Z, Le D-N, Aly AA. Nanoscale heat and mass transport of magnetized 3-d chemically radiative hybrid nanofluid with orthogonal/inclined magnetic field along rotating sheet. *Case Stud Therm Eng* (2021) 26:101193. doi:10.1016/j.csite.2021.101193

17. Ali Abro K, Atangana A. Dual fractional modeling of rate type fluid through non-local differentiation. In: *Numerical methods for partial differential equations* (2020).

18. Shchigolev VK. Fractional-order derivatives in cosmological models of accelerated expansion. *Mod Phys Lett A* (2021) 36(14):2130014. doi:10.1142/s0217732321300147

19. Abed AM, Rashid ZN, Abedi F, Zeebaree SRM, Sahib MA, Mohamad Jawad AJ, et al. Trajectory tracking of differential drive mobile robots using fractional-order proportional-integral-derivative controller design tuned by an enhanced fruit fly optimization. *Meas Control* (2022) 55(3-4):209–26. doi:10.1177/00202940221092134

20. Shokhanda R, Goswami P, He J-H, Althobaiti A. An approximate solution of the time-fractional two-mode coupled Burgers equation. *Fractal Fractional* (2021) 5(4):196. doi:10.3390/fractalfract5040196

21. Habib S, Batool A, Islam A, Nadeem M, Gepreel KA, He J-H. Study of nonlinear Hirota-Satsuma coupled KdV and coupled mkdv system with time fractional derivative. *Fractals* (2021) 29(05):2150108. doi:10.1142/s0218348x21501085

22. Jin T, Yang X. Monotonicity theorem for the uncertain fractional differential equation and application to uncertain financial market. *Math Comput Simul* (2021) 190:203–21. doi:10.1016/j.matcom.2021.05.018

23. Lin Z, Wang H. Modeling and application of fractional-order economic growth model with time delay. *Fractal Fractional* (2021) 5(3):74. doi:10.3390/fractalfract5030074

24. Al-Nassir S. Dynamic analysis of a harvested fractional-order biological system with its discretization. *Chaos, Solitons and Fractals* (2021) 152:111308. doi:10.1016/j.chaos.2021.111308

25. Mandelbrot BB *Les objets fractals: Forme, hasard et dimension*, Vol. 17 Flammarion Paris (1975).

26. He J-H, Qian M-Y. A fractal approach to the diffusion process of red ink in a saline water. *Therm Sci* (2022) 26:2447–51. doi:10.2298/tsci2203447h

27. Zhou W, Cao Y, Zhao H, Li Z, Feng P, Feng F. Fractal analysis on surface topography of thin films: A review. *Fractal Fractional* (2022) 6(3):135. doi:10.3390/fractalfract6030135

28. He C-H, Liu C, He J-H, Gepreel KA Low frequency property of a fractal vibration model for a concrete beam. *Fractals* (2021) 29(05):2150117. doi:10.1142/s0218348x21501176

29. Vu CC, Truong TTN, Kim JY. Fractal structures in flexible electronic devices. *Mater Today Phys* (2022) 27:100795. doi:10.1016/j.mtphys.2022.100795

30. Khan H, Ahmad F, Tunç O, Idrees M. On fractal-fractional Covid-19 mathematical model. *Chaos, Solitons Fractals* (2022) 157:111937. doi:10.1016/j.chaos.2022.111937

31. Wu TY, Zhang JE. On modeling nonlinear long waves. In: *Mathematics is for solving problems* (1996). p. 233–49.

32. Wang K-L, He C-H. A remark on wang's fractal variational principle. *Fractals* (2019) 27(08):1950134. doi:10.1142/s0218348x19501342

33. Zayed EME, -Abdel Rahman HM. On solving the kay-burger's equation and the Wu-zhang equations using the modified variational iteration method. *Int J Nonlinear Sci Numer Simulation* (2009) 10(9). doi:10.1515/ijnsns.2009.10.9.1093

34. Khater MMA, Attia RAM, Lu D. Numerical solutions of nonlinear fractional Wu-zhang system for water surface versus three approximate schemes. *J Ocean Eng Sci* (2019) 4(2):144–8. doi:10.1016/j.joes.2019.03.002

35. Aljahdaly NH, El-Tantawy SA, Wazwaz A-M, Ashi HA. Adomian decomposition method for modelling the dissipative higher-order rogue waves in a superthermal

collisional plasma. *J Taibah Univ Sci* (2021) 15(1):971–83. doi:10.1080/16583655.2021.2012373

36. Asgari A, Ganji DD, Davodi AG. Extended tanh method and exp-function method and its application to(2+ 1)-dimensional dispersive long wave nonlinear equations. *J Appl Math Stat Inform (Jamsi)* (2010) 6.

37. Zheng H, Xia Y, Bai Y, Lei G. Travelling wave solutions of Wu-zhang system via dynamic analysis. *Discrete Dyn Nat Soc* (2020) , 2020:1–9. doi:10.1155/2020/2845841

38. Kaur B, Gupta RK. Time fractional (2+1)-dimensional Wu-zhang system: Dispersion analysis, similarity reductions, conservation laws, and exact solutions. *Comput Math Appl* (2020) 79(4):1031–48. doi:10.1016/j.camwa.2019.08.014

39. Patel T, Patel H. An analytical approach to solve the fractional-order (2 + 1)-dimensional Wu-zhang equation. *Math Methods Appl Sci* (2022) 46:479–89. doi:10.1002/mma.8522

40. Almeida R. A caputo fractional derivative of a function with respect to another function. *Commun Nonlinear Sci Numer Simul* (2017) 44:460–81. doi:10.1016/j.cnsns.2016.09.006

41. Atangana A, Baleanu D. New fractional derivatives with nonlocal and non-singular kernel: Theory and application to heat transfer model (2016).

42. Caputo M, Fabrizio M. A new definition of fractional derivative without singular kernel. *Prog Fractional Differ Appl* (2015) 1(2):73–85.

43. Anjum N, Ain QT. Application of He's fractional derivative and fractional complex transform for time fractional Camassa-Holm equation. *Therm Sci* (2020) 24:3023–30. doi:10.2298/tsci190930450a

44. Anjum N, He J-H, Ain QT, Tian D. Li-He's modified homotopy perturbation method for doubly-clamped electrically actuated microbeams-based microelectromechanical system. *Facta Universitatis, Ser Mech Eng* (2021) 19(4):601. doi:10.22190/fume210112025a

45. Baitiche Z, Derbazi C, Alzabut J, Esmael Samei M, Kaabar MKA, Siri Z. Monotone iterative method for caputo fractional differential equation with nonlinear boundary conditions. *Fractal and Fractional* (2021) 5(3):81. doi:10.3390/fractalfract5030081

46. Do QH, Ngo HTB, Razzaghi M. A generalized fractional-order Chebyshev wavelet method for two-dimensional distributed-order fractional differential equations. *Commun Nonlinear Sci Numer Simul* (2021) 95:105597. doi:10.1016/j.cnsns.2020.105597

47. Hashemi MS, Hajikhah S, Mustafa Inc. Generalized squared remainder minimization method for solving multi-term fractional differential equations. *Nonlinear Anal Model Control* (2021) 26(1):57–71. doi:10.15388/namc.2021.26.20560

48. Tian Y, Liu J. A modified exp-function method for fractional partial differential equations. *Therm Sci* (2021) 25:1237–41. doi:10.2298/tsci200428017t

49. He J-H, He C-H, Alsolami AA. A good initial guess for approximating nonlinear oscillators by the homotopy perturbation method. *Facta Univ. Ser Mech Eng* (2023) 21(1):21–9.

50. He J-H, El-Dib YO. The enhanced homotopy perturbation method for axial vibration of strings. *Facta Univ. Ser Mech Eng* (2021) 19(4):735–50. doi:10.22190/fume210125033h

51. He J-H. Homotopy perturbation technique. *Comput Methods Appl Mech Eng* (1999) 178(3-4):257–62. doi:10.1016/s0045-7825(99)00018-3

52. He C-H, El-Dib YO. A heuristic review on the homotopy perturbation method for non-conservative oscillators. *J Low Frequency Noise, Vibration Active Control* (2021) 41(2):572–603. doi:10.1177/14613484211059264

53. Schiff JL. *The Laplace transform*. New York: Springer (1999).

54. Ain QT, Anjum N, Din A, Zeb A, Djilali S, Khan ZA. On the analysis of Caputo fractional order dynamics of Middle East lungs coronavirus (MERS-CoV) model. *Alexandria Eng J* (2022) 61(7):5123–31. doi:10.1016/j.aej.2021.10.016

55. Tuan NH, Mohammadi H, Rezapour S. A mathematical model for COVID-19 transmission by using the caputo fractional derivative. *Chaos, Solitons and Fractals* (2020) 140:110107. doi:10.1016/j.chaos.2020.110107

56. Alizadeh S, Baleanu D, Rezapour S. Analyzing transient response of the parallel RCL circuit by using the caputo-fabrizio fractional derivative. *Adv Differ. Equations* (2020) 2020, 55, doi:10.1186/s13662-020-2527-0

57. Atangana A, Gómez-Aguilar JF. Decolonisation of fractional calculus rules: Breaking commutativity and associativity to capture more natural phenomena. *The Eur Phys J Plus* (2018) 133(4):166. doi:10.1140/epjp/i2018-12021-3

58. Ain QT, He J-H. On two-scale dimension and its applications. *Therm Sci* (2019) 23:1707–12. doi:10.2298/tsci190408138a

59. Anjum N, Ain QT, Li X-X. Two-scale mathematical model for tsunami wave. *GEM - Int J Geomathematics* (2021) 12(1):10. doi:10.1007/s13137-021-00177-z

10.3389/fphy.2023.1178154

Nomenclature

Parameter	Description
$\mathcal{U}$	Velocity in the x direction
$\mathcal{V}$	Velocity in the y direction
$\mathcal{W}$	Elevation of water waves
ζ	Fractional parameter
x, y	Dimensions
t	Time
a, b, c, d	Non-zero arbitrary constants
$\mathbf{L}$	Laplace transform
$\mathcal{R}$	Residual errors

frontiers | Frontiers in Physics

TYPE Original Research
PUBLISHED 21 July 2023
DOI 10.3389/fphy.2023.1216451

OPEN ACCESS

EDITED BY
Hamid M. Sedighi,
Shahid Chamran University of Ahvaz, Iran

REVIEWED BY
Muhammad Nadeem,
Qujing Normal University, China
Naveed Anjum,
Government College University, Faisalabad, Pakistan
Fernane Khaireddine,
8 May 1945 University of Guelma, Algeria

*CORRESPONDENCE
Wael W. Mohammed,
wael.mohammed@mans.edu.eg

RECEIVED 03 May 2023
ACCEPTED 10 July 2023
PUBLISHED 21 July 2023

CITATION
Al-Askar FM and Mohammed WW (2023), Abundant optical solutions for the Sasa-Satsuma equation with M-truncated derivative.
Front. Phys. 11:1216451.
doi: 10.3389/fphy.2023.1216451

Abundant optical solutions for the Sasa-Satsuma equation with M-truncated derivative

Farah M. Al-Askar [1] and Wael W. Mohammed [2,3]*

[1]Department of Mathematical Science, College of Science, Princess Nourah Bint Abdulrahman University, Riyadh, Saudi Arabia, [2]Department of Mathematics, College of Science, University of Ha'il, Ha'il, Saudi Arabia, [3]Department of Mathematics, Faculty of Science, Mansoura University, Mansoura, Egypt

Here, we look at the Sasa-Satsuma equation with M-truncated derivative (SSE-MTD). The analytical solutions in the form of trigonometric, hyperbolic, elliptic, and rational functions are constructed using the Jacobi elliptic function and generalizing Riccati equation mapping methods. Because the Sasa–Satsuma equation is applied to explain the propagation of femtosecond pulses in optical fibers, the acquired solutions can be employed to explain a wide range of important physical phenomena. Moreover, we apply the MATLAB tool to generate a series of graphs to address the effect of the M-truncated derivative on the exact solution of the SSE-MTD.

KEYWORDS

Sasa-Satsuma equation, M-truncated derivative, optical solitons, generalizing Riccati equation mapping method, analytical solutions

1 Introduction

Many authors have centered their attention on fractional nonlinear differential equations (FNLDEs) in the noble age of technology and science to examine complex mathematical models that are used in research area and real life, such as neuroscience, robotics, fluid dynamics, quantum mechanics, plasma physics, optical fibers, and so on. A lot studies have been published about some aspects of fractional differential equations, such as finding exact and numerical solutions, the existence and uniqueness of solutions, and the stability of solutions [1–7]. Therefore, it is essential to discover the exact solutions to these equations in order to understand the physical phenomenon and overcome the resulting obstacles. Recently, acquiring soliton solutions to important equations has emerged as a major field of study. Numerous researchers defended numerous novel methods to evaluate soliton solutions including $(G'/G, 1/G)$-expansion method [8] (G'/G)-expansion [9, 10], generalized (G'/G)-expansion [11], exp-function method [12], Jacobi elliptic function expansion [13], sine-cosine procedure [14], auxiliary equation scheme [15], first-integral method [16], sine-Gordon expansion technique [17], generalized Kudryashov approach [18], $\exp(-\phi(\varsigma))$-expansion method [19], homotopy perturbation method with Aboodh transform [20], He–Laplace method, He's variational iteration method [21, 22], and others.

Abbreviations: 2D, Two dimension; 3D, Three dimension; FNLDEs, Fractional nonlinear differential equations; GREM-method, generalizing Riccati equation mapping method; JEF-method, Jacobi elliptic function method; MTD, M-truncated derivative; ODE, Ordinary differential equation; SSE, Sasa-Satsuma equation; SW, Solitary waves.

In contrast, a new differentiation operator has grown up, that includes the concepts of fractional differentiation and fractal derivative. Therefore, various kinds of fractional derivatives were proposed by several mathematicians. The most well-known ones are the ones proposed by Grunwald-Letnikov, He's fractional derivative, Atangana-Baleanu's derivative, Riemann-Liouville, Marchaud, Riesz, Caputo, Hadamard, Kober, and Erdelyi [23–26]. The bulk of fractional derivative types do not follow classic derivative equations like the chain rule, quotient rule, and product rule. Sousa et al. [27] have developed a new derivative known as the M-truncated derivative (MTD), which is a natural extension of the classical derivative. The MTD for u: $[0,\infty) \to \mathbb{R}$ of order $\delta \in (0, 1]$ is indicated as

$$\mathcal{M}_{j,t}^{\delta,\beta} u(t) = \lim_{h\to 0} \frac{u\left(t\mathcal{E}_{j,\beta}\left(ht^{-\delta}\right)\right) - u(t)}{h},$$

where $\mathcal{E}_{j,\beta}(t)$, for $t \in \mathbb{C}$ and $\beta > 0$, is the truncated Mittag-Leffler function and is defined as:

$$\mathcal{E}_{j,\beta}(t) = \sum_{k=0}^{j} \frac{t^k}{\Gamma(\beta k + 1)}.$$

The MTD has the following characteristics for any real integers a and b [27]:

(1) $\mathcal{M}_{j,t}^{\delta,\beta}(au + bv) = a\mathcal{M}_{j,t}^{\delta,\beta}(u) + b\mathcal{M}_{j,t}^{\delta,\beta}(v)$,

(2) $\mathcal{M}_{j,t}^{\delta,\beta}(u \circ v)(t) = u'(v(t))\mathcal{M}_{j,t}^{\delta,\beta} v(t)$,

(3) $\mathcal{M}_{j,t}^{\delta,\beta}(uv) = u\mathcal{M}_{j,t}^{\delta,\beta} v + v\mathcal{M}_{j,t}^{\delta,\beta} u$,

(4) $\mathcal{M}_{j,t}^{\delta,\beta}(u)(t) = \frac{t^{1-\delta}}{\Gamma(\beta+1)} \frac{du}{dt}$,

(5) $\mathcal{M}_{j,t}^{\delta,\beta}(t^{\nu}) = \frac{\nu}{\Gamma(\beta+1)} t^{\nu-\delta}$.

There are many authors have considered some nonlinear partial differential equations with M-truncated derivative such as [28–31] and the references therein. In this article, we examine the Sasa-Satsuma equation with M-truncated derivative (SSE-MTD):

$$i\mathcal{M}_{j,t}^{\delta,\beta}\mathcal{W} + \frac{1}{2}\mathcal{W}_{xx} + i\left[\alpha_1\mathcal{W}_{xxx} + \alpha_2\mathcal{W}\left(|\mathcal{W}|^2\right)_x + \alpha_3|\mathcal{W}|^2\mathcal{W}_x\right] + \alpha_4|\mathcal{W}|^2\mathcal{W} = 0, \tag{1}$$

where $\mathcal{W} = \mathcal{W}(x,t)$ is the optical soliton profile, $i = \sqrt{-1}$. α_k, for $k = 1, 2, 3, 4$, are real constants. $\mathcal{W}_t$ defines the temporal evolution of optical soliton molecules, $\mathcal{W}_{xx}$ is the group velocity dispersion. $\mathcal{W}_{xxx}$ represents the third-order dispersion, while $\mathcal{W}(|\mathcal{W}|^2)_x$ provides the stimulated Raman scattering, $|\mathcal{W}|^2\mathcal{W}_x$ is the self-steepening and $|\mathcal{W}|^2\mathcal{W}$ is Kerr-law fiber nonlinearity.

If we set $\delta = 1$ and $\beta = 0$, then we have the Sasa-Satsuma (SS) equation (32, 33):

$$i\mathcal{W}_t + \frac{1}{2}\mathcal{W}_{xx} + i\left[\alpha_1\mathcal{W}_{xxx} + \alpha_2|\mathcal{W}|^2\mathcal{W}_x + \alpha_3\mathcal{W}\left(|\mathcal{W}|^2\right)_x\right] + \alpha_4|\mathcal{W}|^2\mathcal{W} = 0. \tag{2}$$

The SS Eq. 2, which was found while studying the integrability of Schrödinger equation, reduced to nonlinear Schrödinger equation when $\alpha_1 = \alpha_2 = \alpha_3 = 0$ as follows:

$$i\mathcal{W}_t + \frac{1}{2}\mathcal{W}_{xx} + \alpha_4|\mathcal{W}|^2\mathcal{W} = 0. \tag{3}$$

In 1991, Sasa and Satsuma [34] created Eq. 2. This equation has additional components that explain third-order dispersion, self-steepening, and self-frequency shift, which are prevalent in many areas of physics, such as ultrashort pulse propagation in optical fibers [35, 36]. Due to the importance of SS Eq. 2, many authors have obtained its exact solutions by using various methods such as new auxiliary equation method [37], extended trial equation and generalized Kudryashov methods [38], inverse scattering transform [39], improved F-expansion methods and improved auxiliary [40], Riemann problem method [41], unified transform method [42], Bäcklund transformation [43], Darboux transformation [44].

Our main objective of this work is to find the exact solutions of the SSE-MTD (1). The solutions in the form of hyperbolic, trigonometric, elliptic, and rational functions are constructed by utilizing the Jacobi elliptic function method (JEF-method) and generalizing Riccati equation mapping method (GREM-method). Because the Sasa–Satsuma equation is applied to clarify the propagation of femtosecond pulses in optical fibers, the solutions obtained can be employed to study a wide range of important physical phenomena. Furthermore, we utilize the MATLAB tool to generate a series of graphs to examine the effect of the M-truncated derivative on the exact solution of the SSE-MTD (1).

The following is how the paper is organized: In the next section, we describe the methods employed in this paper. The wave equation for the SSE-MTD (1) is developed in Section 3. In Section 4, we employ the JEF-method and the GREM-method to get the precise solutions of the SSE-MTD (1). In Section 5, we study the effect of the MTD on the solution of Eq. 1. Finally, the findings of the article are presented.

2 Description of the methods

In this section, we describe the methods employed in this paper.

2.1 GREM-method

It is useful to outline the essential steps of GREM-method mentioned in [45] as follows:

1. We begin by looking at a general kind of PDEs with MTD as follows

$$\mathcal{P}\left(\mathcal{W}, \mathcal{M}_{j,t}^{\delta,\beta}\mathcal{W}, \mathcal{W}_x, \mathcal{W}_{xx}, \ldots\right) = 0. \tag{4}$$

2. We use Eq. 4 to obtain the traveling wave solution

$$\mathcal{W}(t,x) = \mathcal{X}(\eta_\delta), \quad \eta_\delta = \eta_1 x + \frac{\Gamma(\beta+1)\eta_2}{\delta} t^{\delta}. \tag{5}$$

3. Using the next changes

$$\begin{aligned} \mathcal{M}_{j,t}^{\delta,\beta}\mathcal{W} &= \eta_2\mathcal{X}', \\ u_x &= \eta_1\mathcal{X}', \\ &\vdots \quad \vdots \quad \vdots \\ u_{x^n} &= \eta_1^n\mathcal{X}^{(n)}. \end{aligned} \tag{6}$$

4. After then, substituting (6) into (4) to get ordinary differential equation (ODE)

$$\mathcal{P}\left(\eta_2\mathcal{X}', \eta_1\mathcal{X}', \eta_1^n\mathcal{X}^{(n)}\right) = 0. \tag{7}$$

5. Putting the following Riccati-Bernoulli equation

$$\mathcal{X}' = s\mathcal{X}^2 + r\mathcal{X} + p, \tag{8}$$

where s, r, p are constants, into Eq. 8. Then we balance each coefficient of $\mathcal{X}^k$ to zero to get a system of ODE. We solve this system to attain the value of s, r and p. It is straightforward to obtain the non-traveling wave solutions to Eq. 4 by solving Eq. 8 and utilizing Eq. 5.

2.2 JEF-method

While, we summarize here the main steps of the JEF-method described by Fan et al. [46] as follows.

1. We repeat the first four steps from the previous subsection in order to obtain Eq. 7.
2. Assuming the solution of Eq. 7 in this type

$$\mathcal{X}(\eta_\delta) = \sum_{k=0}^{N} a_k[\mathcal{F}(\eta_\delta)]^k, \tag{9}$$

where N is a positive integer that will be determined and $\mathcal{F}(\eta_\delta) = \mathrm{sn}(\mathcal{K}\eta_\delta, m)$ or $\mathcal{F}(\eta_\delta) = cn(\mathcal{K}\eta_\delta, m)$ or $\mathcal{F}(\eta_\delta) = dn(\mathcal{K}\eta_\delta, m)$ for $0 < m < 1$. The Jacobi elliptic functions $\mathrm{sn}(\mathcal{K}\eta_\delta, m)$, $cn(\mathcal{K}\eta_\delta, m)$, $dn(\mathcal{K}\eta_\delta, m)$ are periodic and have features of triangular functions as follows: $\mathrm{sn}^2(\mathcal{K}\eta_\delta, m) + cn^2(\mathcal{K}\eta_\delta, m) = 1$, $dn^2(\mathcal{K}\eta_\delta, m) = 1 - m^2\mathrm{sn}^2(\mathcal{K}\eta_\delta, m)$, $[\mathrm{sn}(\mathcal{K}\eta_\delta, m)]' = cn(\mathcal{K}\eta_\delta, m)dn(\mathcal{K}\eta_\delta, m)$, $[cn(\mathcal{K}\eta_\delta, m)]' = -\mathrm{sn}(\mathcal{K}\eta_\delta, m)dn(\mathcal{K}\eta_\delta, m)$, $[dn(\mathcal{K}\eta_\delta, m)]' = -m^2\mathrm{sn}(\mathcal{K}\eta_\delta, m)cn(\mathcal{K}\eta_\delta, m)$.

If $m \to 1$, then $\mathrm{sn}(\mathcal{K}\eta_\delta, 1) \to \tanh(\mathcal{K}\eta_\delta)$, $cn(\mathcal{K}\eta_\delta, 1) \to \mathrm{sech}(\mathcal{K}\eta_\delta)$ and $dn(\mathcal{K}\eta_\delta, 1) \to \mathrm{sech}(\mathcal{K}\eta_\delta)$.

3. Usually, to determine the parameter N, we balance the highest order linear terms in the resulting equation with the highest order nonlinear terms. To determine the order, we follow these steps: Firstly, we define the degree of $\mathcal{F}$ as $D[\mathcal{F}] = N$. Secondly, we calculated the highest order nonlinear terms and the highest order nonlinear terms as

$$D\left[\frac{d^n\mathcal{F}}{d\eta^n}\right] = N + n,$$

and

$$D\left[\mathcal{F}^p\left(\frac{d^n\mathcal{F}}{d\eta^n}\right)^s\right] = pN + s(N + n).$$

4. After we determine N, we substitute (9) into the ODE (7) in order to attain an equation in powers of $\mathcal{F}$.
5. Equating each coefficients of powers of $\mathcal{F}$ in the resulting equation to zero. This will provide a set of equations containing the a_k ($k = 0, 1, \ldots N$) and $\mathcal{K}$. We solve these equations to attain the values of a_k ($k = 0, 1, \ldots N$) and $\mathcal{K}$ and substitute with these value into Eq. 9.

3 Traveling wave Eq. For SSE-MTD

To derive the wave equation for SSE-MTD (1), we use

$$\mathcal{W}(x,t) = \mathcal{X}(\eta_\delta)e^{i\mu_\delta},\ \mu_\delta = \mu_1 x + \frac{\mu_2\Gamma(\beta+1)}{\delta}t^\delta \text{ and}$$
$$\eta_\delta = \eta_1 x + \frac{\eta_2\Gamma(\beta+1)}{\delta}t^\delta, \tag{10}$$

where $\mathcal{X}$ is a real function, μ_1, μ_2, η_1, and η_2 are non-zero constants. We note that

$$\begin{aligned}
\mathcal{M}_{j,t}^{\delta,\beta}\mathcal{W} &= [\eta_2\mathcal{X}' + i\mu_2\mathcal{X}]e^{i\mu_\delta},\\
\mathcal{W}_x &= (\eta_1\mathcal{X}' + i\mu_1\mathcal{X})e^{i\mu_\delta},\ (|\mathcal{W}|^2)_x = \eta_1(\mathcal{X}^2)'e^{i\mu_\delta},\\
\mathcal{W}_{xx} &= \left(\eta_1^2\mathcal{X}'' + 2i\mu_1\eta_1\mathcal{X}' - \mu_1^2\mathcal{X}\right)e^{i\mu_\delta},\\
\mathcal{W}_{xxx} &= \left(\eta_1^3\mathcal{X}''' + 3i\mu_1\eta_1^2\mathcal{X}'' - 3\eta_1\mu_1^2\mathcal{X}' - i\mu_1^3\mathcal{X}\right)e^{i\mu_\delta}.
\end{aligned} \tag{11}$$

Inserting Eq. 11 into Eq. 1, we have for real part

$$\left(\frac{1}{2}\eta_1^2 - 3\alpha_1\mu_1\eta_1^2\right)\mathcal{X}'' + \left(-\mu_2 - \frac{1}{2}\mu_1^2 + \alpha_1\mu_1^3\right)\mathcal{X} + [\alpha_4 - \alpha_1\mu_1]\mathcal{X}^3 = 0, \tag{12}$$

and for imaginary part

$$\alpha_1\eta_1^3\mathcal{X}''' + (\eta_2 + \mu_1\eta_1 - 3\alpha_1\eta_1\mu_1^2)\mathcal{X}' + \eta_1(\alpha_2 + 2\alpha_3)\mathcal{X}^2\mathcal{X}' = 0. \tag{13}$$

Integrating (13) once, we get

$$[\alpha_1\eta_1^3\mathcal{X}'' + (\eta_2 + \mu_1\eta_1 - 3\alpha_1\eta_1\mu_1^2)\mathcal{X} + \frac{1}{3}\eta_1(\alpha_2 + 2\alpha_3)\mathcal{X}^3 = C, \tag{14}$$

where C is the integral constant. If we compare the coefficients of Eqs (12) and (14), we have

$$\begin{aligned}
\eta_1 &= \frac{1}{2\alpha_1} - 3\mu_1,\\
\eta_2 &= -2\gamma_1\mu_1\eta_1 + 3\alpha_1\eta_1\mu_1^2 - \mu_2 - \gamma_1\mu_1^2 + \alpha_1\mu_1^3,\\
\alpha_4 &= \alpha_1\mu_1 + \frac{1}{3}\eta_1(\alpha_2 + 2\alpha_3),
\end{aligned}$$

and

$$C = 0.$$

Now, we can rewrite Eq. 12 as

$$\mathcal{X}'' - \ell_1\mathcal{X}^3 - \ell_2\mathcal{X} = 0, \tag{15}$$

where

$$\ell_1 = \frac{2\alpha_1\mu_1 - 2\alpha_4}{(\eta_1^2 - 6\alpha_1\mu_1\eta_1^2)}, \text{and } \ell_2 = \frac{(2\mu_2 + \mu_1^2 - 2\alpha_1\mu_1^3)}{(\eta_1^2 - 6\alpha_1\mu_1\eta_1^2)}. \tag{16}$$

Balancing $\mathcal{X}''$ with $\mathcal{X}^3$ in Eq. 15 to calculate the parameter N as

$$N + 2 = 3N \Rightarrow N = 1.$$

4 Exact solutions of SSE-MTD

Two various methods such as GREM-method and JEF-method are used to attain the solutions to Eq. 15. The solutions to the SSE-MTD (1) are then determined.

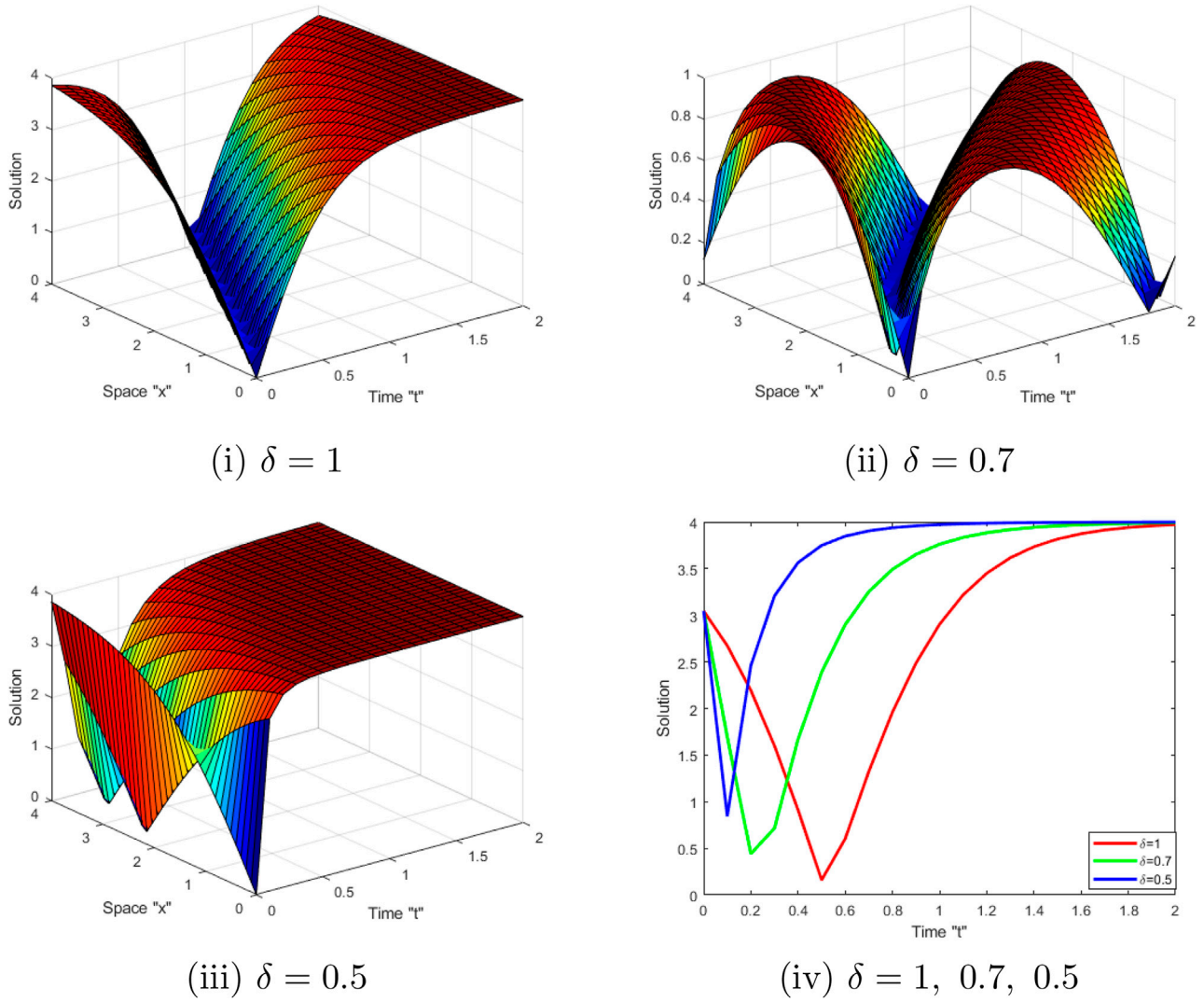

FIGURE 1
(i–iii) display 3D-shape of solution $|\mathcal{W}(x,t)|$ in Eq. 26 with δ =1,0.7,0.5 **(iv)** display 2D-shape of Eq. 26 with different values of δ.

4.1 REM-method

Utilizing Eq. 8, we obtain

$$\mathcal{X}''' = 2s^2\mathcal{X}^3 + 3sr\mathcal{X}^2 + (2sp + r^2)\mathcal{X} + rp. \tag{17}$$

Substituting (17) into (15), we have

$$(2s^2 - \ell_1)\mathcal{X}^3 + 3sr\mathcal{X}^2 + (2sp + r^2 - \ell_2)\mathcal{X} + rp = 0.$$

We put each coefficient of $\mathcal{X}^i$ equal zero in order to get

$$2s^2 - \ell_1 = 0,\ 3sr = 0,\ 2sp + r^2 - \ell_2 = 0, \text{ and } rp = 0.$$

Solving these equations, we have

$$s = \pm\sqrt{\frac{\ell_1}{2}}, \tag{18}$$

$$r = 0, \tag{19}$$

and

$$p = \frac{\ell_2}{2s} = \pm\frac{\ell_2}{\sqrt{2\ell_1}}, \tag{20}$$

where ℓ_1 and ℓ_2 are stated in Eq. 16. There are different sets for the solution of Eq. 8 relying on p and s as follows:

Set I: When $ps > 0$, thus the solutions of Eq. 8 are:

$$\mathcal{X}_1(\eta_\delta) = \sqrt{\frac{p}{s}}\tan\left(\sqrt{ps}\,\eta_\delta\right),$$

$$\mathcal{X}_2(\eta_\delta) = -\sqrt{\frac{p}{s}}\cot\left(\sqrt{ps}\,\eta_\delta\right),$$

$$\mathcal{X}_3(\eta_\delta) = \sqrt{\frac{p}{s}}\left(\tan\left(\sqrt{4ps}\,\eta_\delta\right) \pm \sec\left(\sqrt{4ps}\,\eta_\delta\right)\right),$$

$$\mathcal{X}_4(\eta_\delta) = -\sqrt{\frac{p}{s}}\left(\cot\left(\sqrt{4ps}\,\eta_\delta\right) \pm \csc\left(\sqrt{4ps}\,\eta_\delta\right)\right),$$

$$\mathcal{X}_5(\eta_\delta) = \frac{1}{2}\sqrt{\frac{p}{s}}\left(\tan\left(\frac{1}{2}\sqrt{ps}\,\eta_\delta\right) - \cot\left(\frac{1}{2}\sqrt{ps}\,\eta_\delta\right)\right),$$

Then, SSE-MTD (1) has the trigonometric functions solution:

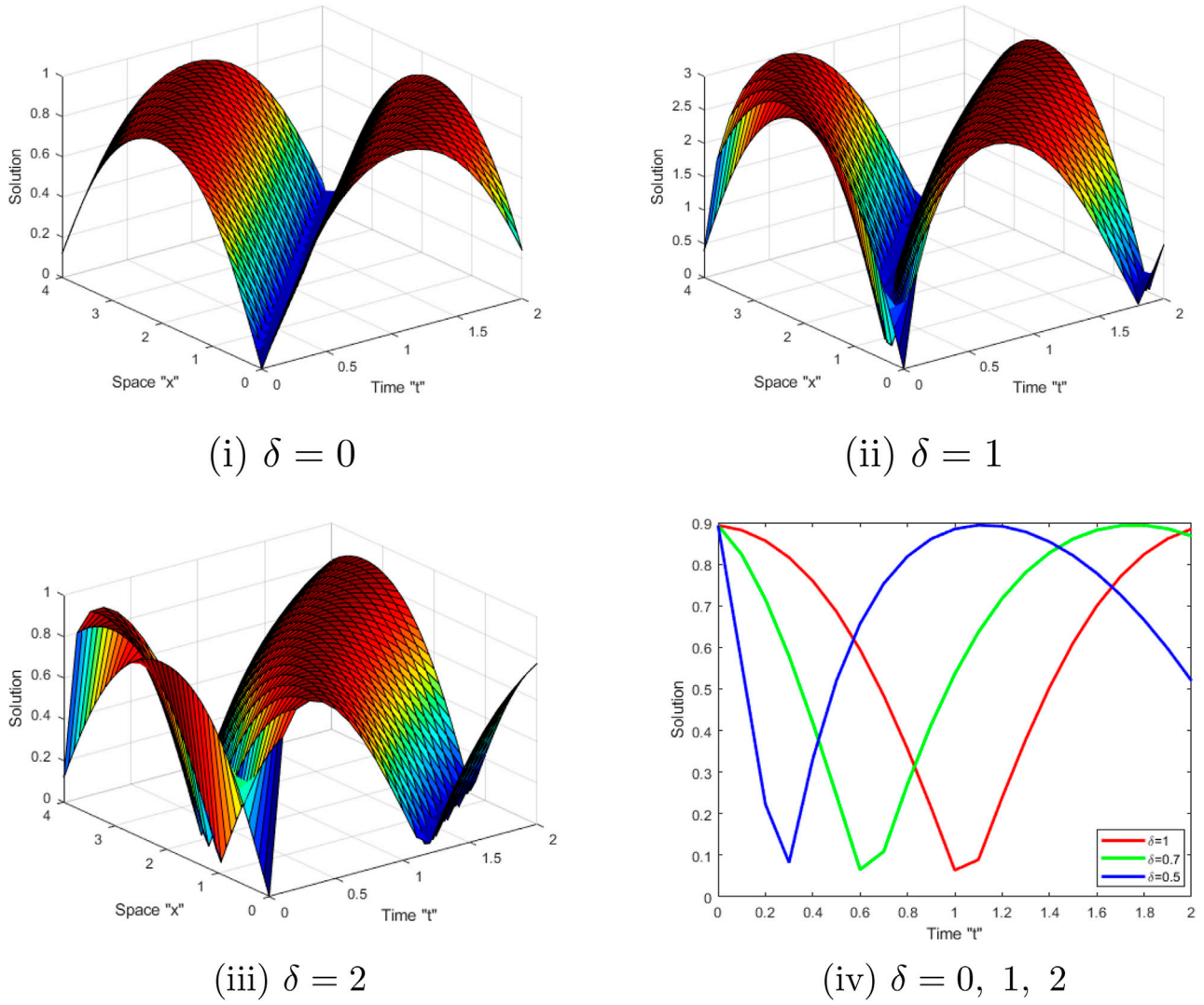

FIGURE 2
(i–iii) display 3D-shape of solution $|\mathcal{W}(x,t)|$ in Eq. 34 with δ = 1,0.7,0.5 **(iv)** display 2D-shape of Eq. 34 with different values of δ.

$$\mathcal{W}_1(x,t) = \sqrt{\frac{p}{s}}\tan\left(\sqrt{ps}\,\eta_\delta\right)e^{i\mu_\delta}, \tag{21}$$

$$\mathcal{W}_2(x,t) = -\sqrt{\frac{p}{s}}\cot\left(\sqrt{ps}\,\eta_\delta\right)e^{i\mu_\delta}, \tag{22}$$

$$\mathcal{W}_3(x,t) = \sqrt{\frac{p}{s}}\left(\tan\left(\sqrt{4ps}\,\eta_\delta\right) \pm \sec\left(\sqrt{4ps}\,\eta_\delta\right)\right)e^{i\mu_\delta}, \tag{23}$$

$$\mathcal{W}_4(x,t) = -\sqrt{\frac{p}{s}}\left(\cot\left(\sqrt{4ps}\,\eta_\delta\right) \pm \csc\left(\sqrt{4ps}\,\eta_\delta\right)\right)e^{\left(\gamma\mathcal{W}(t)-\frac{1}{2}\gamma^2 t\right)}, \tag{24}$$

$$\mathcal{W}_5(x,t) = \frac{1}{2}\sqrt{\frac{p}{s}}\left(\tan\left(\frac{1}{2}\sqrt{ps}\,\eta_\delta\right) - \cot\left(\frac{1}{2}\sqrt{ps}\,\eta_\delta\right)\right)e^{i\mu_\delta}, \tag{25}$$

where $\eta_\delta = \eta_1 x + \frac{\eta_2\Gamma(\beta+1)}{\delta}t^\delta$.

Family II: When $ps < 0$, thus the solutions of Eq. 8 are:

$$\mathcal{X}_6(\eta_\delta) = -\sqrt{\frac{-p}{s}}\tanh\left(\sqrt{-ps}\,\eta_\delta\right),$$

$$\mathcal{X}_7(\eta_\delta) = -\sqrt{\frac{-p}{s}}\coth\left(\sqrt{-ps}\,\eta_\delta\right),$$

$$\mathcal{X}_8(\eta_\delta) = -\sqrt{\frac{-p}{s}}\left(\tanh\left(\sqrt{-4ps}\,\eta_\delta\right) \pm i\,\mathrm{sech}\left(\sqrt{-4ps}\,\eta_\delta\right)\right),$$

$$\mathcal{X}_9(\eta_\delta) = -\sqrt{\frac{-p}{s}}\left(\coth\left(\sqrt{-4ps}\,\eta_\delta\right) \pm \mathrm{csch}\left(\sqrt{-4ps}\,\eta_\delta\right)\right),$$

$$\mathcal{X}_{10}(\eta_\delta) = \frac{-1}{2}\sqrt{\frac{-p}{s}}\left(\tanh\left(\frac{1}{2}\sqrt{-ps}\,\eta_\delta\right) + \coth\left(\frac{1}{2}\sqrt{-ps}\,\eta_\delta\right)\right).$$

Then, SSE-MTD (1) has the hyperbolic functions solution:

$$\mathcal{W}_6(x,t) = -\sqrt{\frac{-p}{s}}\tanh\left(\sqrt{-ps}\,\eta_\delta\right)e^{i\mu_\delta}, \tag{26}$$

$$\mathcal{W}_7(x,t) = -\sqrt{\frac{-p}{s}}\coth\left(\sqrt{-ps}\,\eta_\delta\right)e^{i\mu_\delta}, \tag{27}$$

$$\mathcal{W}_8(x,t) = -\sqrt{\frac{-p}{s}}\left(\tanh\left(\sqrt{-4ps}\,\eta_\delta\right) \pm i\,\mathrm{sech}\left(\sqrt{-4ps}\,\eta_\delta\right)\right)e^{i\mu_\delta}, \tag{28}$$

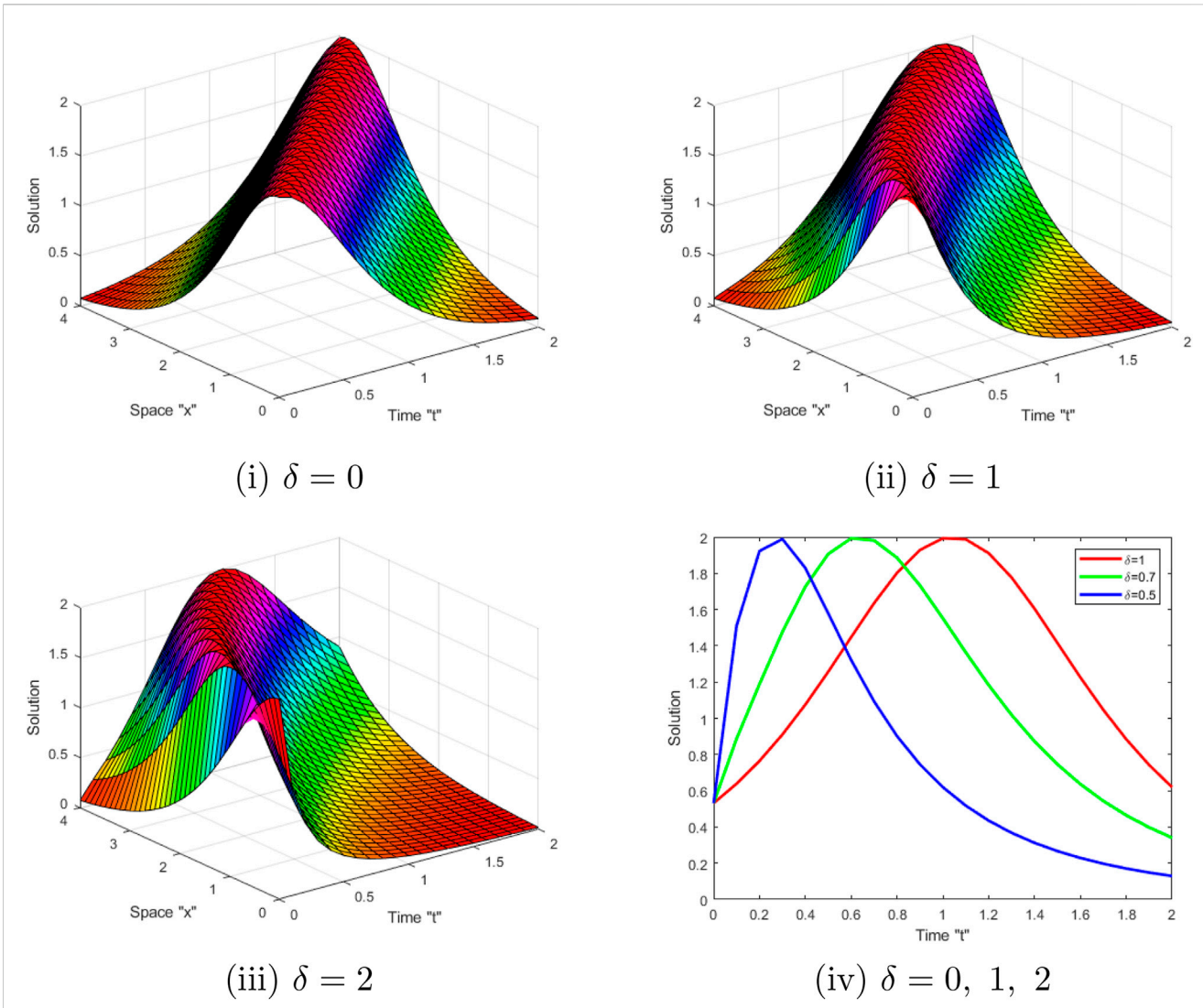

FIGURE 3
(i–iii) display 3D-shape of solution $|\mathcal{W}(x,t)|$ in Eq. 38 with δ = 1, 0.7,0.5 **(iv)** display 2D-shape of Eq. 38 with different values of δ.

$$\mathcal{W}_9(x,t) = -\sqrt{\frac{-p}{s}}\left(\coth\left(\sqrt{-4ps}\,\eta_\delta\right) \pm \operatorname{csch}\left(\sqrt{-4ps}\,\eta_\delta\right)\right)e^{i\mu_\delta}, \quad (29)$$

$$\mathcal{W}_{10}(x,t) = \frac{-1}{2}\sqrt{\frac{-p}{s}}\left(\tanh\left(\frac{1}{2}\sqrt{-ps}\,\eta_\delta\right) + \coth\left(\frac{1}{2}\sqrt{-ps}\,\eta_\delta\right)\right)e^{i\mu_\delta}, \quad (30)$$

where $\eta_\delta = \eta_1 x + \frac{\eta_2\Gamma(\beta+1)}{\delta}t^\delta$.

Family III: When $p = 0$, $s \neq 0$, then the solution of Eq. 8 is

$$\mathcal{X}_{11}(\eta_\delta) = \frac{-1}{s\eta_\delta}.$$

Then, we get the rational function solution of SSE-MTD (1) as

$$\mathcal{W}_{11}(x,t) = \left(\frac{-1}{s\left(\eta_1 x + \frac{\eta_2\Gamma(\beta+1)}{\delta}t^\delta\right)}\right)e^{i\mu_\delta}. \quad (31)$$

Remark 1: *If we Put $\beta = 0$ and $\delta = 0$ in Eqs. (21) and (26), then we get the solutions (13) and (14) that stated in [40].*

4.2 JEF-method

We assume the solutions of Eq. 15, with $N = 1$, are

$$\mathcal{X}(\eta_\delta) = a + b\mathcal{F}(\eta_\delta). \quad (32)$$

First, let $\mathcal{F}(\eta_\delta) = sn(\mathcal{K}\eta_\delta, m)$. Differentiate Eq. 32 two times, we have

$$\mathcal{X}''(\eta_\delta) = -(m^2+1)b\mathcal{K}^2 sn(\mathcal{K}\eta_\delta, m) + 2m^2 b\mathcal{K}^2 sn^3(\mathcal{K}\eta_\delta, m). \quad (33)$$

Setting Eqs 32, 33 into Eq. 15, we obtain

$$(2m^2 b\mathcal{K}^2 - \ell_1 b^3)sn^3(\mathcal{K}\eta_\delta, m) - 3\ell_1 ab^2 sn^2(\mathcal{K}\eta_\delta, m)$$
$$-[(m^2+1)b\mathcal{K}^2 + 3\ell_1 a^2 b + \ell_2 b]sn(\mathcal{K}\eta_\delta, m) - (\ell_1 a^3 + a\ell_2) = 0.$$

Plugging each coefficient of $[\mathrm{sn}(\mathcal{K}\eta_\delta, m)]^n$ equal zero, we attain

$$\ell_1 a^3 + a\ell_2 = 0,$$
$$(m^2+1)b\mathcal{K}^2 + 3\ell_1 a^2 b + \ell_2 b = 0,$$
$$3\ell_1 a b^2 sn^2 = 0,$$

and

$$2m^2 b\mathcal{K}^2 - \ell_1 b^3 = 0.$$

We obtain when we solve these equations

$$a = 0,\ b = \pm\sqrt{\frac{-2m^2\ell_2}{(m^2+1)\ell_1}}\ \mathcal{K}^2 = \frac{-\ell_2}{(m^2+1)}.$$

Consequently, the solution of Eq. 15 is

$$\mathcal{X}(\eta_\delta) = \pm\sqrt{\frac{-2m^2\ell_2}{(m^2+1)\ell_1}}\,sn\left(\sqrt{\frac{-\ell_2}{(m^2+1)}}\eta_\delta, m\right).$$

As a result, the solution of the SSE-MTD (1), for $\ell_2 < 0$ and $\ell_1 > 0$, is

$$\mathcal{W}(x,t) = \pm\sqrt{\frac{-2m^2\ell_2}{(m^2+1)\ell_1}}\,sn\left(\sqrt{\frac{-\ell_2}{(m^2+1)}}\eta_\delta, m\right)e^{i\mu_\delta}, \tag{34}$$

where $\eta_\delta = \eta_1 x + \frac{\eta_2\Gamma(\beta+1)}{\delta}t^\delta$. When $m \to 1$, the solution (34) tends to:

$$\mathcal{W}(x,t) = \pm\sqrt{\frac{-\ell_2}{\ell_1}}\tanh\left(\sqrt{\frac{-\ell_2}{2}}(\eta_1 x + \eta_2 t), m\right)e^{i\mu_\delta}. \tag{35}$$

Similarly, we can replace $\mathcal{F}(\eta_\delta)$ in (32) with $cn(\mathcal{K}\eta_\delta, m)$ or $dn(\mathcal{K}\eta_\delta, m)$ to derive the solutions of Eq. 15 as follows:

$$\mathcal{X}(\eta_\delta) = \pm\sqrt{\frac{-2m^2\ell_2}{(2m^2-1)\ell_1}}\,cn\left(\sqrt{\frac{\ell_2}{(2m^2-1)}}\eta_\delta, m\right),$$

and

$$\mathcal{X}(\eta_\delta) = \pm\sqrt{\frac{-2m^2\ell_2}{(2-m^2)\ell_1}}\,dn\left(\sqrt{\frac{\ell_2}{(2-m^2)}}\eta_\delta, m\right).$$

Consequently, the solutions of the SSE-MTD (1) are as follows:

$$\mathcal{W}(x,t) = \pm\sqrt{\frac{-2m^2\ell_2}{(2m^2-1)\ell_1}}\,cn\left(\sqrt{\frac{-\ell_2}{(2m^2-1)}}\eta_\delta, m\right)e^{i\mu_\delta}, \tag{36}$$

for $\frac{\ell_2}{(2m^2-1)} > 0$, $\ell_1 < 0$, and

$$\mathcal{W}(x,t) = \pm\sqrt{\frac{-2m^2\ell_2}{(2-m^2)\ell_1}}\,dn\left(\sqrt{\frac{\ell_2}{(2-m^2)}}\eta_\delta, m\right)e^{i\mu_\delta}, \tag{37}$$

for $\ell_2 > 0$, $\ell_1 < 0$, respectively. If $m \to 1$, then the solutions (36) and (37) turn to:

$$\mathcal{W}(x,t) = \pm\sqrt{\frac{-2\ell_2}{\ell_1}}\,\mathrm{sech}\left(\sqrt{\ell_2}\,(\eta_1 x + \eta_4 t)\right)e^{i\mu_\delta}, \tag{38}$$

for $\ell_2 > 0$, $\ell_1 < 0$.

Remark 2: *If we Put $\beta = 0$ and $\delta = 0$ in Eqs.* (34) *and* (36)*, then we get the solutions (48) and (49) that stated in [40].*

5 Discussion and effects of M-truncated derivative

Discussion: For the Sasa-Satsuma equation with a M-truncated derivative, we found the optical solutions in this paper. Two effective methods, the REM-method and JEF-method, were used to arrive at these results. The REM-method has provided optical singular periodic (21) and (22), singular optical solution (27), and dark optical solution (26). While JEF-method has provided elliptic solutions. Dark optical solution can interpret solitary waves (SW) with less intensity than the background [47]. SW with discontinuous derivatives can be illustrated using singular solitons [48, 49]. These kinds of SW are effective because of their efficacy and applicability in optical long-distance communications. Optical fibers can be thought of as thin, long strands of pure-ultra glass that allow electromagnetic radiations to travel unimpeded from one location to another.

Effects of M-truncated derivative: Now, we examine the influence of MTD on the exact solution of the SSE-MTD (1). Several graphical representations depict the behavior of some obtained solutions, including (26) (34) and (38). Let us fix the parameters $\alpha_1 = \frac{1}{2}$, $\mu_1 = \mu_2 = \alpha_4 = \eta_1 = 1$, $\alpha_2 = 2$, $\eta_2 = -2$, $x \in [0, 4]$ and $t \in [0, 2]$ to simulate these graphs.

Now, we deduce from Figures 1, 2, 3 that when the derivative order δ of M-truncated derivative increases, the surface moves into the right.

6 Conclusion

In this study, the Sasa-Satsuma equation with M-truncated derivative (SSE-MTD) was examined. We acquired the exact solutions by utilizing Jacobi elliptic function and generalizing Riccati equation mapping methods. Because of the application of the Sasa–Satsuma equation in explaining the propagation of femtosecond pulses in optical fibers, these solutions may explain a wide range of interesting and complex physical phenomena. Furthermore, using the MATLAB program, the M-truncated derivative effects on the exact solutions of SSE-MTD (1) were illustrated. We concluded that when the derivatives order increases the surface moves into the right. In the future work, we can consider Sasa-Satsuma equation with stochastic term.

Data availability statement

The original contributions presented in the study are included in the article/Supplementary Material, further inquiries can be directed to the corresponding author.

Author contributions

WM: software, data curation, formal analysis, investigation, methodology, writing—original draft. FA-A: data curation, investigation, formal analysis, writing—original draft. All authors contributed to the article and approved the submitted version.

Acknowledgments

Princess Nourah bint Abdulrahman University Researcher Supporting Project number (PNURSP2023R 273), Princess Nourah bint Abdulrahman University, Riyadh, Saudi Arabia.

Conflict of interest

The authors declare that the research was conducted in the absence of any commercial or financial relationships that could be construed as a potential conflict of interest.

Publisher's note

All claims expressed in this article are solely those of the authors and do not necessarily represent those of their affiliated organizations, or those of the publisher, the editors and the reviewers. Any product that may be evaluated in this article, or claim that may be made by its manufacturer, is not guaranteed or endorsed by the publisher.

References

1. Lyu W, Wang Z. Global classical solutions for a class of reaction-diffusion system with density-suppressed motility. *Electron Res Archive* (2022) 30(3):995–1015. doi:10.3934/era.2022052

2. Xie X, Wang T, Zhang W. Existence of solutions for the (p,q)-Laplacian equation with nonlocal Choquard reaction. *Appl Math Lett* (2023) 135:108418. doi:10.1016/j.aml.2022.108418

3. Zhang J, Xie J, Shi W, Huo Y, Ren Z, He D. Resonance and bifurcation of fractional quintic Mathieu–Duffing system. *Chaos: Interdiscip J Nonlinear Sci* (2023) 33(2):023131. doi:10.1063/5.0138864

4. Alshammari M, Iqbal N, Botmart T. The solution of fractional-order system of KdV equations with exponential-decay kernel. *Results Phys* (2022) 38:105615. doi:10.1016/j.rinp.2022.105615

5. Hussain S, Madi EN, Iqbal N, Botmart T, Karaca Y, Mohammed WW. Fractional dynamics of vector-borne infection with sexual transmission rate and vaccination. *Mathematics* (2021) 9(23):3118. doi:10.3390/math9233118

6. Alshammari M, Mohammed WW, Yar M. Novel Analysis of fuzzy fractional Klein-Gordon model via Semianalytical method. *J Funct Spaces* (2022) 2022:1–9. doi:10.1155/2022/4020269

7. Qt Ain QT, Anjum N, Din A, ZebDjilali AS, Khan ZA. On the analysis of Caputo fractional order dynamics of Middle East Lungs Coronavirus (MERS-CoV) model. *Alex Eng J* (2022) 61(7):5123–31. doi:10.1016/j.aej.2021.10.016

8. Akbulut A, Kaplan M, Tascan F. Conservation laws and exact solutions of Phi-four (Phi-4) equation via the $(G'/G, 1/G)$ -expansion method. *Z für Naturforschung A* (2016) 71(5):439–46. doi:10.1515/zna-2016-0010

9. Wang ML, Li XZ, Zhang JL. The (G'/G)-expansion method and travelling wave solutions of nonlinear evolution equations in mathematical physics. *Phys Lett A* (2008) 372:417–23. doi:10.1016/j.physleta.2007.07.051

10. Zhang H. New application of the (G'/G)-expansion method. *Commun Nonlinear Sci Numer Simul* (2009) 14:3220–5. doi:10.1016/j.cnsns.2009.01.006

11. Naher H, Abdullah FA. New approach of (G'/G) -expansion method and new approach of generalized (G'/G) -expansion method for nonlinear evolution equation. *AIP Adv* (2013) 3(3):032116. doi:10.1063/1.4794947

12. He JH, Wu XH. Exp-function method for nonlinear wave equations. *Chaos Solitons Fractals* (2006) 30(3):700–8. doi:10.1016/j.chaos.2006.03.020

13. Yan ZL. Abundant families of Jacobi elliptic function solutions of the (2+1)-dimensional integrable Davey–Stewartson-type equation via a new method. *Chaos Solitons Fractals* (2003) 18:299–309. doi:10.1016/s0960-0779(02)00653-7

14. Wazwaz AM. The sine-cosine method for obtaining solutions with compact and noncompact structures. *Appl Math a Comput* (2004) 159(2):559–76. doi:10.1016/j.amc.2003.08.136

15. Jiong S. Auxiliary equation method for solving nonlinear partial differential equations. *Phys Lett A* (2003) 309:387–96. doi:10.1016/S0375-9601(03)00196-8

16. Lu B. The first integral method for some time fractional differential equations. *J Math Anal Appl* (2012) 395(2):684–93. doi:10.1016/j.jmaa.2012.05.066

17. Baskonus HM, Bulut H, Sulaiman TA. New complex hyperbolic structures to the lonngren-wave equation by using sine-gordon expansion method. *Appl Math Nonlinear Sci* (2019) 4(1):129–38. doi:10.2478/amns.2019.1.00013

18. Arnous AH, Mirzazadeh M. Application of the generalized Kudryashov method to the Eckhaus equation. *Nonlinear Anal Modell Control* (2016) 21(5):577–86. doi:10.15388/na.2016.5.1

19. Khan K, Akbar MA. The $\exp(-\phi(\varsigma))$-expansion method for finding travelling wave solutions of Vakhnenko-Parkes equation. *Int J Dyn Syst Differ Equ* (2014) 5:72–83. doi:10.1504/ijdsde.2014.067119

20. Tao H, Anjum N, Yang Y-J. The Aboodh transformation-based homotopy perturbation method: New hope for fractional calculus. *Front Phys* (2023) 11:1168795. doi:10.3389/fphy.2023.1168795

21. Anjum N, He C-H, He J-H. Two-scale fractal theory for the population dynamics. *Fractals* (2021) 29:2150182. doi:10.1142/S0218348X21501826

22. Anjum N, Ain QT, Li XX. Two-scale mathematical model for tsunami wave. *Int J Geomath* (2021) 12:10. doi:10.1007/s13137-021-00177-z

23. Katugampola UN. New approach to a generalized fractional integral. *Appl Math Comput* (2011) 218(3):860–5. doi:10.1016/j.amc.2011.03.062

24. Katugampola UN. New approach to generalized fractional derivatives. *Bull Math Anal Appl B* (2014) 6(4):1–15.

25. Kilbas AA, Srivastava HM, Trujillo JJ. *Theory and applications of fractional differential equations*. Amsterdam, Netherlands: Elsevier (2016).

26. Samko SG, Kilbas AA, Marichev OI. *Fractional integrals and derivatives, theory and applications*. Yverdon, Switzerland: Gordon and Breach (1993).

27. Sousa JV, de Oliveira EC. A new truncated M fractional derivative type unifying some fractional derivative types with classical properties. *Int J Anal Appl* (2018) 16(1):83–96. doi:10.28924/2291-8639-16-2018-83

28. Al-Askar FM, Cesarano C, Mohammed WW. Abundant solitary wave solutions for the boiti–leon–manna–pempinelli equation with M-truncated derivative. *Axioms* (2023) 12(5):466. doi:10.3390/axioms12050466

29. Mohammed WW, Cesarano C, Al-Askar FM. Solutions to the (4+1)-dimensional time-fractional fokas equation with M-truncated derivative. *Mathematics* (2023) 11(1):194. doi:10.3390/math11010194

30. Yusuf A, Inc M, Baleanu D. Optical solitons with M-truncated and beta derivatives in nonlinear optics. *Front Phys* (2019) 7:126. doi:10.3389/fphy.2019.00126

31. Ozkan A, Ozkan EM, Yildirim O. On exact solutions of some space–time fractional differential equations with M-truncated derivative. *Fractal and Fractional* (2023) 7(3):255. doi:10.3390/fractalfract7030255

32. Bogning JR, Tchaho CT, Kafne TC. Solitary wave solutions of the modified sasa-satsuma nonlinear partial differential equation. *Am J Comput Math* (2013) 3:131–7. doi:10.5923/j.ajcam.20130302.11

33. Yildirim Y. Optical solitons to sasa-satsuma model in birefringent fibers with trial equation approach. *Optik* (2019) 185:269–74. doi:10.1016/j.ijleo.2019.03.016

34. Sasa N, Satsuma J. New-type of soliton solutions for a higher-order nonlinear Schrödinger equation. *J Phys Soc Jpn* (1991) 60:409–17. doi:10.1143/jpsj.60.409

35. Mihalache D, Truta N, Crasovan LC. Painlevé analysis and bright solitary waves of the higher-order nonlinear Schrödinger equation containing third-order dispersion and self-steepening term. *Phys Rev E* (1997) 56(1):1064–70. doi:10.1103/physreve.56.1064

36. Solli D, Ropers C, Koonath P, Jalali B. Optical rogue waves. *Nature* (2007) 450(7172):1054–7. doi:10.1038/nature06402

37. Khater MM, Seadawy AR, Lu D. Dispersive optical soliton solutions for higher order nonlinear Sasa-Satsuma equation in mono mode fibers via new auxiliary equation method. *Superlatt Microstruct* (2018) 113:346–58. doi:10.1016/j.spmi.2017.11.011

38. Chen S. Twisted rogue-wave pairs in the Sasa-Satsuma equation. *Phys Rev E* (2013) 88(2):023202. doi:10.1103/physreve.88.023202

39. Tuluce DS, Pandir Y, Bulut H. New soliton solutions for Sasa–Satsuma equation. *Waves Random Complex Medium* (2015) 25(3):417–28. doi:10.1080/17455030.2015.1042945

40. Seadawy AR, Nasreen N, Dian-chen LU. Optical soliton and elliptic functions solutions of Sasa-satsuma dynamical equation and its applications. *Appl Math J Chin Univ*. (2021) 36(2):229–42. doi:10.1007/s11766-021-3844-0

41. Xu T, Wang D, Li M, Liang H. Soliton and breather solutions of the Sasa–Satsuma equation via the Darboux transformation. *Phys Scr* (2014) 7:075207. doi:10.1088/0031-8949/89/7/075207

42. Xu J, Fan E. The unified transform method for the Sasa–Satsuma equation on the half-line. *Proc R Soc A* (2013) 469(2159):20130068. doi:10.1098/rspa.2013.0068

43. Liu Y, Gao YT, Xu T, Lü X, Sun ZY, Meng XH, et al. Soliton solution, bäcklund transformation, and conservation laws for the Sasa-Satsuma equation in the optical fiber communications. *Z Nat A* (2010) 65(4):291–300. doi:10.1515/zna-2010-0405

44. Wright OC, III. Sasa-Satsuma equation, unstable plane waves and heteroclinic connections. *Chaos Soliton Fract* (2007) 33(2):374–87. doi:10.1016/j.chaos.2006.09.034

45. Zhu SD. The generalizing Riccati equation mapping method in non-linear evolution equation: Application to (2+1)-dimensional boiti–leon–pempinelle equation. *Chaos, Solitons Fractals* (2008) 37:1335–42. doi:10.1016/j.chaos.2006.10.015

46. Fan E, Zhang J. Applications of the Jacobi elliptic function method to special-type nonlinear equations. *Phys Lett A* (2002) 305:383–92. doi:10.1016/s0375-9601(02)01516-5

47. Scott AC. *Encyclopedia of nonlinear science*. New York, NY: Routledge, Taylor and Francis Group (2005).

48. Rosenau P, Hyman JM, Staley M. Multidimensional compactons. *Phys Rev Lett* (2007) 98:024101. doi:10.1103/PhysRevLett.98.024101

49. Camassa R, Holm DD. An integrable shallow water equation with peaked solitons. *Phys Rev Lett* (1993) 71:1661–4. doi:10.1103/PhysRevLett.71.1661

Nomenclature

$\mathcal{M}_{j,t}^{\delta,\beta}$	M-truncated derivative operator
$\mathcal{E}_{j,\beta}(t)$	Truncated Mittag-Leffler function
$\Gamma(\cdot)$	Gamma function
β	Positive real number
δ	Fractional derivative order
a and b	Real constants
α_k, for $k = 1, 2, 3, 4$	Real constants
x and t	Independent variables
$\mathcal{X}$	Solution of wave equation
η_δ	The wave variable
μ_δ	The phase component
μ_1	The wave frequency
μ_2	The wave number
η_1	The wave frequency
η_2	The wave velocity
Sn	The elliptic sine
Cn	The elliptic cosine
Dn	The delta amplitude
M	Modulus

frontiers | Frontiers in Physics

TYPE Original Research
PUBLISHED 02 August 2023
DOI 10.3389/fphy.2023.1238901

OPEN ACCESS

EDITED BY
Ji-Huan He,
Soochow University, China

REVIEWED BY
Muhammad Nadeem,
Qujing Normal University, China
Yajie Li,
Henan University of Urban Construction, China
Ain Qura Tul,
Guizhou University, China

*CORRESPONDENCE
Jian-Gang Zhang,
Zhangjg7715776@126.com

RECEIVED 12 June 2023
ACCEPTED 18 July 2023
PUBLISHED 02 August 2023

CITATION
Zhang J-G, Wang F and Wang H-N (2023), Fractional stochastic vibration system under recycling noise.
Front. Phys. 11:1238901.
doi: 10.3389/fphy.2023.1238901

Fractional stochastic vibration system under recycling noise

Jian-Gang Zhang*, Fang Wang and Hui-Nan Wang

School of Mathematics and Physics, Lanzhou Jiaotong University, Lanzhou, China

The fractional stochastic vibration system is quite different from the traditional one, and its application potential is enormous if the noise can be deployed correctly and the connection between the fractional order and the noise property is unlocked. This article uses a fractional modification of the well-known van der Pol oscillator with multiplicative and additive recycling noises as an example to study its stationary response and its stochastic bifurcation. First, based on the principle of the minimum mean square error, the fractional derivative is equivalent to a linear combination of damping and restoring forces, and the original system is simplified into an equivalent integer order system. Second, the Itô differential equations and One-dimensional Markov process are obtained according to the stochastic averaging method, using Oseledec multiplicative ergodic theorem and maximal Lyapunov exponent to judge local stability, and judging global stability is done by using the singularity theory. Lastly, the stochastic D-bifurcation behavior of the model is analyzed by using the Lyapunov exponent of the dynamical system invariant measure, and the stationary probability density function of the system is solved according to the FPK equation. The results show that the fractional order and noise property can greatly affect the system's dynamical properties. This paper offers a profound, original, and challenging window for investigating fractional stochastic vibration systems.

KEYWORDS

van der Pol system, fractional derivative, recycling noise, stochastic averaging method, stochastic bifurcation

1 Introduction

Fractional derivative [1, 2] is an extension of the theory of integer derivatives, and the study of fractional derivatives has a history of over 300 years. Some new materials have appeared, e.g., viscoelastic materials, nanomaterials, cement mortar, 3D-printed materials, and porous materials [3–8], which are different from either a solid or a fluid, and their constitutive relation is extremely difficult to be expressed correctly by the traditional calculus though much effort has been made to solve the problem, for example, using the fractal viscoelastic model [9] and the fractal rheological model [10]; the intractable constitutive relation has not yet been solved.

Considering its memory property, we consider that fractional calculus might be the best candidate for stochastic dynamical systems [11, 12]. Stochastic disturbances are widespread in nature, and fractional stochastic systems have become a hot spot in both mathematics and physics to deal with noise excitation. For example, energy-harvesting devices [13–15] are always subject to random excitation, and a fractional model can effectively reveal the bifurcation properties and multiple attractors of the energy-harvesting system, for example, Ref. [16]. Fractional models for Gaussian white noise also caught much attention [17–21], and the fractional convolution kernel neural network is a suitable mathematical tool for fault diagnosis [22–24]. Duffing oscillator [25, 26] is extended to its fractional partner under noise

[27, 28]. Van der Pol oscillator [29] is another widely used model for the analysis of fractional stochastic P-bifurcation [30, 31].

In reality, noise exists in all aspects of practical applications, especially in nonlinear systems. The properties of stationary response, energy-harvesting efficiency, stability, and bifurcation will be greatly affected by noise excitation. At present, the research on the dynamic behavior of systems driven by recycling noise has attracted widespread attention from domestic and foreign scholars and achieved fruitful results, especially in the birhythmic biological system [32], stochastic resonance in asymmetric bistable systems [33], and the double entropic stochastic resonance phenomenon [34]. In this article, the fractional van der Pol model with recycling noise is adopted to investigate its dynamical properties.

2 Model description

Balthazar van der Pol is a famous electronic engineer in the Netherlands. In 1927, he first deduced the famous van der Pol equation in order to describe the oscillation effect of triodes in electronic circuits, as shown below:

$$\ddot{x} - \mu(1 - x^2)\dot{x} + x = 0$$

Afterward, as a classic nonlinear dynamic system, it is often used in mathematics and some nonlinear dynamic systems to demonstrate its dynamic behavior characteristics. In continuous research, the highest number of nonlinear terms considered is also constantly increasing, and there are also various methods for solving approximate solutions of such equations [35, 36]. From the classical van der Pol equation, changing the order of the equation can obtain systems with different dynamic behaviors, thereby better obtaining the dynamic behavior characteristics of the system. Therefore, we use the following equation to introduce the fractional generalized van der Pol model with multiplicative and additive recycling noise:

$$\begin{aligned}&\ddot{x} - \left(-\varepsilon + \alpha_1 x^2 - \alpha_2 x^4 + \alpha_3 x^6 - \alpha_4 x^8\right)\dot{x} + \omega^2 x + {}_0^cD^p x \\ &\quad = \eta_1(t) + x(t)\eta_2(t),\end{aligned} \tag{1}$$

where ε is the damping coefficient, $\alpha_1, \alpha_2, \alpha_3, \alpha_4$ are nonlinear damping coefficients, ω is the frequency, $\eta_1(t)$ and $\eta_2(t)$ are independent recycling noises, i.e., $D_1 \neq D_2$, $\eta_i(t) = \xi_i(t) + k\xi_i(t-\tau)$, $(i = 1, 2)$. The power spectral density of recycling noise is obtained as:

$$S_i(\omega) = 2D_i\left[1 + k^2 + 2k\cos(\omega\tau)\right], (i = 1, 2). \tag{2}$$

${}_0^cD^p[x(t)]$ is the Caputo fractional derivative [1, 2] of p $(0 \le p \le 1)$ order about $x(t)$ defined as:

$${}_0^cD^p[x(t)] = \frac{1}{\Gamma(m-p)}\int_0^t \frac{x^{(m)}(u)}{(t-u)^{1+p-m}}du, \quad m-1 < p \le m, m \in N. \tag{3}$$

There are other definitions of fractional derivatives, for example, two-scale fractal derivative [37–41] and He's fractional derivative [42]. The Caputo fractional derivative has memory property [43, 44], so it is used for the present study.

The ${}_0^cD^p x$ term in Eq. 1 can be expressed in a combination of spring stiffness and damping terms [45–48], hence, Eq. 1 becomes:

$$\begin{aligned}&\ddot{x} - \left(-\varepsilon + \alpha_1 x^2 - \alpha_2 x^4 + \alpha_3 x^6 - \alpha_4 x^8 + C(p)\right)\dot{x} \\ &\quad + \left(\omega^2 + K(p)\right)x = \eta_1(t) + x(t)\eta_2(t),\end{aligned} \tag{4}$$

where C and K are the equivalent damping and stiffness coefficients of fractional damping, respectively.

In order to identify C and K, we introduce an error function, which reads

$$e = -C(p)\dot{x} + K(p)x - {}_0^cD^p[x(t)], \tag{5}$$

According to the minimum mean square method [44], we have

$$\begin{cases}\partial E(e^2)/\partial(C(p)) = 0, \\ \partial E(e^2)/\partial(K(p)) = 0.\end{cases} \tag{6}$$

Equation 6 leads to the following equations:

$$\begin{cases}E\left[-C(p)\dot{x}^2 + K(p)x\dot{x} - \dot{x}\,{}_0^cD^p x\right] = \lim\limits_{T\to\infty}\frac{1}{T}\int_0^T\left(-C(p)\dot{x}^2 + K(p)x\dot{x} - \dot{x}\,{}_0^cD^p x\right)dt = 0, \\ E\left[-C(p)x\dot{x} + K(p)x^2 - x\,{}_0^cD^p x\right] = \lim\limits_{T\to\infty}\frac{1}{T}\int_0^T\left(-C(p)x\dot{x} + K(p)x^2 - x\,{}_0^cD^p x\right)dt = 0.\end{cases} \tag{7}$$

Assuming that

$$x(t) = a(t)\cos\varphi(t) = a(t)\cos(\omega t + \theta) \tag{8}$$

and $\dot{a}(t) \approx 0$, we have

$$\begin{cases}\dot{x}(t) = -a(t)\omega\sin\varphi(t), \\ \ddot{x}(t) = -a(t)\omega^2\cos\varphi(t).\end{cases} \tag{9}$$

Considering Eq. 8, 9, we re-write Eq. 7 in the form

$$\begin{aligned}&\lim_{T\to\infty}\frac{1}{T}\int_0^T\left(-C(p)\dot{x}^2 + K(p)x\dot{x} - \dot{x}\,{}_0^cD^p x\right)dt \\ &\quad = \lim_{T\to\infty}\frac{1}{T}\int_0^T\left(-C(p)a^2(t)\omega^2\sin^2\varphi(t) - K(p)a^2(t)\omega\varphi(t)\cos\varphi(t)\right. \\ &\qquad \left. + a(t)\omega\sin\varphi(t)\,{}_0^cD^p x\right)d\varphi \\ &\quad \approx -\frac{C(p)a^2\omega}{2} + \frac{1}{\Gamma(1-p)}\lim_{T\to\infty}\frac{1}{T}\int_o^T\left[\left(a\omega\sin\varphi\right)\int_0^t\frac{\dot{x}(t-\tau)}{\tau^p}d\tau\right]d\varphi \\ &\quad = \frac{-C(p)a^2\omega}{2} - \frac{1}{\Gamma(1-p)}\lim_{T\to\infty}\frac{1}{T}\int_0^T a^2\omega\sin\varphi \\ &\qquad \times\left(\int_0^t\frac{\sin\varphi\cos(\omega\tau) - \cos\varphi\sin(\omega\tau)}{\tau^p}d\tau\right)dt = 0,\end{aligned}$$

For the same reason, we have

$$\begin{aligned}&\lim_{T\to\infty}\frac{1}{T}\int_0^T\left(-C(p)x\dot{x} + K(p)x^2 - x\,{}_0^cD^p x\right)dt \\ &\quad = \lim_{T\to\infty}\frac{1}{T}\int_0^T\left(-C(p)a^2(t)\omega\sin\varphi(t)\cos\varphi(t) + K(p)a^2(t)\cos^2\varphi(t)\right. \\ &\qquad \left. - a(t)\cos\varphi(t)\,{}_0^cD^p x\right)d\varphi \\ &\quad \approx \frac{K(p)a^2}{2\omega} - \frac{1}{\Gamma(1-p)}\lim_{T\to\infty}\frac{1}{T}\int_o^T\left[\left(a\cos\varphi\right)\int_0^t\frac{\dot{x}(t-\tau)}{\tau^p}d\tau\right]d\varphi \\ &\quad = \frac{K(p)a^2}{2\omega} + \frac{1}{\Gamma(1-p)}\lim_{T\to\infty}\frac{1}{T}\int_0^T a^2 \\ &\qquad \times\cos\varphi\left(\int_0^t\frac{\sin\varphi\cos(\omega\tau) - \cos\varphi\sin(\omega\tau)}{\tau^p}d\tau\right)dt = 0.\end{aligned}$$

Hence

TABLE 1 Global stability analysis.

Condition		State	Category	Conclusion
$H_1/H_3 < 1$	$c_a < 1$	$a = 0$	Attract natural boundary	The trivial solution of Eq. 26 is stable in the sense of probability, and the original system is probabilistically stable at the balance point
	$c_l > -1$	$a = +\infty$	Exclude natural boundary	
$H_1/H_3 > 1$	$c_a > 1$	$a = 0$	Exclude natural boundary	The trivial solution of Eq. 26 is unstable in the sense of probability, and the original system is probabilistically unstable at the balance point
	$c_l < -1$	$a = +\infty$	Attract natural boundary	
$H_1/H_3 = 1$	$c_a = 1$	$a = 0$	Strict natural boundary	The critical condition of system bifurcation

$$\begin{cases} \lim\limits_{T\to\infty}\frac{1}{T}\int_0^T(-C(p)\dot{x}^2+K(p)x\dot{x}-\dot{x}_0^c D^p x)dt \\ =\frac{-C(p)a^2\omega}{2}-\frac{1}{\Gamma(1-p)}\lim\limits_{T\to\infty}\frac{1}{T}\int_0^T a^2\omega\sin\varphi\left(\int_0^t\frac{\sin\varphi\cos(\omega\tau)-\cos\varphi\sin(\omega\tau)}{\tau^p}d\tau\right)dt=0, \\ \lim\limits_{T\to\infty}\frac{1}{T}\int_0^T(-C(p)x\dot{x}+K(p)x^2-x_0^c D^p x)dt \\ =\frac{K(p)a^2}{2\omega}+\frac{1}{\Gamma(1-p)}\lim\limits_{T\to\infty}\frac{1}{T}\int_0^T a^2\cos\varphi\left(\int_0^t\frac{\sin\varphi\cos(\omega\tau)-\cos\varphi\sin(\omega\tau)}{\tau^p}d\tau\right)dt=0. \end{cases} \tag{10}$$

To simplify Eq. 10 further, we use the following asymptotic integrals

$$\begin{cases} \int_0^t\frac{\cos(\omega\tau)}{\tau^p}d\tau=\omega^{p-1}\left(\Gamma(1-p)\sin\left(\frac{p\pi}{2}\right)+\frac{\sin(\omega t)}{(\omega t)^p}\right)+o\left((\omega t)^{-p-1}\right), \\ \int_0^t\frac{\sin(\omega\tau)}{\tau^p}d\tau=\omega^{p-1}\left(\Gamma(1-p)\cos\left(\frac{p\pi}{2}\right)-\frac{\cos(\omega t)}{(\omega t)^p}\right)+o\left((\omega t)^{-p-1}\right). \end{cases} \tag{11}$$

In view of Eq. 11, the integral averaging of Eq. 10 with respect to φ results in

$$\begin{cases} C(p)=-\omega^{p-1}\sin\left(\frac{p\pi}{2}\right), \\ K(p)=\omega^p\sin\left(\frac{p\pi}{2}\right). \end{cases} \tag{12}$$

Hence, the equivalent system (4) can be written in the form

$$\ddot{x}-\lambda x+{\omega_0}^2 x=\eta_1(t)+x(t)\eta_2(t), \tag{13}$$

where

$$\begin{cases} \lambda=-\varepsilon+\alpha_1x^2-\alpha_2x^4+\alpha_3x^6-\alpha_4x^8-\omega^{p-1}\sin\left(\frac{p\pi}{2}\right), \\ {\omega_0}^2=\omega^2+\omega^p\cos\left(\frac{p\pi}{2}\right). \end{cases} \tag{14}$$

3 Model processing

Now the problem becomes relatively simple; we assume that the solution of Eq. 13 can be expressed as [49].

$$\begin{cases} X=x(t)=a(t)\cos\Phi(t), \\ Y=\dot{x}(t)=-a(t)\omega_0\sin\Phi(t), \\ \Phi(t)=\omega_0 t+\theta(t), \end{cases} \tag{15}$$

where $a(t)$ and $\theta(t)$ are the amplitude and initial phase of the system, respectively.

We re-write Eq. 13 in the form

$$\begin{cases} \dot{x}=y, \\ \dot{y}=\lambda y-{\omega_0}^2x(t)+\eta_1(t)+x(t)\eta_2(t). \end{cases} \tag{16}$$

By Eq. 15 and the stochastic averaging method [50], Eq. 16 becomes

$$\begin{cases} \frac{da}{dt}=F_{11}(a,\theta)+G_{11}(a,\theta)\eta_1(t)+G_{12}(a,\theta)\eta_1(t), \\ \frac{d\theta}{dt}=F_{21}(a,\theta)+G_{21}(a,\theta)\eta_1(t)+G_{22}(a,\theta)\eta_1(t), \end{cases} \tag{17}$$

where

$$\begin{cases} F_{11}(a,\theta)=a\sin^2\Phi\left(\begin{array}{c}-\varepsilon+\alpha_1a^2\cos^2\Phi-\alpha_2a^4\cos^4\Phi+\alpha_3a^6\cos^6\Phi \\ -\alpha_4a^8\cos^8\Phi-\omega^{p-1}\sin\left(\frac{p\pi}{2}\right)\end{array}\right), \\ F_{21}(a,\theta)=\sin\Phi\cos\Phi\left(\begin{array}{c}-\varepsilon+\alpha_1a^2\cos^2\Phi-\alpha_2a^4\cos^4\Phi+\alpha_3a^6\cos^6\Phi \\ -\alpha_4a^8\cos^8\Phi-\omega^{p-1}\sin\left(\frac{p\pi}{2}\right)\end{array}\right), \\ G_{11}(a,\theta)=-\frac{\sin\Phi}{\omega_0}, G_{12}(a,\theta)=-\frac{a\sin\Phi\cos\Phi}{\omega_0}, \\ G_{21}(a,\theta)=-\frac{\cos\Phi}{a\omega_0}, G_{22}(a,\theta)=-\frac{\cos^2\Phi}{\omega_0}. \end{cases} \tag{18}$$

The recycling noise is a stationary process and can be approximated by a 2-D diffusion process. After stochastic averaging, the drift and diffusion coefficients are as follows:

$$\begin{aligned} m_1&=F_{11}+\int_{-\infty}^0\left[\begin{array}{c}\left(\frac{-\cos\Phi}{\omega_0}\right)\left(\frac{-\cos\Phi(t+\tau_1)}{a\omega_0}\right)+\left(\frac{-\cos\Phi\sin\Phi}{\omega_0}\right)\left(\frac{-a\sin2\Phi(t+\tau_1)}{2\omega_0}\right) \\ +\left(\frac{-a(\cos^2\Phi-\sin^2\Phi)}{\omega_0}\right)\left(\frac{-\cos^2\Phi(t+\tau_1)}{\omega_0}\right)\end{array}\right]R(\tau_1)d\tau_1 \\ &=F_{11}+\frac{\cos^2\Phi}{a{\omega_0}^2}S_1(1)+\left[\frac{a\cos^2\Phi\sin^2\Phi+a\cos2\Phi\cos^2\Phi}{{\omega_0}^2}\right]S_2(1), \\ m_2&=F_{21}+\int_{-\infty}^0\left[\begin{array}{c}\left(\frac{\cos\Phi}{a^2\omega_0}\right)\left(\frac{-\sin\Phi(t+\tau_1)}{\omega_0}\right)+\left(\frac{\sin\Phi}{a\omega_0}\right)\left(\frac{-\cos\Phi(t+\tau_1)}{a\omega_0}\right) \\ +\left(\frac{2\cos\Phi\sin\Phi}{\omega_0}\right)\left(\frac{-\cos\Phi^2(t+\tau_1)}{\omega_0}\right)\end{array}\right]R(\tau_1)d\tau_1 \\ &=F_{21}-\frac{2\cos\Phi\sin\Phi}{a^2{\omega_0}^2}S_1(1)-\frac{2\cos^3\Phi\sin\Phi}{{\omega_0}^2}S_2(1), \\ B_{11}&=\int_{-\infty}^{+\infty}\left(\frac{-\sin\Phi}{\omega_0}\right)\left(\frac{-a\sin\Phi(t+\tau_1)}{\omega_0}\right)R(\tau_1)d\tau_1=\frac{2\sin^2\Phi}{{\omega_0}^2}S_1(1), \\ B_{12}&=\int_{-\infty}^{+\infty}\left(\frac{-a\sin2\Phi}{2\omega_0}\right)\left(\frac{-a\sin2\Phi(t+\tau_1)}{2\omega_0}\right)R(\tau_1)d\tau_1=\frac{2a^2\cos^2\Phi\sin^2\Phi}{{\omega_0}^2}S_2(1), \\ B_{21}&=\int_{-\infty}^{+\infty}\left(\frac{-\cos\Phi}{a\omega_0}\right)\left(\frac{-\cos\Phi(t+\tau_1)}{a\omega_0}\right)R(\tau_1)d\tau_1=\frac{2\cos^2\Phi}{a^2{\omega_0}^2}S_1(1), \\ B_{22}&=\int_{-\infty}^{+\infty}\left(\frac{-\cos^2\Phi}{\omega_0}\right)\left(\frac{-\cos^2\Phi(t+\tau_1)}{\omega_0}\right)R(\tau_1)d\tau_1=\frac{2\cos^4\Phi}{{\omega_0}^2}S_2(1), \end{aligned} \tag{19}$$

where $S_i(1)$ is the value of power spectral density of $\eta_i(t)$ at $\omega = 1$.

$$S_i(1) = 2D_i\left[1 + k^2 + 2k\cos(\tau)\right],\ (i = 1, 2) \tag{20}$$

For the deterministic averaging of $\varphi(t)$, we have

$$\begin{aligned}
\bar{m}_{11} &= \frac{1}{2\pi}\int_0^{2\pi}\left[F_{11}(a,\theta) + \frac{\cos^2\Phi}{a{\omega_0}^2}S_1(1) + \frac{a\cos^2\Phi\sin^2\Phi + a\cos 2\Phi\cos^2\Phi}{{\omega_0}^2}S_2(1)\right]d\Phi \\
&= -\frac{1}{2}a\left(\varepsilon + \omega^{p-1}\sin\left(\frac{p\pi}{2}\right)\right) + \frac{\alpha_1 a^3}{8} - \frac{\alpha_2 a^5}{16} + \frac{5\alpha_3 a^7}{128} - \frac{7\alpha_4 a^9}{256} + \frac{S_1(1)}{2a{\omega_0}^2} + \frac{3aS_2(1)}{8{\omega_0}^2} \\
\bar{m}_{22} &= \frac{1}{2\pi}\int_0^{2\pi}\left[F_{21}(a,\theta) - \frac{2\cos\Phi\sin\Phi}{a^2{\omega_0}^2}S_1(1) - \frac{2\cos^3\Phi\sin\Phi}{{\omega_0}^2}S_2(1)\right]d\Phi = 0, \\
\bar{B}_{11} &= \frac{1}{2\pi}\int_0^{2\pi}\frac{2\sin^2\Phi}{{\omega_0}^2}S_1(1)d\Phi = \frac{S_1(1)}{{\omega_0}^2}, \\
\bar{B}_{12} &= \frac{1}{2\pi}\int_0^{2\pi}\frac{2a^2\cos^2\Phi\sin^2\Phi}{{\omega_0}^2}S_2(1)d\Phi = \frac{a^2S_2(1)}{4{\omega_0}^2}, \\
\bar{B}_{21} &= \frac{1}{2\pi}\int_0^{2\pi}\frac{2\cos^2\Phi}{a^2{\omega_0}^2}S_1(1)d\Phi = \frac{S_1(1)}{a^2{\omega_0}^2}, \\
\bar{B}_{22} &= \frac{1}{2\pi}\int_0^{2\pi}\frac{2\cos^4\Phi}{{\omega_0}^2}S_2(1)d\Phi = \frac{3S_2(1)}{4{\omega_0}^2}.
\end{aligned} \tag{21}$$

The corresponding Itô SDE is

$$\begin{cases} da = m_1(a)dt + {\sigma_{11}}^2(a)dB_1(t) + {\sigma_{12}}^2(a)dB_2(t), \\ d\theta = m_2(a)dt + {\sigma_{21}}^2(a)dB_1(t) + {\sigma_{22}}^2(a)dB_2(t), \end{cases} \tag{22}$$

where

$$\begin{cases} m_1(a) = -\frac{1}{2}a\left(\varepsilon + \omega^{p-1}\sin\left(\frac{p\pi}{2}\right)\right) + \frac{\alpha_1 a^3}{8} - \frac{\alpha_2 a^5}{16} \\ +\frac{5\alpha_3 a^7}{128} - \frac{7\alpha_4 a^9}{256} + \frac{S_1(1)}{2a{\omega_0}^2} + \frac{3aS_2(1)}{8{\omega_0}^2}, \\ m_2(a) = 0, \\ {\sigma_{11}}^2(a) = \frac{S_1(1)}{{\omega_0}^2}, {\sigma_{12}}^2(a) = \frac{a^2S_2(1)}{4{\omega_0}^2}, \\ {\sigma_{21}}^2(a) = \frac{S_1(1)}{a^2{\omega_0}^2}, {\sigma_{22}}^2(a) = \frac{3S_2(1)}{4{\omega_0}^2}. \end{cases} \tag{23}$$

The one-dimensional Markov Process can be expressed as:

$$\begin{aligned} da = &\left(\frac{H_1 a}{8} + \frac{\alpha_1 a^3}{8} - \frac{\alpha_2 a^5}{16} + \frac{5\alpha_3 a^7}{128} - \frac{7\alpha_4 a^9}{256} + \frac{H_2}{2a}\right)dt \\ &+ (H_2)^{\frac{1}{2}}dB_1(t) + \left(\frac{H_3 a^2}{4}\right)^{\frac{1}{2}}dB_2(t), \end{aligned} \tag{24}$$

where

$$\begin{cases} H_1 = -4\left(\varepsilon + \omega^{p-1}\sin\left(\frac{p\pi}{2}\right)\right) + \frac{3S_2(1)}{{\omega_0}^2}, \\ H_2 = \frac{S_1(1)}{{\omega_0}^2}, H_3 = \frac{S_2(1)}{{\omega_0}^2}. \end{cases} \tag{25}$$

4 Stochastic stability analysis

4.1 The local stochastic stability

Considering the case of $\alpha_1 = \alpha_2 = \alpha_3 = \alpha_4 = H_2 = 0$ and linear Itô stochastic stability, from Eq. 24, we obtain

$$\begin{aligned} da &= \left(\frac{H_1}{8}a\right)dt + \left(\frac{H_3}{4}a^2\right)^{\frac{1}{2}}dB_2(t), \\ m(a) &= \left(\frac{H_1}{8}\right)a, \sigma(a) = \left(\frac{H_3}{4}\right)^{\frac{1}{2}}a. \end{aligned} \tag{26}$$

Therefore, it is obtained that $\dot{m}(0) = H_1/8$ and $\dot{\sigma}_{12}(0) = (H_3/4)^{1/2}$, using Oseledec multiplicative ergodic theorem [51] and maximal Lyapunov exponents to judge local stability. According to Itô stochastic differential equation, the solution of Eq. 26 is

$$a(t) = a(0)\,exp\left(\int_0^t\left[\dot{m}(0) - \frac{(\dot{\sigma}_{12}(0))^2}{2}\right]ds + \int_0^t\dot{\sigma}_{12}(0)dB_2(s)\right),$$

Then the approximate solution of the Lyapunov exponent of Itô stochastic differential equation is obtained

$$\begin{aligned} \lambda &= \lim_{t\to+\infty}\frac{1}{t}ln(\|x(t,t_0)\|) = \lim_{t\to+\infty}\frac{1}{t}ln(a(t))^{\frac{1}{2}} \\ &= \left(\dot{m}(0) - \frac{(\dot{\sigma}_{12}(0))^2}{2}\right)\Big/2 = \frac{1}{2}\left(\frac{H_1}{8} - \frac{H_3}{8}\right). \end{aligned}$$

When $H_1 - H_3 < 0$, i.e., $\lambda < 0$, Eq. 26 is stable in the sense of probability, and Eq. 16 is stable at the balance point. When $H_1 - H_3 > 0$, i.e., $\lambda < 0$, the effect is just the opposite.

4.2 The global stochastic stability

4.2.1 Linear Itô stochastic stability

Judging global stability by the singularity theory, $a = 0$ is the first kind of singular boundary of Eq. 26. $a = +\infty$ is the second kind of singular boundary problem of Eq. 26. Calculating the diffusion index, drift indices, and characteristic value at boundary $a = 0$ and $a = +\infty$, respectively, yields

$$\begin{aligned} \alpha_a = 2, \beta_a = 1, c_a &= \lim_{a\to0^+}\frac{2m_a(a-0)^{(\alpha_a-\beta_a)}}{{\sigma_{12}}^2(a)} \\ &= \lim_{a\to0^+}\left(\frac{2H_1}{8}a^2\right)\Big/\left(\frac{H_3}{4}a^2\right) = \frac{H_1}{H_3}, \\ \alpha_l = 2, \beta_l = 1, c_l &= -\lim_{a\to+\infty}\frac{2m_a(a-0)^{(\alpha_l-\beta_l)}}{{\sigma_{12}}^2(a)} \\ &= -\lim_{a\to+\infty}\left(\frac{2H_1}{8}a^2\right)\Big/\left(\frac{H_3}{4}a^2\right) = -\frac{H_1}{H_3}. \end{aligned}$$

And the following conclusions are drawn, as shown in Table 1.

4.2.2 Stability of nonlinear Itô stochastic differential equation

When $\alpha_1, \alpha_2, \alpha_3, \alpha_4, H_2 \neq 0$, $a = 0$ is the first kind of singular boundary of Eq. 24. When $a = +\infty$ and $m_a = +\infty$, $a = +\infty$ is the second kind of singular boundary problem of Eq. 24. Calculating the diffusion index, drift indices, and characteristic value at boundary $a = 0$ and $a = +\infty$, respectively, yields

$$\begin{aligned}
&\alpha_a = 2, \beta_a = 1, c_a = \lim_{a\to0^+}\frac{2m_a(a-0)^{(\alpha_a-\beta_a)}}{{\sigma_{11}}^2(a) + {\sigma_{12}}^2(a)} \\
&= \lim_{a\to0^+}\begin{pmatrix} -a\left(\varepsilon + \omega^{p-1}\sin\left(\frac{p\pi}{2}\right)\right) + \frac{\alpha_1 a^3}{4} - \frac{\alpha_2 a^5}{8} \\ +\frac{5\alpha_3 a^7}{64} - \frac{7\alpha_4 a^9}{128} + \frac{S_1(1)}{a{\omega_0}^2} + \frac{3aS_2(1)}{4{\omega_0}^2} \end{pmatrix}a\Big/\left(\frac{S_1(1)}{{\omega_0}^2} + \frac{a^2S_2(1)}{4{\omega_0}^2}\right) \\
&= \lim_{a\to0^+}\frac{{\omega_0}^2\begin{pmatrix} -128a^2\left(\varepsilon + \omega^{p-1}\sin\left(\frac{p\pi}{2}\right)\right) + 32\alpha_1 a^4 - 16\alpha_2 a^6 \\ +10\alpha_3 a^8 - 7\alpha_4 a^{10} + 128S_1(1) + 96a^2S_2(1) \end{pmatrix}}{128S_1(1) + 32a^2S_2(1)} = 1, \lim\alpha_l = 2, \beta_l \\
&= 9, c_l = -\lim_{a\to+\infty}\frac{2m_a(a-0)^{(\alpha_l-\beta_l)}}{{\sigma_{11}}^2(a) + {\sigma_{12}}^2(a)} \\
&= -\lim_{a\to+\infty}\begin{pmatrix} -a\left(\varepsilon + \omega^{p-1}\sin\left(\frac{p\pi}{2}\right)\right) + \frac{\alpha_1 a^3}{4} - \frac{\alpha_2 a^5}{8} \\ +\frac{5\alpha_3 a^7}{64} - \frac{7\alpha_4 a^9}{128} + \frac{S_1(1)}{a{\omega_0}^2} + \frac{3aS_2(1)}{4{\omega_0}^2} \end{pmatrix}a^{-7}\Big/\left(\frac{S_1(1)}{{\omega_0}^2} + \frac{a^2S_2(1)}{4{\omega_0}^2}\right) \\
&= -\lim_{a\to+\infty}\frac{{\omega_0}^2\begin{pmatrix} -128a^2\left(\varepsilon + \omega^{p-1}\sin\left(\frac{p\pi}{2}\right)\right) + 32\alpha_1 a^4 - 16\alpha_2 a^6 \\ +10\alpha_3 a^8 - 7\alpha_4 a^{10} + 128S_1(1) + 96a^2S_2(1) \end{pmatrix}}{128S_1(1)a^8 + 32S_2(1)a^{10}} = -\frac{7\alpha_4{\omega_0}^2}{32S_2(1)}.
\end{aligned}$$

Conclusion: when $a = 0$ and $c_a = 1$ are a strict natural boundary; when $a = +\infty$, $c_l > -1$, and $(\alpha_4\omega_0{}^2)/S_2(1) < 32/7$, the boundary is an exclude natural boundary; when $c_l < -1$ and $(\alpha_4\omega_0{}^2)/S_2(1) > 32/7$, the boundary is an attract natural boundary; when $c_l = -1$ and $(\alpha_4\omega_0{}^2)/S_2(1) = 32/7$, the boundary is a strict natural boundary. Therefore, $c_a = 1$ is a critical condition of system bifurcation.

5 Stochastic bifurcation analysis

5.1 D-bifurcation

If $H_2 = H_3 = 0$, Eq. 13 becomes a deterministic system without a stochastic bifurcation phenomenon. Therefore, discussing the situation of $H_3 \neq 0$ and $\alpha_1 = \alpha_2 = \alpha_3 = \alpha_4 = H_2 = 0$, let $\sigma_{12}(a) = (H_3/4)^{1/2}a$ and $m(a) = (H_1/8 - H_3/8)a$, then the continuous dynamic system generated by Eq. 26 is

$$\psi_1(t)x = x + \int_0^t m(\psi_1(s)x)ds + \int_0^t \sigma(\psi_1(s)x) \circ dB, \tag{27}$$

Equation 27 is the only strong solution of Eq. 26 with x as the initial value. When $m(0) = 0$ and $\sigma_{12}(0) = 0$, let $m(a)$ be bounded, for all $a \neq 0$, the elliptic condition $\sigma_{12}(0) \neq 0$ is satisfied, so there is only one stationary probability density. Therefore, the FPK equation corresponding to Eq. 26 is obtained.

$$\frac{\partial p}{\partial t} = -\frac{\partial}{\partial a}\left[\left(\frac{H_1}{8}a\right)p\right] - \frac{\partial^2}{\partial a^2}\left[\left(\frac{H_3}{4}a^2\right)p\right]. \tag{28}$$

Let $\partial p/\partial t = 0$ get the stationary probability density corresponding to Eq. 28

$$p(a) = c\left|\sigma_{12}{}^{-1}(a)\right| exp\left(\int_0^a \frac{2m(u)}{\sigma_{12}{}^2(u)}du\right). \tag{29}$$

At this time, Eq. 27 has a non-trivial stationary state and a fixed-point equilibrium state. Assuming the invariant measures of these two kinds of stationary states are υ_1 and ϑ_1, respectively, the density is Eq. 29 and $\vartheta_1(x)$, respectively. Hence, the solution of Eq. 28 is

$$a(t) = a(0)\, exp\left[\int_0^t \left(\dot{m}(a) + \frac{\sigma_{12}(a)\ddot{\sigma}_{12}(a)}{2}\right)ds + \int_0^t \dot{\sigma}_{12}(a)dB_2\right]. \tag{30}$$

The Lyapunov exponent of ψ_1 with respect to estimate u can be defined as follows

$$\lambda_{\psi_1}(u) = \lim_{t\to+\infty}\frac{1}{t}ln\|a(t)\|, \tag{31}$$

Substituting Eq. 30 into Eq. 31, here $\sigma_{12}(0) = 0$ and $\dot{\sigma}_{12}(0) = 0$, its Lyapunov exponent of the fixed-point reads

$$\begin{aligned}\lambda_{\psi_1}(\vartheta_1) &= \lim_{t\to+\infty}\frac{1}{t}\left[ln\|a(0)\| + \dot{m}(0)\int_0^t ds + \dot{\sigma}_{12}(0)\int_0^t dB_2(s)\right] \\ &= \dot{m}(0) + \dot{\sigma}_{12}(0)\lim_{t\to+\infty}\frac{B_2(t)}{t} = \dot{m}(0) = \frac{H_1}{8} - \frac{H_3}{8}.\end{aligned} \tag{32}$$

Invariant estimate υ_1 with Eq. 29 as density. Substituting Eq. 30 into Eq. 31. Assuming that $\dot{\sigma}$ and $\dot{m} + \sigma\dot{\sigma}$ are bounded and integrable, respectively, the Lyapunov exponent can be obtained

$$\begin{aligned}\lambda_{\psi_1}(\upsilon_1) &= \lim_{t\to+\infty}\frac{1}{t}\int_0^t [\dot{m}(a) + \sigma_{12}(a)\ddot{\sigma}_{12}(a)]ds \\ &= \int_R\left[\dot{m}(a) + \frac{\sigma_{12}(a)\ddot{\sigma}_{12}(a)}{2}\right]p(a)da = -2\int_R\left[\frac{m(a)}{\sigma_{12}(a)}\right]^2 \\ p(a)da\dot{m}(0) &= -2H_2{}^{3/2}\left(\frac{H_1}{8} - \frac{H_3}{8}\right)exp\left(\frac{8}{H_3}\left(\frac{H_1}{8} - \frac{H_3}{8}\right)\right).\end{aligned} \tag{33}$$

Let $\alpha = H_1 - H_3$, when $\alpha < 0$ and $H_1 < H_3$, ϑ_1 is stable, υ_1 is unstable; when $\alpha > 0$ and $H_1 > H_3$, ϑ_1 is unstable, υ_1 is stable. So α is a D-bifurcation point of Eq. 13.

5.2 P-bifurcation

5.2.1 Stochastic P-bifurcation under additive recycling noise

When additive noise just exists, $D_1 \neq 0$ and $D_2 = 0$. The following is an analysis of the stochastic P-bifurcation of the system in this case. Eq. 22, 23 show that the Itô stochastic differential equation corresponding to $a(t)$ does not depend upon $\theta(t)$, and it is a 1-D diffusion process; its corresponding FPK equation can be expressed as

$$\frac{\partial p(a,t)}{\partial t} = -\frac{\partial}{\partial a}\left[m_1(a)p(a,t)\right] + \frac{1}{2}\frac{\partial^2}{\partial a^2}\left[\sigma_{11}{}^2(a)p(a,t)\right], \tag{34}$$

the corresponding boundary conditions are

$$\begin{cases} p = c, c \in (-\infty, +\infty), & when\ a = 0. \\ p \to 0, \dfrac{\partial p}{\partial a} \to 0, & when\ a \to \infty. \end{cases} \tag{35}$$

In view of Eq. 35, the stationary probability density of the amplitude is

$$p(a) = \frac{C}{\sigma_{11}{}^2(a)}exp\left[\int_0^a \frac{2m_1(u)}{\sigma_{11}{}^2(u)}du\right], \tag{36}$$

where C is the normalization constant,

$$C = \left[\int_0^\infty\left(\frac{1}{\sigma_{11}{}^2(a)}exp\left[\int_0^a \frac{2m_1(u)}{\sigma_{11}{}^2(u)}du\right]\right)da\right]^{-1}. \tag{37}$$

In view of Eq. 23, from Eq. 36, we obtain

$$p(a) = \frac{Ca\omega_0{}^2}{S_1(1)}exp\left[-\frac{a^2\omega_0{}^2\Delta}{7680S_1(1)}\right], \tag{38}$$

where

$$\begin{cases} \Delta = 3840\varepsilon + 3840\omega^{p-1}\, sin\left(\dfrac{p\pi}{2}\right) - 480\alpha_1 a^2 + 160\alpha_2 a^4 - 75\alpha_3 + 42\alpha_4 a^8, \\ \omega_0{}^2 = \omega^2 + \omega^p\, cos\left(\dfrac{p\pi}{2}\right), \\ S_1(1) = 2D_1\left[1 + k^2 + 2kcos(\tau)\right]. \end{cases} \tag{39}$$

The original system response meets $a(t) = \sqrt{x^2(t) + \dot{x}^2(t)}$, in view of Eq. 38, the joint probability density function of the system is

$$p(a) = \frac{C\sqrt{x^2(t) + \dot{x}^2(t)}\omega_0{}^2}{S_1(t)}exp\left[-\frac{(x^2(t) + \dot{x}^2(t))\omega_0{}^2}{3840S_1(t)}\Delta\right]. \tag{40}$$

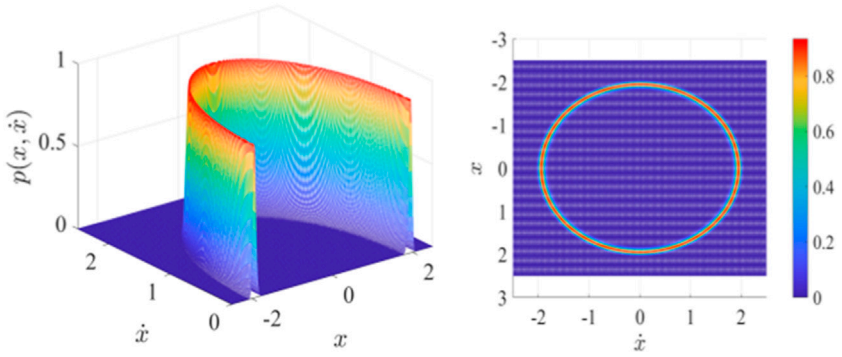

FIGURE 1
Joint probability density function section and top view of Eq. 13 when **p** = **0.06**.

5.2.1.1 Influence of fractional order

As fractional damping is a combination of the equivalent stiff and equivalent damping, the fractional order is of paramount importance; its value can be calculated by He-Liu's fractal formulation [52] for practical applications. According to Eq. 12, when $p = 1$, fractional damping becomes a damping term, while when $p = 0$, it is a stiff term.

Setting $\tau = 2, k = 0.4, \varepsilon = -0.1, \alpha_1 = 1.51, \alpha_2 = 2.85, \alpha_3 = 1.693, \alpha_4 = 0.312$, and $\omega = 1$ in Eq. 13 as that in Refs [30, 53], the stochastic P-bifurcation is studied hereby. Keeping $D_1 = 0.005$ constant, we draw the joint probability density function section and top view of Eq. 13 under the influence of different fractional orders.

When $p = 0.06$, the joint probability density function diagram shows a crater shape; there is only one peak in the section, and there is only a large limit cycle. The response is shown as a vibration far beyond the origin (Figure 1).

When $p = 0.139$, from the section, it can be clearly seen that there are two peaks, but the second peak has a much larger amplitude. At this time, the system has a balance point and a large limit cycle; hence, the system response switches between two peaks, and the probability of a large amplitude vibration is high, as shown in Figure 2.

When $p = 0.141$, the section has three peaks, showing two peaks in addition to the origin. A balance point now coexists with a large and small limit cycle in the system, and the system response switches between the three peaks, which is a multimodal response. Due to the existence of the double limit point set, the relative heights of the joint probability density function peaks at the three peaks are different, implying that the system response peaks are different, as shown in Figure 3.

When $p = 0.145$, the section has two peaks, in contrast to Figure 2, the relative height of the peak changes, with the second peak being significantly smaller. At this time, the system has both a balance point and a small limit cycle; hence, the system response switches between two peaks, and the probability of a small amplitude vibration is high, as shown in Figure 4.

Based on the above discussions, we conclude that the fractional order can cause stochastic P-bifurcation behavior in the system. From Figure 5, we find that an increasing fractional order will change the stationary response from a single mode to a dual mode and then to a tristable mode. The peak value changes from a single peak to two peaks and then to three peaks, so stochastic P-bifurcation occurs. Increasing the value of p to 0.145 again, the tristable disappears and the bistable appears; the peak value changes from three peaks to two peaks, so stochastic P-bifurcation occurs.

5.2.1.2 Influence of noise intensity

Keeping the above parameters unchanged, and fixing $p = 0.14$, we draw the joint probability density function section and top view of Eq. 13 under the influence of different noise intensity.

When $D_1 = 0.03$, the joint probability density function diagram shows a crater shape, there is only one peak in the section, and there is only a large limit cycle. The response is shown as a vibration far beyond its origin, as shown in Figure 6.

When $D_1 = 0.015$, from the section, it can be clearly seen that there are two peaks, but the first peak is much smaller. At this time, the system has both a balance point and a large limit cycle; hence, the system response switches between two peaks, and the probability of a large amplitude vibration is high, as shown in Figure 7.

When $D_1 = 0.005$, the section has three peaks, showing two peaks in addition to the origin. A balance point now coexists with a large and small limit cycle in the system, and the system response switches among the three peaks, which is a multimodal response. Due to the existence of the double limit point set, the relative heights of the joint probability density function peaks at the three peaks are different, implying that the vibration frequency of the system response peak is different, as shown in Figure 8.

When $D_1 = 0.0013$, the section has two peaks, in contrast to Figure 7; the relative height of the peak changes, with the first peak being much larger. At this point, the system has a balance point and a small limit cycle, the system response switches between two peaks, and the probability of a small amplitude vibration is high, as shown in Figure 9.

Based on the above discussions, it can be verified that changing the noise intensity affects greatly stochastic P-bifurcation property. From Figure 10, it can also be seen that with noise intensity being reduced, the stationary

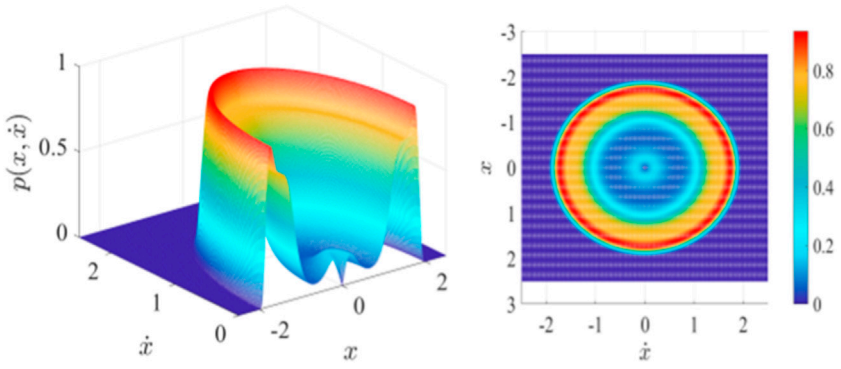

FIGURE 2
Joint probability density function section and top view of Eq. 13 when **p** = **0.137**.

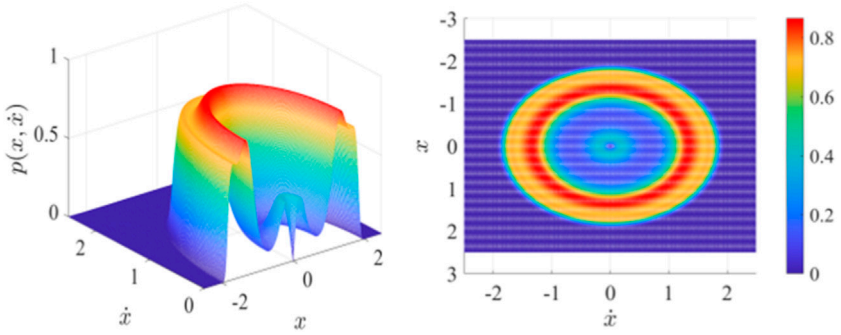

FIGURE 3
Joint probability density function section and top view of Eq. 13 when **p** = **0.14**.

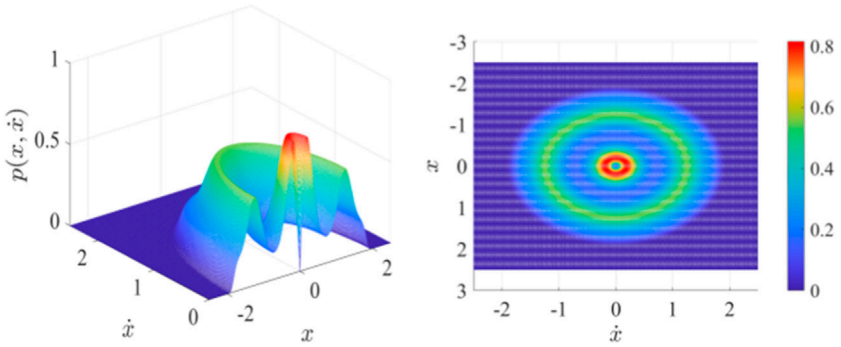

FIGURE 4
Joint probability density function section and top view of Eq. 13 when **p** = **0.143**.

response of the system switches from a single mode to a dual mode and then to a tristable mode. The peak value of the stationary probability density function curve changes from a single peak to two peaks and then three peaks, so stochastic P-bifurcation occurs. Decreasing the value of D_1 to 0.0013 again, the tristable disappears and the bistable appears; the peak value changes from three peaks to two peaks, so stochastic P-bifurcation occurs.

5.2.2 Additive and multiplicative recycling noise

When $D_1 \neq 0$ and $D_2 \neq 0$, the expression of the stationary probability density function of the amplitude of Eq. 13 is

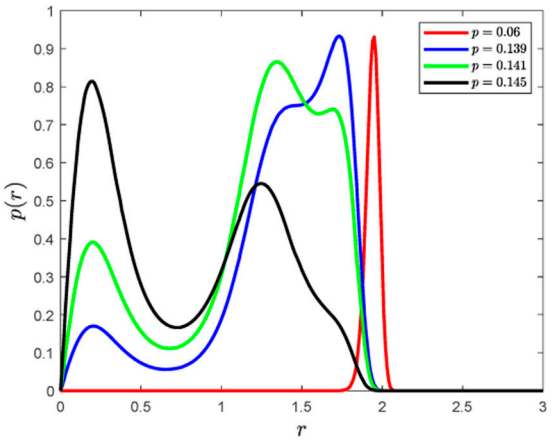

FIGURE 5
Stationary probability density function diagram of Eq. 13 when $\mathbf{D_1 = 0.005}$.

$$p(a) = \frac{C}{\sigma_{11}^2(a) + \sigma_{12}^2(a)} exp\left[\int_0^a \frac{2m(u)}{\sigma_{11}^2(u) + \sigma_{12}^2(u)} du\right], \quad (41)$$

where C is the normalization constant,

$$C = \left[\int_0^\infty \left(\frac{1}{\sigma_{11}^2(a) + \sigma_{12}^2(a)} exp\left[\int_0^a \frac{2m_1(u)}{\sigma_{11}^2(u) + \sigma_{12}^2(u)} du\right]\right) da\right]^{-1}. \quad (42)$$

In view of Eq. 23, from Eq. 42, we have

$$p(a) = 4Ca\omega_0^2 \left[4S_1(1) + a^2 S_2(1)\right]^{-\frac{\Delta_1}{S_2^5(1)}} exp\left(\frac{\Delta_2}{768 S_2^4(1)}\right), \quad (43)$$

where

$$\begin{cases} \Delta_1 = 2\omega_0^2\left[\left(\varepsilon + \omega^{p-1} sin\left(\frac{p\pi}{2}\right)\right) S_2^4 + \alpha_1 S_1 S_2^3 + 2\alpha_2 S_1^2 S_2^2 + 5\alpha_3 S_1^3 S_2 + 14\alpha_4 S_1^4\right], \\ \Delta_1 = a^2\omega_0^2\left(384\alpha_1 S_2^3 + 768\alpha_2 S_1 S_2^2 + 1920\alpha_3 S_1^2 S_2 + 5376\alpha_4 S_1^3\right) \\ +a^4\omega_0^2\left(-96\alpha_2 S_2^3 - 240\alpha_3 S_1 S_2^2 - 672\alpha_4 S_1^2 S_2\right) \\ +a^6\omega_0^2\left(40\alpha_3 S_2^3 + 112\alpha_4 S_1 S_2^2\right) - 21a^8\omega_0^2\alpha_4 S_2^3, \\ \omega_0^2 = \omega^2 + \omega^p cos\left(\frac{p\pi}{2}\right), \\ S_1(1) = 2D_1\left[1 + k^2 + 2kcos(\tau)\right], S_2(1) = 2D_2\left[1 + k^2 + 2kcos(\tau)\right]. \end{cases} \quad (44)$$

Keeping the above parameters unchanged, we draw the joint probability density function section and top view of Eq. 13 under the influence of different fractional orders and noise intensity.

When $p = 0.05$, let $D_1 = 0.5$ and $D_2 = 1$. The joint probability density function diagram shows a crater shape; there is only one peak in the section, and there is only a large limit cycle. The response is shown as a vibration far away from the origin. At the same time, reducing the value of noise intensity reveals that the peak of the joint

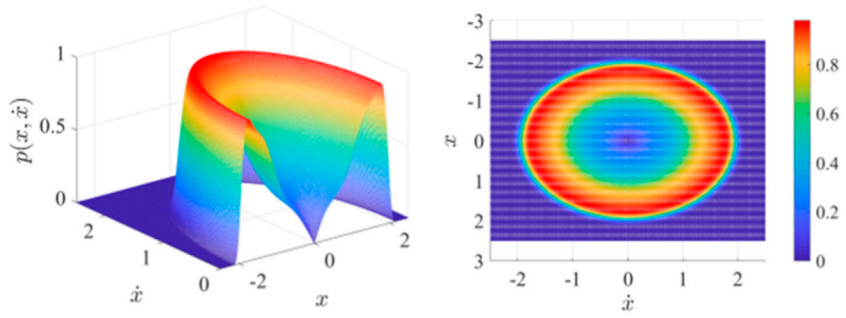

FIGURE 6
Joint probability density function section and top view of Eq. 13 when $\mathbf{D_1 = 0.03}$.

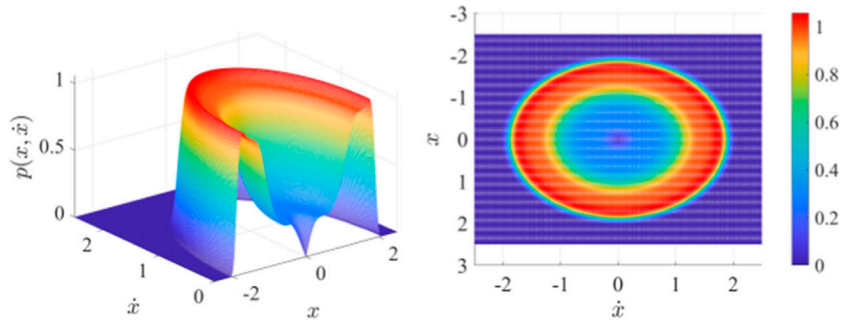

FIGURE 7
Joint probability density function section and top view of Eq. 13 when $\mathbf{D_1 = 0.015}$.

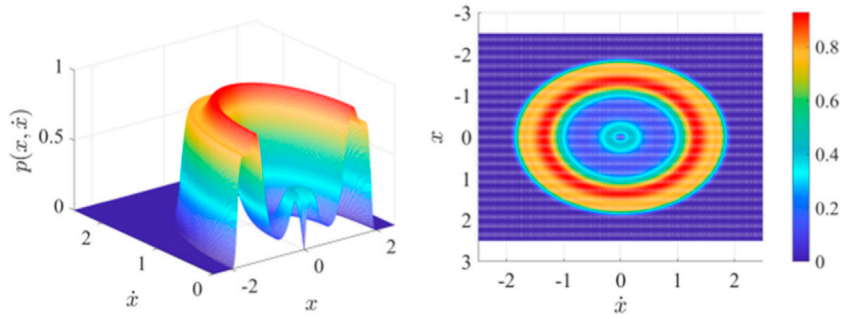

FIGURE 8
Joint probability density function section and top view of Eq. 13 when $D_1 = 0.005$.

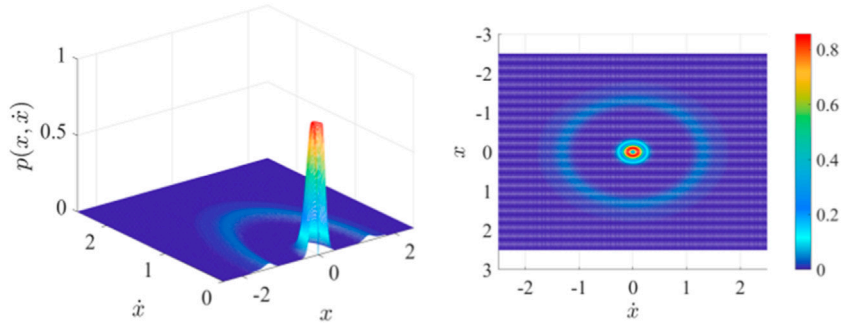

FIGURE 9
Joint probability density function section and top view of Eq. 13 when $D_1 = 0.0013$.

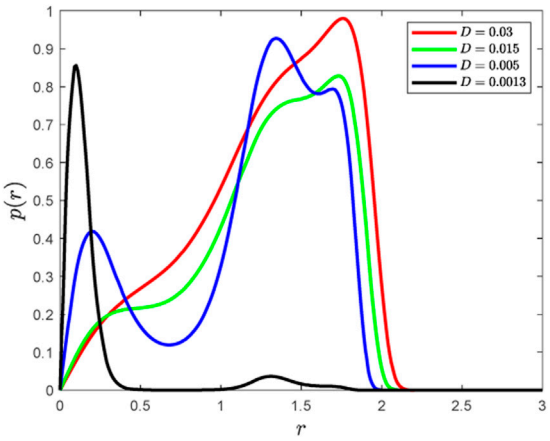

FIGURE 10
Stationary probability density function diagram of Eq. 13 when $p = 0.141$.

probability density does not change with only one peak. However, the system only has a limit cycle, which has been in a monostable. Therefore, there is no stochastic P-bifurcation phenomenon occurring, as shown in Figure 11.

When $p = 0.1$, let $D_1 = 0.002$ and $D_2 = 0.01$. From the section, it can be clearly seen that there are two peaks, but the second peak has a much larger amplitude. At this time, the system has both a balance point and a limit cycle; hence, the system response switches between two peaks, and the large amplitude vibration has a higher probability. When the simultaneous improvement of the noise intensifies to $D_1 = 0.008$ and $D_2 = 0.2$, the peak value of the stationary probability density function curve changes from two peaks to one peak. There is only a large limit cycle, and the system response becomes a vibration far from the origin. Therefore, increasing the noise intensity induces a stochastic P-bifurcation property, as shown in Figure 12.

When $p = 0.14$, let $D_1 = 0.003$ and $D_2 = 0.01$. The section has a peak near the origin. There is only a balance point in the system at this time, and the response is shown as a vibration closer to the origin. When simultaneously improving its noise intensity to $D_1 = 0.004$ and $D_2 = 0.1$, the peak value of the stationary probability density function curve changes from a single peak to two peaks. At this time, the system has both a balance point and a limit cycle; hence, the system response switches between two peaks, and the probability of a large amplitude vibration is small. Therefore, increasing the noise intensity induces the stochastic P-bifurcation phenomenon. Further increasing the noise intensity to $D_1 = 0.006$ and $D_2 = 0.15$, the peak value of the section changes relatively, and the first peak is lower. The system response switches between two peaks, and the probability of a small one is

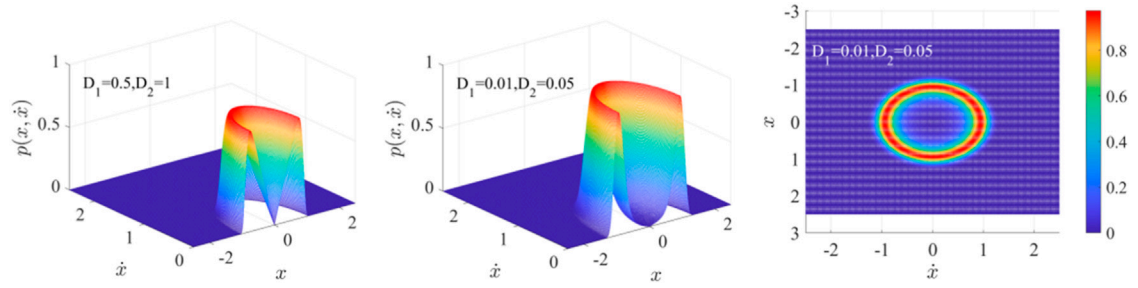

FIGURE 11
Joint probability density function section and top view of Eq. 13 when **p** = **0.05**.

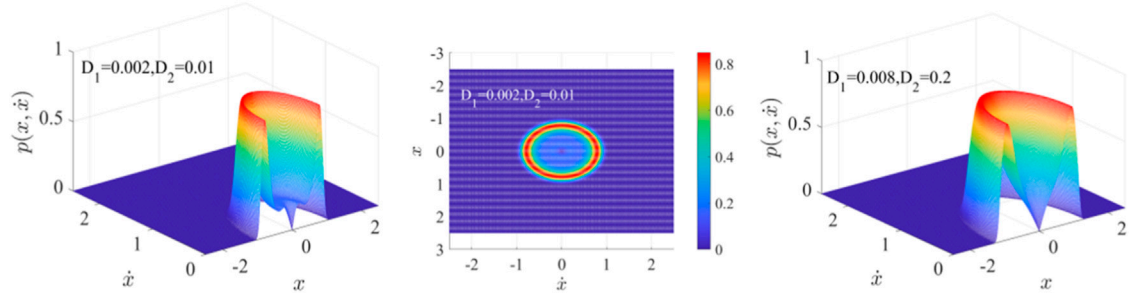

FIGURE 12
Joint probability density function section and top view of Eq. 13 when **p** = **0.1**.

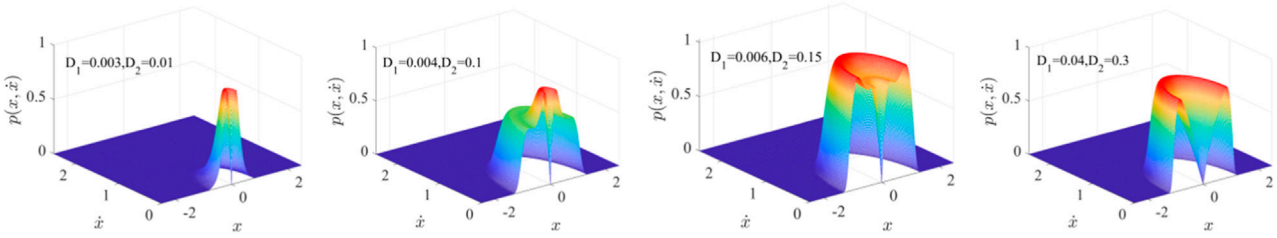

FIGURE 13
Joint probability density function section and top view of Eq. 13 when **p** = **0.14**.

small. Continuing to increase the value of noise intensity to $D_1 = 0.04$ and $D_2 = 0.3$, the peak value of the curve changes from two peaks to a single peak. There is only a limit cycle in the system at this time, and the response is shown as a vibration far away from the origin. Therefore, increasing the noise intensity induces the second stochastic P-bifurcation phenomenon, as show in Figure 13.

6 Conclusion

In this paper, the stationary response and the stochastic bifurcation of the fractional van der Pol equation under multiplicative and additive recycling noise excitations are investigated. By the least square method, we obtain an equivalent integral nonlinear stochastic system. The Itô differential equation and One-dimensional Markov process are obtained according to the stochastic averaging method. We discuss the local and global stochastic stability and analyze the conditions for inducing D-bifurcation and P-bifurcation in the system. The analysis shows that when $\alpha < 0$ and $H_1 < H_3$, the point equilibrium state becomes stable, and the non-trivial stationary state becomes unstable; when $\alpha > 0$ and $H_1 > H_3$, the result is the opposite. So α is a D-bifurcation point of the original system. When only additive noise exists, the fractional order and the noise intensity will greatly affect the system's property. It was found that reducing the order p or increasing the noise intensity D_1 can cause nonlinear jumping or significant oscillation in the system, leading to system instability. Through increasing the order p or reducing the noise intensity D_1, the system response is in a monostable state or a small disturbance near the balance point. Similarly, when additive and

multiplicative noise coexist, selecting appropriate parameters can maintain the system response at a monostable or small disturbance near the balance point. Therefore, in practical engineering, to avoid the potential adverse effects of high noise intensity on the system, the occurrence of stochastic bifurcation behavior can be controlled by changing the noise intensity or fractional order. In the future, we will combine theory with practice to explore the impact of recycling noise on the stationary response and stochastic bifurcation of systems in wind turbines. We will study the impact of changing noise intensity and fractional order on the system, and how to handle these adverse effects to achieve optimal system performance.

Data availability statement

The original contributions presented in the study are included in the article/Supplementary material, further inquiries can be directed to the corresponding author.

Author contributions

J-GZ: supervision, writing–review and editing, funding acquisition, investigation, and project administration. FW: writing–original draft, writing–review and editing, and software. H-NW: writing–review and editing and software. All authors contributed to the article and approved the submitted version.

Funding

This study was supported by the key project of the Gansu Province natural science foundation of China (No. 23JRRA882).

Conflict of interest

The authors declare that the research was conducted in the absence of any commercial or financial relationships that could be construed as a potential conflict of interest.

Publisher's note

All claims expressed in this article are solely those of the authors and do not necessarily represent those of their affiliated organizations, or those of the publisher, the editors and the reviewers. Any product that may be evaluated in this article, or claim that may be made by its manufacturer, is not guaranteed or endorsed by the publisher.

References

1. He JH. A tutorial review on fractal spacetime and fractional calculus. *Int J Theor Phys* (2014) 53:3698–718. doi:10.1007/s10773-014-2123-8

2. He JH. Fractal calculus and its geometrical explanation. *Phys* (2018) 10:272–6. doi:10.1016/j.rinp.2018.06.011

3. He CH, Liu C. Fractal approach to the fluidity of a cement mortar. *Nonlinear Engineering-modeling Appl* (2022) 11(1):1–5. doi:10.1515/nleng-2022-0001

4. Zuo YT, Liu HJ. Fractal approach to mechanical and electrical properties of graphene/sic composites. *Facta Universitatis: Ser Mech Eng* (2021) 19(2):271–84. doi:10.22190/fume201212003z

5. He CH, Liu C. Fractal dimensions of a porous concrete and its effect on the concrete's strength. *Facta Universitatis Ser Mech Eng* (2023) 21(1):137–50. doi:10.22190/FUME221215005H

6. Jankowski P. Detection of nonlocal calibration parameters and range interaction for dynamic of FGM porous nanobeams under electro-mechanical loads. *Facta Universitatis Ser Mech Eng* (2022) 20(3):457–78. doi:10.22190/fume210207007j

7. He CH, Shen Y, Ji FY, He JH. Taylor series solution for fractal Bratu-type equation arising in electrospinning process. *Fractals* (2020) 28(1):2050011. doi:10.1142/s0218348x20500115

8. Liu FJ, Zhang T, He CH, Tian D. Thermal oscillation arising in a heat shock of a porous hierarchy and its application. *Facta Universitatis Ser Mech Eng* (2022) 20(3):633–45. doi:10.22190/fume210317054l

9. Liang YH, Wang KJ. A new fractal viscoelastic element: Promise and applications to Maxwell-Rheological model. *Therm Sci* (2021) 25(2):1221–7. doi:10.2298/tsci200301015l

10. Zuo YT. Effect of Sic particles on viscosity of 3-D print paste a fractal rheological model and experimental verification. *Therm Sci* (2021) 25(3):2405–9. doi:10.2298/tsci200710131z

11. Long Y, Xu BB, Chen DY, Ye W. Dynamic characteristics for a hydro-turbine governing system with viscoelastic materials described by fractional calculus. *Appl Math Model* (2018) 58:128–39. doi:10.1016/j.apm.2017.09.052

12. Wang L, Xue LL, Xu W, Yue XL. Stochastic P-bifurcation analysis of a fractional smooth and discontinuous oscillator via the generalized cell mapping method. *Int J Non-Linear Mech* (2017) 96:56–63. doi:10.1016/j.ijnonlinmec.2017.08.003

13. He CH, Amer TS, Tian D, Abolila AF, Galal AA. Controlling the kinematics of a spring-pendulum system using an energy harvesting device. *J Low Frequency Noise: Vibration Active Control* (2022) 41(3):1234–57. doi:10.1177/14613484221077474

14. He CH, Ei-Dib YO. A heuristic review on the homotopy perturbation method for non-conservative oscillators. *J Low FrequCency Noise, Vibration Active Control* (2022) 41(2):572–603. doi:10.1177/14613484211059264

15. He JH, Ei-Dib YO. The reducing rank method to solve third-order Duffing equation with the homotopy perturbation. *Numer Methods Differential Equations* (2021) 37(2):1800–8. doi:10.1002/num.22609

16. Zhang WT, Xu W, Niu LZ, Tang YN. Bifurcations analysis of a multiple attractors energy harvesting system with fractional derivative damping under random excitation. *Commun Nonlinear Sci Numer Simulation* (2023) 118:107069. doi:10.1016/j.cnsns.2022.107069

17. Hu DL, Mao XC, Han L. Stochastic stability analysis of a fractional viscoelastic plate excited by Gaussian white noise. *Mech Syst Signal Process* (2022) 177:109181. doi:10.1016/j.ymssp.2022.109181

18. Li YJ, Wu ZQ, Lan QX, Cai YJ, Xu HF, Sun YT. Stochastic transition behaviors in a Tri-Stable van der Pol oscillator with fractional delayed element subject to Gaussian White Noise. *Therm Sci* (2022) 26(3):2713–25. doi:10.2298/tsci22037131

19. Li YJ, Wu ZQ, Lan QX, Cai YJ, Xu HF, Sun YT. Transition behaviors of system energy in a bi-stable van Ver Pol oscillator with fractional derivative element driven by multiplicative Gaussian white noise. *Therm Sci* (2022) 26(3):2727–36. doi:10.2298/tsci22037271

20. Li YJ, Wu ZQ, Wang F, Zhang GQ, Wang YC. Stochastic P-bifurcation in a generalized Van der Pol oscillator with fractional delayed feedback excited by combined Gaussian white noise excitations. *J Low Frequency Noise, Vibration Active Control* (2021) 40(1):91–103. doi:10.1177/1461348419878534

21. Din A, Ain QT. Stochastic optimal control analysis of a mathematical model: Theory and application to non-singular kernels. *fractal and fractional* (2022) 6:279. doi:10.3390/fractalfract6050279

22. Zhu R, Wang MX, Xu SY, Li K, Han QP, Tong X, et al. Fault diagnosis of rolling bearing based on singular spectrum analysis and wide convolution kernel neural network. *J Low Frequency Noise, Vibration Active Control* (2022) 41(4):1307–21. doi:10.1177/14613484221104639

23. Kuo PH, Tseng YR, Luan PC, Yau HT. Novel fractional-order convolutional neural network based chatter diagnosis approach in turning process with chaos error mapping. *Nonlinear Dyn* (2023) 111:7547–64. doi:10.1007/s11071-023-08252-w

24. Kuo PH, Chen YW, Hsieh TH, Jywe WY, Yau HT. A thermal displacement prediction system with an automatic Lrgtvac-PSO optimized branch Structured

bidirectional GRU neural network. *IEEE Sensors Journa* (2023) 23:12574–86. doi:10.1109/JSEN.2023.3269064

25. He JH, Jiao ML, Gepreel KA, Khan Y. Homotopy perturbation method for strongly nonlinear oscillators. *Mathematics Comput Simulation* (2023) 204:243–58. doi:10.1016/j.matcom.2022.08.005

26. He JH, Jiao ML, He CH. Homotopy perturbation method for fractal Duffing oscillator with arbitrary conditions. *Fractals* (2022) 30. doi:10.1142/S0218348X22501651

27. Chen LC, Zhu WQ. Stochastic jump and bifurcation of Duffing oscillator with fractional derivative damping under combined harmonic and white noise excitations. *Int J Non-Linear Mech* (2011) 46:1324–9. doi:10.1016/j.ijnonlinmec.2011.07.002

28. Chen LC, Zhu WQ. Stationary response of duffing oscillator with fractional derivative damping under combined harmonic and wide band noise excitations. *Chin J Appl Mech* (2010) 3:517–21.

29. He CH, Tian D, Moatimid GM, Salman HF, Zekry MH. Hybrid Rayleigh–van der pol–duffing oscillator: Stability analysis and controller. *J Low Frequency Noise, Vibration Active Control* (2022) 41(1):244–68. doi:10.1177/14613484211026407

30. Li YJ, Wu ZQ. Stochastic P-bifurcation in a tri-stable Van der Pol system with fractional derivative under Gaussian white noise. *J Vibroengineering* (2019) 21:803–15. doi:10.21595/jve.2019.20118

31. Li YJ, Wu ZQ, Lan QX, Hao Y, Zhang XY. Stochastic P bifurcation in a tri-stable van der Pol oscillator with fractional derivative excited by combined Gaussian white noises. *J Vibration Shock* (2021) 40(16):275–93. doi:10.21595/jve.2019.20118

32. Chamgoué AC, Yamapi R, Woafo P. Bifurcations in a biorhythmic biological system with time-delayed noise. *Nonlinear Dyn* (2013) 73:2157–73. doi:10.1007/s11071-013-0931-7

33. Wu YZ, Sun ZK. Residence-times distribution function in asymmetric bistable system driven by noise recycling. *Acta Phys Sin* (2020) 69(12):120501. doi:10.7498/aps.69.20201752

34. Guo XY, Cao TQ. Phenomenon of double entropic stochastic resonance with recycled noise. *Chin J Phys* (2022) 77:721–32. doi:10.1016/j.cjph.2021.10.020

35. He KY, Nadeem M, Habib S, Sedighi HM, Huang DH. Analytical approach for the temperature distribution in the casting-mould heterogeneous system. *Int J Numer Methods Heat Fluid Flow* (2021) 32:1168–82. doi:10.1108/HFF-03-2021-0180

36. Fang JH, Nadeem M, Habib M, Karim S, Wahash HA. A new iterative method for the approximate solution of klein-gordon and sine-gordon equations. *J Funct Spaces* (2022) 2022:1–9. doi:10.1155/2022/5365810

37. He JH, Kou SJ, He CH, Zhang ZW, Gepreel KA. Fractal oscillation and its frequency-amplitude property. *Fractals* (2021) 29(4):2150105. doi:10.1142/s0218348x2150105x

38. He JH, Moatimid G, Zekry M. Forced nonlinear oscillator in a fractal space. *Facta Universitatis, Ser Mech Eng* (2022) 20(1):001–20. doi:10.22190/fume220118004h

39. Tian D, Ain QT, Anjum N, He CH, Cheng B. Fractal N/MEMS: From pull-in instability to pull-in stability. *Fractals* (2021) 29:2150030. doi:10.1142/S0218348X21500304

40. He CH. A variational principle for a fractal nano/microelectromechanical (N/MEMS) system. *International J Numer Methods Heat Fluid Flow* (2023) 33(1):351–9. doi:10.1108/hff-03-2022-0191

41. Ain QT, Sathiyaraj Karim S, Nadeem M, Mwanakatwe PK, Kandege Mwanakatwe P. ABC fractional derivative for the alcohol drinking model using two-scale fractal dimension. *Complexity* (2022) 2022:1–11. doi:10.1155/2022/8531858

42. Wang Y, An JY. Amplitude-frequency relationship to a fractional Duffing oscillator arising in microphysics and tsunami motion. *J Low Frequency Noise Vibration Active Control* (2019) 38(3-4):1008–12. doi:10.1177/1461348418795813

43. Mendes EM, Salgado GH, Aguirre LA. Numerical solution of Caputo fractional differential equations with infinity memory effect at initial condition. *Commun Nonlinear Sci Numer Simulation* (2019) 69:237–47. doi:10.1016/j.cnsns.2018.09.022

44. Zeng HJ, Wang YX, Xiao M, Wang Y. Fractional solitons: New phenomena and exact solutions. *Front Phys* (2023) 11:1177335. doi:10.3389/fphy.2023.1177335

45. Chen LC, Wang WH, Li ZS, Zhu WQ. Stationary response of Duffing oscillator with hardening stiffness and fractional derivative. *Int J Non-Linear Mech* (2013) 48:44–50. doi:10.1016/j.ijnonlinmec.2012.08.001

46. Li W, Zhang MT, Zhao JF. Stochastic bifurcations of generalized Duffing-van der Pol system with fractional derivative under colored noise. *Chin Phys B* (2017) 26:090501. doi:10.1088/1674-1056/26/9/090501

47. Chen LC, Li ZS, Zhuang QQ, Zhu WQ. First-passage failure of single-degree-of-freedom nonlinear oscillators with fractional derivative. *J Vibration Control* (2013) 19:2154–63. doi:10.1177/1077546312456057

48. Chen LC, Zhu WQ. Stochastic response of fractional-order van der Pol oscillator. *Theor Appl Mech Lett* (2014) 4:013010. doi:10.1063/2.1401310

49. Spanos PD, Zeldin BA. Random vibration of systems with frequency-dependent parameters or fractional derivatives. *J Eng Mech* (1997) 123(3):290–2. doi:10.1061/(asce)0733-9399(1997)123:3(290)

50. Zhu WQ. *Nonlinear stochastic dynamics and control: Hamilton theoretical framework*. Beijing, China: Science Press (2003).

51. Oseledec VI. A multiplicative ergodic theorem. Lyapunov characteristic numbers for dynamical systems. *Trans Mosc Math. Soc* (1968) 19(2):197–231.

52. He CH, Liu C. Fractal dimensions of a porous concrete and its effect on the concrete's strength. *Facta Universitatis Ser Mech Eng* (2023) 21(1):137–50. doi:10.22190/FUME221215005H

53. Zhang XY, Wu ZQ. Bifurcations in tri-stable Duffing–Van der Pol oscillator with recycling noise. *Mod Phys Lett B* (2018) 32(20):1850228. doi:10.1142/s0217984918502287

frontiers | Frontiers in Physics

TYPE Mini Review
PUBLISHED 06 October 2023
DOI 10.3389/fphy.2023.1251608

OPEN ACCESS

EDITED BY
Chun-Hui He,
Xi'an University of Architecture and Technology, China

REVIEWED BY
Naveed Anjum,
Government College University, Faisalabad, Pakistan

*CORRESPONDENCE
Yu Liu,
liuyu@suda.edu.cn

RECEIVED 02 July 2023
ACCEPTED 19 September 2023
PUBLISHED 06 October 2023

CITATION
Liu Y, Chen H and Chen L (2023), The mechanism of the capillary oscillation and its application to fabrics' sweat permeability.
Front. Phys. 11:1251608.
doi: 10.3389/fphy.2023.1251608

The mechanism of the capillary oscillation and its application to fabrics' sweat permeability

Yu Liu[1,2]*, Hongxia Chen[3] and Lifen Chen[2]

[1]National Engineering Laboratory for Modern Silk, College of Textile and Clothing Engineering, Soochow University, Suzhou, China, [2]Jiangsu Sunshine Group, Wuxi, Jiangsu, China, [3]Department of Laboratory and Equipment Management, Soochow University, Suzhou, China

The capillary effect plays an important role in air and moisture permeability, and it can be used for thermal enhancement and energy harvesting. However, the capillary oscillation has not been extremely studied, and its mechanism for fabrics' sweat permeability was rare and preliminary. This paper studies the frequency property of the capillary oscillation in a zig-zag porosity of a fabric with a multiple layer structure. The theoretical analysis reveals that small porosity and low frequency of the zig-zag porosity are beneficial to the high sweat permeability. The proposed capillary oscillation probably paves a new avenue for designing fabrics with high moisture permeability, particularly in sportswear and military apparel in extreme cold environments.

KEYWORDS

capillary flow, capillary oscillator, low-frequency property, sweat permeability, fabric, hierarchical structure

1 Introduction

The capillary effect [1–3] appears everywhere in our everyday life and engineering, and the capillary fluid [4] can be used for enhancing heat conduction in micro/nanodevices or in a porous hierarchy [5, 6]. The capillary effect can also be effectively applied in the microelectromechanical system (MEMS) [7, 8] and energy-harvesting devices [9, 10] and can greatly affect the mechanical and thermal properties of porous materials [11–14]. The application of capillary oscillation to fabrics' sweat permeability has significant implications in textile engineering. Sportswear garments that are designed with high sweat permeability are preferred to enhance breathability and prevent excessive moisture buildup. This is crucial as excessive moisture buildup can lead to discomfort and distraction during physical activity, ultimately hindering the performance of the wearer. Similarly, garments with excellent sweat permeability are necessary to allow for rapid absorption of sweat and minimize skin irritation in undergarments. The fabrics' sweat permeability from the inner side to the environment has triggered rocketing interest in sportswear and military apparel in an extreme cold environment. If the sweat cannot be transferred through the cloth after an active motion, it will greatly affect the comfort property and even be life-threatening due to the icy fabric.

The capillary oscillation and its relationship with sweat permeability are crucial for developing new materials with improved performance characteristics in textile. However, the capillary fluid's oscillation property was hardly analyzed. Jin et al. revealed the frequency property mathematically [1]. Han and He applied the capillary oscillation to fabric's self-cleanliness [15]. Xiao, et al. studied the capillary oscillation in a short small tube [16]. Saxena studied moisture permeability through nylon and cotton fabrics [17]. Midha et al. researched

the laundering times on moisture permeability [18]. As the capillary thread moves up and down, it displaces a small amount of liquid from the surface of the fabric into the surrounding air. The process reduces the local surface tension at the contact point between the fabric and the skin, making the fabric more hydrophilic and thus more susceptible to sweat absorption. Ha et al. showed that air and moisture permeability plays an important role in the clothing microclimate [19]. Raja et al. conducted an experiment on the sweat transfer of multi-weave structure fabrics [20]. Guan et al. studied the clothing–human body system [21]. Liu et al. researched the thermal property of a microstructure [22]. The oscillatory motion of the capillary wall can create micro-cracks and pores in the fabric, which can facilitate the passage of sweat molecules and enhance sweat permeability. Furthermore, these micro-cracks can also provide additional channels for moisture transfer from the skin to the surrounding environment, further improving sweat evaporation and cooling performance.

All the aforementioned theoretical and experimental studies revealed that the capillary effect on fabrics' sweat permeability is of extreme importance for both everyday life and advanced applications. When sweat interacts with a fabric surface, capillary oscillation enhances the transfer of sweat from the skin to the fabric's surface. This process results in increased sweat permeability, which is essential for regulating body temperature. In this paper, we will show the mechanism of the capillary oscillation and its great effect on the fabric's air/moisture permeability.

2 Capillary oscillation

When a small tube is gradually immersed into a fluid, the fluid rises along the tube. This phenomenon, commonly referred to as the capillary effect [2, 3], is a familiar observation to anyone who has witnessed the wetting process of a napkin when it comes into contact with water. It can be explained by the geometrical potential theory [23]. The capillary rise is vulnerable to an environmental perturbation, and the capillary fluid will vibrate periodically [1]. The periodicity of the capillary oscillator is determined by the combined action of the gravity and surface tension of the liquid, and this periodicity is more obvious in the pull-in solution. Pull-in instability and periodic behavior are two key phenomena in microelectromechanical system (MEMS) dynamics, and differential equations can well describe these nonlinear aspects [24–26]. The capillary rise without any perturbation can be expressed as [27].

$$h \propto \frac{1}{r^n}, \tag{1}$$

where h is the capillary rise, r is the equivalent capillary radius, and n is a positive parameter depending on the tube's geometry.

Equation 1 shows that a smaller porosity leads to a higher capillary rise, which can explain why a nanofiber membrane has high permeability [28]. The nanofiber membrane can be produced via the electrospinning technology [29] and has the potential application in optimizing design of the sportswear and military apparel in an extreme cold environment.

A mathematical model was established in Ref. [1], and Bin et al. conducted a numerical simulation of the capillary oscillation [2].

The dynamical motion of the capillary fluid through a zig-zag porous structure of a fabric can be modelled using the following equation [1]:

$$x'' + \varepsilon \sin(\omega x) + \omega_0^2 x = 0,\ x(0) = A,\ x'(0) = 0, \tag{2}$$

where x is the center of the capillary fluid when it is still, ω is the frequency of zig-zag porosity, ω_0 is a parameter relative to the capillary effect, ε is a geometric parameter relative to fabric's geometry, and A is the amplitude.

When $\omega_0 = 0$, Eq. 2 becomes a famous pendulum oscillator [30]. When x<<1, Eq. 2 can be approximately expressed as

$$x'' + (\varepsilon\omega + \omega_0^2)x - \frac{1}{6}\varepsilon\omega^3 x^3 = 0,\ x(0) = A,\ x'(0) = 0. \tag{3}$$

This is the duffing oscillator [31]. To provide insights into the periodic property of Eq. 3, we quote the frequency formulation of Ji-Huan He [32, 33]. Consider a general nonlinear oscillator in the form

$$x'' + p(x) = 0,\ x(0) = A,\ x'(0) = 0, \tag{4}$$

where p is a nonlinear function of x and $p/x > 0$. Ji-Huan He's frequency formulation reads [32, 33].

$$\Omega^2 = \left\{\frac{p(x)}{x}\right\}\Big|_{x=\frac{\sqrt{3}}{2}A}, \tag{5}$$

where Ω is the frequency of the nonlinear oscillator.

The square of the frequency of Eq. 3 is

$$\begin{aligned}\Omega^2 &= \left\{\frac{(\varepsilon\omega + \omega_0^2)x - \frac{1}{6}\varepsilon\omega^3 x^3}{x}\right\}\Big|_{x=\frac{\sqrt{3}}{2}A} \\ &= \left\{\varepsilon\omega + \omega_0^2 - \frac{1}{6}\varepsilon\omega^3 x^2\right\}\Big|_{x=\frac{\sqrt{3}}{2}A} \\ &= \varepsilon\omega + \omega_0^2 - \frac{1}{8}\varepsilon\omega^3 \mathrm{A}^2,\end{aligned} \tag{6}$$

where Ω is the capillary fluid's vibrating frequency and A is the amplitude. This frequency formulation is a simple yet effective tool for the fast and accurate identification of the periodic property of a nonlinear oscillator [34–36]. Eq. 4 can also be derived using various numerical methods, such as the homotopy perturbation method [37, 38], the variational iteration method [24, 39], Wang's variational approach [40], or asymptotic methods [25, 26].

3 Fabrics' sweat permeability

A higher vibrating amplitude of the capillary motion implies that sweat can be transferred to a farther distant. When the capillary rise is less than the thickness of the fabric, the capillary oscillation is the main factor for the sweat permeability. According to Eq. 4, a higher amplitude requires a low frequency, and this low-frequency property is the mechanism underlying the sweat permeability. The period of the capillary oscillation is

$$T = \frac{2\pi}{\Omega} = \frac{2\pi}{\sqrt{\varepsilon\omega + \omega_0^2 - \frac{1}{8}\varepsilon\omega^3 \mathrm{A}^2}}, \tag{7}$$

where A is the amplitude of the capillary fluid's periodic motion. According to Eq. 7, a large amplitude implies a large period, which infers an extremely slowly motion. This can explain why the capillary rise seems to be stable at the initial stage when the

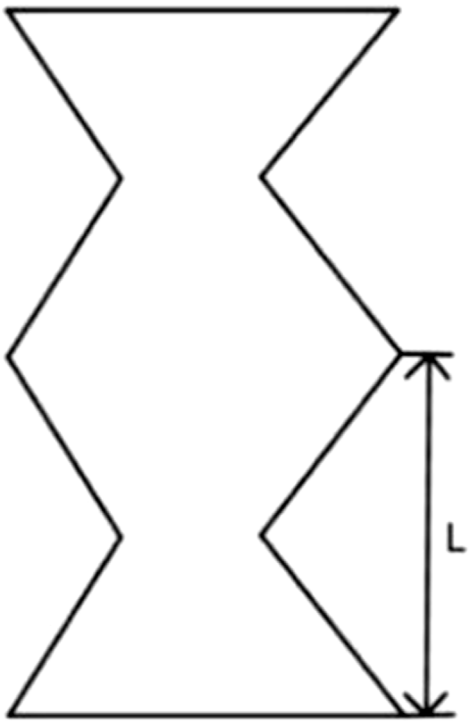

FIGURE 1
Zig-zag capillary tube.

small tube is immersed into water and keeps convincingly unchanged for few hours; however, it might change after 24 h or longer. As the permeability thickness reaches h+A, where h is the capillary height, the capillary fluid's periodic motion will continue to oscillate within the capillary. This oscillation will cause the fluid to move back and forth along the length of the capillary, creating a wave-like motion. A will increase as the thickness of the permeability increases, leading to an increase in the overall flow rate through the capillary. When the fabric's thickness is less than h+A, a good permeability is predicted.

The maximal amplitude of the capillary fluid reaches when the frequency becomes zero:

$$\Omega = \sqrt{\varepsilon\omega + \omega_0^2 - \frac{1}{8}\varepsilon\omega^3 \mathrm{A}^2} = 0. \tag{8}$$

The maximal amplitude reads

$$A_{\max} = \sqrt{\frac{8\left(\varepsilon\omega + \omega_0^2\right)}{\varepsilon\omega^3}}. \tag{9}$$

Equation 9 shows that the frequency of zig-zag porosity is the main factor affecting the moisture/air permeability.

4 Fabrics with multiple layers and hierarchical structure

To ensure good sweat permeability, the fabric should have a large zig-zag period, as shown in Figure 1.

$$L = \frac{2\pi}{\omega}, \tag{10}$$

where L is the zig-zag period. A larger L leads to a thicker fabric, and the multiple-layer structure is always adopted in practical applications.

In order to decrease the thickness of the fabric with good air/moisture permeability, we can adopt a hierarchical structure from a nano/micro-inner layer to a macro-outside layer, and the thickness of each layer should satisfy the following inequality 11:

$$H_n < r_n + \sqrt{\frac{8\left(\varepsilon_n\omega_n + \omega_{n0}^2\right)}{\varepsilon\omega_n^3}}, \tag{11}$$

where H_n is the thickness of the nth layer of the hierarchy, r_n is the nth layer's capillary rise, and ω_n is the zig-zag frequency of the nth layer [1].

The inner wall of blood vessels is unsmooth, leading to a zig-zag inner surface, so that the blood can be transferred to a farther distance than that of the smooth inner surface.

If the porosity is smooth enough in each layer, inequality 11 should be modified as

$$H_n < r_n, \tag{12}$$

which means the thickness of each layer should be less than its capillary rise. Many natural hierarchical systems can transport water for a long distance [41].

5 Conclusion

This paper proposes the capillary oscillation model to design hierarchical fabrics with good air/moisture permeability, which is of critical importance for the clothing design, especially for sportswear and military apparel in an extreme cold environment, where the sweat permeability plays an important role in human's comfort and safety. This theoretical analysis enables scientists to understand the capillary oscillation and its role in air/water transportation. Capillary oscillation is the periodic oscillation of liquid in a capillary tube due to the interaction between surface tension and viscous forces. In the context of fabric moisture absorption and perspiration, capillary oscillation plays an important role in determining the wicking and transport of moisture in the fabric. When a fabric comes into contact with moisture, capillary forces cause the liquid to be drawn into the fabric's capillary channels. The capillary oscillation then helps distribute the moisture throughout the fabric, allowing it to be absorbed and transported more efficiently. This is because the oscillation creates a pumping effect that helps move the liquid through the capillary channels. In addition, capillary oscillation can also help enhance the fabric's moisture absorption and perspiration properties. By promoting the movement of moisture through the fabric, capillary oscillation can help increase the rate of moisture absorption and perspiration, thereby improving the fabric's overall comfort and performance. Overall, the relationship between capillary oscillation and moisture absorption and perspiration properties of fabrics is complex, with many factors influencing the process. However, it is clear that capillary oscillation plays an important role in determining the wicking and transport of moisture in the fabrics and can help

enhance the fabric's moisture absorption and perspiration properties. Understanding this relationship and applying advanced techniques like nanotechnology and optimized yarn structure can lead to the development of innovative textile materials with superior sweat permeability and performance. Because this paper gives a self-contained theoretical model for the sweat permeability for the first time, the future holds exciting possibilities for improving garment design and enhancing human wellbeing as technology advances and researchers continue to explore this topic.

Author contributions

All authors listed have made a substantial, direct, and intellectual contribution to the work and approved it for publication.

Funding

This work was supported by the Large-scale Scientific Instruments Open and Shared Independent Research Project of Jiangsu Province (TC2023A042), National Nature Science Foundation of China (51403146), and Nature Science Foundation of Jiangsu Province (BK20161288).

Conflict of interest

Authors YL and LC were employed by the company Jiangsu Sunshine Group.

The remaining author declares that the research was conducted in the absence of any commercial or financial relationships that could be construed as a potential conflict of interest.

Publisher's note

References

1. Xiao J, Liu MN, Pan F, Li YP, Fan J. Low frequency of a deforming capillary vibration, part 1: Mathematical model. *J Low Freq Noise V A* (2019) 38(3-4):1676–80. doi:10.1177/14613484198562

2. Bin C, Lu JF, Xia ZZ. Numerical investigation of the fractal capillary oscillator. *J Low Freq N A* (2023) 42(2):579–88. doi:10.1177/14613484221131245

3. Pasandideh-Fard M, Qiao YM, Chandra S, Mostaghimi J. Capillary effects during droplet impact on a solid surface. *Phys Fluids* (1996) 8(3):650–9. doi:10.1063/1.868850

4. Deegan RD, Bakajin O, Dupont TF, Huber G, Witten TA. Capillary flow as the cause of ring stains from dried liquid drops. *Nature* (1997) 389(6653):827–9. doi:10.1038/39827

5. Liu FJ, Zhang T, He CH, Tian D. Thermal oscillation arising in a heat shock of a porous hierarchy and its application. *Facta Univ-ser Mech* (2022) 20(3):633–45. doi:10.22190/FUME210317054L

6. Xue RJ, Liu FJ. A Fractional model and its application to heat prevention coating with cocoon-like hierarchy. *Therm Sci* (2022) 26(3):2493–8. doi:10.2298/TSCI2203493X

7. Guo JG, Zhou LJ, Zhao YP. Instability analysis of torsional MEMS/NEMS actuators under capillary force. *J Colloid Interf Sci* (2009) 331(2):458–62. doi:10.1016/j.jcis.2008.11.069

8. He CH. A variational principle for a fractal nano/microelectromechanical (N/MEMS) system. *Int J Numer Method H* (2023) 33(1):351–9. doi:10.1108/HFF-03-2022-0191

9. Li C, Liu K, Liu H, Yang B, Hu X. Capillary driven electrokinetic generator for environmental energy harvesting. *Mater Res Bull* (2017) 90:81–6. doi:10.1016/j.materresbull.2017.02.022

10. He CH, Amer TS, Tian D, Abolila AF, Galal AA. Controlling the kinematics of a spring-pendulum system using an energy harvesting device. *J Low Freq N A* (2022) 41(3):1234–57. doi:10.1177/14613484221077474

11. Jamali A, Mendes J, Nagaratnam B, Lim M. A new four stage model of capillary pressure in early age concrete: Insights from high capacity tensiometers. *Cement Concrete Res* (2022) 161:106955–67. doi:10.1016/j.cemconres.2022.106955

12. He CH, Liu C. Fractal dimensions of a porous concrete and its effect on the concrete's strength. *Facta Univ-ser Mech* (2023) 21(1):137–50. doi:10.22190/FUME221215005H

13. He CH, Liu C, He JH, SedighiShokri HMA, Gepreel KA. A fractal model for the internal temperature response of a porous concrete. *Appl Comput Math-bak* (2022) 21(1):71–7. doi:10.30546/1683-6154.21.1.2022.71

14. Xiao QH, Wu Z, Qiu JS, Dong ZY, Shi SS. Capillary water absorption performance and damage constitutive model of recycled concrete under freeze-thaw action. *Constr Build Mater* (2022) 353(24):129120–0. doi:10.1016/j.conbuildmat.2022.129120

15. Han CY, He JH. Effect of fabric surface's cleanliness on its moisture/air permeability. *Therm Sci* (2021) 25(2):1517–21. doi:10.2298/TSCI2102517H

16. Xiao JF, Liu X, Luo YM, Cai JC, Xu JF. Oscillations of free surface at the edge of short capillary tubes. *Colloid Surf A* (2020) 591:124572. doi:10.1016/j.colsurfa.2020.124572

17. Saxena RK. Studies on water vapour transfer through nylon and cotton fabrics. *Indian J Fibre Text* (1999) 24(3):188–92.

18. Midha V, Kumar SS, Kumar MN. Investigation on permeability and moisture management properties of different denim fabrics after repeated laundering. *Indian J Fibre Text* (2017) 108(1):71–7. doi:10.1080/00405000.2016.1153873

19. Ha M, Tokura H, Yanai Y, Moriyama T, Tsuchiya N. Combined effects of fabric air permeability and moisture absorption on clothing microclimate and subjective sensation during intermittent exercise at 27 degrees C. *Ergonomics* (1999) 42(7):964–79. doi:10.1080/001401399185243

20. Raja D, Babu VR, Senthilkumar M, Ramakrishnan G, Kannan N. A dynamic sweat transfer tester for analyzing transverse sweat transfer properties of multi-weave structure fabrics. *J Ind Tex* (2014) 44(2):211–31. doi:10.1177/1528083713481836

21. Guan MH, Annaheim S, Camenzind M, Li J, Mandal S, Psikuta A, et al. Moisture transfer of the clothing-human body system during continuous sweating under radiant heat. *Text Res J* (2019) 89(21):4537–53. doi:10.1177/0040517519835767

22. Liu TQ, Yan WT, Yang X, Wang SF. Thermal performance of wickless and orientation independent thin vapor chambers with wettability patterned micro structure. *Therm Sci* (2022) 26(5):4391–400. doi:10.2298/TSCI211106017L

23. Tian D, Li XX, He JH. Geometrical potential and nanofiber membrane's highly selective adsorption property. *Adsorpt Sci Technol* (2019) 37(5-6):367–88. doi:10.1177/0263617418813826

24. Anjum N, He JH, He CH, Ashiq A. A brief review on the asymptotic methods for the periodic behaviour of microelectromechanical systems. *J Appl Comput Mech* (2022) 8(3):1120–40. doi:10.22055/jacm.2022.39404.3401

25. Anjum N, Rahman JU, He JH, Alam MN, Suleman M. An efficient analytical approach for the periodicity of nano/microelectromechanical systems' oscillators. *Math Probl Eng* (2022) 2022:1–12. doi:10.1155/2022/9712199

26. Shokravi M. Dynamic pull-in and pull-out analysis of viscoelastic nanoplates under electrostatic and casimir forces via sinusoidal shear deformation theory. *J Microelectron Reliab* (2017) 71(4):17–28. doi:10.1016/j.microrel.2017.02.006

27. Fan J, Zhang YR, Liu Y, Wang WH, Cao FY, Yang QQ, et al. Explanation of the cell orientation in a nanofiber membrane by the geometric potential theory. *Result Phys* (2019) 15:102537–41. doi:10.1016/j.rinp.2019.102537

28. Yalcinkaya F, Yalcinkaya B, Hruza J, Hrabak P. Effect of nanofibrous membrane structures on the treatment of wastewater microfiltration. *Sci Adv Mater* (2017) 9(5):747–57. doi:10.1166/sam.2017.3027

29. Liu LG, Liu YQ, Li YY, Shen Y, He JH. Dropping in electrospinning process: A general strategy for fabrication of microspheres. *Therm Sci* (2021) 25(2):1295–303. doi:10.2298/TSCI191228025L

30. He JH, Amer TS, Elnaggar S, Galal AA. Periodic property and instability of a rotating pendulum system. *Axioms* (2021) 10(3):191–206. doi:10.3390/axioms10030191

31. He CH, Tian D, Moatimid GM, Salman HF, Zekry MH. Hybrid Rayleigh–van der pol–duffing oscillator: Stability analysis and controller. *J Low Freq N A* (2022) 41(1): 244–68. doi:10.1177/14613484211026407

32. He JH. The simplest approach to nonlinear oscillators. *Results Phys* (2019) 15: 102546–8. doi:10.1016/j.rinp.2019.102546

33. He JH. The simpler, the better: Analytical methods for nonlinear oscillators and fractional oscillators. *J Low Freq N A* (2019) 38(3-4):1252–60. doi:10.1177/1461348419844145

34. Feng GQ, Niu JY. An analytical solution of the fractal toda oscillator. *Results Phys* (2023) 44:106208–15. doi:10.1016/j.rinp.2023.106208

35. Elias-Zuniga A, Palacios-Pineda LM, Jimenez-Cedeno IH, Martinez-Romero O, Trejo DO. He's frequency-amplitude formulation for nonlinear oscillators using Jacobi elliptic functions. *J Low Freq N A* (2020) 39(4):þ1216–23. doi:10.1177/1461348420972820

36. He CH, Liu C. A modified frequency-amplitude formulation for fractal vibration systems. *Fractals* (2022) 30(3):2250046–8. doi:10.1142/S0218348X22500463

37. He CH, El-Dib YO. A heuristic review on the homotopy perturbation method for non-conservative oscillators. *J Low Freq N A* (2021) 41(2):572–603. doi:10.1177/14613484211059264

38. He JH, He CH, Alsolami AA. A good initial guess for approximating nonlinear oscillators by the homotopy perturbation method. *Facta Univ-ser Mech* (2023) 21(1): 021–9. doi:10.22190/FUME230108006H

39. Wang SQ, He JH. Variational iteration method for solving integro-differential equations. *Phys Lett A* (2007) 367(3):188–91. doi:10.1016/j.physleta.2007.02.049

40. Wang SQ. A variational approach to nonlinear two-point boundary value problems. *Comput Math Appl* (2009) 58(11):2452–5. doi:10.1016/j.camwa.2009.03.050

41. Chen HW, Zhang PF, Zhang LW, Iu HLL, Jiang Y, Zhang DY, et al. Continuous directional water transport on the peristome surface of nepenthes alata. *Nature* (2016) 532:85–9. doi:10.1038/nature17189

frontiers | Frontiers in Physics

TYPE Original Research
PUBLISHED 17 October 2023
DOI 10.3389/fphy.2023.1232828

OPEN ACCESS

EDITED BY
Dragan Marinkovic,
Technical University of Berlin, Germany

REVIEWED BY
S. A. Edalatpanah,
Ayandegan Institute of Higher Education (AIHE), Iran
Arzu Akbulut,
Bursa Uludağ University, Türkiye
Shah Muhammad,
King Saud University, Saudi Arabia
Ain Qura Tul,
Guizhou University, China

*CORRESPONDENCE
Anam Nigar,
nigaranam@yahoo.com

RECEIVED 01 June 2023
ACCEPTED 17 August 2023
PUBLISHED 17 October 2023

CITATION
Ali A, Nigar A, Nadeem M, Jat Baloch MY, Farooq A, Alrefaei AF and Hussain R (2023), Complex solutions for nonlinear fractional partial differential equations via the fractional conformable residual power series technique and modified auxiliary equation method.
Front. Phys. 11:1232828.
doi: 10.3389/fphy.2023.1232828

Complex solutions for nonlinear fractional partial differential equations via the fractional conformable residual power series technique and modified auxiliary equation method

Asghar Ali[1], Anam Nigar[2]*, Muhammad Nadeem[3], Muhammad Yousuf Jat Baloch[4], Atiya Farooq[5], Abdulwahed Fahad Alrefaei[6] and Rashida Hussain[5]

[1]Mirpur University of Science and Technology (MUST), Mirpur, Pakistan, [2]School of Electronics and Information Engineering, Changchun University of Science and Technology, Changchun, China, [3]School of Mathematics and Statistics, Qujing Normal University, Qujing, China, [4]College of New Energy and Environment, Jilin University, Changchun, China, [5]Department of Mathematics, Mirpur University of Science and Technology, Mirpur, Pakistan, [6]Department of Zoology, College of Science, King Saud University, Riyadh, Saudi Arabia

The fractional-order nonlinear Gardner and Cahn–Hilliard equations are often used to model ultra-short burst beams of light, complex fields of optics, photonic transmission systems, ions, and other fields of mathematical physics and engineering. This study has two main objectives. First, the main objective of this investigation is to solve the fractional-order nonlinear Gardner and Cahn–Hilliard equations by using the modified auxiliary equation method, which is not found in the literature. Second, the exact and approximate solutions of these equations are obtained by utilizing the fractional conformable residual power series algorithm and the modified auxiliary equation method. For the analytical and numerical solutions to two equations, we employ two separate techniques and establish consistency between the precise answers that are derived and the compatible numerical solution. To the best of our knowledge, this method of solving equations has never been investigated in this manner. The 2D and 3D contours have been defined using appropriate parametric values to support the physical compatibility of the results. The assessed findings suggested that the approach used in this study to recover inclusive and standard solutions is approachable, efficient, and faster in computing and can be considered a useful tool in resolving more complex phenomena that arise in the field of engineering, mathematical physics, and optical fiber.

KEYWORDS

fractional conformable residual power series algorithm, nonlinear partial differential equations, fractional-order nonlinear Cahn–Hilliard equation, modified auxiliary equation method, approximate solution

1 Introduction

In complicated areas of fields that can be modeled by various types of partial differential equations, many linear and nonlinear solutions appear. The nonlinear partial differential equations (NLPDEs) are crucial for studying a variety of issues. Understanding virtually nonlinear partial differential equations requires an effort to determine precise solutions to nonlinear equations [1–3]. Fractional calculus, which is the study of integrals and derivatives of any arbitrary real or complex order, has gained significant recognition over the past 30 years or so largely because of its well-established applications in numerous and varied disciplines of technical knowledge [4].

Fractional differential equations have received considerable attention over the past 20 years as a result of their capacity to accurately reproduce a broad range of events in a variety of scientific and technical fields. In science and engineering, fractional differential equations can be used to represent a variety of physical applications [5]. Fractional differential equations have been used to tackle numerous engineering and scientific problems [6]. The differential equation in fractional nonlinear partial differential equations (FNLPDEs) has nonlinear variables which create complex behaviors and phenomena not seen in linear equations. Complex patterns, chaotic dynamics, solitons, and shocks can all occur as a result of nonlinearity. The interaction between nonlinearity and fractional derivatives makes it particularly difficult to comprehend and analyze the dynamics of FNLPDEs.

The usage of fractional differential equations (FDEs) is widespread throughout many scientific disciplines due to their various applications in physics and engineering. Fractional partial differential equations (FPDEs) have grown in

TABLE 1 Comparison of analytical solutions via the MSSE technique and numerical solutions computed via the modified VI technique for the model under investigation.

Iteration	Analytical	Numerical	Absolute error	Relative error
1	6.2	23	17	2.8333
2	2.2	11	9	4.5
3	−19.2	−22	3	0.15789
4	−75.2	−94	19	0.25333
5	−190.2	−229	39	0.20526
6	−394.2	−457	63	0.1599
7	−723.2	−814	91	0.12586
8	−1219.2	−1342	123	0.1009
9	−1930.2	−2089	159	0.082383
21	−52894.2	−53797	903	0.017072
22	−63498.2	−64489	991	0.015607
23	−75619.2	−76702	1083	0.014322
24	−89395.2	−90574	1179	0.013189
25	$-1.0497e+05$	$-1.0625e+05$	1279	0.012184
26	$-1.2249e+05$	$-1.2388e+05$	1383	0.01129
27	$-1.4212e+05$	$-1.4361e+05$	1491	0.010491
28	$-1.6402e+05$	$-1.6562e+05$	1603	0.0097733
29	$-1.8835e+05$	$-1.9007e+05$	1719	0.0091266
30	$-2.1529e+05$	$-2.1713e+05$	1839	0.008542
31	$-2.4502e+05$	$-2.4698e+05$	1963	0.0080116
32	$-2.7772e+05$	$-2.7981e+05$	2091	0.0075291
33	$-3.1359e+05$	$-3.1582e+05$	2,223	0.0070888
34	$-3.5283e+05$	$-3.5519e+05$	2,359	0.0066859
35	$-3.9564e+05$	$-3.9813e+05$	2,499	0.0063164
36	$-4.4222e+05$	$-4.4486e+05$	2,643	0.0059767
37	$-4.928e+05$	$-4.9559e+05$	2,791	0.0056636

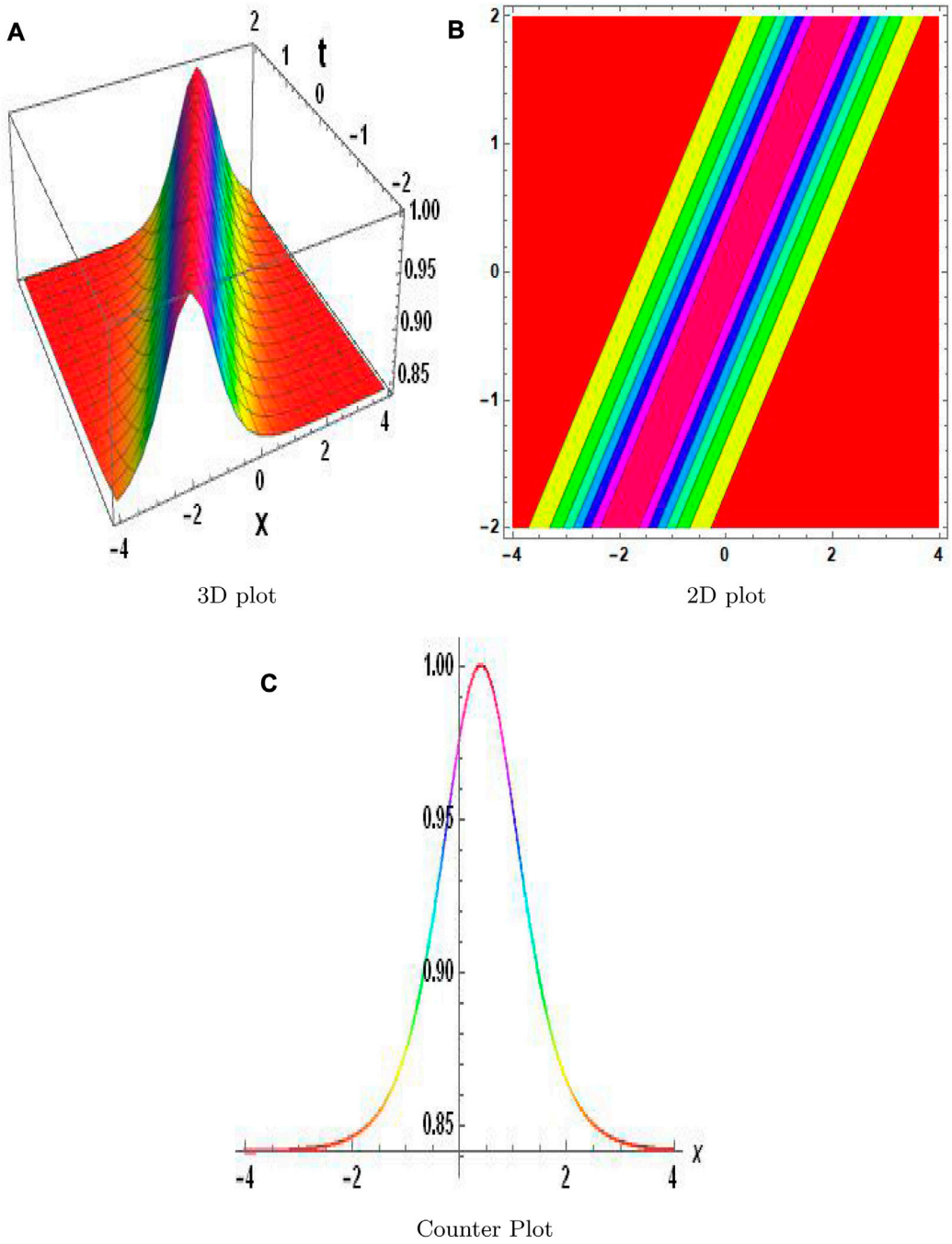

FIGURE 1
Physical depiction of $v_{1,1}$ at $\sigma = 0.4$, $\theta = -1.4$, and $\eta = 0.5$.

significance and reputation among FDEs in recent years as a result of their demonstrated utility in a wide range of extremely diverse scientific and engineering disciplines [7]. Many fractional types of equations are solved using novel transform [8] and zz transform with the Mittag-Leffler kernel [9]. Since they cannot be solved precisely, the majority of nonlinear FDEs require approximate and numerical solutions such as the Adomian decomposition method [10], spectral collocation method [11], Euler method and homotopy analysis method [12], Laplace residual power series [13], variational iteration transform method [14], and homotopy analysis method [15]. FNLPDEs find applications in various cutting-edge areas of research. For example, in materials science, FNLPDEs are used to model diffusion and transport in heterogeneous media. In finance, they are employed to describe complex price dynamics and risk management. In biology, FNLPDEs are utilized to study the spread of diseases and population dynamics. The unique combination of nonlinearity and fractional derivatives in

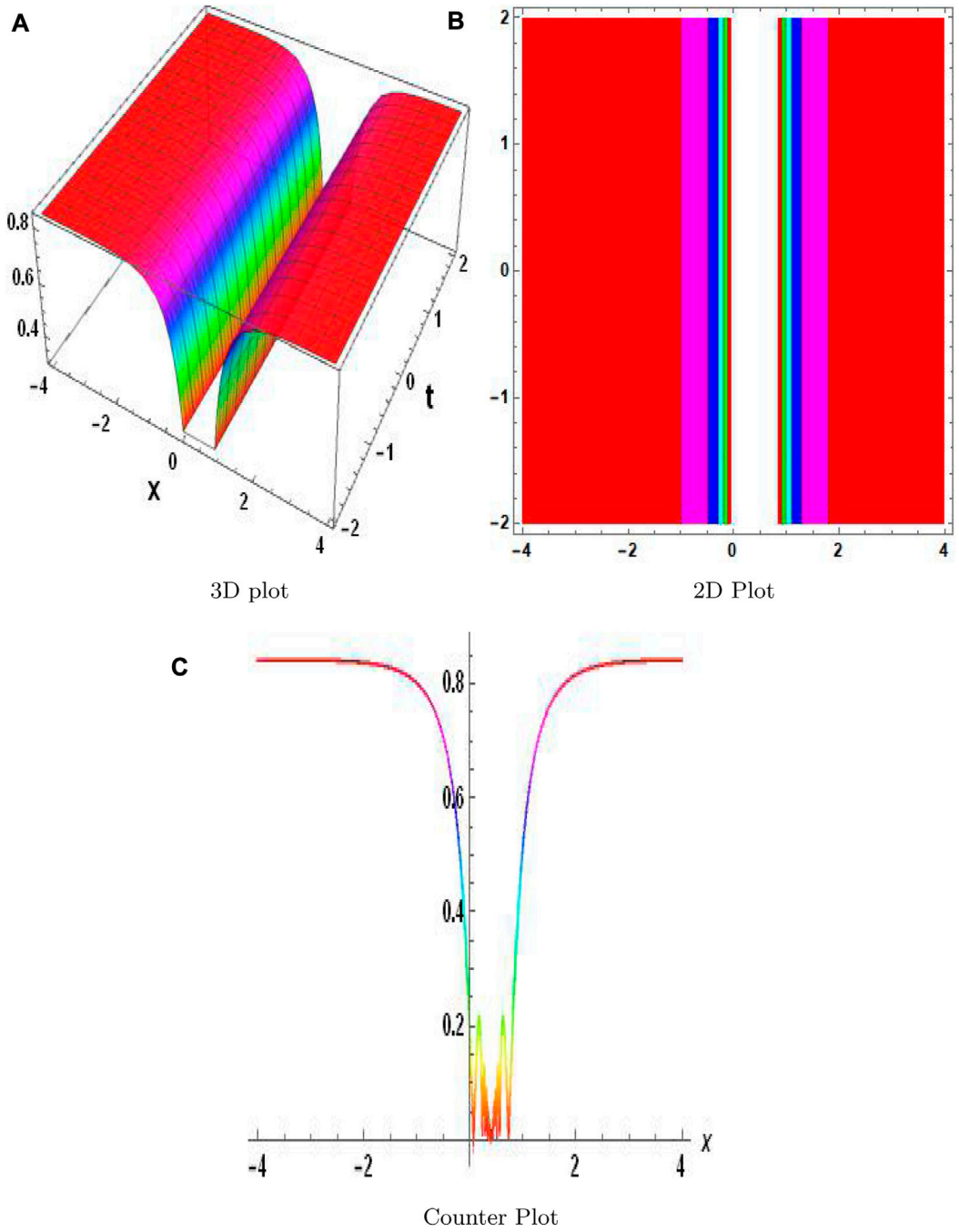

FIGURE 2
Physical depiction of $v_{1,2}$ at $\sigma = 0.34$, $\theta = -2.4$, and $\eta = 1.5$.

FNLPDEs provides a versatile framework for modeling these emerging phenomena.

One of the most recent methods developed in this field is the auxiliary equation method proposed by Khater [16]. Although this approach was employed in numerous research studies [17], a modified auxiliary equation approach (also known as the modified Khater method) was developed to get precise traveling wave solutions. The soliton and other solitary wave solutions of the equations are obtained in this research paper using the modified auxiliary equation approach. It enhances the auxiliary equation method. This article describes a method that modifies the auxiliary differential equation methodology for solving nonlinear partial differential equations [18]. Over the past 30 years, fresh and state-of-the-art methods for investigating nonlinear differential systems with fractional-order equations have been created, along with new computer methods and symbolic programming. Analytical methodologies, new mathematical theories, and computational systems that enable us to study nonlinear complicated phenomena have triggered this revolution in understanding. Furthermore, the sub-equation

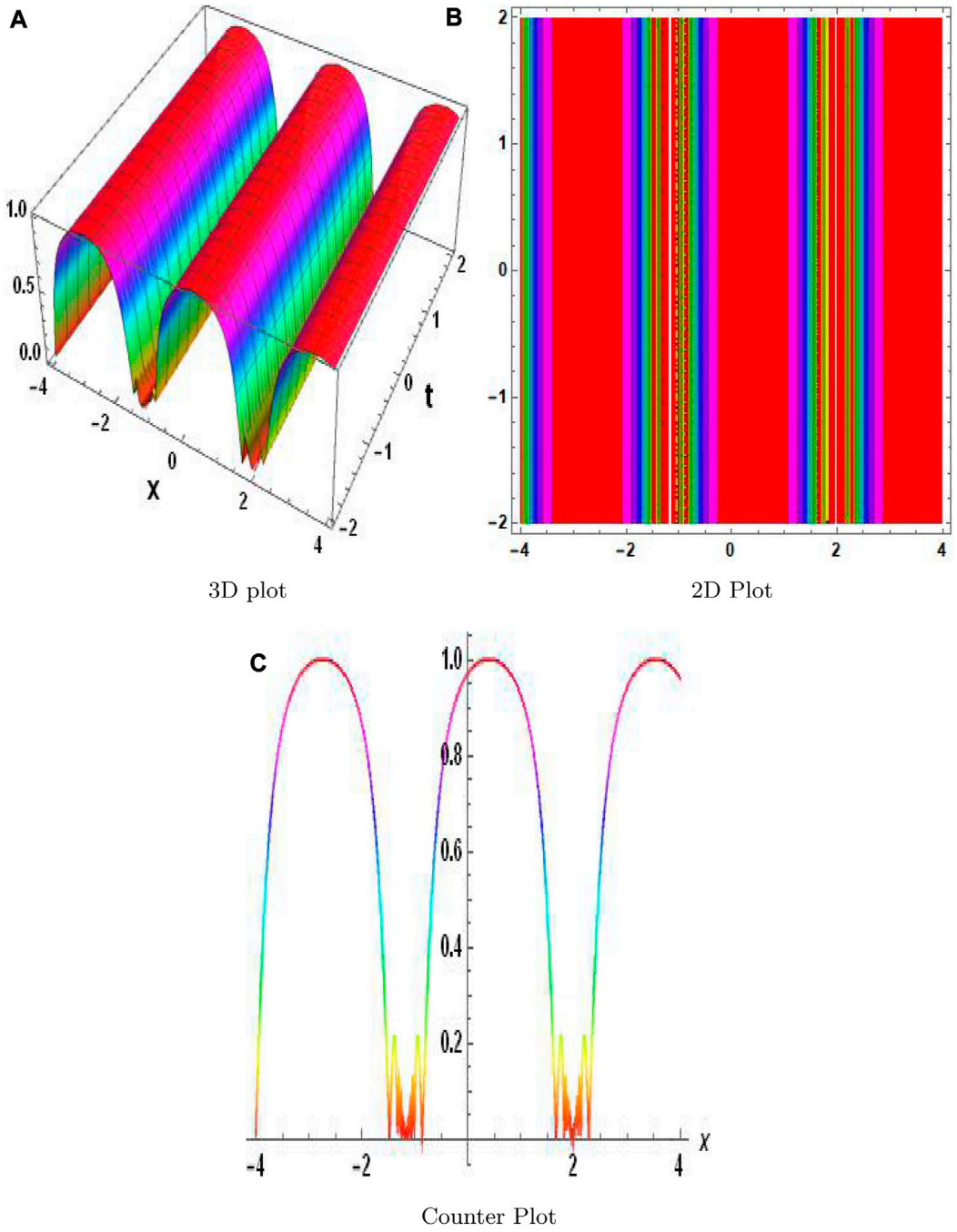

FIGURE 3
Physical depiction of $v_{1,3}$ at $\sigma = -0.4$, $\theta = 0.4$, and $\eta = -0.5$.

method [19], modified Kudryashov method [20], and F-expansion method [21–23] are just a few of the methods that have been used.

A semi-approximate approach called numerical simulations was developed specifically for addressing challenging nonlinear temporal FPDEs that can appear in a variety of scientific fields. This approach, which was devised and developed by Abu Arqub for the study of fuzzy differential equations, is used for generalizing the expansion of the Taylor series of arbitrary order and minimizing the residual error identified to detect the unknown compounds. This method has the ability to immediately solve nonlinear terms without any constraints, transformations, linearizations, or changes to the models. As a result, it has attracted considerable attention and has become an energizing focus of the research community [24, 25].

The Gardner equation [26] is developed to illustrate the description of solitary inner waves in shallow water and combines the KdV and modified KdV equations. The Gardner equation is frequently used in various branches of physics, such as plasma theories, quantum area theories, fluid mechanics, and physics [27].

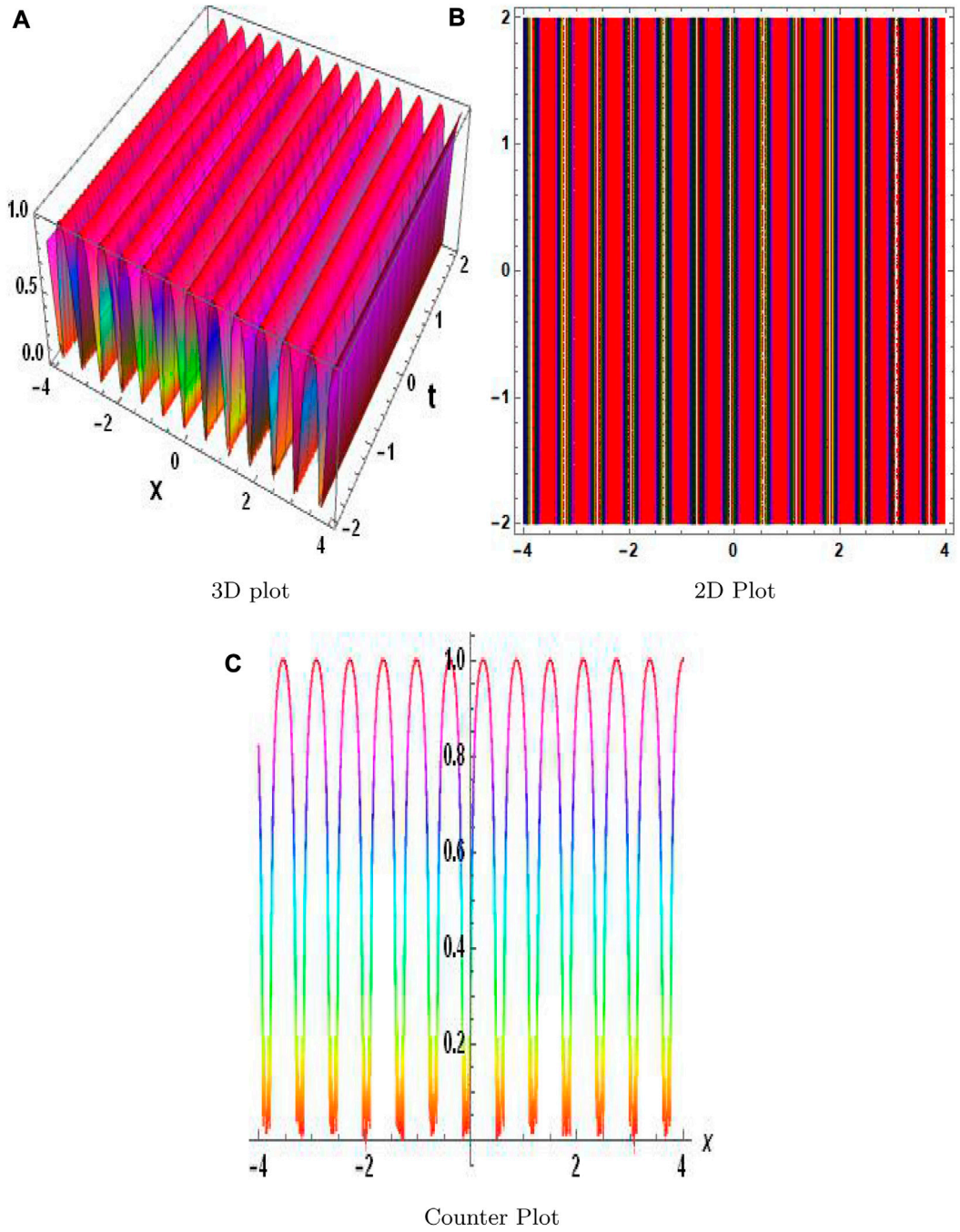

FIGURE 4
Physical depiction of $v_{1,4}$ at $\sigma = 0.44$, $\theta = -0.54$, and $\eta = 2.5$.

Numerous wave phenomena in the plasma and solid phases are also covered [28]. We recognize the conformable fractional-order nonlinear Gardner (FG) equation in the following form:

$$\partial_t^{\alpha} w(x,t) + 6\left(w - \lambda^2 w^2\right)\frac{\partial w}{\partial x} - \frac{\partial^3 w}{\partial x^3} = 0, \tag{1}$$

with an initial condition

$$w(x,0) = \frac{1}{2} + \frac{1}{2}\tanh\left(\frac{x}{2}\right),$$

and boundary condition

$$w(0,t) = \frac{1}{2} + \frac{1}{2}\tanh\left(\frac{-t}{2}\right),$$

$$w(1,t) = \frac{1}{2} + \frac{1}{2}\tanh\left(\frac{1-t}{2}\right).$$

A binary alloy's phase separation under a critical temperature is illustrated by the Cahn–Hilliard equation, which was first proposed by Cahn and Hilliard in 1958 [29]. The spinodal decomposition,

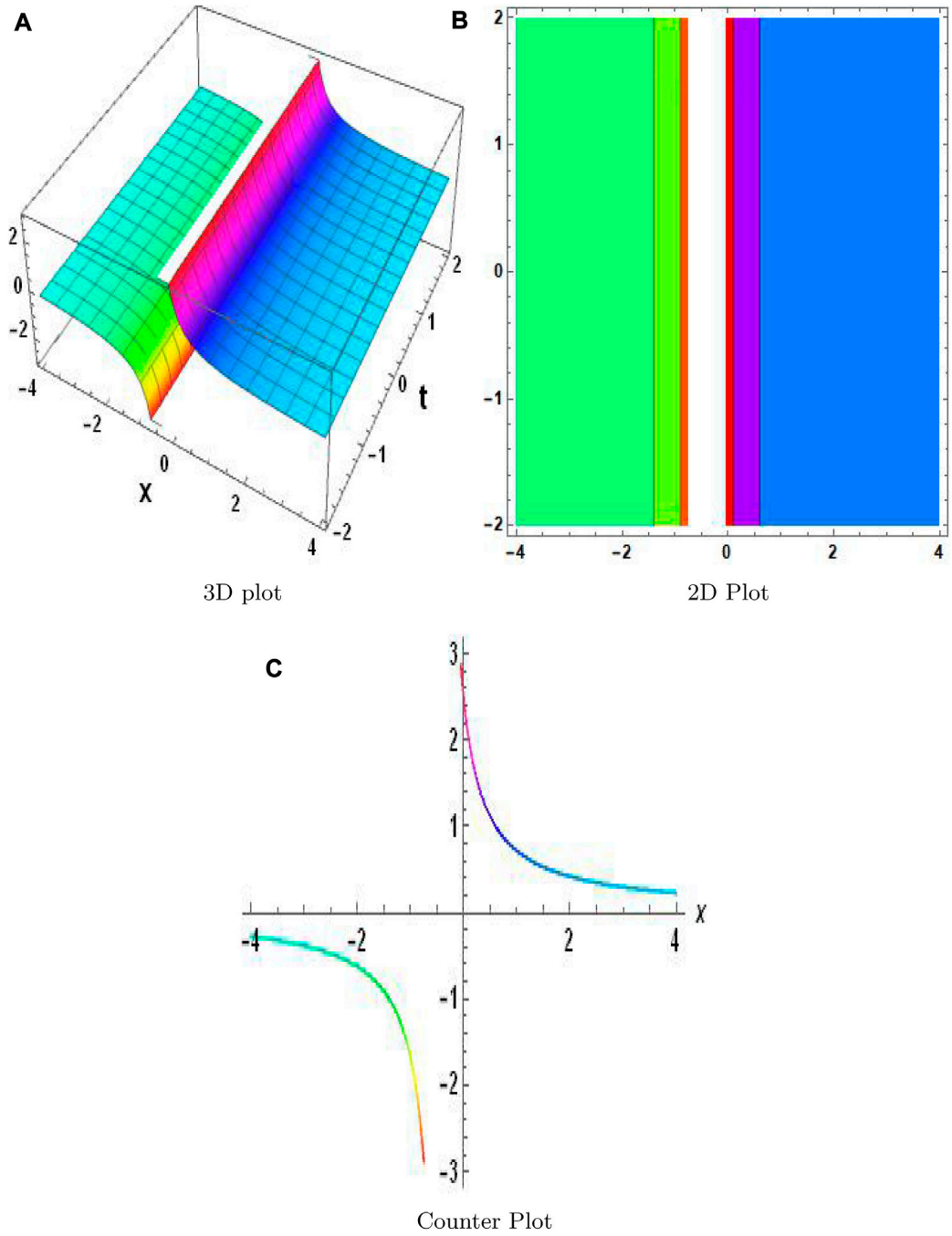

FIGURE 5
Physical depiction of $v_{1,5}$ at $\sigma = 1.4$, $\theta = -1.24$, and $\eta = 1.4$.

phase separation, and phase ordering dynamics are three fascinating physical phenomena that depend critically on this equation [30]. In this framework, the fractional Cahn–Hilliard (FCH) equation [31] is expressed as follows:

$$\partial_t^{\alpha} w(x,t) - \frac{\partial w}{\partial x} - 6w\left(\frac{\partial w}{\partial x}\right)^2 - \left(3w^2 - 1\right)\frac{\partial^2 w}{\partial x^2} + \frac{\partial^4 w}{\partial x^4} = 0, \qquad (2)$$

with an initial condition

$$w(x,0) = \tanh\left(\frac{\sqrt{2}\,(x)}{2}\right),$$

and boundary condition

$$w(0,t) = \tanh\left(\frac{\sqrt{2}\,(t)}{2}\right),$$

$$w(1,t) = \tanh\left(\frac{\sqrt{2}\,(1+t)}{2}\right).$$

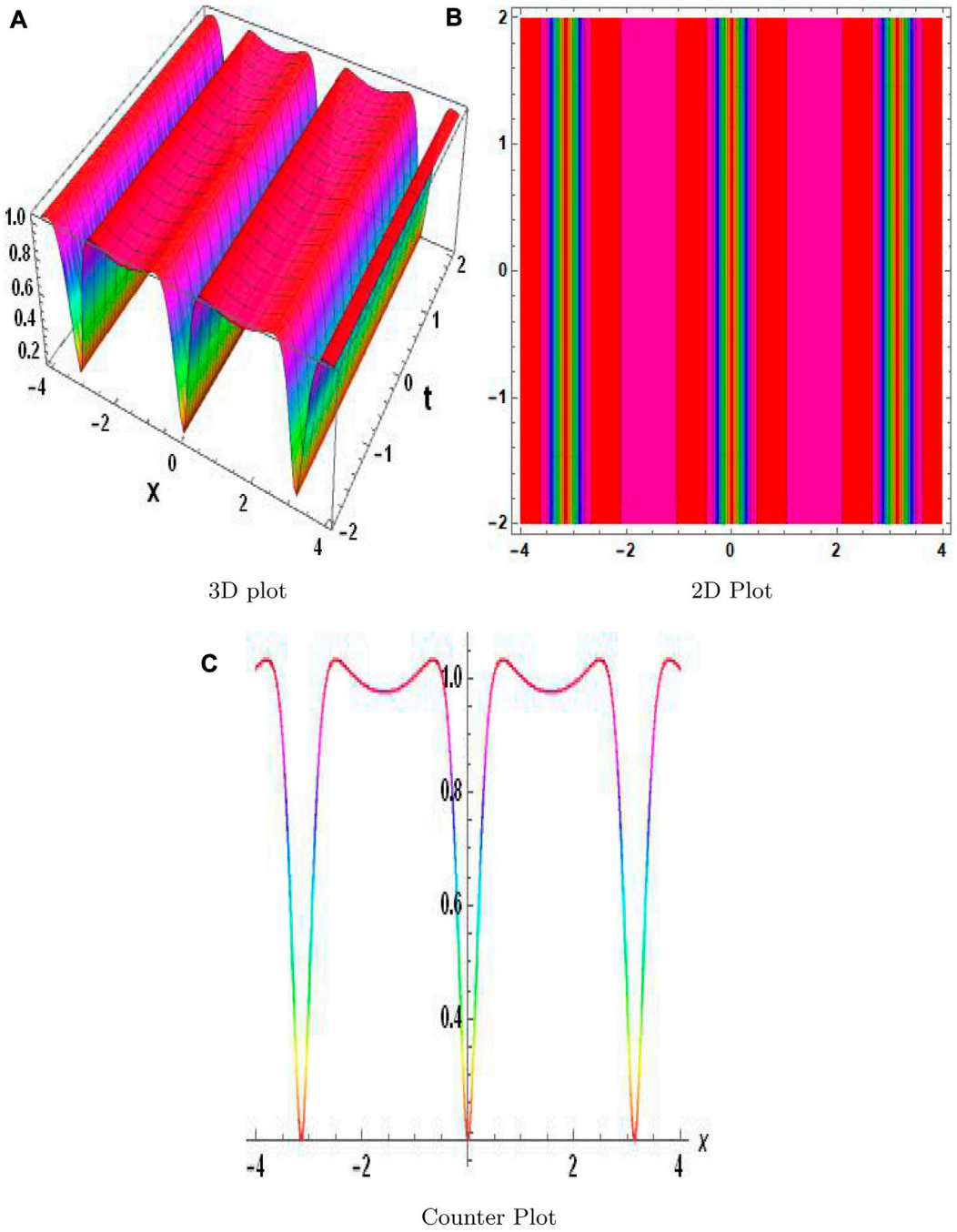

FIGURE 6
Physical depiction of $v_{2,1}$ at $\sigma = -0.4$, $\theta = -1.4$, and $\eta = -0.5$.

The methodology of this paper includes the following: Section 2 discusses the modified auxiliary equation method (MAEM) and also solves the equations. Section 3 discusses the semi-analytical fractional conformable residual power series algorithm and contains an explanation of the system to a solution. Section 4 examines the stability property of the equations. Section 5 contains the discussion and results of the system to illustrate the approximate delicacy. Section 6 presents the conclusion.

Preliminaries

Definition 1: The α-order fractional conformable derivative of a function $w(x, t)$ of order $\alpha\epsilon(0, 1)$ is given as

$$\frac{\partial^{\alpha} w(t)}{\partial t} = \lim_{\epsilon \to 0} \frac{w\left(\epsilon t^{1-\alpha} + t\right) - w(t)}{\epsilon}, t > 0.$$

Moreover, if the previous limit exists at a point s; $s > 0$ in $(0, s)$, then $w(t)$ is called α-differentiable so that $\frac{\partial^{\alpha} w(s)}{\partial t} = \lim_{t \to s^{+}} \frac{\partial^{\alpha} w(t)}{\partial t}$.

Definition 2: The multiple time-fractional series (MTFS) expansion $t_0 > 0$ is given as

$$\sum_{i=0}^{\infty} \zeta_i(x)(t - t_0)^{i\alpha} = \zeta_0(x) + \zeta_1(x)(t - t_0)^{\alpha} + \ldots,$$

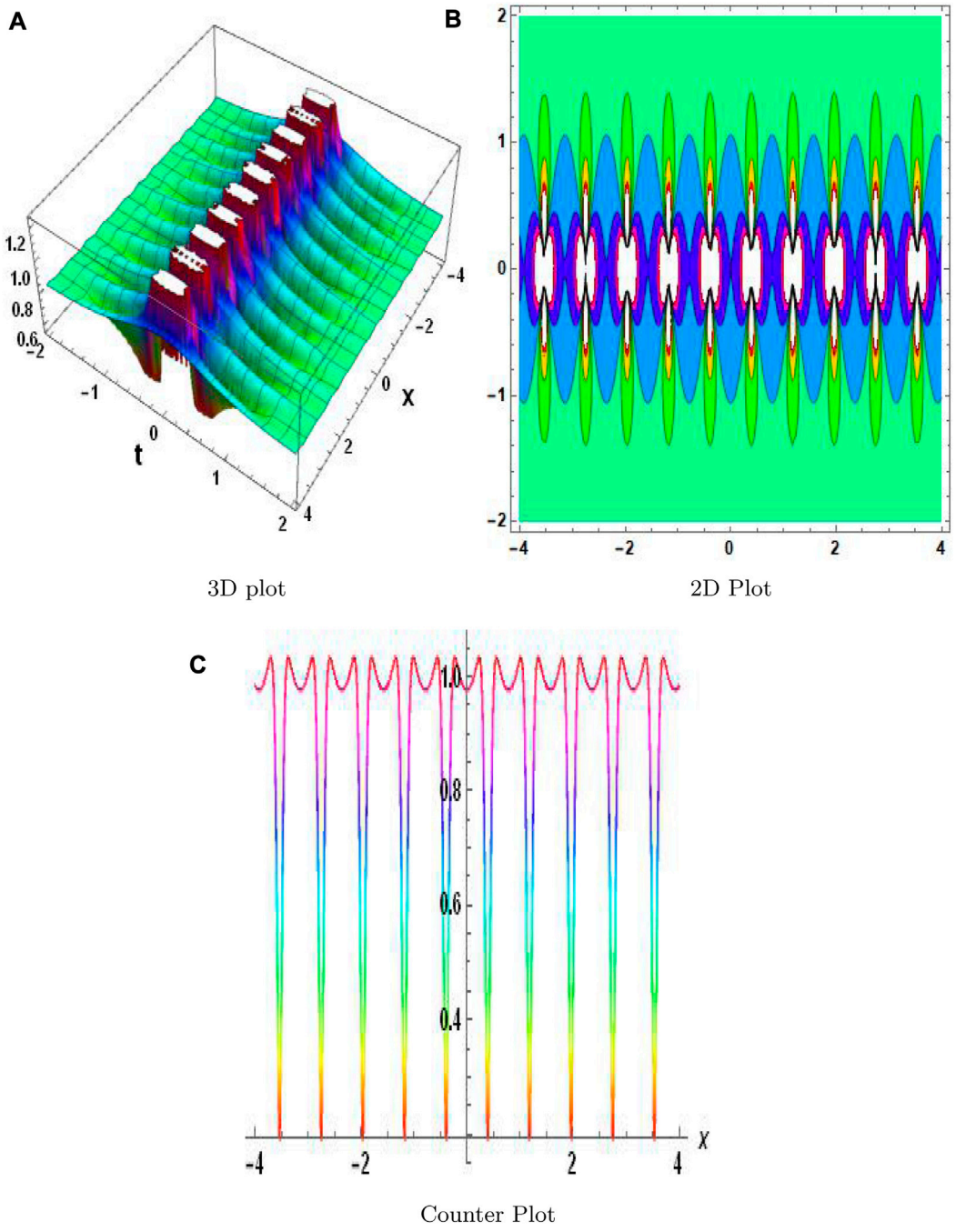

FIGURE 7
Physical depiction of $v_{2,2}$ at $\sigma = 0.74$, $\theta = -1.74$, and $\eta = 0.75$.

where $\epsilon(n-1, n)$, $t\epsilon(t_0, t_0 + r^{1/\alpha})$, $r > 0$, $r^{1/\alpha}$ is a radius of convergence and $\zeta_i(x)$ indicates unknown coefficients of the expansion. When $\alpha = 1$, then the expansion in Definition 2 reduces to the usual series expansion at $t_0 > 0$, with a radius of convergence r that converges uniformly on $|t - t_0| < r$. Many other definitions are provided in [32].

2 Methodology

2.1 Modified auxiliary equation method

First, we introduce the MAEM [33]. Let us consider FNLPDEs.

$$F\left(v, v_t^{\alpha}, v_{xx}, , v_{xt}, , \ldots\right) = 0, \tag{3}$$

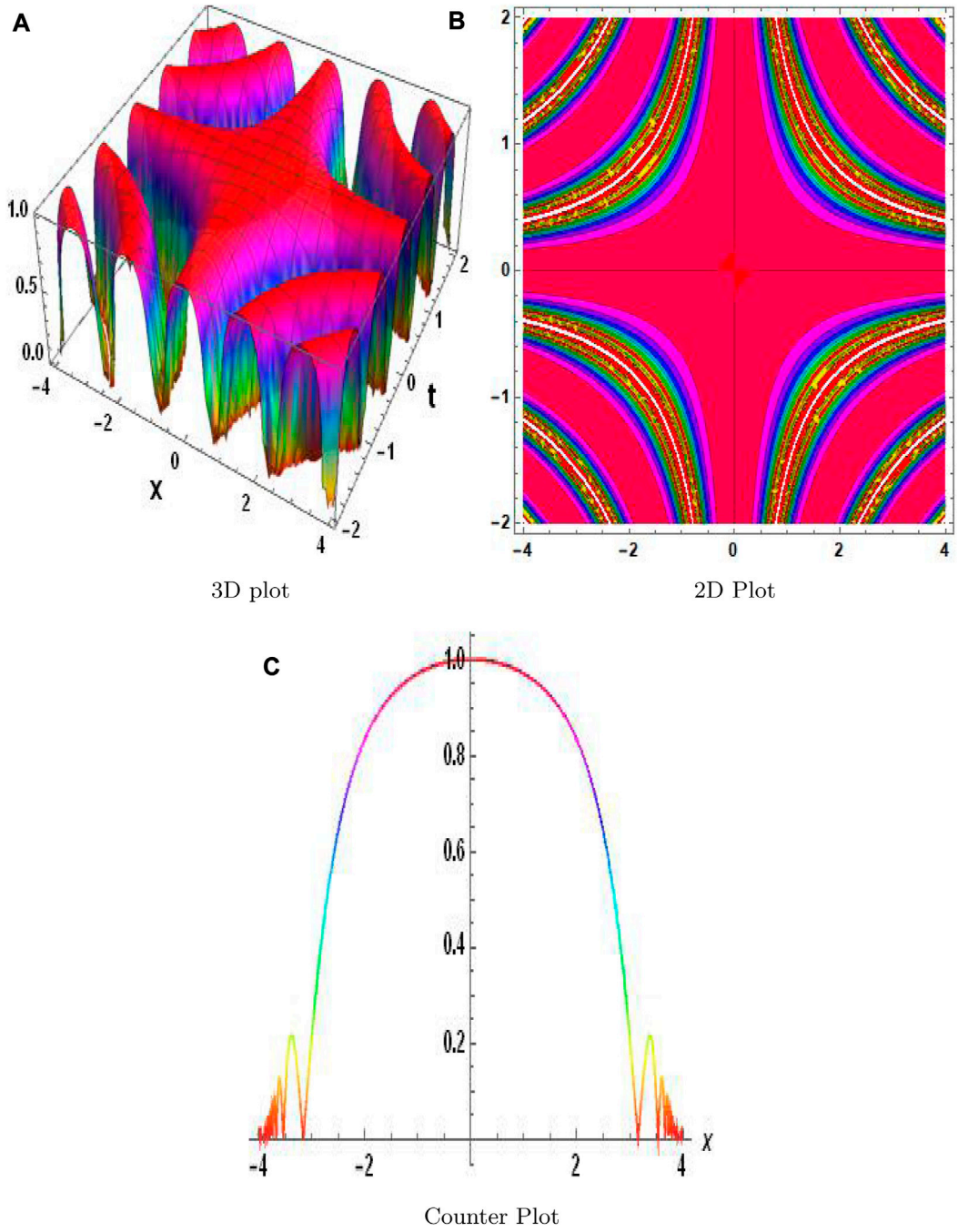

FIGURE 8
Physical depiction of $v_{2,3}$ at $\sigma = 1.4$, $\theta = -3.4$, and $\eta = 3.5$.

where F is the function's polynomial. In Eq. 3, v is a function of the spatial variables x and t and represents the propagation of the wave profile. To modify the following, Eq. 3 is transformed into an ordinary differential equation as

$$v = V(\eta), \eta = x - \frac{vt^{\alpha}}{\alpha}, \tag{4}$$

where α represents arbitrary constants. Eq. 3 is converted into an ODE of the kind using transforms from Eq. 4.

$$M(V, V', V'', \ldots) = 0, \tag{5}$$

where M stands for the polynomial involving the function V and its regular derivatives $V' = dV/d\eta$. The solution to Eq. 5 is

$$V(\eta) = a_0 + \sum_{i=1}^{m} \left(a_i L^{i\phi(\eta)} + a_{-i} (L)^{-i\phi(\eta)} \right), \tag{6}$$

where a_0 and a_i are unknown constants. Function $\phi'(\eta)$ is expressed as

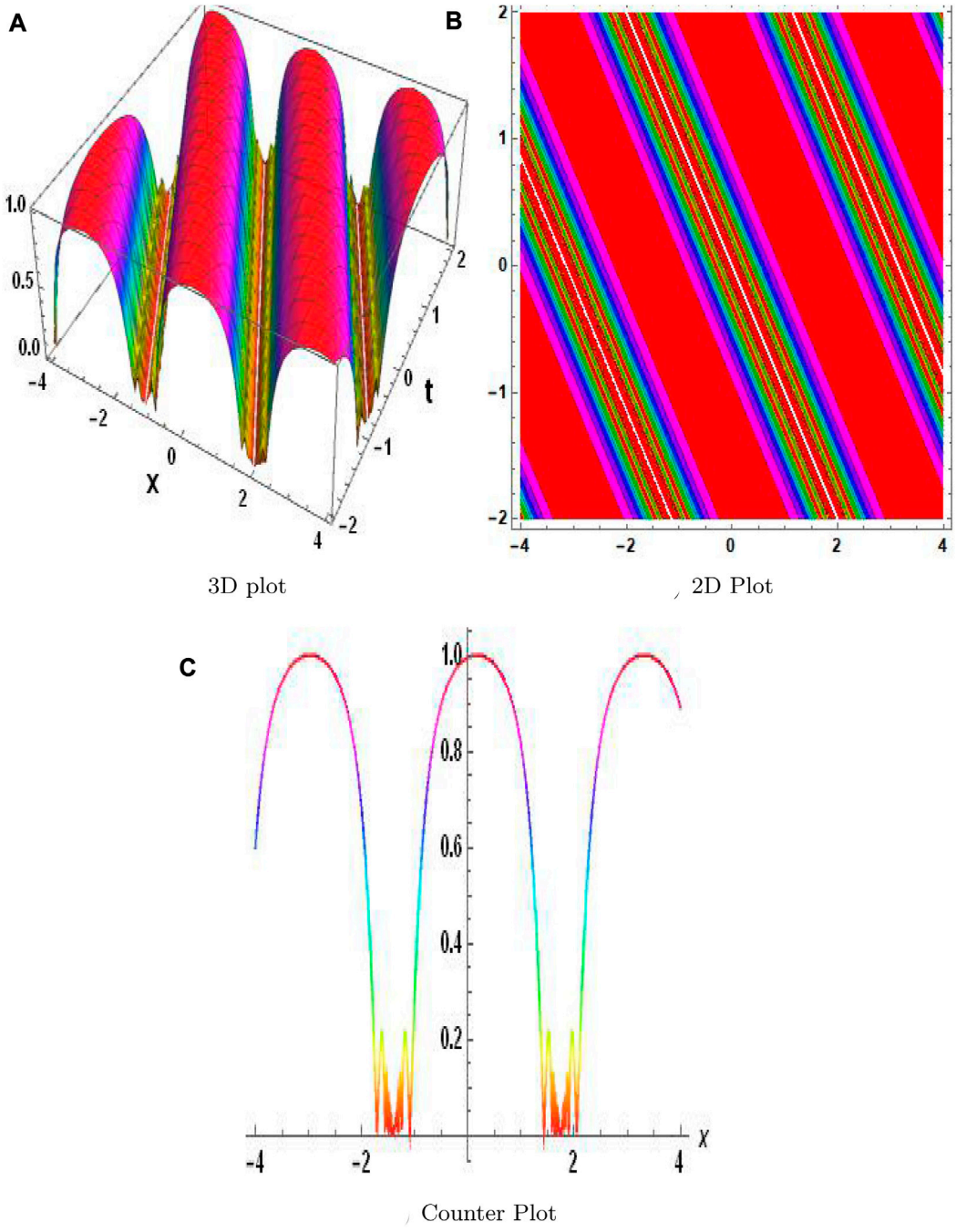

FIGURE 9
Physical depiction of $v_{2,4}$ at $\sigma = -0.3$, $\theta = -1.3$, and $\eta = 0.35$.

$$\phi'(\eta) = \frac{\theta L^{\phi(\eta)} + \vartheta L^{-\phi(\eta)} + \sigma}{\ln(L)}, \tag{7}$$

where σ, θ, and ϑ are arbitrary constants and $L \neq 1$, $L > 0$. On the basis of the (HBP), we may calculate N. The formal solution to Eq. 5 is obtained by replacing the N in Eq. 6. By substituting the ODE Eq. 7 formal solution into Eq. 5 and setting the coefficients of $L^{i\phi(\eta)}$, $i = 0, \pm1, \pm2 \ldots$ to zero, the system of linear equations is produced. The unknown constants a_0, a_i, and a_{-i} can be found by solving this system of equations. The following solutions for auxiliary Eq. 7 are taken into consideration as follows:

Case I: When $\vartheta \neq 0$, $\sigma^2 - 4\theta\vartheta < 0$,

$$L^{\phi(\eta)} = \frac{-\sigma + \sqrt{-\sigma^2 + 4\theta\vartheta}\tan\left(\frac{1}{2}\sqrt{-\sigma^2 + 4\theta\vartheta}\,\eta\right)}{2\vartheta}, \tag{8}$$

or

$$L^{\phi(\eta)} = -\frac{\sigma + \sqrt{-\sigma^2 + 4\theta\vartheta}\cot\left(\frac{1}{2}\sqrt{-\sigma^2 + 4\theta\vartheta}\,\eta\right)}{2\vartheta}. \tag{9}$$

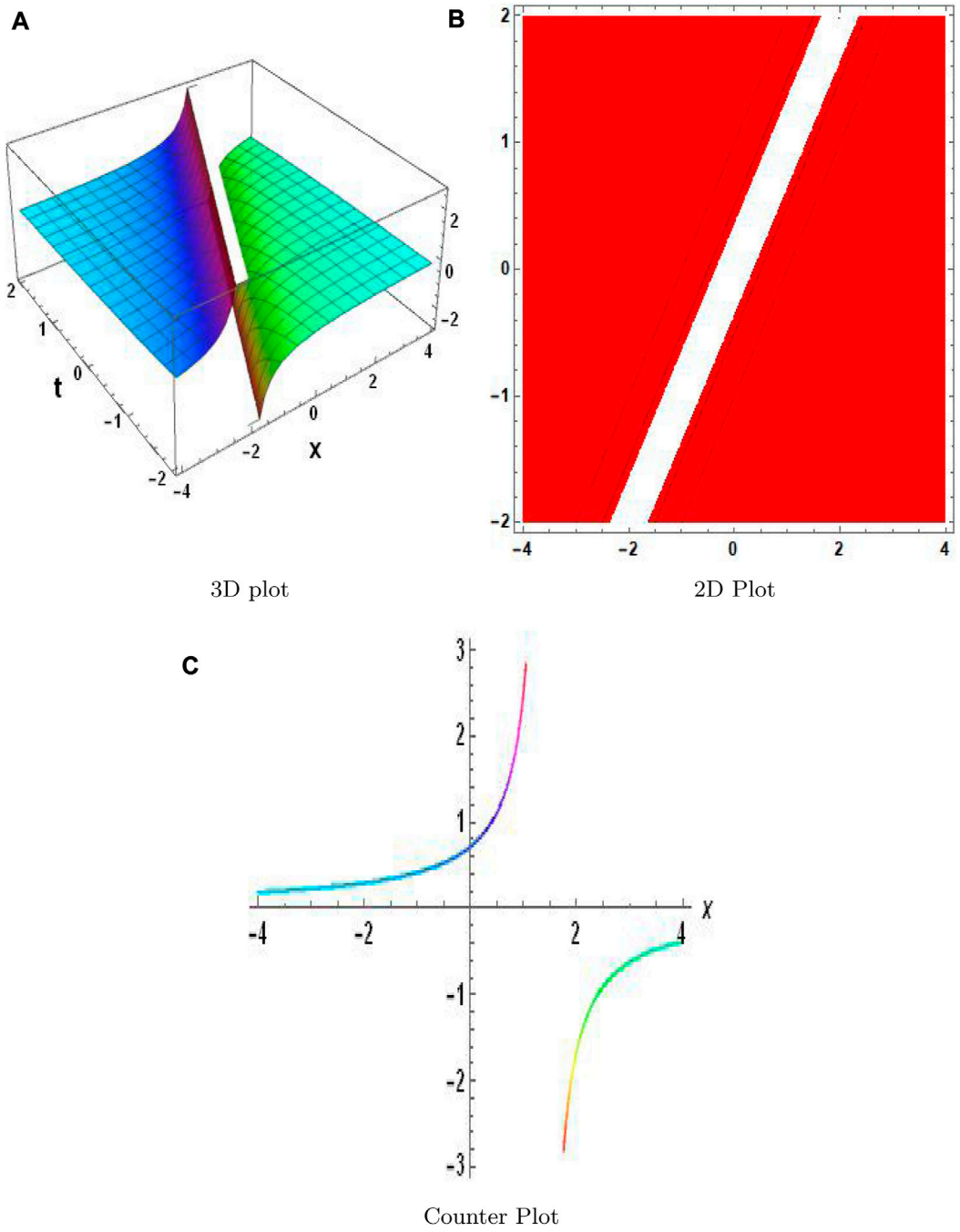

FIGURE 10
Physical depiction of $v_{2,5}$ at $\sigma = 0.4$, $\theta = -1.4$, and $\eta = 0.5$. **(A)** is 3-D plot, **(B)** is 2-D plot, and **(C)** is contour plot.

Case II: When $\vartheta \neq 0$, $\sigma^2 - 4\theta\vartheta > 0$,

$$L^{\phi}(\eta) = -\frac{\sigma + \sqrt{-\sigma^2 + 4\theta\vartheta}\tanh\left(\frac{1}{2}\sqrt{-\sigma^2 + 4\theta\vartheta}\,\eta\right)}{2\vartheta}, \tag{10}$$

or

$$L^{\phi}(\eta) = -\frac{\sigma + \sqrt{-\sigma^2 + 4\theta\vartheta}\coth\left(\frac{1}{2}\sqrt{-\sigma^2 + 4\theta\vartheta}\,\eta\right)}{2\vartheta}. \tag{11}$$

Case III: When $\vartheta \neq 0$, $\sigma^2 - 4\theta\vartheta = 0$,

$$L^{\phi}(\eta) = -\frac{\sigma\eta + 2}{2\vartheta\eta}. \tag{12}$$

By substituting the unknown values for a_0, a_i, a_i and the aforementioned cases into Eq. 6, using transformations from Eq. 4, it is possible to obtain the closed-form solutions to Eq. 1 and Eq. 2.

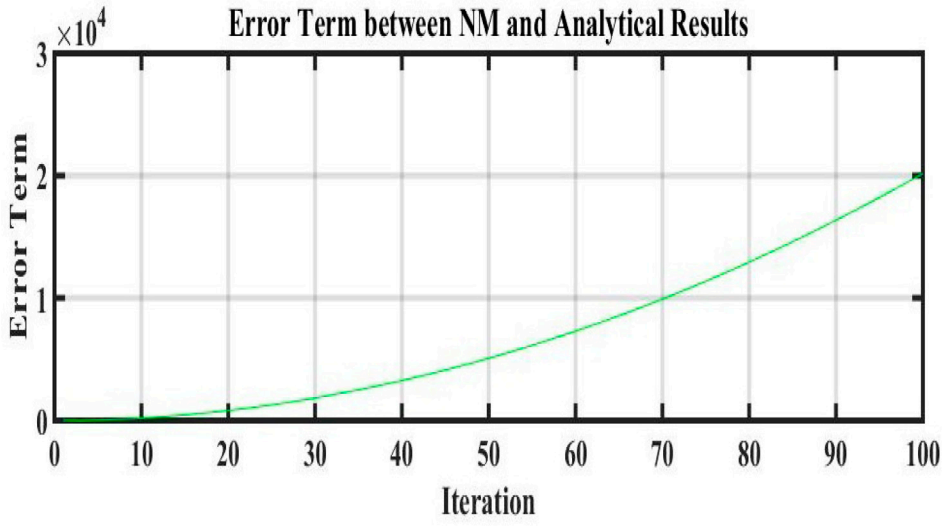

FIGURE 11
Comparison of error terms between numerical and analytical results by using values of Table 1.

2.1.1 Application to the fractional-order nonlinear Gardner equation

The governing Eq. 1 transforms into the following ODE using the following conformable derivative transformation from Eq. 4:

$$-\nu V' + V^{(3)} + 6\left(V - \lambda^2 V^2\right)V' = 0,$$
$$-\nu V + V'' - 2\lambda^2 V^3 + 3V^2 = 0. \tag{13}$$

By changing the degree of the highest-order derivative term and nonlinear with HBP, $N = 1$ is calculated. According to the formal solution in Eq. 13 derived from Eq. 6, we obtain

$$V(\eta) = a_0 + a_1 L^{\phi(\eta)} + \frac{a_{-1}}{L^{\phi(\eta)}}. \tag{14}$$

When Eq. 14 is substituted with Eq. 7 in Eq. 13, the coefficients of powers of $L^{i\phi(\eta)}$, $i = 0, \pm1, \pm2 \ldots$ are set to zero, resulting in a linear equation system. The following sets of solutions are found by using Mathematica software.

Set 1:

$$a_1 = 0, a_{-1} = \frac{\vartheta}{\lambda}, a_0 = 0, \nu = \frac{1}{\lambda^2}, \theta = 0, \sigma = -\frac{1}{\lambda}. \tag{15}$$

Set 2:

$$a_1 = -\frac{1}{16\lambda^3\vartheta}, a_{-1} = -\frac{\vartheta}{\lambda}, a_0 = \frac{1}{2\lambda^2}, \nu = \frac{1}{\lambda^2}, \theta = -\frac{1}{16\lambda^2\vartheta}, \sigma = 0. \tag{16}$$

Set 3:

$$a_1 = \frac{1}{16\lambda^3\vartheta}, a_{-1} = \frac{\vartheta}{\lambda}, a_0 = \frac{1}{2\lambda^2}, \nu = \frac{1}{\lambda^2}, \theta = -\frac{1}{16\lambda^2\vartheta}, \sigma = 0. \tag{17}$$

Set 4:

$$a_1 = 0, a_{-1} = -\frac{\vartheta}{\lambda}, a_0 = \frac{1}{\lambda^2}, \nu = \frac{1}{\lambda^2}, \theta = 0, \sigma = -\frac{1}{\lambda}. \tag{18}$$

Set 5:

$$a_1 = 0, a_{-1} = \frac{\vartheta}{\lambda}, a_0 = \frac{1}{\lambda^2}, \nu = \frac{1}{\lambda^2}, \theta = 0, \sigma = \frac{1}{\lambda}. \tag{19}$$

Family 1. Solutions to Eq. 1 are derived by substituting the values from Set 1 into Eq. 15.

Case I: When $\vartheta \neq 0$, $\sigma^2 - 4\theta\vartheta < 0$,

$$\nu_{1,1} = \frac{2\vartheta^2}{\lambda\left(\sqrt{4\theta\vartheta - \sigma^2}\,\tan\left(\frac{1}{2}\eta\sqrt{4\theta\vartheta - \sigma^2}\right) - \sigma\right)}, \tag{20}$$

or

$$\nu_{1,2} = -\frac{2\vartheta^2}{\lambda\left(\sqrt{4\theta\vartheta - \sigma^2}\,\cot\left(\frac{1}{2}\eta\sqrt{4\theta\vartheta - \sigma^2}\right) + \sigma\right)}. \tag{21}$$

Case II: When $\vartheta \neq 0$, $\sigma^2 - 4\theta\vartheta > 0$,

$$\nu_{1,3} = -\frac{2\vartheta^2}{\lambda\left(\sqrt{4\theta\vartheta - \sigma^2}\tanh\left(\frac{1}{2}\eta\sqrt{4\theta\vartheta - \sigma^2}\right) + \sigma\right)}, \tag{22}$$

or

$$\nu_{1,4} = -\frac{2\vartheta^2}{\lambda\left(\sqrt{4\theta\vartheta - \sigma^2}\coth\left(\frac{1}{2}\eta\sqrt{4\theta\vartheta - \sigma^2}\right) + \sigma\right)}. \tag{23}$$

Case III: When $\vartheta \neq 0$, $\sigma^2 - 4\theta\vartheta = 0$,

$$\nu_{1,5} = -\frac{2\vartheta^2\left(x - \frac{t^\alpha}{\alpha\lambda^2}\right)}{\lambda\left(2 - \frac{x - \frac{t^\alpha}{\alpha\lambda^2}}{\lambda}\right)}. \tag{24}$$

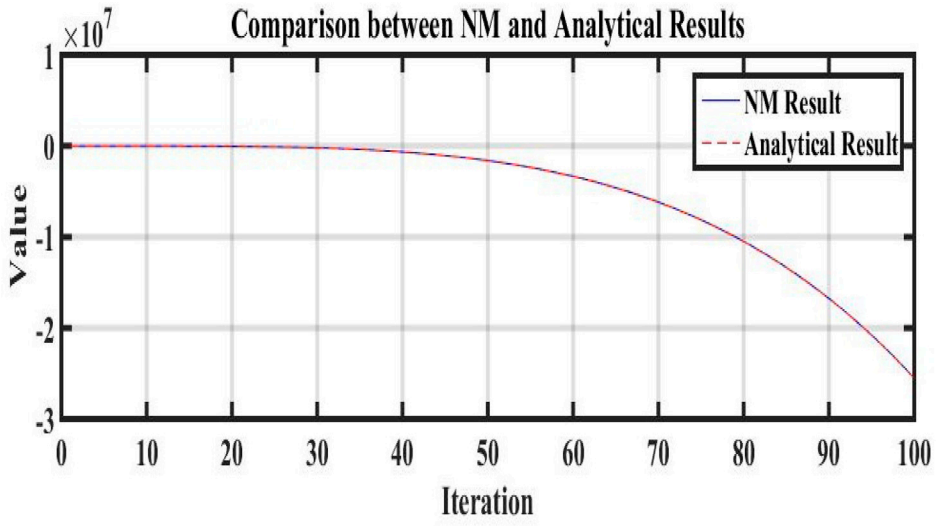

FIGURE 12
Comparison between numerical and analytical results by using values of Table 1.

Family 2. Solutions to Eq. 1 are derived by substituting the values from Set 2 into Eq. 16.

Case I: When $\vartheta \neq 0$, $\sigma^2 - 4\theta\vartheta < 0$,

$$\nu_{1,6} = \frac{1}{2\lambda^2} - \frac{\sqrt{4\theta\vartheta - \sigma^2}\tan\left(\frac{1}{2}\eta\sqrt{4\theta\vartheta - \sigma^2}\right) - \sigma}{32\lambda^3\vartheta^2} - \frac{2\vartheta^2}{\lambda\left(\sqrt{4\theta\vartheta - \sigma^2}\tan\left(\frac{1}{2}\eta\sqrt{4\theta\vartheta - \sigma^2}\right) - \sigma\right)}, \tag{25}$$

or

$$\nu_{1,7} = \frac{1}{2\lambda^2} + \frac{\sqrt{4\theta\vartheta - \sigma^2}\cot\left(\frac{1}{2}\eta\sqrt{4\theta\vartheta - \sigma^2}\right) + \sigma}{32\lambda^3\vartheta^2} + \frac{2\vartheta^2}{\lambda\left(\sqrt{4\theta\vartheta - \sigma^2}\cot\left(\frac{1}{2}\eta\sqrt{4\theta\vartheta - \sigma^2}\right) + \sigma\right)}. \tag{26}$$

Case II: When $\vartheta \neq 0$, $\sigma^2 - 4\theta\vartheta > 0$,

$$\nu_{1,8} = \frac{1}{2\lambda^2} + \frac{\sqrt{4\theta\vartheta - \sigma^2}\tanh\left(\frac{1}{2}\eta\sqrt{4\theta\vartheta - \sigma^2}\right) + \sigma}{32\lambda^3\vartheta^2} + \frac{2\vartheta^2}{\lambda\left(\sqrt{4\theta\vartheta - \sigma^2}\tanh\left(\frac{1}{2}\eta\sqrt{4\theta\vartheta - \sigma^2}\right) + \sigma\right)}, \tag{27}$$

or

$$\nu_{1,9} = \frac{1}{2\lambda^2} + \frac{\sqrt{4\theta\vartheta - \sigma^2}\coth\left(\frac{1}{2}\eta\sqrt{4\theta\vartheta - \sigma^2}\right) + \sigma}{32\lambda^3\vartheta^2} + \frac{2\vartheta^2}{\lambda\left(\sqrt{4\theta\vartheta - \sigma^2}\coth\left(\frac{1}{2}\eta\sqrt{4\theta\vartheta - \sigma^2}\right) + \sigma\right)}. \tag{28}$$

Case III: When $\vartheta \neq 0$, $\sigma^2 - 4\theta\vartheta = 0$,

$$\nu_{1,10} = \frac{1}{2\lambda^2} + \frac{2\vartheta^2\left(x - \frac{t^\alpha}{\alpha\lambda^2}\right)}{\lambda\left(\sigma\left(x - \frac{t^\alpha}{\alpha\lambda^2}\right) + 2\right)} + \frac{\sigma\left(x - \frac{t^\alpha}{\alpha\lambda^2}\right) + 2}{32\lambda^3\vartheta^2\left(x - \frac{t^\alpha}{\alpha\lambda^2}\right)}. \tag{29}$$

2.1.2 Application to the fractional-order nonlinear Cahn–Hilliard equation

The governing Eq. 2 transforms into the following ODE using the traveling wave transformations from Eq. 4:

$$-\nu V' + V^{(4)} - \left(3V^2 - 1\right)V'' - 6VV'^2 - V' = 0.$$

Then, integrating the aforementioned equation, we obtain

$$(-\nu - 1)V + V^{(3)} + \left(1 - 3V^2\right)V' = 0. \tag{30}$$

By adjusting the highest-order derivative term's degree and nonlinear using homogeneous balance principal, $N = 1$ is calculated. According to the formal solution of Eq. 30 derived from Eq. 6, we obtain

$$V(\eta) = a_0 + a_1 L^{\phi(\eta)} + \frac{a_{-1}}{L^{\phi(\eta)}}. \tag{31}$$

When Eq. 31 is substituted with Eq. 7 into Eq. 30, the coefficients of powers of $L^{i\phi(\eta)}$, $i = 0, \pm1, \pm2 \ldots$ are set to zero, resulting in a linear equation system. The following sets of solutions are found using Mathematica software.

Set 1:

$$a_1 = -\frac{5\sqrt{3}}{32\vartheta}, a_{-1} = -\frac{2\vartheta}{\sqrt{3}}, a_0 = \frac{1}{4\sqrt{3}}, \nu = -1, \sigma = 0, \theta = -\frac{15}{64\vartheta}. \tag{32}$$

Set 2:

$$a_1 = 0, a_{-1} = \frac{2\vartheta}{\sqrt{3}}, a_0 = \frac{1}{27}\left(4\sqrt{3} - 5\sqrt{30}\right), \nu = -1, \sigma = \frac{1}{9}\left(5 - 4\sqrt{10}\right), \theta = 0. \tag{33}$$

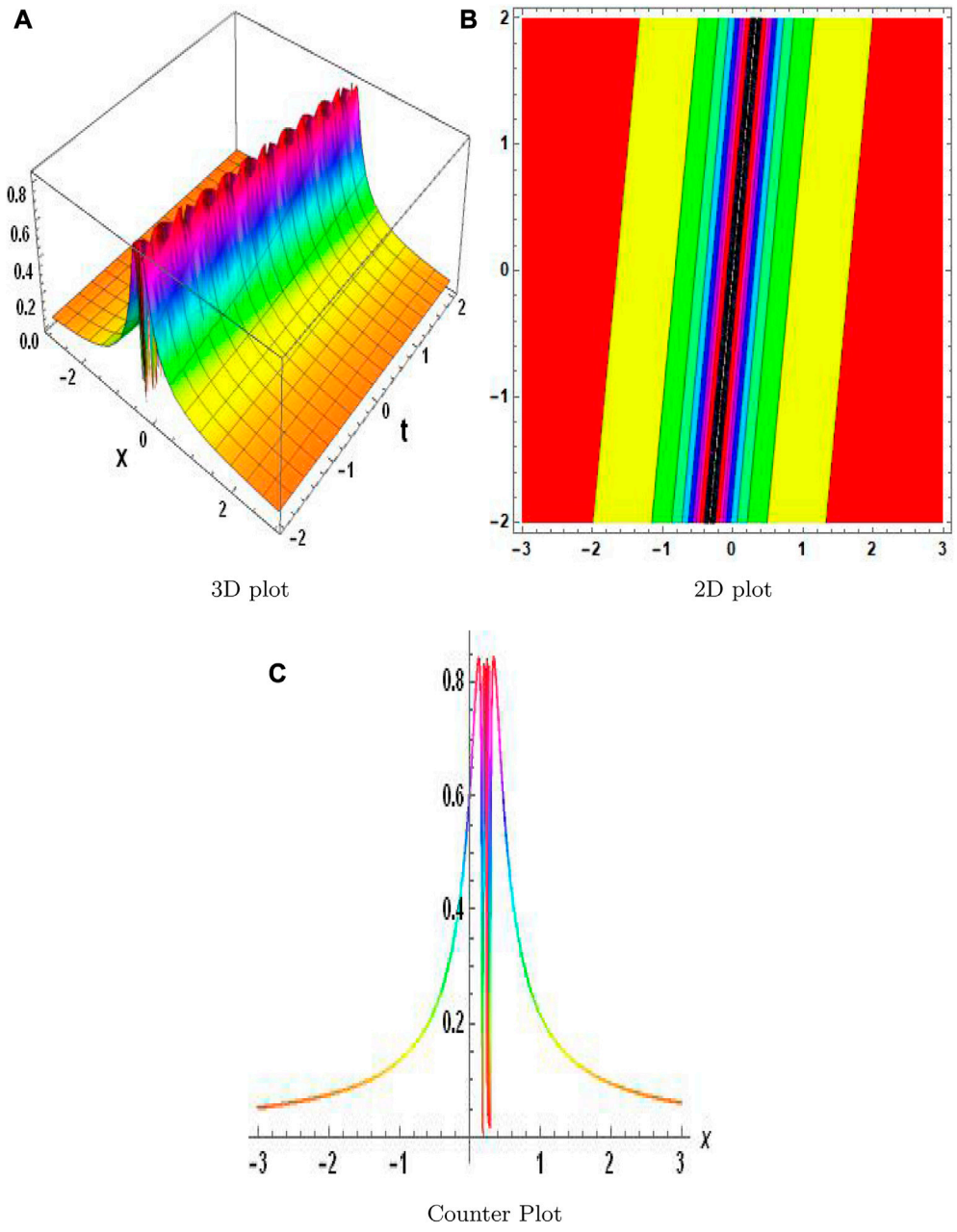

FIGURE 13
Physical depiction of H in Eq. 92 under $\sigma = 0.5$, $v = 2.4$, $\lambda = 1.4$, and $\vartheta = 0.4$.

Set 3:

$$a_1 = \frac{5\sqrt{3}}{32\vartheta}, a_{-1} = \frac{2\vartheta}{\sqrt{3}}, a_0 = -\frac{1}{4\sqrt{3}}, v = -1, \sigma = 0, \theta = -\frac{15}{64\vartheta}.$$

Set 4:

$$a_1 = 0, a_{-1} = \frac{2\vartheta}{\sqrt{3}}, a_0 = \frac{1}{27}\left(4\sqrt{3} + 5\sqrt{30}\right), v = -1,$$
$$\sigma = \frac{1}{9}\left(4\sqrt{10} + 5\right), \theta = 0.$$

Set 5:

$$a_1 = 0, a_{-1} = -\frac{2\vartheta}{\sqrt{3}}, a_0 = \frac{1}{27}\left(5\sqrt{30} - 4\sqrt{3}\right),$$
$$v = -1, \sigma = \frac{1}{9}\left(5 - 4\sqrt{10}\right), \theta = 0.$$

Family 1. Solutions to Eq. 2 are derived by substituting the values from Set 1 into Eq. 32.

Case I: When $\vartheta \neq 0$, $\sigma^2 - 4\theta\vartheta < 0$,

$$v_{2,1} = \frac{1}{4\sqrt{3}} - \frac{4\vartheta^2}{\sqrt{3}\left(\sqrt{4\theta\vartheta-\sigma^2}\,\tan\left(\frac{1}{2}\eta\sqrt{4\theta\vartheta-\sigma^2}\right)-\sigma\right)} - \frac{5\sqrt{3}\left(\sqrt{4\theta\vartheta-\sigma^2}\,\tan\left(\frac{1}{2}\eta\sqrt{4\theta\vartheta-\sigma^2}\right)-\sigma\right)}{64\vartheta^2}, \tag{34}$$

or

$$v_{2,2} = \frac{1}{4\sqrt{3}} + \frac{4\vartheta^2}{\sqrt{3}\left(\sqrt{4\theta\vartheta-\sigma^2}\,\cot\left(\frac{1}{2}\eta\sqrt{4\theta\vartheta-\sigma^2}\right)+\sigma\right)} + \frac{5\sqrt{3}\left(\sqrt{4\theta\vartheta-\sigma^2}\,\cot\left(\frac{1}{2}\eta\sqrt{4\theta\vartheta-\sigma^2}\right)+\sigma\right)}{64\vartheta^2}. \tag{35}$$

Case II: When $\vartheta \neq 0$, $\sigma^2 - 4\theta\vartheta > 0$,

$$v_{2,3} = \frac{1}{4\sqrt{3}} + \frac{4\vartheta^2}{\sqrt{3}\left(\sqrt{4\theta\vartheta-\sigma^2}\tanh\left(\frac{1}{2}\eta\sqrt{4\theta\vartheta-\sigma^2}\right)+\sigma\right)} + \frac{5\sqrt{3}\left(\sqrt{4\theta\vartheta-\sigma^2}\tanh\left(\frac{1}{2}\eta\sqrt{4\theta\vartheta-\sigma^2}\right)+\sigma\right)}{64\vartheta^2}, \tag{36}$$

or

$$v_{2,4} = \frac{1}{4\sqrt{3}} + \frac{4\vartheta^2}{\sqrt{3}\left(\sqrt{4\theta\vartheta-\sigma^2}\coth\left(\frac{1}{2}\eta\sqrt{4\theta\vartheta-\sigma^2}\right)+\sigma\right)} + \frac{5\sqrt{3}\left(\sqrt{4\theta\vartheta-\sigma^2}\coth\left(\frac{1}{2}\eta\sqrt{4\theta\vartheta-\sigma^2}\right)+\sigma\right)}{64\vartheta^2}. \tag{37}$$

Case III: When $\vartheta \neq 0$, $\sigma^2 - 4\theta\vartheta = 0$,

$$v_{2,5} = \frac{1}{4\sqrt{3}} + \frac{4\eta\vartheta^2}{\sqrt{3}(\eta\sigma+2)} + \frac{5\sqrt{3}(\eta\sigma+2)}{64\eta\vartheta^2}. \tag{38}$$

3 Numerical investigation using the fractional conformable residual power series algorithm

In this section, a newly developed approach is utilized to produce accurate approximations of the time-fractional equations supplied with a given initial condition inside a finite spatiotemporal domain [34]. This approach uses a newly designed algorithm. Let us consider the following nonlinear time-fractional equations to achieve our goal:

$$\partial_t^\alpha w(x,t) + N\left(w, w^2, w_x, w_{xx}\right) + \ldots = 0, \tag{39}$$

with an initial condition

$$w(x,0) = w_0(x). \tag{40}$$

The numerical simulation that is being provided assumes that the solution to Eqs 39, 40 has a multiple time-fractional series (MTFS) expansion of approximately $t_0 = 0$ of the following form:

$$w(x,t) = \sum_{i=1}^{m} \frac{t^{i\alpha}\zeta_i(x)}{i!\alpha^i}. \tag{41}$$

The mth truncated solution of $w(x, t)$ of Eq. 40 is defined as

$$w_m = \zeta_0(x) + \sum_{i=1}^{m} \frac{t^{i\alpha}\zeta_i(x)}{i!\alpha^i}. \tag{42}$$

Initially, the residual error $R_s(x, t)$ of Eqs 39, 40 is given as

$$\mathcal{R}_s(x,t) = \partial_t^\alpha w(x,t) + N\left(w, w^2, w_x, w_{xx}\right) + \ldots. \tag{43}$$

The $R_s(x, t)$ mth residual error should be truncated so that

$$\mathcal{R}_s^m(x,t) = \partial_t^\alpha w_m(x,t) + N\left(w_m, w_m^2, w_{x,m}, w_{xx,m}\right) + \ldots. \tag{44}$$

By replacing the mth truncated residual error in Eq. 44 with the truncated MTFS solution in Eq. 42, we obtain

$$\begin{aligned}\partial_t^{\alpha(m-1)}\mathcal{R}_s^2(x,t) = \partial_t^{m\alpha}&\left(\zeta_0(x) + \sum_{i=1}^{m}\frac{t^{i\alpha}\zeta_i(x)}{i!\alpha^i}\right) + N\left(\left(\sum_{i=1}^{m}\frac{t^{i\alpha}\zeta_i(x)}{i!\alpha^i} + \zeta_0(x)\right)\right),\\ &N\left(\left(\sum_{i=1}^{m}\frac{t^{i\alpha}\zeta_i(x)}{i!\alpha^i} + \zeta_0(x)\right)^2,\right.\\ &\left(\sum_{i=1}^{m}\frac{t^{i\alpha}\zeta_i(x)}{i!\alpha^i} + \zeta_0(x)\right)_x,\\ &\left.\left(\sum_{i=1}^{m}\frac{t^{i\alpha}\zeta_i(x)}{i!\alpha^i} + \zeta_0(x)\right)_{xx}\right) + \ldots.\end{aligned} \tag{45}$$

To make the major steps of the provided FCRPSA in determining the m-term truncated solution's unknown coefficients $\zeta_i(x)$ more clear (Eq. 42), set $m = 1$ and equate $R_s^1(x,t)$ to zero at $t = 0$. Therefore, $\zeta_1(x)$ is obtained. Thereafter, set $m = 2$, apply operator ∂_t^α on both sides of the resulting relevant equation, and solve $\partial_t^\alpha \mathcal{R}_s^2(x,0)$. Then, $\zeta_2(x)$ is also obtained. The unknown coefficient $\zeta_i(x)$ of the MTFS expansion would be discovered if we continue solving in this manner (Eq. 42).

3.1 Numerical simulation of the fractional-order nonlinear Gardner equation

Let us consider the equation

$$D_t^\alpha(x,t) + 6\left(w - \lambda^2 w^2\right)\frac{\partial w}{\partial x} - \frac{\partial^3 w}{\partial x^3} = 0, \tag{46}$$

with an initial condition

$$w(0,t) = \frac{1}{2}\tanh\left(\frac{x}{2}\right) + \frac{1}{2}. \tag{47}$$

We use the fractional conformable residual power series algorithm to solve this equation. For this, the m-truncated term is taken as

$$w_m = \zeta_0(x) + \sum_{i=1}^{m}\frac{t^{i\alpha}\zeta_i(x)}{i!\alpha^i}, \tag{48}$$

and the residual error function is

$$\mathcal{R}_s^m(x,t) = \frac{\partial^\alpha w_m}{\partial t} + 6w_m - \lambda^2 w_m^2\frac{\partial w_m}{\partial x} + \frac{\partial^3 w_m}{\partial x^3}. \tag{49}$$

For m = 0,

$$w_0(x,t) = \frac{1}{2}\tanh\left(\frac{x}{2}\right) + \frac{1}{2}.$$

For m = 1, the truncated term is

$$w_1(x,t) = \zeta_0(x) + \frac{\zeta_1(x)t^\alpha}{\alpha}, \tag{50}$$

$$\zeta_0(x) = w_0(x,t) = \frac{1}{2}\tanh\left(\frac{x}{2}\right) + \frac{1}{2}, \tag{51}$$

$$w_1(x,t) = \frac{1}{2}\tanh\left(\frac{x}{2}\right) + \frac{1}{2} + \frac{\zeta_1(x)t^\alpha}{\alpha}. \tag{52}$$

Therefore, the first residual error function is

$$\mathcal{R}_s^1(x,t) = \frac{\partial^\alpha w_1}{\partial t} + 6w_1 - \lambda^2 w_1^2\frac{\partial w_1}{\partial x} + \frac{\partial^3 w_1}{\partial x^3}. \tag{53}$$

Substituting Eq. 50 into Eq. 53,we obtain

$$\mathcal{R}_s^1(x,t) = 6\left(\left(\frac{t^\alpha\zeta_1(x)}{\alpha} + \zeta_0(x)\right) - \lambda^2\left(\frac{t^\alpha\zeta_1(x)}{\alpha} + \zeta_0(x)\right)^2\right)\left(\frac{t^\alpha\zeta_1'(x)}{\alpha} + \zeta_0'(x)\right) + \left(\frac{t^\alpha\zeta_1^3(x)}{\alpha} + \zeta_0^3(x)\right) + \zeta_1(x). \tag{54}$$

Thus, $R_s^1(x,t)$ at t = 0 results in

$$6\left(\zeta_0(x) - \lambda^2\zeta_0(x)^2\right)\zeta_0'(x) + \zeta_0^3(x) + \zeta_1(x) = 0, \tag{55}$$

$$\zeta_1(x) = \frac{1}{8}\mathrm{sech}^4\left(\frac{x}{2}\right)\left(3\left(\lambda^2-1\right)\sinh(x) + \left(3\lambda^2-4\right)\cosh(x) - 1\right). \tag{56}$$

So, the first series solution $w_1(x, t)$ is provided by

$$w_1(x,t) = \frac{1}{2} + \frac{1}{2}\tanh\left(\frac{x}{2}\right) + \frac{1}{8}\mathrm{sech}^4\left(\frac{x}{2}\right) \times \left(3\left(\lambda^2-1\right)\sinh(x) + \left(3\lambda^2-4\right)\cosh(x) - 1\right)\frac{t^\alpha}{\alpha}. \tag{57}$$

For m = 2, the truncated term is

$$w_2(x,t) = \frac{\zeta_2(x)t^{2\alpha}}{2\alpha^2} + \frac{\zeta_1(x)t^\alpha}{\alpha} + \zeta_0(x), \tag{58}$$

$$w_2(x,t) = \frac{1}{2} + \frac{1}{2}\tanh\left(\frac{x}{2}\right) + \frac{1}{8}\mathrm{sech}^4\left(\frac{x}{2}\right) \times \left(3\left(\lambda^2-1\right)\sinh(x) + \left(3\lambda^2-4\right)\cosh(x) - 1\right)\frac{t^\alpha}{\alpha} + \frac{\zeta_2(x)t^{2\alpha}}{2\alpha^2}, \tag{59}$$

and the second residual error function is obtained by substituting Eq. 58 into Eq. 59

$$\begin{aligned}\mathcal{R}_s^2(x,t) = {} & \frac{\partial^\alpha}{\partial t}\left(\frac{t^{2\alpha}\zeta_2(x)}{2\alpha^2} + \frac{t^\alpha\zeta_1(x)}{\alpha} + \zeta_0(x)\right) \\ & + 6\left(\left(\frac{t^{2\alpha}\zeta_2(x)}{2\alpha^2} + \frac{t^\alpha\zeta_1(x)}{\alpha} + \zeta_0(x)\right)\right. \\ & \left.-\lambda^2\left(\frac{t^{2\alpha}\zeta_2(x)}{2\alpha^2} + \frac{t^\alpha\zeta_1(x)}{\alpha} + \zeta_0(x)\right)^2\right) \\ & \frac{\partial^2}{\partial x^2}\left(\frac{t^{2\alpha}\zeta_2(x)}{2\alpha^2} + \frac{t^\alpha\zeta_1(x)}{\alpha} + \zeta_0(x)\right) \\ & + \frac{\partial^3}{\partial x^3}\left(\frac{t^{2\alpha}\zeta_2(x)}{2\alpha^2} + \frac{t^\alpha\zeta_1(x)}{\alpha} + \zeta_0(x)\right),\end{aligned} \tag{60}$$

$$\begin{aligned}\mathcal{R}_s^2(x,t) = {} & \left(\frac{t^\alpha\zeta_2(x)}{\alpha} + \zeta_1(x)\right) \\ & + 6\left(\left(\frac{t^{2\alpha}\zeta_2(x)}{2\alpha^2} + \frac{t^\alpha\zeta_1(x)}{\alpha} + \zeta_0(x)\right)\right. \\ & \left.-6\lambda^2\left(\frac{t^{2\alpha}\zeta_2(x)}{2\alpha^2} + \frac{t^\alpha\zeta_1(x)}{\alpha} + \zeta_0(x)\right)^2\right) \\ & \left(\frac{t^{2\alpha}\zeta_2'(x)}{2\alpha^2} + \frac{t^\alpha\zeta_1'(x)}{\alpha} + \zeta_0'(x)\right) \\ & + \left(\frac{t^{2\alpha}\zeta_2^3(x)}{2\alpha^2} + \frac{t^\alpha\zeta_1^3(x)}{\alpha} + \zeta_0^3(x)\right).\end{aligned} \tag{61}$$

Then, d^α/dt is applied on both sides of Eq. 61 and thus at t = 0, we obtain

$$\begin{aligned}\left(-\zeta_1^3(x)\right)\left(\zeta_2(x)\right. = {} & 12\lambda^2\zeta_0(x)\zeta_1(x)\zeta_0'(x) + 6\lambda^2\zeta_0(x)^2\zeta_1'(x) \\ & \left.-6\zeta_1(x)\zeta_0'(x) - 6\zeta_0(x)\zeta_1'(x)\right),\end{aligned} \tag{62}$$

$$\begin{aligned}\zeta_2(x) = {} & -\frac{1}{64}\mathrm{sech}^7\left(\frac{x}{2}\right)\left(18\lambda^4\cosh\left(\frac{5x}{2}\right) - 42\lambda^2\cosh\left(\frac{5x}{2}\right)\right. \\ & \left.-24\left(\lambda^2-1\right)\cosh\left(\frac{x}{2}\right)\right) - \frac{1}{64}\mathrm{sech}^7\left(\frac{x}{2}\right) \\ & \left(-6\left(15\lambda^4 - 37\lambda^2 + 22\right)\cosh\left(\frac{3x}{2}\right) + 24\cosh\left(\frac{5x}{2}\right)\right) \\ & -\frac{1}{64}\mathrm{sech}^7\left(\frac{x}{2}\right)\left(-204\lambda^2\sinh\left(\frac{x}{2}\right) + 222\lambda^2\sinh\left(\frac{3x}{2}\right)\right. \\ & \left.+206\sinh\left(\frac{x}{2}\right) - 129\sinh\left(\frac{3x}{2}\right)\right) - \frac{1}{64}\mathrm{sech}^7\left(\frac{x}{2}\right) \\ & \left(-90\lambda^4\sinh\left(\frac{3x}{2}\right) + 18\lambda^4\sinh\left(\frac{5x}{2}\right) - 42\lambda^2\sinh\left(\frac{5x}{2}\right)\right. \\ & \left.+25\sinh\left(\frac{5x}{2}\right)\right),\end{aligned} \tag{63}$$

$$\begin{aligned}w_2(x,t) = {} & \frac{1}{2} + \frac{1}{2}\tanh\left(\frac{x}{2}\right) + \frac{1}{8}\mathrm{sech}^4\left(\frac{x}{2}\right)\left(3\left(\lambda^2-1\right)\sinh(x)\right. \\ & \left.+\left(3\lambda^2-4\right)\cosh(x) - 1\right)\frac{t^\alpha}{\alpha} - \frac{1}{64}\mathrm{sech}^7\left(\frac{x}{2}\right) \\ & \left(18\lambda^4\cosh\left(\frac{5x}{2}\right) - 42\lambda^2\cosh\left(\frac{5x}{2}\right)\right. \\ & \left.-24\left(\lambda^2-1\right)\cosh\left(\frac{x}{2}\right)\right) - \frac{1}{64}\mathrm{sech}^7\left(\frac{x}{2}\right) \\ & \left(-6\left(15\lambda^4 - 37\lambda^2 + 22\right)\cosh\left(\frac{3x}{2}\right) + 24\cosh\left(\frac{5x}{2}\right)\right) \\ & -\frac{1}{64}\mathrm{sech}^7\left(\frac{x}{2}\right)\left(-204\lambda^2\sinh\left(\frac{x}{2}\right) + 222\lambda^2\sinh\left(\frac{3x}{2}\right)\right. \\ & \left.+206\sinh\left(\frac{x}{2}\right) - 129\sinh\left(\frac{3x}{2}\right)\right) - \frac{1}{64}\mathrm{sech}^7\left(\frac{x}{2}\right) \\ & \left(-90\lambda^4\sinh\left(\frac{3x}{2}\right) + 18\lambda^4\sinh\left(\frac{5x}{2}\right) - 42\lambda^2\sinh\left(\frac{5x}{2}\right)\right. \\ & \left.+25\sinh\left(\frac{5x}{2}\right)\right)\frac{t^{2\alpha}}{2\alpha^2}.\end{aligned} \tag{64}$$

Similarly, through this process, we obtain

$$w_n(x,t) = \frac{1}{2} + \frac{1}{2}\tanh\left(\frac{x}{2}\right) + \frac{1}{8}\operatorname{sech}^4\left(\frac{x}{2}\right)\left(3\left(\lambda^2-1\right)\sinh(x) + \left(3\lambda^2-4\right)\cosh(x) - 1\right)\frac{t^\alpha}{\alpha} - \frac{1}{64}\operatorname{sech}^7\left(\frac{x}{2}\right)\left(18\lambda^4\cosh\left(\frac{5x}{2}\right) - 42\lambda^2\cosh\left(\frac{5x}{2}\right) - 24\left(\lambda^2-1\right)\cosh\left(\frac{x}{2}\right)\right) - \frac{1}{64}\operatorname{sech}^7\left(\frac{x}{2}\right)\left(-6\left(15\lambda^4 - 37\lambda^2 + 22\right)\cosh\left(\frac{3x}{2}\right) + 24\cosh\left(\frac{5x}{2}\right)\right) - \frac{1}{64}\operatorname{sech}^7\left(\frac{x}{2}\right)\left(-204\lambda^2\sinh\left(\frac{x}{2}\right) + 222\lambda^2\sinh\left(\frac{3x}{2}\right) + +206\sinh\left(\frac{x}{2}\right)\right)\frac{t^{2\alpha}}{2\alpha^2} + \ldots. \tag{65}$$

If $\alpha = 1$, we obtain the exact solution

$$w(x,t) = \frac{1}{2}\tanh\left(\frac{x-t}{2}\right) + \frac{1}{2}. \tag{66}$$

3.2 Numerical simulation of the fractional-order nonlinear Cahn–Hilliard equation

Let us consider the equation

$$\frac{\partial^\alpha w}{\partial t} = \frac{\partial w}{\partial x} - 6w\left(\frac{\partial w}{\partial x}\right)^2 + \left(3w^2-1\right)\frac{\partial^2 w}{\partial x^2} - \frac{\partial^4 w}{\partial x^4}, \tag{67}$$

with an initial condition

$$w(x,0) = \tanh\left(\frac{\sqrt{2}\,x}{2}\right). \tag{68}$$

We use the fractional conformable residual power series algorithm for solving this equation. For this, the m-truncated term is

$$w_m = \zeta_0(x) + \sum_{i=1}^{m}\frac{t^{i\alpha}\zeta_i(x)}{i!\alpha^i}, \tag{69}$$

and the residual error function is

$$\mathcal{R}_s^m(x,t) = \frac{\partial^\alpha w_m}{\partial t} - \frac{\partial w_m}{\partial x} - 6w_m\left(\frac{\partial w_m}{\partial x}\right)^2 - 3w_m^2 - 1\frac{\partial^2 w_m}{\partial x^2} + \frac{\partial^4 w_m}{\partial x^4}. \tag{70}$$

For m = 0,

$$w_0(x,t) = \tanh\left(\frac{\sqrt{2}\,x}{2}\right).$$

For m = 1, the truncated term is

$$w_1(x,t) = \zeta_0(x) + \frac{\zeta_1(x)t^\alpha}{\alpha}, \tag{71}$$

$$\zeta_0(x) = w_0(x,t) = \tanh\left(\frac{\sqrt{2}\,x}{2}\right), \tag{72}$$

$$w_1(x,t) = \tanh\left(\frac{\sqrt{2}\,x}{2}\right) + \frac{\zeta_1(x)t^\alpha}{\alpha}. \tag{73}$$

Therefore, the first residual error function is

$$\mathcal{R}_s^1(x,t) = \frac{\partial^\alpha w_1}{\partial t} - w_1 - 6w_1\left(\frac{\partial w_1}{\partial x}\right)^2 - \left(3w_1^2-1\right)\frac{\partial^2 w_1}{\partial x^2} + \frac{\partial^4 w_1}{\partial x^4}. \tag{74}$$

Substituting Eq. 71 into Eq. 74, we obtain

$$\mathcal{R}_s^1(x,t) = \frac{\partial^\alpha}{\partial t}\left(\frac{\zeta_1(x)t^\alpha}{\alpha} + \zeta_0(x)\right) - \frac{\partial}{\partial x}\left(\zeta_0(x) + \frac{\zeta_1(x)t^\alpha}{\alpha}\right) - 6\left(\zeta_0(x) + \frac{\zeta_1(x)t^\alpha}{\alpha}\right)\left(\frac{\partial}{\partial x}\zeta_0 + \frac{\zeta_1 x t^\alpha}{\alpha}\right)^2 - \left(3\left(\zeta_0(x) + \frac{\zeta_1 x t^\alpha}{\alpha}\right)^2 - 1\right)\frac{\partial^2}{\partial x^2}\left(\frac{\zeta_1(x)t^\alpha}{\alpha} + \zeta_0(x)\right) + \frac{\partial^4}{\partial x^4}\left(\zeta_0(x) + \frac{\zeta_1(x)t^\alpha}{\alpha}\right). \tag{75}$$

Thus, $R_s^1(x,t)$ at t = 0,

$$-6\zeta_0(x)\zeta_0'(x)^2 - \left(3\zeta_0(x)^2 - 1\right)\zeta_0''(x) - \zeta_0(x) + \zeta_0^4(x) + \zeta_1(x) = 0, \tag{76}$$

$$\zeta_1(x) = \frac{\operatorname{sech}^2\left(\frac{x}{\sqrt{2}}\right)}{\sqrt{2}}. \tag{77}$$

Therefore, the first series solution $w_1(x, t)$ is provided by

$$w_1(x,t) = \tanh\left(\frac{\sqrt{2}\,x}{2}\right) + \frac{\operatorname{sech}^2\left(\frac{x}{\sqrt{2}}\right)}{\sqrt{2}}\frac{t^\alpha}{\alpha}. \tag{78}$$

For m = 2, the truncated term is

$$w_2(x,t) = \frac{\zeta_2(x)t^{2\alpha}}{2\alpha^2} + \frac{\zeta_1(x)t^\alpha}{\alpha} + \zeta_0(x), \tag{79}$$

$$w_2(x,t) = \tanh\left(\frac{\sqrt{2}\,x}{2}\right) + \frac{\operatorname{sech}^2\left(\frac{x}{\sqrt{2}}\right)}{\sqrt{2}}\frac{t^\alpha}{\alpha} + \frac{\zeta_2(x)t^{2\alpha}}{2\alpha^2}. \tag{80}$$

Substituting Eq. 79 into Eq. 80, the second residual error function is

$$\mathcal{R}_s^2(x,t) = \frac{\partial^\alpha}{\partial t}\left(\frac{t^{2\alpha}\zeta_2(x)}{2\alpha^2} + \frac{t^\alpha\zeta_1(x)}{\alpha} + \zeta_0(x)\right) - \frac{\partial}{\partial x}\left(\frac{t^{2\alpha}\zeta_2(x)}{2\alpha^2} + \frac{t^\alpha\zeta_1(x)}{\alpha} + \zeta_0(x)\right) - 6\left(\frac{t^{2\alpha}\zeta_2(x)}{2\alpha^2} + \frac{\zeta_1 x t^\alpha}{\alpha} + \zeta_0(x)\right)\frac{\partial}{\partial x}\left(\frac{t^{2\alpha}\zeta_2(x)}{2\alpha^2} + \frac{t^\alpha\zeta_1(x)}{\alpha} + \zeta_0(x)\right)^2 - \left(3\left(\frac{t^{2\alpha}\zeta_2(x)}{2\alpha^2} + \frac{\zeta_1 x t^\alpha}{\alpha} + \zeta_0(x)\right)^2 - 1\right)\frac{\partial^2}{\partial x^2}\left(\frac{t^{2\alpha}\zeta_2(x)}{2\alpha^2} + \frac{t^\alpha\zeta_1(x)}{\alpha} + \zeta_0(x)\right) + \frac{\partial^4}{\partial x^4}\left(\frac{t^{2\alpha}\zeta_2(x)}{2\alpha^2} + \frac{\zeta_1 x t^\alpha}{\alpha} + \zeta_0(x)\right), \tag{81}$$

$$\mathcal{R}_s^2(x,t) = \left(\frac{t^\alpha \zeta_2(x)}{\alpha} + \zeta_1(x)\right) - \left(\frac{t^{2\alpha}\zeta_2'(x)}{2\alpha^2} + \frac{t^\alpha \zeta_1'(x)}{\alpha} + \zeta_0'(x)\right) - 6\left(\frac{t^{2\alpha}\zeta_2(x)}{2\alpha^2} + \frac{t^\alpha \zeta_1(x)}{\alpha} + \zeta_0(x)\right)\left(\frac{t^{2\alpha}\zeta_2'(x)}{2\alpha^2} + \frac{t^\alpha \zeta_1'(x)}{\alpha} + \zeta_0'(x)\right)^2 - \left(3\left(\frac{t^{2\alpha}\zeta_2(x)}{2\alpha^2} + \frac{t^\alpha \zeta_1(x)}{\alpha} + \zeta_0(x)\right)^2 - 1\right)\left(\frac{t^{2\alpha}\zeta_2''(x)}{2\alpha^2} + \frac{t^\alpha \zeta_1''(x)}{\alpha} + \zeta_0''(x)\right) + \left(\frac{t^{2\alpha}\zeta_2^4(x)}{2\alpha^2} + \frac{t^\alpha \zeta_1^4(x)}{\alpha} + \zeta_0^4(x)\right). \tag{82}$$

Then, d^α/dt is applied on both sides of Eq. 82 and thus at t = 0, we obtain

$$\zeta_2(x) = 12\zeta_0(x)\zeta_0'(x)\zeta_1'(x) + 6\zeta_1(x)\zeta_0'(x)^2 + 3\zeta_0(x)^2\zeta_1''(x) + 6\zeta_1(x)\zeta_0(x)\zeta_0''(x) - \zeta_1''(x) + \zeta_1(x) - \zeta_1^4(x), \tag{83}$$

$$\zeta_2(x) = \tanh\left(\frac{x}{\sqrt{2}}\right)\left(-\operatorname{sech}^2\left(\frac{x}{\sqrt{2}}\right)\right), \tag{84}$$

$$w_2(x,t) = \frac{t^{2\alpha}\tanh\left(\frac{x}{\sqrt{2}}\right)\left(-\operatorname{sech}^2\left(\frac{x}{\sqrt{2}}\right)\right)}{2\alpha^2} + \frac{t^\alpha \operatorname{sech}^2\left(\frac{x}{\sqrt{2}}\right)}{\sqrt{2}\alpha} + \tanh\left(\frac{\sqrt{2}\,x}{2}\right). \tag{85}$$

Similarly, through this process, we obtain

$$w_3(x,t) = \frac{1}{16}\operatorname{sech}^6\left(\frac{x}{\sqrt{2}}\right)\left(\tanh\left(\frac{x}{\sqrt{2}}\right)\left(\sqrt{2}\sinh\left(2\sqrt{2}\,x\right)\right)\right) \frac{1}{16}\operatorname{sech}^6\left(\frac{x}{\sqrt{2}}\right)\left(\left(-224\cosh\left(\sqrt{2}\,x\right) + 4\cosh\left(2\sqrt{2}\,x\right) + 492\right) - 4\sqrt{2}\right), \tag{86}$$

$$w_n(x,t) = \frac{t^{2\alpha}\tanh\left(\frac{x}{\sqrt{2}}\right)\left(-\operatorname{sech}^2\left(\frac{x}{\sqrt{2}}\right)\right)}{2\alpha^2} + \frac{t^\alpha \operatorname{sech}^2\left(\frac{x}{\sqrt{2}}\right)}{\sqrt{2}\alpha} + \tanh\left(\frac{\sqrt{2}\,x}{2}\right) + \frac{1}{16}\operatorname{sech}^6\left(\frac{x}{\sqrt{2}}\right)\left(\tanh\left(\frac{x}{\sqrt{2}}\right)\left(\sqrt{2}\sinh\left(2\sqrt{2}\,x\right) - 224\cosh\left(\sqrt{2}\,x\right) + 4\cosh\left(2\sqrt{2}\,x\right) + 492\right) - 4\sqrt{2}\right) + \ldots. \tag{87}$$

If $\alpha = 1$, we obtain the exact solution

$$w(x,t) = \tanh\left(\frac{\sqrt{2}\,(x+t)}{2}\right). \tag{88}$$

4 Stability analysis

In this section, we examine the stability property [35] for Eqs 1, 2. Understanding the stability of an equilibrium solution may be gained by linearizing the FNLPDE around it. In order to investigate the rise or decay of minor perturbations, eigenvalue analysis is performed on the linearized equation, which has fractional derivatives. By solving the characteristic equation linked to the linearized system, the eigenvalues may be found. The equilibrium is stable if all of the eigenvalues have negative real portions; otherwise, it is unstable. Nevertheless, it is crucial to keep in mind that the fractional character of the derivatives makes the eigenvalue analysis more complicated. A Hamiltonian system is used to investigate the stability feature of the nonlinear fractional equations. The Hamiltonian system's momentum is represented using the following formula:

$$H = 1\Big/2\int_{-k}^{k} w^2(x), dx. \tag{89}$$

Consequently, the condition for the stability of solutions is as follows:

$$\frac{\partial H}{\partial v} > 0. \tag{90}$$

For example, we check the stability property for Eq. 24, and we obtain

$$H = \frac{2\vartheta^4\left(\frac{\sigma(-(v-10))+\frac{4}{\sigma(v-10)-2}-4\log(10\sigma+\sigma(-v)+2)}{\sigma^3} - \frac{\sigma(-(v+10))+\frac{4}{\sigma(v+10)-2}-4\log(2-\sigma(v+10))}{\sigma^3}\right)}{\lambda^2}. \tag{91}$$

Therefore,

$$\frac{\partial H}{\partial v}|v = 2 = 1.6 > 0. \tag{92}$$

So, this solution is stable on the interval $x\epsilon[-10, 10]$. Similarly, we can check the stability of other obtained solutions with our novel technique.

5 Results and discussion

The MAEM and methods for fractional conformable residual power series are designed particularly to handle fractional equations. They take into account the special characteristics and behaviors related to fractional calculus and are designed to operate with fractional derivatives. These techniques offer specialized tools that are ideally suited for studying FNLPDEs with fractional-order derivatives. When compared to other numerical techniques, the MAEM and fractional conformable residual power series algorithms can provide computational efficiency. They frequently require shortening series expansions or solving auxiliary equations, which can lower the complexity and expense of computing. This benefit may be especially important when handling complex or computationally difficult FNLPDEs. Table 1 presents a comparison of the absolute error $|w - w_2|$ of both equations. These results clearly demonstrate the accuracy and effectiveness of the numerical technique. The results of the MAEM include the periodic and singular solutions. Utilizing 3D surface plots, 2D contour plots, density graphs, and 2D line graphs, the graphical simulation of a few retrieved solutions is discussed. The graphs are created for appropriate values of the arbitrary parameters α, λ, and ϑ.

Figure 1 shows the 3D, 2D, and counterplot graphs at $\alpha = 1$, $\lambda = 1$, $\vartheta = -1$, and $t = 5$ of $v_{1,1}(x, t)$. Similarly, Figure 2 shows the 3D, 2D, and counterplot graphs at $\alpha = 1$, $\lambda = 1$, $\vartheta = 1$, and $t = 10$, which is a periodic solitary wave of $v_{1,3}(x, t)$. Figure 3 shows the 3D, 2D, and counterplot graphs at $\alpha = 1$, $\lambda = 1$, $\vartheta = -1$, and $t = 0.5, 1, 1.5$ of $v_{1,5}(x, t)$. Similarly, Figure 4 shows the 3D, 2D, and counterplot graphs at $\alpha = 1$ and $t = 5$ of $v_{1,7}(x, t)$. Figure 5 shows the 3D, 2D, and counterplot graphs at $\theta = 1$ and $\vartheta = 0.1$ of $v_{2,2}(x, t)$. Similarly, Figure 6 shows the 3D, 2D, and counterplot graphs at $\theta = 1$ and $\vartheta = 0.1$, which is periodic solitary wave of $v_{2,4}(x, t)$. Figure 7 shows the 3D, 2D, and counterplot graphs at $\alpha = 1$, which is a singular soliton solution of $v_{2,5}(x, t)$. Figure 8 shows the 3D, 2D, and counterplot graphs at $\theta = 1$ and $\vartheta = 0.1$, which is periodic solitary wave of $v_{2,4}(x, t)$. Figure 9 shows the 3D, 2D, and counterplot graphs at $\alpha = 1$, which is a singular soliton solution of $v_{2,5}(x, t)$. Figure 10 shows the 3D, 2D, and counterplot graphs at $\theta = 1$ and $\vartheta = 0.1$, which is a periodic solitary wave of $v_{2,4}(x, t)$. Figure 11 shows the comparison of error terms between numerical and analytical techniques. Figure 12 shows the comparison between numerical and analytical techniques. Figure 13 shows the stability analysis of governing equations. Fundamental mathematical techniques used to describe and examine real-world occurrences in science and engineering include trigonometric, hyperbolic, and rational functions. In order to represent oscillatory motion and periodic phenomena like waves and tides, trigonometric functions like sine and cosine are used. Heat conduction, population expansion, and fluid dynamics are the three areas where hyperbolic functions, such as hyperbolic sine and cosine, are used to depict exponential growth and decay. Rational functions, which are polynomial ratios, have asymptotes, holes, and other graph characteristics that make them useful for simulating complex systems in financial analysis, control systems, population dynamics, and circuit design.

6 Conclusion

The nonlinear fractional Cahn–Hilliard and Gardner equations have been addressed in this paper using a unique methodology. This analytical technique is useful for creating partial differential equations and discovering approximate solutions under the right initial circumstances. The effectiveness of the suggested method is also shown by the precise results obtained utilizing MAEM with a smaller number of series terms. The application of this method to two different physical models demonstrates its accuracy and efficiency in handling fractional nonlinear equations, leading to stunning and complicated graphics. Additionally, the approximation series' quick convergence is noted. We can see how the graphs change as a result of changing parameter values. When the calculations and simulations performed in Mathematica 11 were compared to previous numerical findings, it became clear that this numerical method is capable of handling difficult fractional equations in higher dimensions. The analytical approach used here is also notable for being straightforward, reliable, and succinct when solving nonlinear partial differential equations. The overall findings of the study emphasize the importance of this strategy in improving our knowledge and management of such difficult equations.

Data availability statement

The original contributions presented in the study are included in the article/Supplementary Material; further inquiries can be directed to the corresponding author.

Author contributions

AA: writing, conceptualization, formal analysis, supervision, and review and editing. AN: review implementation and editing. MN: formal analysis and review and editing. MJB: formal analysis and review and editing. AF: formal analysis and writing the original draft. AFA: formal analysis and review and editing. RH: formal analysis and review and editing. All authors contributed to the article and approved the submitted version.

Acknowledgments

The authors extend their appreciation to the Researchers Supporting Project (No. RSP2023R218), King Saud University, Riyadh, Saudi Arabia.

Conflict of interest

The authors declare that the research was conducted in the absence of any commercial or financial relationships that could be construed as a potential conflict of interest.

Publisher's note

All claims expressed in this article are solely those of the authors and do not necessarily represent those of their affiliated organizations, or those of the publisher, the editors, and the reviewers. Any product that may be evaluated in this article, or claim that may be made by its manufacturer, is not guaranteed or endorsed by the publisher.

References

1. Ali A, Ahmad J, Javed S. Solitary wave solutions for the originating waves that propagate of the fractional Wazwaz-Benjamin-Bona-Mahony system. *Alexandria Eng J* (2023) 69:121–33. doi:10.1016/j.aej.2023.01.063

2. Ali A, Ahmad J, Javed S. Exploring the dynamic nature of soliton solutions to the fractional coupled nonlinear Schrödinger model with their sensitivity analysis. *Opt Quan Elect* (2023) 55(9):810. doi:10.1007/s11082-023-05033-y

3. Wang KJ. Traveling wave solutions of the Gardner equation in dusty plasmas. *Results Phys* (2022) 33:105207. doi:10.1016/j.rinp.2022.105207

4. Kudryashov NA. Optical solitons of the model with generalized anti-cubic nonlinearity. *Optik* (2022) 257:168746. doi:10.1016/j.ijleo.2022.168746

5. Wang KJ. Variational principle and diverse wave structures of the modified Benjamin-Bona-Mahony equation arising in the optical illusions field. *Axioms* (2022) 11(9):445. doi:10.3390/axioms11090445

6. Ali A, Ahmad J, Javed S, Rehman SU. Analysis of chaotic structures, bifurcation and soliton solutions to fractional Boussinesq model. *Physica Scripta* (2023) 98:075217. doi:10.1088/1402-4896/acdcee

7. Islam SR, Arafat SY, Wang H. Abundant closed-form wave solutions to the simplified modified Camassa-Holm equation. *J Ocean Eng Sci* (2022) 8:238–45. doi:10.1016/j.joes.2022.01.012

8. Shakeel M, El-Zahar ER, Shah NA, Chung JD. Generalized exp-function method to find closed form solutions of nonlinear dispersive modified benjamin–bona–mahony equation defined by seismic sea waves. *Mathematics* (2022) 10(7):1026. doi:10.3390/math10071026

9. Joseph SP. Exact traveling wave doubly periodic solutions for generalized double sine-gordon equation. *Int J Appl Comput Math* (2022) 8(1):42–19. doi:10.1007/s40819-021-01236-7

10. Athron P, Fowlie A, Lu CT, Wu L, Wu Y, Zhu B. *The* W *boson mass and muon* g *– 2: Hadronic uncertainties or new physics?* (2022). arXiv preprint arXiv:2204.03996.

11. Seidel A. *Integral approach for hybrid manufacturing of large structural titanium space components* (2022).

12. Saifullah S, Ahmad S, Alyami MA, Inc M. Analysis of interaction of lump solutions with kink-soliton solutions of the generalized perturbed KdV equation using Hirota-bilinear approach. *Phys Lett A* (2022) 454:128503. doi:10.1016/j.physleta.2022.128503

13. Liu SZ, Wang J, Zhang DJ. The fokas–lenells equations: bilinear approach. *Stud Appl Math* (2022) 148(2):651–88. doi:10.1111/sapm.12454

14. Khater MM. Prorogation of waves in shallow water through unidirectional Dullin–Gottwald–Holm model; computational simulations. *Int J Mod Phys B* (2022) 37:2350071. doi:10.1142/s0217979223500716

15. Muniyappan A, Sahasraari LN, Anitha S, Ilakiya S, Biswas A, Yıldırım Y, et al. Family of optical solitons for perturbed Fokas–Lenells equation. *Optik* (2022) 249:168224. doi:10.1016/j.ijleo.2021.168224

16. He XJ, Lü X. M-lump solution, soliton solution and rational solution to a (3+ 1)-dimensional nonlinear model. *Mathematics Comput Simulation* (2022) 197:327–40. doi:10.1016/j.matcom.2022.02.014

17. Zhang T, Li M, Chen J, Wang Y, Miao L, Lu Y, et al. Multi-component ZnO alloys: bandgap engineering, hetero-structures, and optoelectronic devices. *Mater Sci Eng R: Rep* (2022) 147:100661. doi:10.1016/j.mser.2021.100661

18. Min R, Hu X, Pereira L, Soares MS, Silva LC, Wang G, et al. Polymer optical fiber for monitoring human physiological and body function: A comprehensive review on mechanisms, materials, and applications. *Opt Laser Technolog* (2022) 147:107626. doi:10.1016/j.optlastec.2021.107626

19. Lechelon M, Meriguet Y, Gori M, Ruffenach S, Nardecchia I, Floriani E, et al. Experimental evidence for long-distance electrodynamic intermolecular forces. *Sci Adv* (2022) 8(7):eabl5855. doi:10.1126/sciadv.abl5855

20. Tarla S, Ali KK, Yilmazer R, Yusuf A. Investigation of the dynamical behavior of the Hirota-Maccari system in single-mode fibers. *Opt Quan Elect* (2022) 54(10):613–2. doi:10.1007/s11082-022-04021-y

21. Ahmad J, Rizwanullah M, Suthar T, Albarqi HA, Ahmad MZ, Vuddanda PR, et al. Receptor-targeted surface-engineered nanomaterials for breast cancer imaging and theranostic applications. *The Eur Phys J D* (2022) 76(1):1–44. doi:10.1615/CritRevTherDrugCarrierSyst.2022040686

22. Dubey S, Chakraverty S. Application of modified extended tanh method in solving fractional order coupled wave equations. *Math Comput Simulation* (2022) 198:509–20. doi:10.1016/j.matcom.2022.03.007

23. Siddique I, Mehdi KB, Jarad F, Elbrolosy ME, Elmandouh AA. Novel precise solutions and bifurcation of traveling wave solutions for the nonlinear fractional (3+ 1)-dimensional WBBM equation. *Int J Mod Phys B* (2022) 37:2350011. doi:10.1142/s021797922350011x

24. Jiang Y, Wang F, Salama SA, Botmart T, Khater MM. Computational investigation on a nonlinear dispersion model with the weak non-local nonlinearity in quantum mechanics. *Results Phys* (2022) 38:105583. doi:10.1016/j.rinp.2022.105583

25. Bilal M, Rehman SU, Ahmad J. The study of new optical soliton solutions to the time-space fractional nonlinear dynamical model with novel mechanisms. *J Ocean Eng Sci* (2022). doi:10.1016/j.joes.2022.05.027

26. Fu Z, Liu S, Liu S. New kinds of solutions to Gardner equation. *Chaos, Solitons & Fractals* (2004) 20(2):301–9. doi:10.1016/s0960-0779(03)00383-7

27. Chen W, Sun H, Li XC. *Fractional derivative modelling in mechanics and engeneering*. Springer (2022).

28. Abouelregal AE, Fahmy MA. Generalized Moore-Gibson-Thompson thermoelastic fractional derivative model without singular kernels for an infinite orthotropic thermoelastic body with temperature-dependent properties. *ZAMM-Journal Appl Math Mechanics/Zeitschrift für Angew Mathematik Mechanik* (2022) 102:e202100533. doi:10.1002/zamm.202100533

29. Zhu Y, Tang T, Zhao S, Joralmon D, Poit Z, Ahire B, et al. Recent advancements and applications in 3D printing of functional optics. *Additive Manufacturing* (2022) 52:102682. doi:10.1016/j.addma.2022.102682

30. Li Q, Shan W, Wang P, Cui H. Breather, lump and N-soliton wave solutions of the (2+ 1)-dimensional coupled nonlinear partial differential equation with variable coefficients. *Commun Nonlinear Sci Numer Simulation* (2022) 106:106098. doi:10.1016/j.cnsns.2021.106098

31. Prakasha DG, Veeresha P, Baskonus HM. Two novel computational techniques for fractional Gardner and Cahn-Hilliard equations. *Comput Math Methods* (2019) 1(2):e1021. doi:10.1002/cmm4.1021

32. Aniqa A, Ahmad J. Soliton solution of fractional Sharma-Tasso-Olever equation via an efficient (G′/G)-expansion method. *Ain Shams Eng J* (2022) 13(1):101528. doi:10.1016/j.asej.2021.06.014

33. Khater M, Lu D, Attia RA. Dispersive long wave of nonlinear fractional Wu-Zhang system via a modified auxiliary equation method. *AIP Adv* (2019) 9(2). doi:10.1063/1.5087647

34. Scarmozzino R, Gopinath A, Pregla R, Helfert S. Numerical techniques for modeling guided-wave photonic devices. *IEEE J Selected Top Quan Elect* (2000) 6(1):150–62. doi:10.1109/2944.826883

35. Ali A, Ahmad J, Javed S. Stability analysis and novel complex solutions to the malaria model utilising conformable derivatives. *The Eur Phys J Plus* (2023) 138(3):259–17. doi:10.1140/epjp/s13360-023-03851-3

frontiers | Frontiers in Physics

TYPE Original Research
PUBLISHED 20 October 2023
DOI 10.3389/fphy.2023.1246884

OPEN ACCESS

EDITED BY
Yusry El-Dib,
Ain Shams University, Egypt

REVIEWED BY
Youssri Hassan Youssri,
Cairo University, Egypt
Muhammad Nadeem,
Qujing Normal University, China

*CORRESPONDENCE
Muhammad Rafiullah,
rafiullaharain@gmail.com
Naveed Anjum,
xsnaveed@yahoo.com

†These authors have contributed equally to this work

RECEIVED 24 June 2023
ACCEPTED 04 October 2023
PUBLISHED 20 October 2023

CITATION
Buhe E, Rafiullah M, Jabeen D and Anjum N (2023), Application of homotopy perturbation method to solve a nonlinear mathematical model of depletion of forest resources.
Front. Phys. 11:1246884.
doi: 10.3389/fphy.2023.1246884

Application of homotopy perturbation method to solve a nonlinear mathematical model of depletion of forest resources

Eerdun Buhe[1†], Muhammad Rafiullah[2*†], Dure Jabeen[3†] and Naveed Anjum[4*†]

[1]School of Mathematical Sciences, Hohhot University for Nationalities, Inner Mongolia, China, [2]Department of Mathematics, COMSATS University Islamabad, Lahore, Pakistan, [3]Department of Electronics Engineering, Sir Syed University of Engineering and Technology, Karachi, Pakistan, [4]Department of Mathematics, GC University, Faisalabad, Pakistan

Reduction in forest resources due to increasing global warming and population growth is a critical situation the World faces today. As these reserves decrease, it alarms new challenges that require urgent attention. In this paper, we provide a semi-analytical solution to a nonlinear mathematical model that studies the depletion of forest resources due to population growth and its pressure. With the help of the homotopy perturbation method (HPM), we determine an approximate series solution with few perturbation terms, which is one of the essential power of the HPM method. We compare our semi-analytical results with numerical solutions obtained using the Runge-Kutta 4th-order (RK-4) method. Furthermore, we analyze the model's behaviour and dynamics by changing the parametric coefficients that represent the depletion rate of forest resources and the growth rate of population pressure and present these findings using various graphs.

KEYWORDS

semi-analytical solution, system of non-linear differential equations, homotopy perturbation method, depletion of forest resources, mathematical mobel

1 Introduction

The world faces an alarming issue today due to the depletion of forest resources caused by deforestation, fires, illegal logging, and other factors. Many countries will lose their remaining forests by 2030 if this trend continues, according to a recent report [1]. Urgent action is needed to address this challenge, including better coordination and control of the timber industry and communities that depend on the forests [2]. Mathematics provides some powerful tools to tackle such problems with the help of differential equations which can offer a way to solve dynamical systems making them essential to science, engineering and humanity. Some studies have used the mathematical modeling of forest depletion and suggested solutions using various numerical and analytical methods. Gompil et al. [3] proposed numerical and simulated results for a forest depletion model, while Eswari et al. [4] examined the homotopy perturbation method (HPM) to solve the mathematical model for the depletion of forest resources. Nugraheni et al. [5] proposed stability analysis and numerical simulations for a mangrove forest resource dynamical model. Didiharyono and Kasse [6] studied the stability of a mathematical model for deforestation and presented numerical simulations of the system. All these studies offer useful insights into the dynamics of forest resources and propose possible solutions to handle this critical global problem. This paper concentrates on the study of the

TABLE 1 Error in $B(t)$, $N(t)$ and $P(t)$ by using HPM and RK 4th order.

t	$e_{B(t)}$	$e_{N(t)}$	$e_{P(t)}$
0	0	0	0
0.0040	$7.02229385e-11$	$3.8795633e-12$	$1.11022302e-15$
0.0080	$2.84295254e-10$	$1.5518253e-11$	$7.77156117e-15$
0.0120	$6.60833165e-10$	$3.4923175e-11$	$2.13162820e-14$
0.0160	$1.24834542e-09$	$6.2129856e-11$	$3.57491813e-14$
0.0200	$2.14010853e-09$	$9.7180929e-11$	$3.15303338e-14$
0.0240	$3.48907391e-09$	$1.4013323e-10$	$2.64233079e-14$
0.0280	$5.52271828e-09$	$1.9115020e-10$	$1.93400850e-13$
0.032	$8.55785131e-09$	$2.5035973e-10$	$5.49560397e-13$
0.0360	$1.30154624e-08$	$3.1803182e-10$	$1.20303766e-12$
0.0400	$1.94354861e-08$	$3.9440806e-10$	$2.29549712e-12$
0.0440	$2.84915344e-08$	$4.7988635e-10$	$4.00479649e-12$
0.0480	$4.10056628e-08$	$5.74907232e-10$	$6.55009380e-12$
0.0520	$5.79630068e-08$	$6.79982292e-10$	$1.01949559e-11$
0.0560	$8.05264832e-08$	$7.95743915e-10$	$1.52524659e-11$
0.0600	$1.10051416e-07$	$9.22938170e-10$	$2.20889972e-11$
0.0640	$1.48100092e-07$	$1.06238928e-09$	$3.11282111e-11$

depletion of forest resources, employing a mathematical model suggested by Misra, Lata, and Shukla [7]. This mathematical model consists of the cumulative density of forest resources, the density of the population, and population pressure, represented by the variables B, N, and P, respectively. In this model, the connection between forest and population density is considered as a prey-predator logistic model. The forest density decreases as housing and development increase, impacting its growth rate. Population pressure growth is proportional to population density in the model [7]. The authors have investigated existence and uniqueness of the global positive solution and provided numerical simulations to study this model. The cumulative density of forests and population size, are modelled using comprehensive equations with dynamic relations similar to a prey-predator system. The model signifies the depletion of forest resources provoked by population growth, reduction of forest areas for expansion purposes and the depletion by the pressure of the population. In addition, the model considers that the increase in population pressure is proportional to population density. This model consists of dimensionless differential equations. The suggested model [7] can be represented as:

$$\begin{aligned}\frac{dB}{dt} &= sB - hB^2 - \alpha BN - \lambda_2 B^2 P,\\ \frac{dN}{dt} &= rN - jN^2 + \pi\alpha BN,\\ \frac{dP}{dt} &= \lambda N - \lambda_0 P,\end{aligned} \tag{1}$$

where $B(0) \geq 0$, $N(0) \geq 0$, $P(0) \geq 0$ and we define variables and constant coefficients of this model in the following table as.

Notation	Description
B	Cumulative density of forest resources
N	Density of population
P	Population pressure
S	Intrinsic growth rate
$h = \frac{s_0}{L}$	Intraspecific growth rate of forestry resources in absence of population
$j = \frac{r_0}{K}$	Intraspecific growth rate of population in absence of forestry resources
A	Depletion rate of forest resources due to population
Λ	Growth rate of population pressure
λ_0	Natural depletion rate
λ_2	Depletion rate due to population pressure
Π	Growth in population due to forest resources (proportionality constant)
R	Intrinsic growth rate human population

Values for the parameters and coefficients are considered, $s = 0.8$, $s_0 = 0.2$, $L = 50$, $\alpha = 0.0001$, $\lambda = 0.2$, $\lambda_0 = 0.1$, $r = 0.2$, $r_0 = 0.1$, $K = 100$, $\pi = 0.004$, $\lambda_2 = 0.0002$, $h = \frac{s_0}{L}$, $j = \frac{r_0}{K}$ and initial conditions $n_1 = B(0) = 30$, $n_2 = N(0) = 35$, $n_3 = P(0) = 1$ as given in (Misra et al., 2014).

The rate of forest depletion is alarming, mainly driven by illegal logging and land clearing activities. This trend poses a serious threat to our ecosystem and immediate action is needed to mitigate its

TABLE 2 $B(t)$ **by using HPM with variation of** α**.**

t	$B(t)$ at $\alpha = 0.0001$	$B(t)$ at $\alpha = 0.0002$	$B(t)$ at $\alpha = 0.0004$
0	30	30	30
0.0400	30.8129	30.8123	30.79938896
0.0800	31.64006505	31.63119549	31.61346378
0.1200	32.48303939	32.46937528	32.44206418
0.1600	33.34108369	33.32237882	33.28500024
0.2000	34.21399144	34.18999515	34.14205247
0.2400	35.10152566	35.07198316	35.01297171
0.2800	36.00341892	35.96807153	35.89747924
0.3200	36.91937333	36.8779588	36.7952667
0.3600	37.84906054	37.80131329	37.70599611
0.4000	38.79212173	38.73777318	38.62929989
0.4400	39.74816763	39.68694645	39.56478085
0.4800	40.7167785	40.6484109	40.51201218
0.5200	41.69750417	41.62171415	41.47053744
0.5600	42.68986396	42.60637366	42.43987062
0.6000	43.69334678	43.60187669	43.41949605
0.6400	44.70741106	44.60768033	44.40886848

TABLE 3 $B(t)$ **by using HPM with variation of** λ**.**

t	$B(t)$ at $\lambda = 0.1$	$B(t)$ at $\lambda = 0.2$	$B(t)$ at $\lambda = 0.3$
0	30	30	30
0.0400	30.81286325	30.81233672	30.81181021
0.0800	31.64226453	31.64006505	31.63786584
0.1200	32.48820566	32.48303939	32.47787449
0.1600	33.35066779	33.34108369	33.33150392
0.2000	34.22961141	34.21399144	34.19838205
0.2400	35.12497633	35.10152566	35.07809694
0.2800	36.03668172	36.00341892	35.97019679
0.3200	36.96462607	36.91937333	36.87418996
0.3600	37.9086872	37.84906054	37.78954498
0.4000	38.86872228	38.79212173	38.71569051
0.4400	39.84456783	39.74816763	39.65201535
0.4800	40.83603966	40.7167785	40.59786848
0.5200	41.84293296	41.69750417	41.55255902
0.5600	42.86502224	42.68986396	42.51535622
0.6000	43.90206134	43.69334678	43.48548951
0.6400	44.95378345	44.70741106	44.46214845

TABLE 4 $B(t)$ by using HPM with variation of λ_2.

t	$B(t)$ at $\lambda_2 = 0.0001$	$B(t)$ at $\lambda_2 = 0.0002$	$B(t)$ at $\lambda_2 = 0.0003$
0	30	30	30
0.0400	30.81659405	30.81233672	30.80808055
0.0800	31.64999511	31.64006505	31.63014111
0.1200	32.50021609	32.48303939	32.46588035
0.1600	33.36724938	33.34108369	33.31495729
0.2000	34.2510668	34.21399144	34.17699131
0.2400	35.15161962	35.10152566	35.05156215
0.2800	36.06883856	36.00341892	35.93820992
0.3200	37.00263378	36.91937333	36.83643509
0.3600	37.9528949	37.84906054	37.74569848
0.4000	38.91949097	38.79212173	38.6654213
0.4400	39.9022705	39.74816763	39.59498509
0.4800	40.90106144	40.7167785	40.53373176
0.5200	41.9156712	41.69750417	41.4809636
0.5600	42.94588662	42.68986396	42.43594323
0.6000	43.991474	43.69334678	43.39789368
0.6400	45.05217908	44.70741106	44.36599828

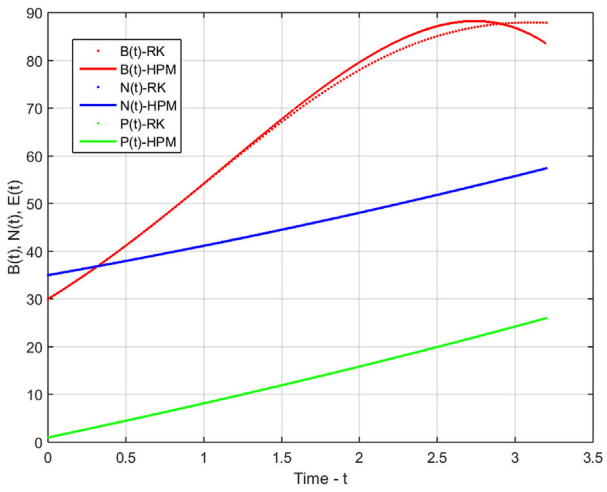

FIGURE 1
Solution for model 1.

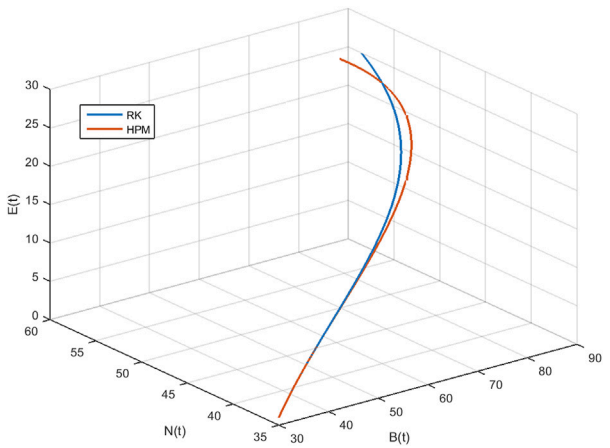

FIGURE 2
Solution for model 1 in 3D.

impact. Without decisive measures, the depletion of forest resources will have long-lasting consequences on the environment and our wellbeing. It is imperative to find sustainable solutions and enforce regulations to curb the rampant destruction of forests and preserve them for future generations.

Many dynamical problems in science and engineering cannot be solved analytically (exactly) and can be approximated numerically. There is another technique named as series solution (semi-analytical techniques) which is more closer to analytical results. For this purpose a wide range of methods have been developed to find approximate solutions that are as close as possible to the exact solutions. Among these methods are the Taylor series method [8], which approximates functions as power series; the Picard method [9], which iteratively computes solutions from initial conditions; the Adomian decomposition method [10], which decomposes a differential equation into simpler sub problems; the variational iteration method [11], which uses Lagrange multipliers to optimize solutions; and the homotopy perturbation method [12–14,14,15,17–19], which constructs a homotopy that gradually deforms the problem into a simpler one

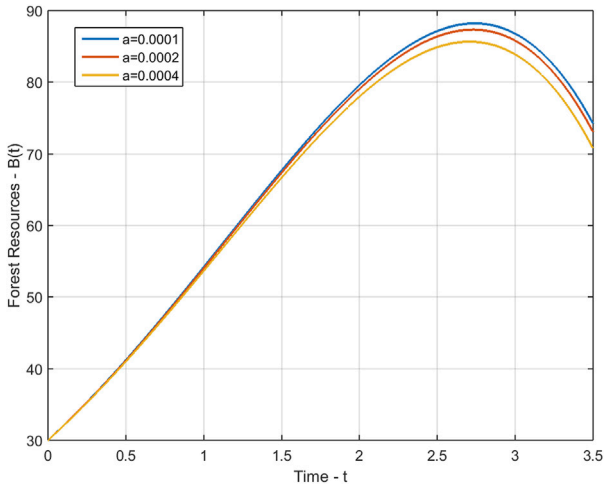

FIGURE 3
Forest resources $B(t)$ and α with the variation of time.

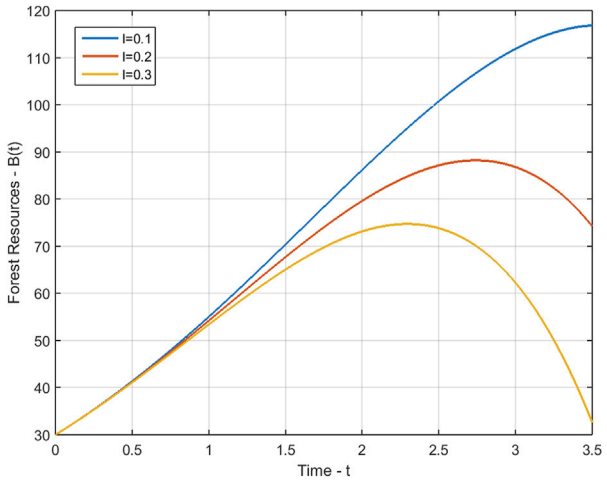

FIGURE 4
Forest resources $B(t)$ and λ with the variation of time.

while adding a perturbation term to the solution. These methods have been applied to a wide range of problems in physics, engineering, various fields and have proven to be highly effective in providing accurate approximations to complex dynamical systems.

Ji Huan He, a mathematician from China proposed a novel semi-analytical method based on homotopy and perturbation techniques in 1999, which was named the homotopy perturbation method (HPM) [12]. He improved and extended the HPM to solve a wide range of problems. In 2004, He used the HPM to non-linear oscillators and asymptotic [13,14]. In 2005, the HPM was applied to solve non-linear wave equations and problems related to limit cycle and bifurcation of non-linear systems [15,16]. In 2008, He employed the HPM to solve boundary value problems [20]. In 2007, Javidi and Golbabai used a revised version of the HPM to solve non-linear Fredholm integral equations [21].Recently, HPM with small variations has been applied to study fractal duffing oscillator problems under arbitrary conditions [22], modified HPM for nonlinear oscillators Anjum and He [23], attachment oscillator arising in nanotechnology [24], conservative nonlinear oscillators [25], non-linear oscillator problems in a fractal space [26] and HPM including Aboodh transformation to solve fractional calculus Tao et al. [27], vibrating magnetic inverted pendulum Moatimid et al. [28], Symmetry-breaking and pull-down motion for the helmholtz–duffing oscillator Niu et al. [29], nonlinear fractional Drinfeld–Sokolov–Wilson Equation Nadeem and Alsayaad [30], trajectory analysis of a zero-pitch-angle e-Sail Niccolai et al. [31], natural convection between two concentric horizontal circular cylinders Abdulameer and Ali Al-Saif [32], nonlocal initial-boundary value problems for parabolic and hyperbolic Al-Hayani and Younis [33], multi-step iterative methods for solving nonlinear equations Saeed et al. [34], telegraph equation Moazzzam et al. [35], triangular linear diophantine fuzzy system of equations Shams et al. [36], condensing coagulation model and Lifshitz-Slyzov equation Arora et al. [37], singular nonlinear system of boundary value problems Pathak et al. [38], rikitake-yype system Ene and Pop [39], heat and mass transfer with 2D unsteady squeezing viscous flow problem Abdul-Ameer and Ali Al-Saif [40], variable Speed Wind Turbine Control Shalbafian and Ganjefar [41], radial thrust problem Niccolai et al. [42], special third grade fluid flow with viscous dissipation effect over a stretching sheet Swain et al. [43], and the frequency–amplitude relationship of a nonlinear oscillator with cubic and quintic nonlinearities He et al. [44]. The HPM has become a widely-used technique to solve a large variety of problems in different fields and many research papers have been published each year using this method as evidenced by a simple search on Google Scholar.

In this paper, we provide an approximate solution of model 1) by using the homotopy perturbation method. The interesting feature of HPM is that it provides the best approximate solution by taking a few numbers of perturbation terms.

2 Homotopy perturbation method

Consider a non-linear differential equation

$$D(\mu) - g(\tau) = 0, \ \tau \in \mho \tag{2}$$

subject to the boundary condition

$$\beta\left(\mu, \frac{\partial \mu}{\partial \tau}\right) = 0, \ \tau \in \Gamma \tag{3}$$

where D is a differential operator, β is boundary operator, Γ is the boundary of the domain $\bar{\mho}$ and $g(\tau)$ is an unknown function. The D, generally consist on two parts, linear and non-linear part, represented as L and N respectively. Therefore, 2) can be written as follows

$$L(\mu) + N(\mu) - g(\tau) = 0, \tag{4}$$

using homotopy method, by taking an embedding parameter q one can construct a homotopy $v(\tau, q)$: $\mho \times [0, 1] \rightarrow R$ for Eq. 4 which satisfies

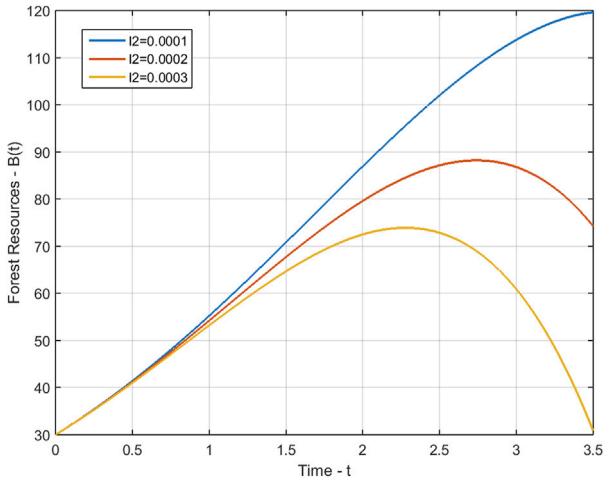

FIGURE 5
Forest resources $B(t)$ and λ_2 with the variation of time.

$$H(w,q) = (1-q)[L(w) - L(\mu_0)] + q[L(w) + N(w) - g(\tau)] = 0, \tag{5}$$

and it is equivalent to

$$H(w,q) = L(w) - L(\mu_0) + qL(\mu_0) + q[N(w) - g(\tau)] = 0, \tag{6}$$

where $q \in [0, 1]$ is an embedding parameter, μ_0 is an initial guess approximation of Eq. 6 which satisfies the initial (or boundary) conditions. It can be written as follows.

$$q = 0, \qquad H(w,0) = L(w) - L(\mu_0), \tag{7}$$

$$q = 1, \qquad H(w,1) = L(w) + N(w) - g(\tau). \tag{8}$$

We suppose the solution in the form of power series for Eq. 5 by taking an embedding parameter q

$$w = w_0 + qw_1 + q^2w_2 + q^3w_3 + \cdots \tag{9}$$

The approximate solution of Eq. 2 can be obtained by setting $q = 1$,

$$\mu = \lim_{q\to 1} w = w_0 + w_1 + w_2 + w_3 + \cdots \tag{10}$$

The convergence of (Eq. 10) has been proved in [12]. The series is convergent for most cases, however, the convergent rate depends upon the nonlinear operator $N(w)$. Furthermore He suggested the following conditions.

1. The second derivative of nonlinear operator $N(w)$ with respect to w must be small, because the parameter q may be relatively large, i.e., $q \to 1$.
2. The norm of $\|L^1(\frac{\partial N}{\partial w})\|$ must be smaller than one, in order that the series converges.

3 Application of HPM

Now we apply HPM on our model, Eq. 1 of depletion of forest resources (non-linear system of differential equations) as

$$\begin{cases} (1-q)(u' - B_0') + q(u' - su + hu^2 + \alpha uv + \lambda_2 u^2 w) = 0, \\ (1-q)(v' - N_0') + q(v' - rv + jv^2 - \pi\alpha uv) = 0, \\ (1-q)(w' - P_0') + q(w' - \lambda v + \lambda_0 w) = 0. \end{cases} \tag{11}$$

The initial guesses for (11) are constant as defined in [7].

$$\begin{aligned} u_0(t) &= B_0(t) = B(0) = n_1 \\ v_0(t) &= N_0(t) = N(0) = n_2 \\ w_0(t) &= P_0(t) = P(0) = n_3 \end{aligned} \tag{12}$$

and we assume the solution of (11) as,

$$\begin{aligned} u &= u_0 + qu_1 + q^2u_2 + q^3u_3 + \cdots, \\ v &= v_0 + qv_1 + q^2v_2 + q^3v_3 + \cdots, \\ w &= w_0 + qw_1 + q^2w_2 + q^3w_3 + \cdots, \end{aligned} \tag{13}$$

by substituting Eq. 13 in Eq. 11 and collecting the terms of powers of q, we obtain

$$q^0: \begin{cases} u_0' = 0, \ u_0(0) = n_1, \\ v_0' = 0, \ v_0(0) = n_2, \\ w_0' = 0, \ w_0(0) = n_3. \end{cases} \tag{14}$$

$$q^1: \begin{cases} u_1' + u_0(\alpha v_0 - s) + u_0^2(h + \lambda_2 w_0) = 0, \ u_1(0) = 0, \\ v_1' - (r + \alpha\pi u_0)v_0 + jv_0^2 = 0, \ v_1(0) = 0, \\ w_1' - \lambda v_0 + \lambda_0 w_0 = 0, \ w_1(0) = 0. \end{cases} \tag{15}$$

$$q^2: \begin{cases} u_2' + \alpha u_0 v_1 + u_1(\alpha v_0 + 2u_0(h + \lambda_2 w_0) - s) + \lambda_2 u_0^2 w_1, \ u_2(0) = 0, \\ v_2' - \alpha\pi u_1 w_0 - (r + \alpha\pi u_0 - 2jv_0)v_1 = 0, \ v_2(0) = 0, \\ w_2' - \lambda v_1 + \lambda_0 w_1 = 0, \ w_2(0) = 0, \end{cases} \tag{16}$$

$$q^3: \begin{cases} u_3' + \alpha u_0 v_2 + u_1^2(h + \lambda_2 w_0) + u_2(\alpha v_0 + 2u_0(h + \lambda_2 w_0)) \\ \quad + u_1(\alpha v_1 + 2\lambda_2 u_0 w_1) + 2\lambda_2 u_0^2 w_2 = 0, \ u_3(0) = 0, \\ v_3' - \alpha\pi u_2 v_0 - \alpha\pi u_1 v_1 + jv_1^2 - rv_2 - \alpha\pi u_0 v_2 + 2jv_0 v_2 = 0, \\ \quad v_3(0) = 0, \\ w_3 - \lambda v_2 + \lambda_0 w_2 = 0, \ w_3(0) = 0. \end{cases} \tag{17}$$

$$q^4: \begin{cases} u_4' + \alpha u_2 v_1 + \alpha u_0 v_3 + u_3(-s + \alpha v_0 + 2u_0(h + \lambda_2 w_0)) + \lambda_2 u_1^2 w_1 \\ \quad + \lambda_2 u_0 u_2 w_1 + u_1(\alpha v_2 + 2u_2(h + \lambda_2 w_0) + 2\lambda_2 u_0 w_2) \\ \quad + \lambda_2 u_0^2 w_4 = 0, \ u_4(0) = 0, \\ v_4' - \alpha\pi u_3 v_0 - \alpha\pi u_2 v_1 - \alpha\pi u_1 v_2 + 2jv_1 v_2 - rv_3 \\ \quad - \alpha\pi u_0 v_3 + 2jv_0 v_3 = 0, \ v_4(0) = 0, \\ w_4 - \lambda v_3 + \lambda_0 w_4 = 0, \ w_4(0) = 0. \end{cases} \tag{18}$$

.
.
.

Now considering $s = 0.8$, $s_0 = 0.2$, $L = 50$, $\alpha = 0.0001$, $\lambda = 0.2$, $\lambda_0 = 0.1$, $r = 0.2$, $r_0 = 0.1$, $K = 100$, $\pi = 0.004$, $\lambda_2 = 0.0002$, $h = \frac{s_0}{L}$, $j = \frac{r_0}{K}$, $n_1 = B(0) = 30$, $n_2 = N(0) = 35$, $n_3 = P(0) = 1$, and simplifying the equations from (Eqs 14–18) we have.

By substituting these values in Eq. 13, we have the solution of model 1) as

$u_0 = 30$	$v_0 = 35$	$w_0 = 1$
$u_1 = 20.115t$	$v_1 = 5.7742t$	$w_1 = 6.9t$
$u_2 = 4.84665t^2$	$v_2 = 0.375578t^2$	$w_2 = 0.232542t^2$
$u_3 = -0.260167t^3$	$v_3 = 0.00519615t^3$	$w_3 = 0.017287t^3$
$u_4 = -0.495765t^4$	$v_4 = -0.000913025t^4$	$w_4 = -0.00017237t^4$

$$B(t) = \lim_{q\to 1} u = 30 + 20.115t + 4.84665t^2 - 0.260167t^3 - 0.495765t^4 - 0.12174t^5 + \cdots, \quad (19)$$

$$N(t) = \lim_{q\to 1} v = 35 + 5.77542t + 0.375578t^2 + 0.00519615t^3 - 0.000913025t^4 - 0.00006t^5 + \cdots, \quad (20)$$

$$P(t) = \lim_{q\to 1} w = 1 + 6.9t + 0.232542t^2 + 0.0172871t^3 - 0.00017237t^4 - 0.000033t^5 + \cdots \quad (21)$$

For $\alpha = 0.0001$, $\alpha = 0.0002$ and $\alpha = 0.0004$, we have.

$B(t)_{\alpha=0.0001} = 30 + 20.115t + 4.84665t^2 - 0.260167t^3 - 0.495765t^4 + \cdots$,

$B(t)_{\alpha=0.0002} = 30 + 20.01t + 4.77438t^2 - 0.274268t^3 - 0.49119t^4 + \cdots$ and.

$B(t)_{\alpha=0.0004} = 30 + 19.8t + 4.63094t^2 - 0.301744t^3 - 0.481988t^4 + \cdots$.

For $\lambda = 0.1$, $\lambda = 0.2$ and $\lambda = 0.3$, we have.

$B(t)_{\lambda=0.1} = 30 + 20.115t + 5.16165t^2 + 0.0854419t^3 - 0.336328t^4 + \cdots$,

$B(t)_{\lambda=0.2} = 30 + 20.115t + 4.84665t^2 - 0.260167t^3 - 0.495765t^4 + \cdots$ and.

$B(t)_{\lambda=0.3} = 30 + 20.115t + 4.53165t^2 - 0.605776t^3 - 0.648587t^4 + \cdots$.

For $\lambda_2 = 0.0001$, $\lambda_2 = 0.0002$ and $\lambda_2 = 0.0003$, we have.

$B(t)_{\lambda_2=0.0001} = 30 + 20.205t + 5.24226t^2 + 0.113954t^3 - 0.334519t^4 + \cdots$,

$B(t)_{\lambda_2=0.0002} = 30 + 20.115t + 4.84665t^2 - 0.260167t^3 - 0.495765t^4 + \cdots$ and.

$B(t)_{\lambda_2=0.0002} = 30 + 20.025t + 4.45157t^2 - 0.629906t^3 - 0.645153t^4 + \cdots$.

3.1 Verification of the solution

To verify the validity of solution, first we check the solution for initial conditions which are satisfied at $t = 0$, secondly we put the solution and its derivatives in the system. If both sides of system are satisfied then we consider the solution is correct or true. For the second condition, we differentiate Eqs 19–21 with respect to t, so we have

$$\frac{dB(t)}{dt} = 20.115 + 9.69329t - 0.780501t^2 - 1.98306t^3 - 0.608698t^4 + \cdots \quad (22)$$

$$\frac{dN(t)}{dt} = 0.77542 + 0.751156t + 0.0155885t^2 - 0.0036521t^3 - 0.000326555t^4 + \cdots \quad (23)$$

$$\frac{dP(t)}{dt} = 6.9 + 0.465084t + 0.0518614t^2 - 0.000689481t^3 - 0.000165368t^4 + \cdots \quad (24)$$

Now using Eqs 19–24 and the values of given parameters in system 1) and we have

$$0. - 1.77636 \times 10^{-15}t + 2.22045 \times 10^{-16}t^3 - 2.22045 \times 10^{-16}t^4 + \cdots = 0 \quad (25)$$

$$0. + 3.46945 \times 10^{-18}t^2 - 8.67362 \times 10^{-19}t^3 + 4.73413 \times 10^{-6}t^5 + \cdots = 0 \quad (26)$$

$$0. - 6.93889 \times 10^{-18}t^2 + 9.75483 \times 10^{-6}t^5 + \cdots = 0 \quad (27)$$

The coefficients of t powers in Eqs 25–27 are around 15 to 19 decimal places correct to zero. So our series solution (5th degree polynomials) satisfies the system up to 4th degree polynomial (where the coefficients are approximately 17 decimal correct to zero). The solution can be improved by taking/adding more terms of power t in it.

3.2 Results and discussions

In this section, we demonstrate the performance of our model 1 through the evaluation of our calculated approximate solutions, $B(t)$, $N(t)$, and $P(t)$. To validate our results, we compare them with the Runge-Kutta 4th-order method and present the absolute error, $e_{B(t)}$, $e_{N(t)}$, and $e_{P(t)}$ in Table 1 for various time steps. The time domain of our Homotopy Perturbation Method (HPM) is divided into sub-intervals and mapped onto $0 \le t \le 400$ with a step size of 0.5 for graphical representation. Our analysis revealed an average absolute error of $6.53290554e-08$, $5.09269781e-10$, and $1.35452205e-11$ for $B(t)$, $N(t)$, and $P(t)$, respectively. In Tables 2–4, we present the cumulative density of forest resources, $B(t)$, for various values of α, λ, and λ_2. These results underscore the versatility and accuracy of our proposed model, which has the potential to contribute significantly to the field of forest resource management. Figure 1 provides a clear illustration of the behaviour of the cumulative density of forest resources $B(t)$, the density of population pressure $P(t)$, and the density of population $N(t)$ as calculated using HPM and RK-4th order method. The solid lines represent the HPM series solution, while the dotted lines show the numerical solution calculated by the RK-4th order method. The graph highlights that the cumulative density of forest resources decreases as the density of population pressure increases. This suggests that controlling population pressure is essential for preserving forests on a large scale. Additionally, Figure 2 depicts the behaviour of model 1 in 3D with respect to HPM and RK method, providing a comprehensive view of the model's behaviour over time. Figure 3, represents the impact of the depletion rate of forest resources due to population, $\alpha = a$, on the cumulative density of forest resources, $B(t)$. It reflects that decreasing the depletion rate of forest resources due to population directs to a growth in the cumulative density of forest resources over time. This emphasizes the significance of controlling the population pressure on forests to control their depletion. In Figure 4, we discuss the impact of the growth rate coefficient of population pressure caused by population $\lambda = l$ on the cumulative density of forest resources $B(t)$. The graph indicates that if we decrease the value of λ, the cumulative density of forest resources increases. Likewise, Figure 5 describes the effect of population pressure λ_2 on $B(t)$. We can see, as the value of λ_2 decreases, the cumulative density of forest resources $B(t)$ increases.

These figures illustrate the significance of controlling population pressure and growth rates to save and preserve forest resources. It also emphasizes the necessity for procedure interventions to control population growth and decrease the depletion of forest resources.

3.3 Technical specification

These calculations are performed on Mathematica® 11.3.0.0 (64-bit) and Matlab® R2015a (8.5.0.197613) 64-bit using a machine Intel(R) Core(TM) i3.2310M CPU @ 2.10 GHz and OS: window 7 Professional (64-bit).

4 Conclusion

In this paper, we used the homotopy perturbation method to obtain a semi-analytical solution for the nonlinear model of the depletion of forest resources. Important characteristic of HPM is that it provides the adequate approximate series solution by taking a few number of perturbation terms which is near to analytical exact solution. Through comparison with the Runge-Kutta method, we established the effectiveness and accuracy of the proposed method. Additionally, we investigated the behaviour of the model by varying the values of the depletion rate of forest resources due to population α, the growth rate coefficient of population pressure caused by population λ, and the depletion rate of its carrying capacity due to population pressure λ_2. The results showed that reducing these coefficients can increase the cumulative density of forest resources $B(t)$. These findings highlight the urgent need for measures to conserve forest resources for the wellbeing of our planet. The presented model and its solution indicate the seriousness of this global issue which needs to be acted upon immediately and effectively to preserve our forest resources. This study suggests that additional investigations and research is needed to build more relevant models for assistance of forest resource experts.

Data availability statement

The original contributions presented in the study are included in the article/Supplementary material, further inquiries can be directed to the corresponding authors.

Author contributions

All authors listed have made a substantial, direct, and intellectual contribution to the work and approved it for publication.

Conflict of interest

The authors declare that the research was conducted in the absence of any commercial or financial relationships that could be construed as a potential conflict of interest.

Publisher's note

References

1. Asongu SA, Jingwa BA. Population growth and forest sustainability in africa. *Int J Green Econ* (2012) 6:145–66. doi:10.1504/ijge.2012.050353

2. Ndoye O, Tieguhong JC. Forest resources and rural livelihoods: the conflict between timber and non-timber forest products in the Congo basin. *Scand J For Res* (2004) 19:36–44. doi:10.1080/14004080410034047

3. Gompil B, Tseveen B, Almasbek J. Modeling and control of Mongolian forest utilization: impact of illegal logging. *Nat Resource Model* (2022) 35:e12333. doi:10.1111/nrm.12333

4. Eswari A, Kumar SS, Raj SV, Priya VS. Analysis of mathematical modeling the depletion of forestry resource: effects of population and industrialization. *Matrix Sci Mathematic (Msmk)* (2019) 3:22–6. doi:10.26480/msmk.02.2019.22.26

5. Nugraheni K, Burhan M, Pancahayani S, Azka M. Stability analysis of mangrove forest resource depletion models due to the opening of fish pond land. In: *Journal of physics: conference series*, 1277. IOP Publishing (2019).012037.

6. Didiharyono D, Kasse I. Mathematical modelling of deforestation due to population density and industrialization. *Jurnal Varian* (2021) 5:9–16. doi:10.30812/varian.v5i1.1412

7. Misra A, Lata K, Shukla J. Effects of population and population pressure on forest resources and their conservation: a modeling study. *Environ Dev sustainability* (2014) 16:361–74. doi:10.1007/s10668-013-9481-x

8. Corliss G, Chang Y. Solving ordinary differential equations using taylor series. *ACM Trans Math Softw (Toms)* (1982) 8:114–44. doi:10.1145/355993.355995

9. Picard É. Sur l'application des méthodes d'approximations successives à l'étude de certaines équations différentielles ordinaires. *J de mathématiques pures appliquées* (1893) 9:217–71.

10. Adomian G. *Solving frontier problems of physics: the decomposition method*, 60. Springer Science and Business Media (2013).

11. Wu Y, He JH. Variational principle for the Kaup-Newell system. *J. comput. appl. mech.* (2023) 54 (3):405–409. doi:10.22059/JCAMECH.2023.365116.875

12. He J-H. Homotopy perturbation technique. *Comp Methods Appl Mech Eng* (1999) 178:257–62. doi:10.1016/s0045-7825(99)00018-3

13. He J-H. The homotopy perturbation method for nonlinear oscillators with discontinuities. *Appl Math Comput* (2004) 151:287–92. doi:10.1016/s0096-3003(03)00341-2

14. He J-H. Asymptotology by homotopy perturbation method. *Appl Maths Comput* (2004) 156:591–6. doi:10.1016/j.amc.2003.08.011

15. He J-H. Limit cycle and bifurcation of nonlinear problems. *Chaos, Solitons and Fractals* (2005) 26:827–33. doi:10.1016/j.chaos.2005.03.007

16. He J-H. Application of homotopy perturbation method to nonlinear wave equations. *Chaos, Solitons and Fractals* (2005) 26:695–700. doi:10.1016/j.chaos.2005.03.006

17. Rafiullah M, Rafiq A. A new approach to solve systems of second order non-linear ordinary differential equations. *Acta Universitatis Apulensis Mathematics-informatics* (2010) 24:189–200.

18. Rafiq A, Rafiullah M. Some new multi-step iterative methods for solving nonlinear equations using modified homotopy perturbation method. *Nonlinear Anal Forum* (2008) 13:185–94.

19. Chakraverty S, Mahato N, Karunakar P, Rao TD. *Advanced numerical and semi-analytical methods for differential equations*. John Wiley and Sons (2019).

20. He J. Homotopy perturbation method for solving boundary value problems. *Phisical Lett* (2006) 350:87–8. doi:10.1016/j.physleta.2005.10.005

21. Javidi M, Golbabai A. Modified homotopy perturbation method for solving non-linear fredholm integral equations. *Chaos, Solitons and Fractals* (2009) 40:1408–12. doi:10.1016/j.chaos.2007.09.026

22. He JH, Jiao ML, He CH. Homotopy perturbation method for fractal duffing oscillator with arbitrary conditions. *FRACTALS (fractals)* (2022) 30:1–10. doi:10.1142/s0218348x22501651

23. Anjum N, He J-H. Two modifications of the homotopy perturbation method for nonlinear oscillators. *J Appl Comput Mech* (2020) 6:1420–5. doi:10.22055/JACM.2020.34850.2482

24. Ali M, Anjum N, Ain QT, He J-H. Homotopy perturbation method for the attachment oscillator arising in nanotechnology. *Fibers Polym* (2021) 22:1601–6. doi:10.1007/s12221-021-0844-x

25. Anjum N, He J-H. Higher-order homotopy perturbation method for conservative nonlinear oscillators generally and microelectromechanical systems' oscillators particularly. *Int J Mod Phys B* (2020) 34:2050313. doi:10.1142/s0217979220503130

26. He J-H, Moatimid GM, Zekry MH. Forced nonlinear oscillator in a fractal space. *Facta Universitatis, Ser Mech Eng* (2022) 20:001–20. doi:10.22190/fume220118004h

27. Tao H, Anjum N, Yang Y-J. The aboodh transformation-based homotopy perturbation method: new hope for fractional calculus. *Front Phys* (2023) 11:310. doi:10.3389/fphy.2023.1168795

28. Moatimid GM, Amer T, Zekry MH. Analytical and numerical study of a vibrating magnetic inverted pendulum. *Archive Appl Mech* (2023) 93:2533–47. doi:10.1007/s00419-023-02395-3

29. Niu J-Y, He C-H, Alsolami AA. Symmetry-breaking and pull-down motion for the helmholtz–duffing oscillator. *J Low Frequency Noise, Vibration Active Control* (2023). doi:10.1177/14613484231193261

30. Nadeem M, Alsayaad Y. A new study for the investigation of nonlinear fractional drinfeld–sokolov–wilson equation. *Math Probl Eng* (2023) 2023:1–9. doi:10.1155/2023/9274115

31. Niccolai L, Quarta AA, Mengali G, Bassetto M. Trajectory analysis of a zero-pitch-angle e-sail with homotopy perturbation technique. *J Guidance, Control Dyn* (2023) 46:734–41. doi:10.2514/1.g007219

32. Abdulameer YA, Ali Al-Saif AJ. Analytical simulation of natural convection between two concentric horizontal circular cylinders: a hybrid fourier transform-homotopy perturbation approach. *Math Model Eng Probl* (2023) 10:886–96. doi:10.18280/mmep.100319

33. Al-Hayani WM, Younis MT. The homotopy perturbation method for solving nonlocal initial-boundary value problems for parabolic and hyperbolic partial differential equations. *Eur J Pure Appl Maths* (2023) 16:1552–67. doi:10.29020/nybg.ejpam.v16i3.4794

34. Saeed HJ, Ali AH, Menzer R, Poclean AD, Arora H. New family of multi-step iterative methods based on homotopy perturbation technique for solving nonlinear equations. *Mathematics* (2023) 11:2603. doi:10.3390/math11122603

35. Moazzzam A, Anjum A, Saleem N, Kuffi EA. Study of telegraph equation via he-fractional laplace homotopy perturbation technique. *Ibn Al-haitham J Pure Appl Sci* (2023) 36:349–64. doi:10.30526/36.3.3239

36. Shams M, Kausar N, Khan N, Shah MA. Modified block homotopy perturbation method for solving triangular linear diophantine fuzzy system of equations. *Adv Mech Eng* (2023) 15:168781322311595. doi:10.1177/16878132231159519

37. Arora G, Kumar R, Mammeri Y. Homotopy perturbation and adomian decomposition methods for condensing coagulation and lifshitz-slyzov models. *GEM-International J Geomathematics* (2023) 14:4. doi:10.1007/s13137-023-00215-y

38. Pathak P, Barnwal AK, Sriwastav N, Singh R, Singh M. An algorithm based on homotopy perturbation theory and its mathematical analysis for singular nonlinear system of boundary value problems. *Math Methods Appl Sci* (2023). doi:10.1002/mma.9299

39. Ene R-D, Pop N. Semi-analytical closed-form solutions for the rikitake-type system through the optimal homotopy perturbation method. *Mathematics* (2023) 11:3078. doi:10.3390/math11143078

40. Abdul-Ameer YA, Ali Al-Saif A-SJ. Fourier-homotopy perturbation method for heat and mass transfer with 2d unsteady squeezing viscous flow problem. *J Comput Appl Mech* (2023) 54:219–35. doi:10.22059/jcamech.2023.356976.817

41. Shalbafian A, Ganjefar S. Variable speed wind turbine control using the homotopy perturbation method. *Int J Precision Eng Manufacturing-Green Tech* (2023) 10:141–50. doi:10.1007/s40684-022-00422-2

42. Niccolai L, Quarta AA, Mengali G. Application of homotopy perturbation method to the radial thrust problem. *Astrodynamics* (2023) 7:251–8. doi:10.1007/s42064-022-0150-4

43. Swain S, Swain BK, Sahoo B. Application of homotopy perturbation method on special third grade fluid flow with viscous dissipation effect over a stretching sheet. *Int J Mod Phys C* (2023) 34:2350060. doi:10.1142/s0129183123500602

44. He J-H, Jiao M-L, Gepreel KA, Khan Y. Homotopy perturbation method for strongly nonlinear oscillators. *Mathematics Comput Simulation* (2023) 204:243–58. doi:10.1016/j.matcom.2022.08.005

frontiers | Frontiers in Physics

TYPE Original Research
PUBLISHED 20 October 2023
DOI 10.3389/fphy.2023.1267673

OPEN ACCESS

EDITED BY
Chun-Hui He,
Xi'an University of Architecture and Technology, China

REVIEWED BY
Marwan Alquran,
Jordan University of Science and Technology, Jordan
Muhammad Nadeem,
Qujing Normal University, China

*CORRESPONDENCE
Farah M. Al-Askar,
famalaskar@pnu.edu.sa

RECEIVED 26 July 2023
ACCEPTED 03 October 2023
PUBLISHED 20 October 2023

CITATION
Al-Askar FM (2023), The solitary wave solutions of the stochastic Heisenberg ferromagnetic spin chain equation using two different analytical methods.
Front. Phys. 11:1267673.
doi: 10.3389/fphy.2023.1267673

The solitary wave solutions of the stochastic Heisenberg ferromagnetic spin chain equation using two different analytical methods

Farah M. Al-Askar*

Department of Mathematical Science, College of Science, Princess Nourah Bint Abdulrahman University, Riyadh, Saudi Arabia

Here, we consider the stochastic (2 + 1)-dimensional Heisenberg ferromagnetic spin chain equation which is forced by the multiplicative Brownian motion in the Stratonovich sense. We utilize the (G'/G)-expansion method and the mapping method to attain the analytical solutions of the stochastic (2 + 1)-dimensional Heisenberg ferromagnetic chain equation. Various types of analytical stochastic solutions, such as the hyperbolic, elliptic, and trigonometric functions, have been obtained. Physicists can utilize these solutions to understand a variety of important physical phenomena because the magnetic soliton has been categorized as one of the interesting groups of nonlinear excitations representing spin dynamics in the semiclassical continuum Heisenberg systems. Moreover, we employ MATLAB tools to plot 3D and 2D graphs for some obtained solutions to address the influence of Brownian motion on these solutions.

KEYWORDS

stochastic Heisenberg ferromagnetic equation, Brownian motion, mapping method, (G'/G)-expansion method, noise

1 Introduction

In many branches of science and mathematics, nonlinear evolution equations (NLEEs) play a crucial role in describing a wide range of phenomena that linear equations are unable to adequately explain. These equations involve nonlinear terms that can lead to diverse and often intricate behaviors, making their study both fascinating and challenging. NLEEs have also found significant applications in various branches of physics and engineering. In fluid dynamics, the famous Navier–Stokes equations describe the behavior of fluids which are inherently nonlinear due to their viscosity and turbulent effects. Understanding and solving these equations is essential for predicting weather patterns, optimizing industrial processes, and designing efficient aerodynamics. Additionally, NLEEs have been instrumental in quantum field theory, providing insights into particle physics and the dynamics of elementary particles.

In mathematics, the study of NLEEs has led to the development of several powerful analytical and numerical techniques. Some of these methods include Jacobi elliptic function [1], $(\frac{G'}{G})$-expansion [2, 3], sine–cosine [4, 5], perturbation [6, 7], exp $(-\phi(\varsigma))$-expansion [8], Hirota's [9], tanh–sech [10, 11], and Riccati–Bernoulli sub-ODE methods [12].

On the other hand, stochastic NLEEs (SNLEEs) play a crucial role in various scientific fields, including physics, finance, and probability theory. These equations incorporate

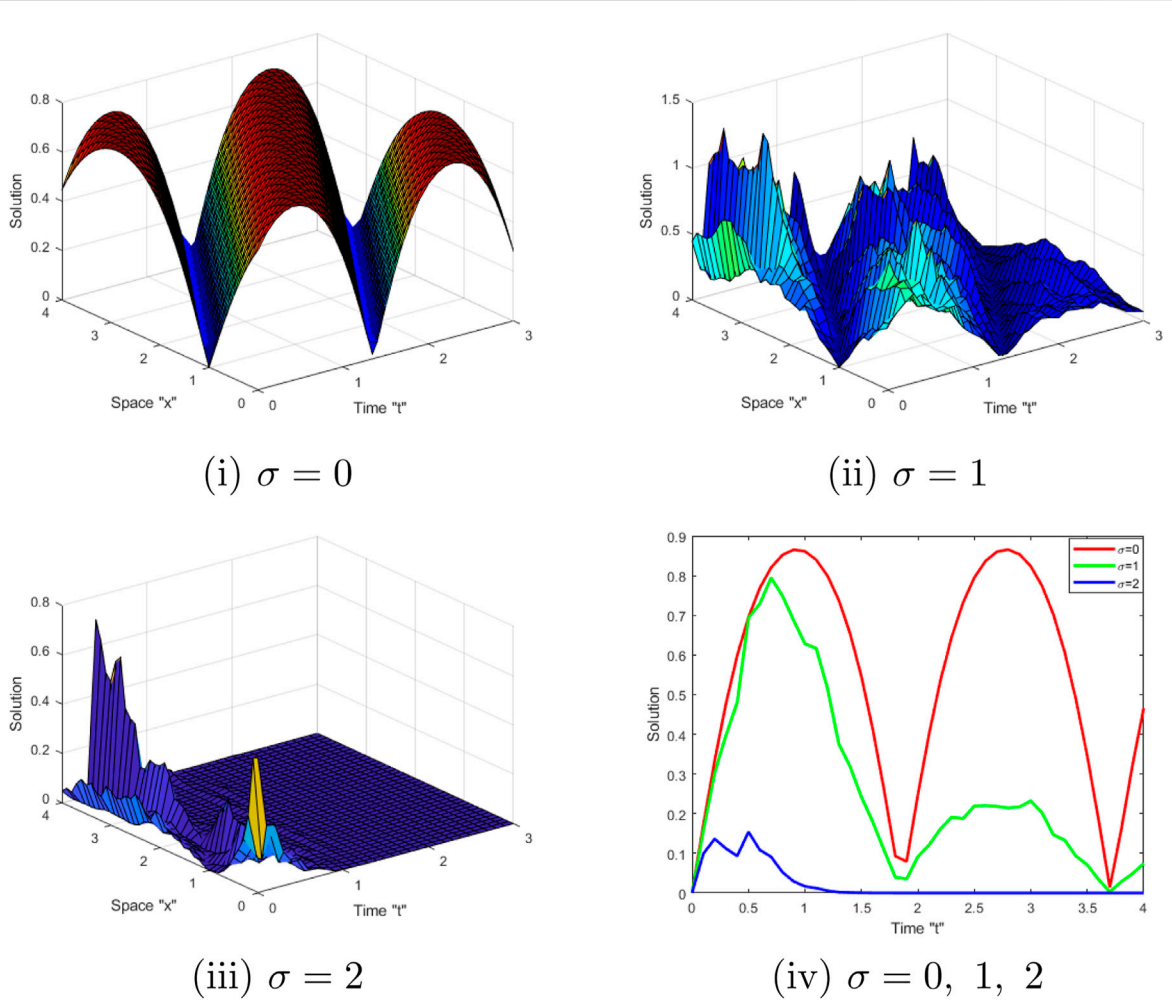

FIGURE 1
(i–iii) 3D profile of the solution $|\psi(x,y,t)|$ defined in Eq. 32, with $\theta_3 = -5$, $\hat{w} = 0.5$, and $\sigma = 0, 1, 2$. (iv) 2D profile of Eq. 32 with various values of σ.

random variations into deterministic equations, adding a stochastic term that captures the inherent uncertainty in the system. The addition of the stochastic term is of paramount importance as it allows us to better model and understand real-world phenomena by accounting for unpredictable factors and fluctuations. Furthermore, the addition of stochastic terms helps capture the complexity and nonlinearity of real-world systems. Many physical and financial systems exhibit a nonlinear behavior, where small changes in the initial conditions or parameters can lead to drastic and unpredictable outcomes. Traditional deterministic NLEEs often fail to accurately capture this nonlinear behavior. By introducing stochastic terms, we can better model the inherent randomness and nonlinearity of these systems, leading to more realistic and insightful solutions.

It looks more significant when considering models of NLEEs with random forces. Therefore, here, we consider one of the most important models in the modern magnetic theory, the stochastic Heisenberg ferromagnetic spin chain equation (SHFSCE), derived using multiplicative Brownian motion in the Stratonovich sense, which has the following form:

$$id\psi + \left[k_1\psi_{xx} + k_2\psi_{yy} + k_3\psi_{xy} - k_4|\psi|^2\psi\right]dt + i\rho\psi \circ d\mathcal{B} = 0, \quad (1)$$

where ψ is a complex stochastic function of the variables x, y, and t and k_i is the constant for $i = 1, 2, 3$, and 4. σ is the noise intensity, and $\mathcal{B}$ is the Brownian motion in one variable t.

A deterministic Heisenberg ferromagnetic equation (DHFE) has been created to interpret magnetic ordering in ferromagnetic materials. It plays an important role in the modern magnetic theory, which describes nonlinear magnet dynamics and is used in optical fibers. Due to the importance of DHFE, many authors have attained the exact solution for this equation by using various methods, such as Hirota's bilinear method [13, 14], Darboux transformation [15–17], sub-ODE method [18], sine-Gordon and modified exp-function expansion methods [19], auxiliary ordinary differential equation [20], Jacobi elliptic functions [21], F-expansion method combined with Jacobi elliptic functions [22], and generalized Riccati mapping method and improved auxiliary equation [23], while many authors have investigated the analytical solutions of fractional DHFE by using various methods, including exp $(-\phi(\varsigma))$-expansion and extended tanh function [24], new extended generalized Kudryashov [25], and generalized Riccati equation mapping methods [26].

The main motivation of this work is to obtain the analytical stochastic solutions of Eq. 1 using the (G'/G)-expansion and

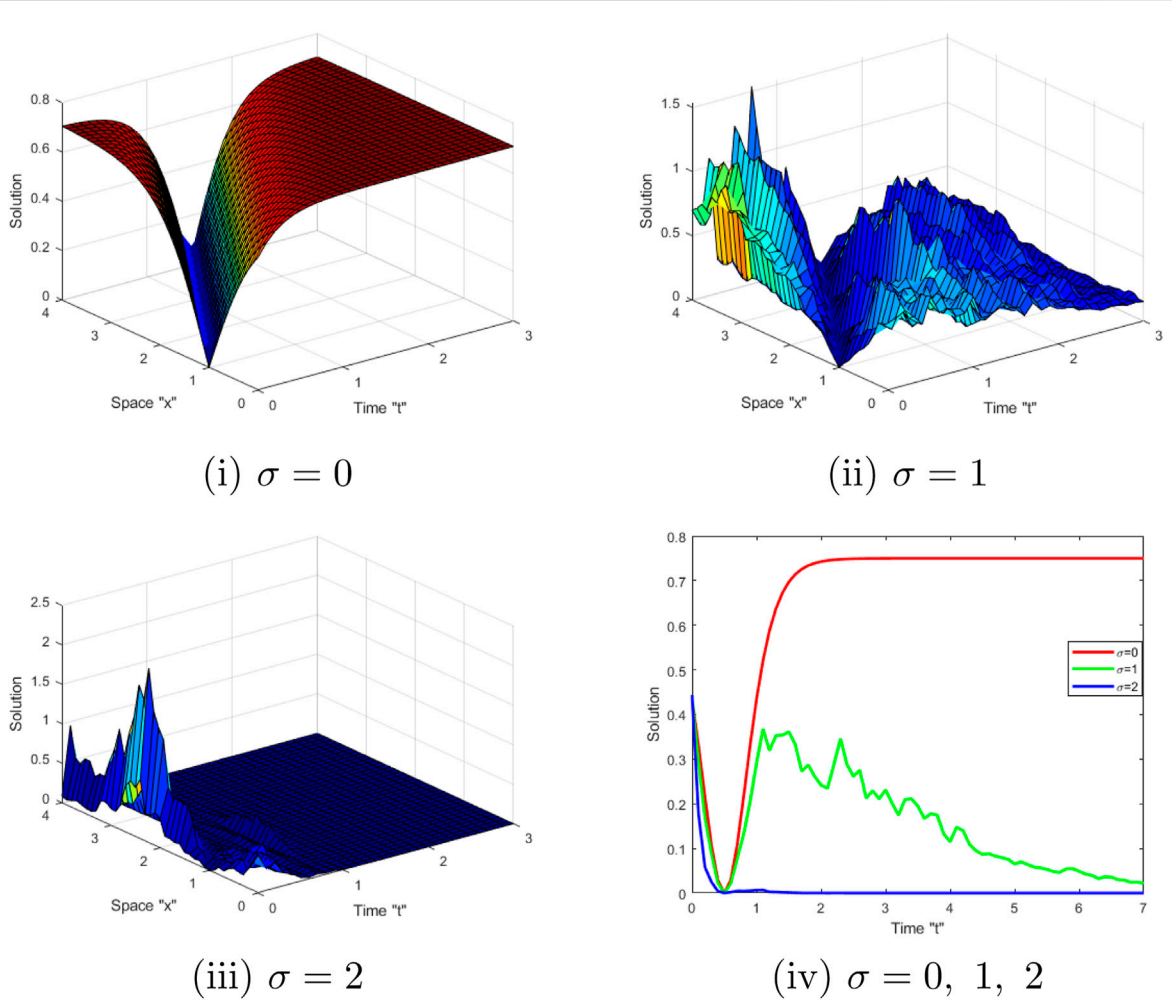

FIGURE 2
(i–iii) 3D profile of the solution $|\psi(x,y,t)|$ defined in Eq. 33, with $\theta_3 = -5$ and $\sigma = 0, 1, 2$ (iv) 2D profile of Eq. 33 with various values of σ.

mapping methods. Physicists could utilize the acquired solution to interpret a variety of fascinating physical phenomena because the magnetic soliton has been categorized as one of the interesting groups of nonlinear excitations representing spin dynamics in the semiclassical continuum Heisenberg systems. Moreover, we show the influence of Brownian motion on the behavior of these solutions using *MATLAB* tools to exhibit some graphical representations.

The remainder of this article is organized as follows: in Section 2, we define the Brownian motion and state the relationship between the Stratonovich and Itô integrals. In Section 3, we derive the wave equation of SHFSCE (1). In Section 4, we apply the $(\frac{G'}{G})$-expansion method to attain the analytical stochastic solution of SHFSCE (1). In Section 5, we discuss the influences of Brownian motion on the analytical solutions of SHFSCE (1). Finally, we outline the article's conclusions in Section 6.

2 Brownian motion

Brownian motion refers to the random movement of microscopic particles suspended in a fluid. It was first observed by the Scottish botanist Robert Brown in 1827 when he noticed pollen grains jiggling randomly in water under a microscope. This discovery paved the way for the development of the kinetic theory of gases and had a profound impact on our understanding of the physical world. Brownian motion has applications in a wide range of scientific disciplines. In physics, it has been used to determine fundamental constants, such as Avogadro's number, by measuring the displacement of particles in a known volume under known conditions. In chemistry, it has been utilized to study the diffusion of molecules, enabling the determination of molecular sizes and diffusion coefficients. In biology, it has been employed to study the movement of microscopic organisms and the dynamics of biological macromolecules.

Now, let us define the Brownian motion $\mathcal{B}(t)$ as follows:

Definition 1. *The stochastic process $\mathcal{B}(t),\ t \geq 0$ is called Brownian motion if it satisfies the following criteria*:

1. $\mathcal{B}(0) = 0$.
2. $\mathcal{B}(t)$ *has independent increments.*
3. $\mathcal{B}(t)$ *is continuous in* t.

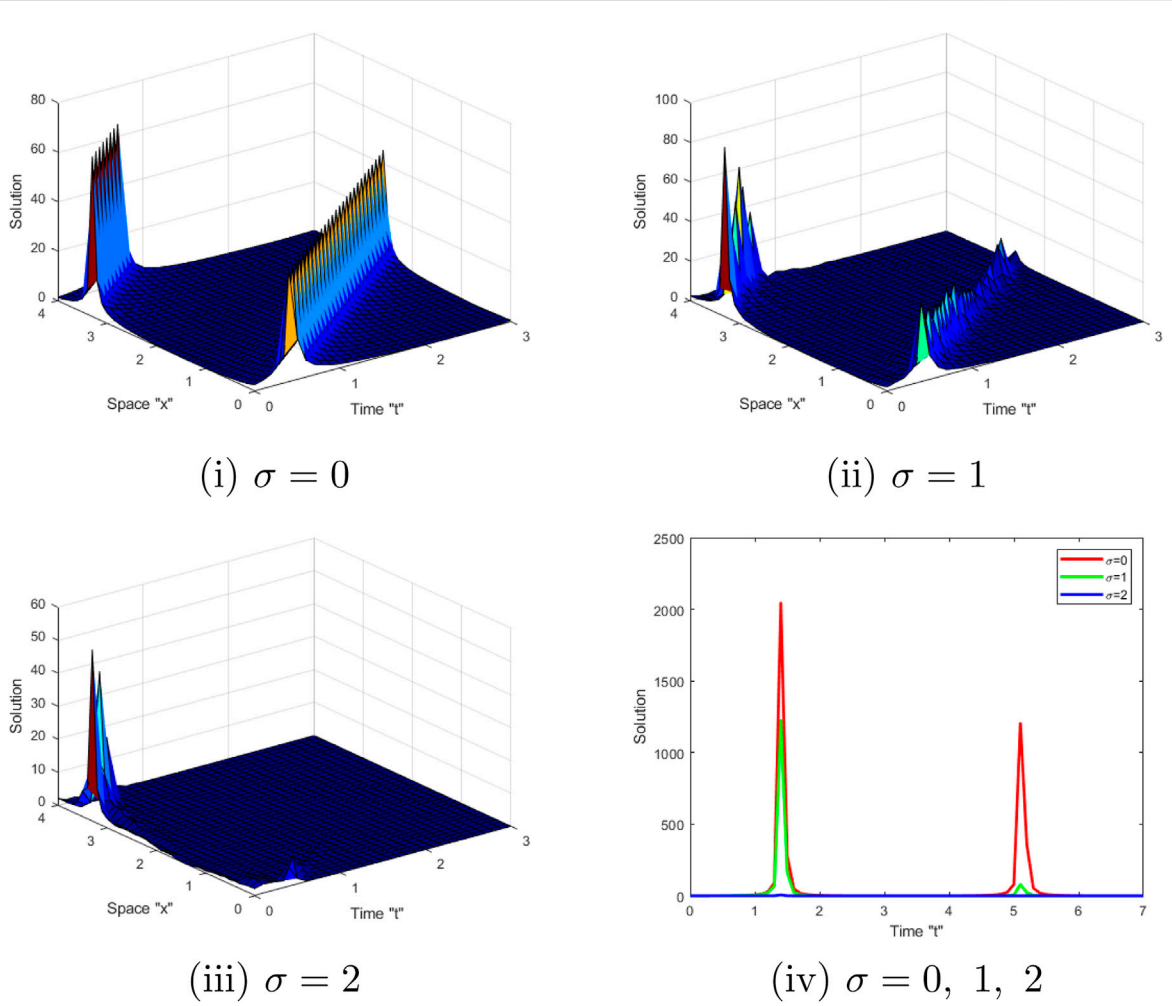

FIGURE 3
(i–iii) 3D profile of the solution $|\psi(x,y,t)|$ defined in Eq. 43, with $\theta_3 = -5$ and $\sigma = 0, 1, 2$. (iv) 2D profile of Eq. 43 with various values of σ.

4. *The increments* $\mathcal{B}(t) - \mathcal{B}(s)$ *are normally distributed with variance* $t - s$ *and mean 0.*

We need the following lemma:

Lemma 1. $\mathbb{E}(e^{\rho\mathcal{B}(t)}) = e^{\frac{1}{2}\rho^2 t}$ *for any real number* ρ.

We note that there are two widely used versions of stochastic integrals, Stratonovich and Itô [27, 28]. Modeling issues usually dictate determination of the acceptable version; however, once the version is selected, a comparable equation of the other version can be established with the same solutions. Thus, it is possible to switch between Itô (denoted by $\int_0^t f d\mathcal{B}$) and Stratonovich (denoted by $\int_0^t f \circ d\mathcal{B}$) integrals using the following relationship:

$$\int_0^t f(s, X_s) d\mathcal{B}(s) = \int_0^t f(s, X_s) \circ d\mathcal{B}(s) - \frac{1}{2}\int_0^t f(s, X_s) \frac{\partial f(s, X_s)}{\partial x} ds, \tag{2}$$

where f is assumed to be sufficiently regular and $\{X_t,\ t \geq 0\}$ is a stochastic process.

3 The wave equation of SHFSCE

To derive the wave equation of SHFSCE, we employ the next wave transformation:

$$\begin{aligned} &\psi(x, y, t) = u(\eta) e^{(i\theta - \sigma\mathcal{B}(t) - \sigma^2 t)},\ \eta = \eta_1 x + \eta_2 y + \eta_3 t, \\ &\theta = \theta_1 x + \theta_2 y + \theta_3 t, \end{aligned} \tag{3}$$

where u is a real deterministic function and η_i and θ_i for all $i = 1, 2$, and 3 are constants. We note that

$$\begin{aligned} \psi_{xx} &= \left[\eta_1^2 u'' + 2i\eta_1\theta_1 u' - \theta_1^2 u\right] e^{(i\theta - \sigma\mathcal{B}(t) - \sigma^2 t)}, \\ \psi_{yy} &= \left[\eta_2^2 u'' + 2i\eta_2\theta_2 u' - \theta_2^2 u\right] e^{(i\theta - \sigma\mathcal{B}(t) - \sigma^2 t)}, \\ \psi_{xy} &= \left[\eta_1\eta_2 u'' + i(\eta_1\theta_2 + \eta_2\theta_1) u' - \theta_1\theta_2 u\right] e^{(i\theta - \sigma\mathcal{B}(t) - \sigma^2 t)}, \end{aligned} \tag{4}$$

and

$$\begin{aligned} d\psi &= \left[\left(\eta_3 u' + i\theta_3 u + \frac{1}{2}\sigma^2 u - \sigma^2 u\right) dt - \sigma u d\mathcal{B}\right] e^{(i\theta - \sigma\mathcal{B}(t) - \sigma^2 t)} dt \\ &= \left[(\eta_3 u' + i\theta_3 u) dt - \left(\frac{1}{2}\sigma^2 u dt + \sigma u d\mathcal{B}\right)\right] e^{(i\theta - \sigma\mathcal{B}(t) - \sigma^2 t)} dt, \end{aligned} \tag{5}$$

where the term $+\frac{1}{2}\sigma^2 u$ represents the Itô correction. By using Eq. 2 in the differential form, we obtain

$$d\psi = [(\eta_3 u' + i\theta_3 u)dt - \sigma u \circ d\mathcal{B}]e^{(i\theta - \sigma\mathcal{B}(t) - \sigma^2 t)}dt. \tag{6}$$

Substituting Eq. 3 into (1) and utilizing Eqs 4, 5, we obtain the following equation for the imaginary part:

$$(\eta_3 + 2k_1\eta_1\theta_1 + 2k_2\eta_2\theta_2 + k_3\eta_1\theta_2 + k_3\eta_2\theta_1)u' = 0, \tag{7}$$

where we assume that

$$\eta_3 = -k_1\eta_1\theta_1 - 2k_2\eta_2\theta_2 - k_3\eta_1\theta_2 - k_3\eta_2\theta_1.$$

Furthermore, we derive the following equation for the real part:

$$u'' - \hbar_1 e^{(2\sigma\mathcal{B}(t) - 2\sigma^2 t)}u^3 - \hbar_2 u = 0, \tag{8}$$

where

$$\hbar_1 = \frac{k_4}{k_1\eta_1^2 + k_2\eta_2^2 + k_3\eta_1\eta_2} \text{ and } \hbar_2 = \frac{\theta_3 + k_1\theta_1^2 + k_2\theta_2^2 + k_3\theta_1\theta_2}{k_1\eta_1^2 + k_2\eta_2^2 + k_3\eta_1\eta_2}.$$

Taking expectation on both sides of Eq. 8, we attain

$$u'' - \hbar_1 u^3 e^{-2\sigma^2 t}\mathbb{E}\left(e^{2\sigma\mathcal{B}(t)}\right) - \hbar_2 u = 0, \tag{9}$$

where u represents the deterministic function. Using Lemma 1, Eq. 9 attains the following form:

$$u'' - \hbar_1 u^3 - \hbar_2 u = 0. \tag{10}$$

4 Exact solutions of SHFSCE

To find the solutions of Eq. 10, we apply the (G'/G)-expansion [2] and mapping methods. Subsequently, we attain the solutions of SHFSCE (1).

4.1 (G'/G)-expansion method

To begin, let us assume that the solution of Eq. 10 has the following form:

$$u = \sum_{i=0}^{N} b_k \left[\frac{G'}{G}\right]^i, \tag{11}$$

where $b_0, b_1, ..., b_N$ denote unknown constants, such that $b_N \neq 0$, and G solves

$$G'' + \lambda G' + \nu G = 0, \tag{12}$$

where λ and ν are undefined constants. By balancing u^3 with u'' in Eq. 10, we obtain

$$N = 1. \tag{13}$$

From Eq. 13, we can rewrite Eq. 11 as

$$u = b_0 + b_1\frac{G'}{G}. \tag{14}$$

Substituting Eq. 14 into Eq. 10 and utilizing Eq. 12, we obtain

$$(2b_1 - \hbar_1 b_1^3)\left[\frac{G'}{G}\right]^3 + (3\lambda b_1 - 3\hbar_1 b_0 b_1^2)\left[\frac{G'}{G}\right]^2 + (\lambda^2 b_1 + 2b_1\nu - 3\hbar_1 b_1 b_0^2 - \hbar_2 b_1)\left[\frac{G'}{G}\right] + (\nu\lambda b_1 - \hbar_1 b_0^2 b_1 - \hbar_2 b_0) = 0.$$

Equating each coefficient of $\left[\frac{G'}{G}\right]^i$ ($i = 3, 2, 1$, and 0) by zero, we obtain

$$2b_1 - \hbar_1 b_1^3 = 0,$$
$$3\lambda b_1 - 3\hbar_1 b_0 b_1^2 = 0,$$
$$\lambda^2 b_1 + 2b_1\nu - 3\hbar_1 b_1 b_0^2 - \hbar_2 b_1 = 0,$$

and

$$\nu\lambda b_1 - \hbar_1 b_0^3 - \hbar_2 b_0 = 0.$$

We obtain the following equation by solving these equations:

$$b_1 = \pm\sqrt{\frac{2}{\hbar_1}}, \quad \lambda = \lambda, \; b_0 = \pm\frac{\lambda}{\sqrt{2\hbar_1}}, \; \nu = \frac{\lambda^2}{4} + \frac{\hbar_2}{2}. \tag{15}$$

The roots of auxiliary Eq. 12 are

$$\frac{-\lambda}{2} \pm \sqrt{\frac{-\hbar_2}{2}}.$$

Depending on $\hbar_2$, a variety of situations might arise, which are as follows:

Case 1: If $\hbar_2 = 0$, then

$$G(\eta) = c_1 \exp\left(\frac{-\lambda}{2}\eta\right) + c_2\eta\exp\left(\frac{-\lambda}{2}\eta\right),$$

where c_1 and c_2 are constants. Hence, by using Eq. 14, the solution of Eq. 10 is

$$u(\eta) = \pm\frac{\lambda}{\sqrt{2\hbar_1}} \pm \sqrt{\frac{2}{\hbar_1}}\left[\frac{-\lambda}{2} + \frac{c_2\exp\left(\frac{-\lambda}{2}\eta\right)}{c_1\exp\left(\frac{-\lambda}{2}\eta\right) + c_2\eta\exp\left(\frac{-\lambda}{2}\eta\right)}\right]. \tag{16}$$

As a result, SHFSCE (1) derives the solution

$$\psi(x,y,t) = \pm\left\{\frac{\lambda}{\sqrt{2\hbar_1}} + \sqrt{\frac{2}{\hbar_1}}\left[\frac{-\lambda}{2} + \frac{c_2\exp\left(\frac{-\lambda}{2}\eta\right)}{c_1\exp\left(\frac{-\lambda}{2}\eta\right) + c_2\eta\exp\left(\frac{-\lambda}{2}\eta\right)}\right]\right\}e^{(i\theta - \sigma\mathcal{B}(t) - \sigma^2 t)}, \tag{17}$$

where $\eta = \eta_1 x + \eta_2 y - (2k_1\eta_1\theta_1 + 2k_2\eta_2\theta_2 + k_3\eta_1\theta_2 + k_3\eta_2\theta_1)t$ and $\theta = \theta_1 x + \theta_2 y + \theta_3 t$.

Case 2: If $\hbar_2 < 0$, then

$$G(\eta) = c_1\exp\left[\left(\frac{-\lambda}{2} + \sqrt{\frac{-\hbar_2}{2}}\right)\eta\right] + c_2\exp\left[\left(\frac{-\lambda}{2} - \sqrt{\frac{-\hbar_2}{2}}\right)\eta\right].$$

Therefore, the solution of Eq. 10 is

$$u(\eta) = \pm\frac{\lambda}{\sqrt{2\hbar_1}} \pm \sqrt{\frac{2}{\hbar_1}}\left[\frac{c_1\left(\frac{-\lambda}{2} + \sqrt{\frac{-\hbar_2}{2}}\right)\exp\left(\left(\frac{-\lambda}{2} + \sqrt{\frac{-\hbar_2}{2}}\right)\eta\right)}{c_1\exp\left(\left(\frac{-\lambda}{2} + \sqrt{\frac{-\hbar_2}{2}}\right)\eta\right) + c_2\exp\left(\left(\frac{-\lambda}{2} - \sqrt{\frac{-\hbar_2}{2}}\right)\eta\right)} + \frac{c_2\left(\frac{-\lambda}{2} - \sqrt{\frac{-\hbar_2}{2}}\right)\exp\left(\left(\frac{-\lambda}{2} - \sqrt{\frac{-\hbar_2}{2}}\right)\eta\right)}{c_1\exp\left(\left(\frac{-\lambda}{2} + \sqrt{\frac{-\hbar_2}{2}}\right)\eta\right) + c_2\exp\left(\left(\frac{-\lambda}{2} - \sqrt{\frac{-\hbar_2}{2}}\right)\eta\right)}\right]. \tag{18}$$

Consequently, the solution of SHFSCE (1) is

$$\psi(x,y,t)=\pm\left\{\frac{\lambda}{\sqrt{2\hbar_1}}+\sqrt{\frac{2}{\hbar_1}}\left[\frac{c_1\left(\frac{-\lambda}{2}+\sqrt{\frac{-\hbar_2}{2}}\right)\exp\left(\left(\frac{-\lambda}{2}+\sqrt{\frac{-\hbar_2}{2}}\right)\eta\right)}{c_1\exp\left(\left(\frac{-\lambda}{2}+\sqrt{\frac{-\hbar_2}{2}}\right)\eta\right)+c_2\exp\left(\left(\frac{-\lambda}{2}-\sqrt{\frac{-\hbar_2}{2}}\right)\eta\right)}+\frac{c_2\left(\frac{-\lambda}{2}-\sqrt{\frac{-\hbar_2}{2}}\right)\exp\left(\left(\frac{-\lambda}{2}-\sqrt{\frac{-\hbar_2}{2}}\right)\eta\right)}{c_1\exp\left(\left(\frac{-\lambda}{2}+\sqrt{\frac{-\hbar_2}{2}}\right)\eta\right)+c_2\exp\left(\left(\frac{-\lambda}{2}-\sqrt{\frac{-\hbar_2}{2}}\right)\eta\right)}\right]\right\}e^{(i\theta-\sigma\mathcal{B}(t)-\sigma^2t)}. \tag{19}$$

Case 3: If $\hbar_2>0$, then

$$G(\eta)=\exp\left(\frac{-\lambda}{2}\eta\right)\left[c_1\cos\left(\sqrt{\frac{\hbar_2}{2}}\eta\right)+c_2\sin\left(\sqrt{\frac{\hbar_2}{2}}\eta\right)\right].$$

Hence, the solution of Eq. 10 is

$$u(\eta)=\pm\frac{\lambda}{\sqrt{2\hbar_1}}\pm\sqrt{\frac{2}{\hbar_1}}\left[\frac{-\lambda}{2}+\frac{-c_1\sqrt{\frac{\hbar_2}{2}}\sin\left(\sqrt{\frac{\hbar_2}{2}}\eta\right)+c_2\sqrt{\frac{\hbar_2}{2}}\cos\left(\sqrt{\frac{\hbar_2}{2}}\eta\right)}{c_1\cos\left(\sqrt{\frac{\hbar_2}{2}}\eta\right)+c_2\sin\left(\sqrt{\frac{\hbar_2}{2}}\eta\right)}\right]. \tag{20}$$

Thus, the solution of SHFSCE (1) is

$$\psi(x,y,t)=\left\{\frac{\lambda}{\sqrt{2\hbar_1}}\pm\sqrt{\frac{2}{\hbar_1}}\left[\frac{-\lambda}{2}+\frac{-c_1\sqrt{\frac{\hbar_2}{2}}\sin\left(\sqrt{\frac{\hbar_2}{2}}\eta\right)+c_2\sqrt{\frac{\hbar_2}{2}}\cos\left(\sqrt{\frac{\hbar_2}{2}}\eta\right)}{c_1\cos\left(\sqrt{\frac{\hbar_2}{2}}\eta\right)+c_2\sin\left(\sqrt{\frac{\hbar_2}{2}}\eta\right)}\right]\right\}e^{(i\theta-\sigma\mathcal{B}(t)-\sigma^2t)}, \tag{21}$$

where $\eta=\eta_1x+\eta_2y-(2k_1\eta_1\theta_1+2k_2\eta_2\theta_2+k_3\eta_1\theta_2+k_3\eta_2\theta_1)t$ and $\theta=\theta_1x+\theta_2y+\theta_3t$.

Special cases

Case 1: Substituting $c_2=0$ and $\lambda=0$ into Eq. 21, we obtain

$$\psi(x,y,t)=\pm\sqrt{\frac{\hbar_2}{\hbar_1}}\tan\left(\sqrt{\frac{\hbar_2}{2}}\eta\right)e^{(i\theta-\sigma\mathcal{B}(t)-\sigma^2t)}. \tag{22}$$

Case 2: Substituting $c_1=0$ and $\lambda=0$ into Eq. 21, we obtain

$$\psi(x,y,t)=\pm\sqrt{\frac{\hbar_2}{\hbar_1}}\cot\left(\sqrt{\frac{\hbar_2}{2}}\eta\right)e^{(i\theta-\sigma\mathcal{B}(t)-\sigma^2t)}. \tag{23}$$

Case 3: If we substitute $c_1=c_2=1$ and $\lambda=0$ into Eq. 21, then

$$\psi(x,y,t)=\pm\sqrt{\frac{\hbar_2}{\hbar_1}}\left[\sec\left(\sqrt{2\hbar_2}\eta\right)+\tan\left(\sqrt{2\hbar_2}\eta\right)\right]e^{(i\theta-\sigma\mathcal{B}(t)-\sigma^2t)}.$$

Case 4: Substituting $c_1=c_2=1$ and $\lambda=\sqrt{2\hbar_1}$ into Eq. 21, we derive

$$\psi(x,y,t)=\left[\pm1\mp2\sqrt{\frac{\hbar_2}{\hbar_1}}\left(\frac{1}{1+\cot\left(\sqrt{2\hbar_2}\eta\right)}\right)\right]e^{(i\theta-\sigma\mathcal{B}(t)-\sigma^2t)}. \tag{24}$$

Case 5: Substituting $c_1=c_2=1$ and $\lambda=-\sqrt{2\hbar_1}$ into Eq. 21, we obtain

$$\psi(x,y,t)=\left[\mp1\pm2\sqrt{\frac{\hbar_2}{\hbar_1}}\left(\frac{1}{1+\tan\left(\sqrt{2\hbar_2}\eta\right)}\right)\right]e^{(i\theta-\sigma\mathcal{B}(t)-\sigma^2t)}. \tag{25}$$

Case 6: Substituting $c_1=c_2=1$ and $\lambda=0$ into Eq. 19, we derive

$$\psi(x,y,t)=\pm\sqrt{\frac{-\hbar_2}{\hbar_1}}\tanh\left(\sqrt{\frac{-\hbar_2}{2}}\eta\right)e^{(i\theta-\sigma\mathcal{B}(t)-\sigma^2t)}. \tag{26}$$

Case 7: Substituting $c_1=1$, $c_2=-1$, and $\lambda=0$ into Eq. 19, we derive

$$\psi(x,y,t)=\pm\sqrt{\frac{-\hbar_2}{\hbar_1}}\coth\left(\sqrt{\frac{-\hbar_2}{2}}\eta\right)e^{(i\theta-\sigma\mathcal{B}(t)-\sigma^2t)}, \tag{27}$$

where $\eta=\eta_1x+\eta_2y-(2k_1\eta_1\theta_1+2k_2\eta_2\theta_2+k_3\eta_1\theta_2+k_3\eta_2\theta_1)t$ and $\theta=\theta_1x+\theta_2y+\theta_3t$.

Remark 3. Eqs 22–27 *with* $\sigma=0$ *coincide with the results reported in* [24].

4.2 Mapping method

Let the solutions of Eq. 10 take the following form:

$$\Psi(\eta)=\ell_0+\ell_1\varphi(\eta), \tag{28}$$

where ℓ_0 and ℓ_1 denote the undetermined constants and φ solves the first elliptic equation:

$$\varphi'=\sqrt{r+q\varphi^2+p\varphi^4}, \tag{29}$$

where the parameters r, q, and p all denote real numbers. Substituting Eq. 28 into Eq. 10, we obtain

$$(2\ell_1p-\hbar_1\ell_1^3)\varphi^3-3\hbar_1\ell_0\ell_1^2\varphi^2+(\ell_1q-3\hbar_1\ell_0^2\ell_1-\ell_1\hbar_2)\varphi+(\hbar_2\ell_0-\hbar_1\ell_0^3)=0.$$

Equating each coefficient of φ^k to zero, we derive

$$2\ell_1p-\hbar_1\ell_1^3=0,$$
$$-3\hbar_1\ell_0\ell_1^2=0,$$
$$\ell_1q-3\hbar_1\ell_0^2\ell_1-\ell_1\hbar_2=0,$$

and

$$-\hbar_2\ell_0-\hbar_1\ell_0^3=0.$$

Solving these equations, we obtain

$$\ell_0=0,\quad \ell_1=\pm\sqrt{\frac{2p}{\hbar_1}},\quad \hbar_1=0,\quad q=\hbar_2. \tag{30}$$

Substituting into Eq. 28, we derive the solutions of Eq. 10 in the following form:

$$u(\eta)=\pm\sqrt{\frac{2p}{\hbar_1}}\varphi(\eta),\ \text{for}\ \frac{p}{\hbar_1}>0.$$

Consequently, the solutions of SHFSCE (1), utilizing Eq. 3, are

$$\psi(x,y,t)=\pm\sqrt{\frac{2p}{\hbar_1}}\varphi(\eta)e^{(i\theta-\sigma\mathcal{B}(t)-\sigma^2t)},\ \text{for}\ \frac{p}{\hbar_1}>0. \tag{31}$$

Depending on p and $\hbar_1$, a variety of cases might arise, which are as follows:

Case 1: If $p=,\hat{w}^2$, $q=-(1+\hat{w}^2)$, and $r=1$, then the solution of Eq. 29 is $\varphi(\eta)=\mathrm{sn}(\eta)$. Hence, Eq. 31 becomes

$$\psi(x,y,t)=\pm\hat{w}\sqrt{\frac{2}{\hbar_1}}sn(\eta)e^{(i\theta-\sigma\mathcal{B}(t)-\sigma^2t)},\ \text{for}\ \hbar_1>0. \tag{32}$$

When $\hat{w}\to1$, then Eq. 32 changes to

$$\psi(x,y,t) = \pm\sqrt{\frac{2}{\hbar_1}}\tanh(\eta)e^{(i\theta-\sigma\mathcal{B}(t)-\sigma^2t)}, \text{ for } \hbar_1>0. \quad (33)$$

Case 2: If $p = 1$, $q = 2\hat{w}^2 - 1$ and $r = -\hat{w}^2(1-\hat{w}^2)$, then the solution of Eq. 29 is $\varphi(\eta) = ds(\eta)$. Thus, Eq. 31 becomes

$$\psi(x,y,t) = \pm\sqrt{\frac{2}{\hbar_1}}ds(\eta)e^{(i\theta-\sigma\mathcal{B}(t)-\sigma^2t)}, \text{ for } \hbar_1>0. \quad (34)$$

When $\hat{w}\to 1$, then Eq. 34 changes to

$$\psi(x,y,t) = \pm\sqrt{\frac{2}{\hbar_1}}\text{csch}(\eta)e^{(i\theta-\sigma\mathcal{B}(t)-\sigma^2t)}, \text{ for } \hbar_1>0. \quad (35)$$

If $\hat{w}\to 0$, then Eq. 34 tends to

$$\psi(x,y,t) = \pm\sqrt{\frac{2}{\hbar_1}}\csc(\eta)e^{(i\theta-\sigma\mathcal{B}(t)-\sigma^2t)}, \text{ for } \hbar_1>0. \quad (36)$$

Case 3: If $p = 1$, $q = 2-\hat{w}^2$, and $r = (1-\hat{w}^2)$, then the solution of Eq. 29 is $\varphi(\eta) = cs(\eta)$. Hence, Eq. 31 becomes

$$\psi(x,y,t) = \pm\sqrt{\frac{2}{\hbar_1}}cs(\eta)e^{(i\theta-\sigma\mathcal{B}(t)-\sigma^2t)}, \text{ for } \hbar_1>0. \quad (37)$$

When $\hat{w}\to 1$, then Eq. 37 transfers to Eq. 35. If $\hat{w}\to 0$, then Eq. 37 tends to

$$\psi(x,y,t) = \pm\sqrt{\frac{2}{\hbar_1}}\cot(\eta)e^{(i\theta-\sigma\mathcal{B}(t)-\sigma^2t)}, \text{ for } \hbar_1>0. \quad (38)$$

Case 4: If $p = \frac{\hat{w}^2}{4}$, $q = \frac{(\hat{w}^2-2)}{2}$, and $r = \frac{1}{4}$, then the solution of Eq. 29 is $\varphi(\eta) = \frac{sn(\eta)}{1+dn(\eta)}$. Thus, Eq. 31 becomes

$$\psi(x,y,t) = \pm\hat{w}\sqrt{\frac{1}{2\hbar_1}}\frac{sn(\eta)}{1+dn(\eta)}e^{(i\theta-\sigma\mathcal{B}(t)-\sigma^2t)}, \text{ for } \hbar_1>0. \quad (39)$$

When $\hat{w}\to 1$, then Eq. 39 transfers to

$$\psi(x,y,t) = \pm\sqrt{\frac{1}{2\hbar_1}}\frac{\tanh(\eta)}{1+\text{sech}(\eta)}e^{(i\theta-\sigma\mathcal{B}(t)-\sigma^2t)}, \text{ for } \hbar_1>0. \quad (40)$$

Case 5: If $p = \frac{(1-\hat{w}^2)^2}{4}$, $q = \frac{(1-\hat{w}^2)^2}{2}$, and $r = \frac{1}{4}$, then the solution of Eq. 29 is $\varphi(\eta) = \frac{sn(\eta)}{dn+cn(\eta)}$. Hence, Eq. 31 becomes

$$\psi(x,y,t) = \pm(1-\hat{w}^2)\sqrt{\frac{1}{2\hbar_1}}\frac{sn(\eta)}{dn+cn(\eta)}e^{(i\theta-\sigma\mathcal{B}(t)-\sigma^2t)}, \text{ for } \hbar_1>0. \quad (41)$$

If $\hat{w}\to 0$, then Eq. 41 tends to

$$\psi(x,y,t) = \pm\sqrt{\frac{1}{2\hbar_1}}\frac{\sin(\eta)}{1+\cos(\eta)}e^{(i\theta-\sigma\mathcal{B}(t)-\sigma^2t)}, \text{ for } \hbar_1>0. \quad (42)$$

Case 6: If $p = \frac{1-\hat{w}^2}{4}$, $q = \frac{(1-\hat{w}^2)}{2}$, and $r = \frac{(1-\hat{w}^2)}{4}$, then the solution of Eq. 29 is $\varphi(\eta) = \frac{cn(\eta)}{1+sn(\eta)}$. Thus, Eq. 31 takes the following form:

$$\psi(x,y,t) = \pm\sqrt{\frac{1-\hat{w}^2}{2\hbar_1}}\frac{cn(\eta)}{1+sn(\eta)}e^{(i\theta-\sigma\mathcal{B}(t)-\sigma^2t)}, \text{ for } \hbar_1>0. \quad (43)$$

If $\hat{w}\to 0$, then Eq. 43 tends to

$$\psi(x,y,t) = \pm\sqrt{\frac{1}{2\hbar_1}}\frac{\cos(\eta)}{1+\sin(\eta)}e^{(i\theta-\sigma\mathcal{B}(t)-\sigma^2t)}, \text{ for } \hbar_1>0. \quad (44)$$

Case 7: If $p = 1$, $q = 0$, and $r = 0$, then the solution of Eq. 29 is $\varphi(\eta) = \frac{c}{\eta}$. Hence, Eq. 31 becomes

$$\psi(x,y,t) = \pm\sqrt{\frac{2}{\hbar_1}}\frac{c}{\eta}e^{(i\theta-\sigma\mathcal{B}(t)-\sigma^2t)}, \text{ for } \hbar_1>0. \quad (45)$$

Case 8: If $p = -1$, $q = 2-\hat{w}^2$, and $r = (\hat{w}^2-1)$, then the solution of Eq. 29 is $\varphi(\eta) = dn(\eta)$. Thus, Eq. 31 becomes

$$\psi(x,y,t) = \pm\sqrt{\frac{-2}{\hbar_1}}dn(\eta)e^{(i\theta-\sigma\mathcal{B}(t)-\sigma^2t)}, \text{ for } \hbar_1<0. \quad (46)$$

When $\hat{w}\to 1$, then Eq. 46 transfers to

$$\psi(x,y,t) = \pm\sqrt{\frac{-2}{\hbar_1}}\text{sech}(\eta)e^{(i\theta-\sigma\mathcal{B}(t)-\sigma^2t)}, \text{ for } \hbar_1<0. \quad (47)$$

If $\hat{w}\to 0$, then Eq. 46 tends to

$$\psi(x,y,t) = \pm\sqrt{\frac{-2}{\hbar_1}}e^{(i\theta-\sigma\mathcal{B}(t)-\sigma^2t)}, \text{ for } \hbar_1<0. \quad (48)$$

Case 9: If $p = -\hat{w}^2$, $q = 2\hat{w}^2-1$ and $r = (1-\hat{w}^2)$, then the solution of Eq. 29 is $\varphi(\eta) = cn(\eta)$. Hence, Eq. 31 becomes

$$\psi(x,y,t) = \pm\hat{w}\sqrt{\frac{-2}{\hbar_1}}cn(\eta)e^{(i\theta-\sigma\mathcal{B}(t)-\sigma^2t)}, \text{ for } \hbar_1<0. \quad (49)$$

When $\hat{w}\to 1$, then Eq. 46 transfers to Eq. 47.

Case 10: If $p = \frac{\hat{w}^2-1}{4}$, $q = \frac{(\hat{w}^2+1)}{2}$, and $r = \frac{(\hat{w}^2-1)}{4}$, then the solution of Eq. 29 is $\varphi(\eta) = \frac{dn(\eta)}{1+sn(\eta)}$. Thus, Eq. 31 has the following form:

$$\psi(x,y,t) = \pm\sqrt{\frac{\hat{w}^2-1}{2\hbar_1}}\frac{dn(\eta)}{1+sn(\eta)}e^{(i\theta-\sigma\mathcal{B}(t)-\sigma^2t)}, \text{ for } \hbar_1<0. \quad (50)$$

Case 11: If $p = \frac{-1}{4}$, $q = \frac{(\hat{w}^2+1)}{2}$, and $r = \frac{-(1-\hat{w}^2)^2}{4}$, then the solution of Eq. 29 is $\varphi(\eta) = \hat{w}cn(\eta) \pm dn(\eta)$. Hence, Eq. 31 becomes

$$\psi(x,y,t) = \pm\sqrt{\frac{-1}{2\hbar_1}}[\hat{w}cn(\eta)\pm dn(\eta)]e^{(i\theta-\sigma\mathcal{B}(t)-\sigma^2t)}, \text{ for } \hbar_1<0. \quad (51)$$

When $\hat{w}\to 1$, then Eq. 51 transfers to Eq. 47.

5 Brownian motion's influence

In this section, we address the influence of Brownian motion on solutions of SHFSCE (1). We provide numerous graphical representations to demonstrate the influence of Brownian motion on the behavior of these solutions. First, let us fix the parameters $k_1 = 2.5$, $k_2 = k_3 = 1.5$, $k_4 = 0.5$, and $\eta_1 = \eta_2 = \theta_1 = \theta_2 = 1$. MATLAB is used to plot some solutions, such as [22], for $x\in[0,4]$, $y = 1$, and $t\in[0,4]$ and for various σ values (noise intensity) as follows:

When examining the surface at $\sigma = 0$, it is apparent from Figure 1, Figure 2, and Figure 3 that there is a fluctuation and that the surface is not smooth. When noise is added and its intensity is increased by a factor of $\sigma = 1$ and 2, the surface becomes substantially flatter after minor transit patterns. This demonstrates that the Brownian motion influences the solutions of SHFSCE and stabilizes them at zero.

6 Conclusion

In this article, we considered SHFSCE (1) forced by multiplicative Brownian motion. The stochastic solutions to this problem were obtained using two separate methods: the (G'/G)-expansion approach and the mapping method. These solutions are much more accurate and helpful in comprehending several critical complicated physical processes. Some previously obtained solutions, such as those described in [24], were extended. Finally, we used MATLAB tools to show the influence of multiplicative Brownian motion on the solutions of SHFSCE using graphical representations.

Data availability statement

The original contributions presented in the study are included in the article/Supplementary Material; further inquiries can be directed to the corresponding author.

Author contributions

FA-A: conceptualization, data curation, formal analysis, funding acquisition, investigation, methodology, software, writing–original draft, and writing–review and editing.

Funding

The author(s) declare that no financial support was received for the research, authorship, and/or publication of this article.

Acknowledgments

Princess Nourah bint Abdulrahman University Researcher Supporting Project number (PNURSP2023R 273), Princess Nourah bint Abdulrahman University, Riyadh, Saudi Arabia.

Conflict of interest

The author declares that the research was conducted in the absence of any commercial or financial relationships that could be construed as a potential conflict of interest.

Publisher's note

All claims expressed in this article are solely those of the authors and do not necessarily represent those of their affiliated organizations, or those of the publisher, the editors, and the reviewers. Any product that may be evaluated in this article, or claim that may be made by its manufacturer, is not guaranteed or endorsed by the publisher.

References

1. Yan ZL. Abundant families of Jacobi elliptic function solutions of the (2+1)-dimensional integrable Davey–Stewartson-type equation via a new method. *Chaos Solitons Fractals* (2003) 18:299–309. doi:10.1016/s0960-0779(02)00653-7

2. Wang ML, Li XZ, Zhang JL. The (G′/G) -expansion method and travelling wave solutions of nonlinear evolution equations in mathematical physics. *Phys Lett A* (2008) 372:417–23. doi:10.1016/j.physleta.2007.07.051

3. Zhang H. New application of the (G′/G) -expansion method. *Commun Nonlinear Sci Numer Simul* (2009) 14:3220–5. doi:10.1016/j.cnsns.2009.01.006

4. Wazwaz AM. A sine-cosine method for handling nonlinear wave equations. *Math Comput Model* (2004) 40:499–508. doi:10.1016/j.mcm.2003.12.010

5. Yan C. A simple transformation for nonlinear waves. *Phys Lett A* (1996) 224:77–84. doi:10.1016/s0375-9601(96)00770-0

6. Mohammed WW. Approximate solution of the Kuramoto-Shivashinsky equation on an unbounded domain. *Chin Ann Math Ser B* (2018) 39:145–62. doi:10.1007/s11401-018-1057-5

7. Mohammed WW. Modulation equation for the stochastic swift–hohenberg equation with cubic and quintic nonlinearities on the real line. *mathematics* (2020) 6:1–12. doi:10.3390/math7121217

8. Khan K, Akbar MA. The exp(−φ(ς)) -expansion method for finding travelling wave solutions of Vakhnenko-Parkes equation. *Int J Dyn Syst Differ Equ* (2014) 5:72–83. doi:10.1504/ijdsde.2014.067119

9. Hirota R. Exact solution of the Korteweg-de Vries equation for multiple collisions of solitons. *Phys Rev Lett* (1971) 27:1192–4. doi:10.1103/physrevlett.27.1192

10. Wazwaz AM. The tanh method: exact solutions of the sine-Gordon and the sinh-Gordon equations. *Appl Math Comput* (2005) 167:1196–210. doi:10.1016/j.amc.2004.08.005

11. Malfliet W, Hereman W. The tanh method. I. Exact solutions of nonlinear evolution and wave equations. *Phys Scr* (1996) 54:563–8. doi:10.1088/0031-8949/54/6/003

12. Yang XF, Deng ZC, Wei Y. A Riccati-Bernoulli sub-ODE method for nonlinear partial differential equations and its application. *Adv Diff Equa* (2015) 1:117–33. doi:10.1186/s13662-015-0452-4

13. Liu DY, Tian B, Jiang Y, Xie XY, Wu XY. Analytic study on a (2+1)-dimensional nonlinear Schrödinger equation in the Heisenberg ferromagnetism. *Comput Math Appl* (2016) 71:2001–7. doi:10.1016/j.camwa.2016.03.020

14. Zhao XH, Tian B, Liu DY, Wu XY, Chai J, Guo YJ. Dark solitons interaction for a (2 +1)-dimensional nonlinear Schrödinger equation in the Heisenberg ferromagnetic spin chain. *Supperlatt Microstruct* (2016) 100:587–95. doi:10.1016/j.spmi.2016.10.014

15. Ling LM, Liu QP. Darboux transformation for a two-component derivative nonlinear Schrödinger equation. *J Phys A* (2010) 43:434023. doi:10.1088/1751-8113/43/43/434023

16. Li CZ, He JS. Darboux transformation and positons of the inhomogeneous Hirota and the Maxwell-Bloch equation. *Sci China-phys Mech Astr* (2014) 57:898–907. doi:10.1007/s11433-013-5296-x

17. Ma WX, Zhang YJ. Darboux transformations of integrable couplings and applications. *Rev Math Phys* (2018) 30:1850003. doi:10.1142/s0129055x18500034

18. Tang GS, Wang SH, Wang GW. Solitons and complexitons solutions of an integrable model of (2+1)-dimensional Heisenberg ferromagnetic spin chain. *Nonlinear Dynam* (2017) 88:2319–27. doi:10.1007/s11071-017-3379-3

19. Sulaiman TA, Akturk T, Bulut H, Baskonus HM. Investigation of various soliton solutions to the Heisenberg ferromagnetic spin chain equation. *J Electromagnet Wave* (2018) 32:1093–105. doi:10.1080/09205071.2017.1417919

20. Wang QM, Gao YT, Su CQ, Mao BQ, Gao Z, Yang JW. Dark solitonic interaction and conservation laws for a higher-order (2 +1)-dimensional nonlinear Schrödinger-type equation in a Heisenberg ferromagnetic spin chain with bilinear and biquadratic interaction. *Ann Phys* (2015) 363:440–56. doi:10.1016/j.aop.2015.10.001

21. Triki H, Wazwaz AM. New solitons and periodic wave solutions for the (2 +1)-dimensional Heisenberg ferromagnetic spin chain equation. *J Electromagn Waves Appl* (2016) 30:788–94. doi:10.1080/09205071.2016.1153986

22. Ma YL, Li BQ, Fu YY. A series of the solutions for the heisenberg ferromagnetic spin chain equation. *Math Methods Appl Sci* (2018) 41:3316–22. doi:10.1002/mma.4818

23. Seadawy AR, Nasreen N, Lu D, Arshad M. Arising wave propagation in nonlinear media for the (2+1)-dimensional Heisenberg ferromagnetic spin chain dynamical model. *Physica A* (2020) 538:122846. doi:10.1016/j.physa.2019.122846

24. Bashar H, Islam SMR, Kumard D. Construction of traveling wave solutions of the (2+1)-dimensional Heisenberg ferromagnetic spin chain equation. *Partial Differential Equations Appl Maths* (2021) 4:100040. doi:10.1016/j.padiff.2021.100040

25. Seadawy AR, Yasmeen A, Raza N, Althobaiti S. Novel solitary waves for fractional (2+1)-dimensional Heisenberg ferromagnetic model via new extendedgeneralized Kudryashov method. *Phys Scr* (2021) 96:125240. doi:10.1088/1402-4896/ac30a4

26. Rani M, Ahmed N, Dragomir SS, Mohyud-Din ST. New travelling wave solutions to (2+1)-Heisenberg ferromagnetic spin chain equation using Atangana's conformable derivative. *Phys Scr* (2021) 96:094007. doi:10.1088/1402-4896/ac07b9

27. Kloeden PE, Platen E. *Numerical solution of stochastic differential equations*. New York: Springer-Verlag (1995).

28. Kloeden PE, Platen E, Schurz H. *Numerical solution of SDE through computer experiments*. New York: Springer-Verlag (1994).

Frontiers in Physics

Investigates complex questions in physics to understand the nature of the physical world

Addresses the biggest questions in physics, from macro to micro, and from theoretical to experimental and applied physics.

Discover the latest Research Topics

See more →

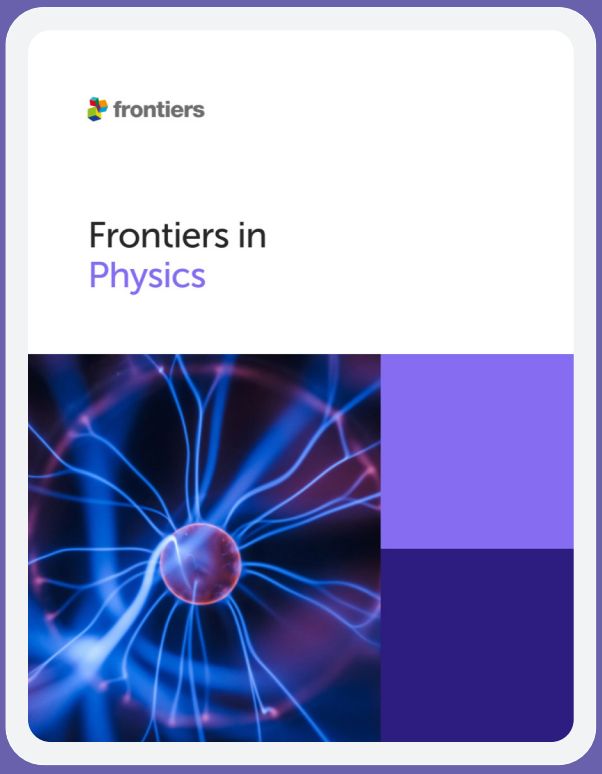

Frontiers

Avenue du Tribunal-Fédéral 34
1005 Lausanne, Switzerland
frontiersin.org

Contact us

+41 (0)21 510 17 00
frontiersin.org/about/contact